Fundamentals of Short-Range FM Radar

Fundamentals of Short-Range FM Radar

Igor V. Komarov
Sergey M. Smolskiy

English translation edited by
David K. Barton

Artech House
Boston • London
www.artechhouse.com

Library of Congress Cataloging-in-Publication Data
Komarov, Igor V.
Fundamentals of short-range FM radar / Igor V. Komarov, Sergey M. Smolskiy.
p. cm. — (Artech House radar library)
Includes bibliographical references and index.
ISBN 1-58053-110-5 (alk. paper)
1. Radar. I. Smolskiy, Sergey M. II. Title. III. Series.

TK6575.K625 2003
621.3848—dc22

2003057715

British Library Cataloguing in Publication Data
Komarov, Igor V.
Fundamentals of short-range FM radar. — (Artech House radar library)
1. Radar 2. Radio frequency modulation
I. Title II. Smolskiy, Sergey M.
621.3'848

ISBN 1-58053-110-5

Cover design by Igor Valdman

685 Canton Street
Norwood, MA 02062

International Standard Book Number: 1-58053-110-5
Library of Congress Catalog Card Number: 2003057715

10 9 8 7 6 5 4 3 2 1

This book is dedicated to the memory of our parents

Contents

Preface

The material offered to readers of this book is based on literature sources and on a small part of the long-term research works of the authors in the area of autodynes and frequency-modulated continuous-wave (FMCW) radar. Most of the material was presented at the Radio Engineering Faculty of the Moscow Power Engineering Institute (Technical University) MPEI in lecture courses on "FMCW Radar," "Theory of Signal Processing," "Short-Range Radar Systems," "Transistor Autodynes," "Oscillation Theory in Radio Engineering," and "Oscillation Stability," and also at lectures, seminars, and scientific and technical conferences at industrial enterprises.

We think that this book may be useful to students and postgraduate students of the appropriate radio engineering specialties, experts (engineers) in the field of radar who want to get acquainted with or are seriously engaged in the theory and development of FMCW radar and autodynes. We hope that it will be interesting to scientific officers and teachers of technical universities - specific experts in these subjects.

Is it possible to design a radar using this book? Our long-term experience in teamwork with industry enables us to give a definite negative answer. This book contains only the fundamentals of the theory of FMCW radar and autodynes, while for their design it is necessary to have a set of additional data that is absent from this book, and we are not going to include it. At the same time, it is obvious that without knowing the fundamentals, it is, in general, impossible to design anything, and studying these fundamentals is necessary in any case.

The book consists of two parts. Part I has been written by Dr. I. Komarov, and Part II by Dr. S. Smolskiy. Auxiliary sections of the book have been prepared by the authors jointly.

Part I contains the fundamental theory of short-range FMCW radar, while Part II covers the theory of radiating autodynes. At first sight, such a combination may seem strange, but we should not jump to conclusions. We note that radiating autodynes, by the principle of their operation, may work only within the structure

of radars, and most effectively in short-range FMCW radars. The experts on FMCW radar, as a rule, are not familiar with autodyne theory. If they apply an autodyne for development of a radar they are interested only in its technical characteristics rather than in theoretical considerations. Experts in autodynes often know little or nothing about FMCW radar theory and methods of signal processing. That is why the simple and unexpected idea came to us: why not present materials on these two subjects in one book devoted to the basics of FMCW radar? Then the expert interested in FMCW radar may get acquainted with autodyne theory and the expert in autodynes can correspondingly get acquainted with the theory of FMCW radar. The reader will judge how effective this combination has been.

During preparation of the book we followed to a certain degree an aphorism of Bertrand Russell: "A book can be either clear, or strict, but it is impossible to combine both these requirements." Therefore, in Part I preference is given to clarity, but not to the detriment of rigor, and in Part II the preference is given to rigor, but not to the detriment of clarity, or so it seems to us.

The material of Part I is written according to the principle "from simple to more complex." Each chapter is like a step on a ladder, on which the reader rises. Chapter 1 is intended for those readers who may have heard of FMCW radars, but have no clear idea about their performance or areas of application. In the beginning of the chapter a brief history of the origin and further development of FMCW radar is given. Then examples of FMCW radar applications are given. Some present examples are well known: first, radio altimeters and meters of level of liquid or powderlike products in closed tanks. Other examples include possible applications of FMCW radar such as navigational radar, precision range meters for fixed or slowly moving targets, meters of very small motions, instruments for measuring minute changes of range (hundredths of a millimeter) as noncontact meters of vibrations and pressure of a gas or liquid, and others.

Chapter 2 is the basis for all further material of Part I. The basic block diagrams of FMCW radar are considered and expressions for transmitted, reflected, and converted signals are deduced. The last term refers to the signal at the output of the RF mixer. In other literature it is frequently called an *intermediate frequency signal* (by analogy to the intermediate frequency signal in a superheterodyne receiver), and also the *range measuring signal.* A feature of the analysis given in this chapter is that the converted signal is considered as the product of the current difference of the phases, instead of as a product of the difference of instantaneous frequencies of transmitted and reflected signals. This method of analysis is exact and general, and it enables us to obtain most simply the necessary relationships, in particular, the basic relationships for the spectrum of the converted signal. It also allows us to explain very simply some features of the converted signal. If desired or necessary it is easy to proceed to frequency interpretations.

The material in Chapter 2 receives further development in Chapter 3, where parameters and characteristics of the converted signal are examined for the most widely used types of periodic frequency modulation: sinusoidal, double sinusoidal,

and various types of linear modulation: symmetrical, asymmetrical, and nonisosceles sawtooth. The greatest attention is given to the analysis of the converted signal with asymmetrical sawtooth modulation because this modulation in many cases obtains the best characteristics of FMCW radar.

Because modern electronic component technology makes possible the application of a frequency synthesizer as an FM oscillator, the features of the converted signal for discrete linear (stepped) modulation are examined in this chapter. At the end of the chapter we estimate the influence on parameters of the converted signal of nonlinearity in the transmitter modulation characteristic.

Chapters 2 and 3 form the basis for the subsequent development.

In Chapter 4 we consider so-called integrated methods of converted signal processing. The term "integrated" may be not absolutely successful, but no other term has been devised. Integrated methods of converted signal processing are defined to be those in which all signal parameters (i.e., amplitude, frequency, and phase) are utilized for processing. The possible methods of signal processing are first briefly considered. A significant part of the material in this chapter (~20%) is devoted to consideration of the influence on radar receiver operation of parasitic amplitude modulation of the transmitted signal and several adequately effective ways to reduce this influence. Then we consider methods of stabilization of frequency deviation and linearization of the transmitter modulation characteristic. In Section 4.4, "Frequency Processing of the Converted Signal," we consider long-known processing methods as well as rather new methods. Descriptions of the earlier methods are given for completeness and to avoid sending the reader to old references that may be almost inaccessible. Here we describe the following: the method of range measurement by calculation of the number of zeros of the converted signal for the modulation period, and the method of using the converted signal frequency deviation with sinusoidal modulation. In the following section we consider methods of range measurement based on measurement of the converted signal's instantaneous frequency, the fixing of this frequency and of the converted signal's frequency deviation. The chapter concludes with a section in which we analyze opportunities of range measurement by measurement of the converted signal's phase shift during the modulation period. We show that this approach allows us to measure range with a margin of error no more than tenths of one percent, using technically achievable deviations of transmitted signal frequency.

In Chapter 5, we consider methods of converted signal processing based on exploiting the characteristics and parameters of its spectrum. We have seen from long-term experience of discussing these questions with colleagues and students, the greatest difficulty in studying this material is the necessity of representing a spectral picture in frequency-range coordinates. For this reason, we consider first the dependence of separate spectral components on range and then the three-dimensional spectral picture in voltage-frequency-range coordinates. Further, on the basis of this analysis, theoretical and real range resolutions are calculated. In development of this question, the range resolution is calculated for application of weighted signal processing, and the physical essence of weighted processing is

explained in detail. The natural continuation of this material is radar scan of range. Various ways of creating the physical spectrum analyzer of the converted signal, and such important parameters of the analyzer as minimal necessary analysis time, are considered. As in Chapter 4, we describe one of the possible processing methods with which the normal operation of the receiver is ensured even when the parasitic amplitude modulation signal is larger than the converted signal. At the end of the chapter, various methods of processing the separate spectral components of the converted signal are presented. Here it is worth noticing the sections in which we discuss opportunities for applying an FM signal instead of multifrequency signals, and methods of using phase relationships.

Part II is devoted first to simple and compact RF devices, called *autodynes*, *self-mixing oscillators*, or *self-generating mixers* by different authors and different scientific schools. In essence, such a cascade is a very complex device consisting of a self-oscillatory system connected by a reciprocal circuit to a transceiving antenna. This RF cascade combines the functions of generating an RF transmission with specific characteristics, radiating it from the antenna, receiving the signal reflected from the target (the measured object) to the same antenna, and generating the response to this time-delayed reflected signal, whose amplitude may be small or large.

The difficulties of combining all these functions, and the essentially nonlinear mode of autodyne operation necessary for generation of the transmission and processing of the converted reflected signal, together with the complexity of active semiconductor RF elements and microwave oscillatory systems, also introduce complexity in the theoretical analysis of these devices and the significant interest of researchers in them. The resulting set of dissertations on this subject is protected now (at least, in Russia). Engineers are interested in autodynes because these devices are simple to produce, extremely small-sized and cheap for mass production, and require only one antenna without expensive microwave duplexing devices. Also, as nonlinear devices, autodynes allow us to offer nonstandard circuit choices, for example, distributed autodynes with power addition, noise-proof autodynes with various types of frequency modulation, autodynes that are well matched to nonstandard antennas, and many others.

What method of description of autodyne FMCW radar characteristics is used in Part II?

Very often in Russian and Western scientific literature the researchers try a simple approach: to find very simple treatments of autodyne processes by resorting to already generated concepts from the theory of other devices. It is possible to find many such examples. One of the first (pioneer) publications on autodynes by American authors R. D. Huntoon and B. G. Miller (*Electronics,* November 1945) examines the autodyne signal as a reaction to varying loading. Other models of the autodyne sometimes postulate a mixer with fixed heterodyne signal amplitude or a synchronized oscillator transferred in the beating mode. Thus, it is possible to try to explain the elementary processes of an autodyne, but as soon as real problems and practical questions are addressed, these treatments start to reveal serious

(sometimes basic) mistakes. It is necessary, even speaking about the fundamentals of autodyne system operation, to address complex models and to climb into a theoretical jungle. We recollect that one known Russian expert in radio engineering, during the defense of a dissertation, slightly paraphrased the words of philosophers about the electron to joke: "The autodyne is as inexhaustible as the atom." It seems to us that in this joke there is a serious element of truth.

Nevertheless, we have decided not to hesitate because of such complexities, in order that the reader realize that simple explanations cannot simply be dismissed. If there is a problem in overlooking a complex question (for example, dynamic properties, speed of resynchronization, transients of the autodyne signal with frequency modulation, nonlinear distortions in FM, etc.), it is necessary to prepare for serious slow work with difficult mathematical literature, with complex computer modeling packages, complex microwave experimental equipment, and all other "amenities" of modern engineering practice.

In Chapter 6 (the first chapter of Part II) we describe the method of symbolical abbreviated equations, which is widely used by Russian scientists, and which allows us easily and elegantly to analyze various processes in single-frequency self-oscillatory systems (systems without FM). To prepare the Western reader for this method the relatively simple case of the single-tuned oscillator is first considered, for which it is shown how to obtain the initial simplified (so-called "abbreviated") equations. A strict substantiation of the method is presented, and then the general abbreviated equations, the equations of the stationary mode, and the general characteristic equation describing local stability of oscillations are determined. Different examples are analyzed: the oscillator with fixed and automatic bias, the analysis of stationary modes with usual and dynamic oscillatory characteristics, the method of usual and dynamic hodographs, cases of soft and rigid excitation of self-oscillations are considered, and stability of modes and transients in the phase plane are analyzed. The general equations are obtained with sufficiently general preconditions on structure of the selective system and autobias circuits, and also on characteristics of inertial active elements. Consideration is given to the case of FM absence, and as far as is known to us, consideration of self-oscillatory systems by members of the American scientific schools is not usually carried out in a similar way.

Chapter 7 is devoted to absolutely new and original theoretical material: application of the symbolical abbreviated equation method to systems with variable parameters, in this case to autodyne systems with FM as used in FMCW radar. At first the previous general abbreviated equations are applied to the case of controlled multiport active elements, and then the case of frequency modulation is considered. A proven procedure for abbreviation of the equations and fast derivation of the equations of specific systems is offered for different types of modulation. For simplification of understanding, simple and more complex examples are considered with sine wave, binary, and triangular (symmetric and asymmetrical) types of frequency modulation.

Part I repeatedly emphasizes that the parasitic amplitude modulation (PAM) that always accompanies frequency modulation, not only in nonlinear systems but also in linear selective systems, is quite harmful to FMCW operation. In Chapter 8 the question of PAM signal definition is considered in detail. We first consider the case of the FM oscillator for discrete frequency tuning, when there is a connection between oscillation amplitude and the mode for different variants of oscillator circuits, and then the case of modulation. We determine the parameters of the FM oscillator mode from the solution of the differential equations and then the in-phase and quadrature PAM components. The dependence of the PAM factor on the mode, on modulation frequency, and on circuit parameters of the oscillator are derived. The cases of frequency control with varicaps, both with smooth and sharp P-N junctions, are separately analyzed.

Chapter 9 is devoted to the important practical question of modulation characteristic nonlinearity in the FM oscillator and to the issue of its linearization. The case of large change of frequency is examined first for smooth and sharp varicaps, and the dependence of modulation characteristic nonlinearity upon the factor of frequency overlapping is considered, first without and then with high-frequency voltage on the varicap. Nonlinear distortions of the modulating function are analyzed, and factors of nonlinear distortions on the second and third harmonics are determined. Methods of linearizing the modulation characteristic using diode-resistive circuits, circuits with voltage detection, diode-transistor compensating circuits, and circuits of modulators with detuned circuits are considered. A technique of engineering calculation of compensating circuits is developed.

In Chapter 10, the basic theoretical chapter of autodyne process analysis, we derive the abbreviated equations for an autodyne with autobias, in which the autodyne signal may be described as due to autodyne self-detecting properties (in an autobias chain), or due to peak detection. The abbreviated equations are linearized for the case of a weak reflected signal and the linearized equivalent circuits of the autodyne are discussed. Autodyne transfer factors in voltage and current are determined, describing the effectiveness of transformation of the reflected signal into a useful autodyne signal. The form and spectral structure of the useful detected signal and the RF autodyne signal are calculated. The cases of different types of frequency modulation are separately considered. The dependence of autodyne sensitivity upon its mode and circuit parameters are derived, and questions of mode optimization are discussed for low and high frequencies of the chosen transistor.

By studying the material of this chapter, the reader will master a technique for approaching the analysis of a specific autodyne circuit and for defining the sensitivity and potential of an FM radar. He or she will also understand the connection and necessary measures for simultaneous maintenance of high autodyne sensitivity, reserve of mode stability, necessary autodyne output power, and required parameters of frequency modulation.

Chapter 11 is devoted to the specific and complex question of analysis of autodyne behavior in the presence of a large synchronizing signal (the useful

signal synchronizing a chain of interconnected autodynes, or a harmful interfering signal at nearby frequency). The presence of this material in a book devoted to fundamentals of FMCW radar can be explained in the following way. We wanted to show that the general approach to autodyne equations may be used for the solution of complicated problems. In this chapter fine and "superfine" methods of nonlinear fluctuation theory are used for consideration of the problem, allowing us to describe the large variety of modes and again to obtain closed formulas for calculation and analysis of autodyne transfer factors. These methods include synchronization theory, bifurcation theory, analysis of dynamic systems behavior on cylindrical phase space, simultaneous influence on autodynes of the detuned synchronizing signal and a reflected signal, questions of maintenance not only of local, but also of global stability, the analysis of special points of the second order and their bifurcations, invariant integrated, and biphase surfaces. It appears that the usual assumption of failure of autodyne operation resulting from locking by strong interference is wrong: with a reasonable choice of mode it is possible not only to keep autodyne mode stability, but also to even increase sensitivity.

This chapter will be complex for the unprepared reader. It can be omitted when studying the fundamentals of FMCW radar. If the reader wishes to get seriously into autodyne subjects, the chapter will help guide him or her to become interested in a surprising and fruitful direction that may open the door to a new world of deep nonlinear phenomena.

Certainly, many questions have not found reflection in the book. From among such questions applicable to Part I, we do not discuss the theory of short-range FMCW radar operation with real (i.e., fluctuating) signals, noise and code modulations, digital processing of the converted signal, questions of short-range FMCW radar design, and a number of others. In Part II such questions as push-pull and ring autodynes, autodynes with stabilization of sensitivity, autodynes with delay lines, autodynes with axisymmetric antennas and antenna arrays, multielement autodynes with power addition in space, laser autodynes, and many other issues are not mentioned. It is obvious that discussion of all these questions in one book is completely unrealistic.

Perhaps the reader will be surprised at the scarcity of the references listed, given the large interest of scientists and engineers in this field. During preparation of the manuscript we met some difficulties with formation of this list. The fact is that, on the one hand, we tried to refer as little as possible to Russian texts and those of the former USSR, as they are seldom translated into other languages and are inaccessible to the Western reader. On the other hand, for obvious reasons, the Western editions are remote from us, and it is very difficult for us to choose really pioneering works from numerous articles and reports. It seems to us that the Western reader who is seriously interested in this problem will find without effort the literature accessible through common information bases and can skillfully compare approaches and results of different authors.

More than 30 years of scientific research in described directions was performed by us, in close contact but in different departments of the Moscow Power

Engineering Institute (Technical University). In the Radio Receiver Department, Dr. Komarov supervised a large group of researchers, teachers, postgraduate students, and students involved in the problems of analysis and synthesis of FMCW radar structures, of theory and practical devices of signal processing, description of signals from interference, and so forth. Autodyne development was carried out in the Radio Transmitter Department under Dr. Smolskiy, supervising an equally large team of researchers, postgraduate students, and students. We also worked during all these years in close contact with many scientific research institutes and industrial design offices. Thus, the results obtained are the work of many, many people, and so it is completely impossible to list all their names. Unfortunately, many of them are already not with us, and we try to do justice to their memory. To all colleagues who are in good health, the authors express great gratitude for long years of teamwork.

S. M. Smolskiy would like to express profound gratitude to the main teacher and the supervisor of his studies since his student years: Dr. V. M. Bogachev, his instructor and friend on many scientific and vital questions, for all the advice given during 35 years of friendship and cooperation, and for all skills (that are actively used today), transferred by working with the youth. It is also a pleasure to recollect years of teamwork with colleagues and pupils Dr. V. G. Lysenko, Dr. S. A. Morosanov, Dr. S. L. Artemenkov, Dr. V. A. Ivanov, Dr. S. N. Bikkenin, Dr. L. N. Laut, and M. A. Solov'ev.

During preparation of the book, invaluable help to the authors was rendered by scientific editor Mr. David K. Barton, whom we thank with our hearts and hope that we have found in him not simply a highly skilled colleague but a friend as well. He has done a huge amount of work, in essence having translated our English text "with a significant Russian accent" into normal technical English, helped us to find the correct terms for the present moment, and asked questions that have undoubtedly improved the text.

We also offer heartfelt thanks to the employees of Artech House with whom we worked, for their extremely benevolent, attentive, and kind attitude to us.

We would be delighted if interested readers would express, through Artech House or directly to us, their questions, remarks, and recommendations for improvement of the book. We firmly believe that any scientific work never happens to be entirely completed. We imagine that the book is similar to an unfinished house: you look to the right at an empty window - one direction for development, on the left at an aperture for a door - another no less interesting picture! You see the best memory of the authors' work before you, and simultaneously express gratitude to them - studying their works and development in different directions.

And we, as all authors of completed books, shall wait eagerly for this development.

Part I

Chapter 1

Introduction to Frequency-Modulated Continuous-Wave Radar

1.1 BRIEF HISTORY

The idea of using FM signals for ranging to a reflecting object (a target) is very old. These signals were used as long ago as the 1920s for ionospheric research. The practical application of frequency-modulated continuous-wave (FMCW) radar started in 1928, when J. O. Bentley filed the American patent [1] on an "airplane altitude indicating system."

Bentley's radar was very simple (Figure 1.1). The transmitter frequency is modulated with a triangular waveform (Figure 1.2), using an electric motor rotating an adjustable capacitor. The transmitted energy is radiated toward the surface. Because the isolation between transmitting and receiving antennas is limited, a small fraction of the transmitted energy (the direct signal) enters the receiving antenna along with the signal reflected from the surface. The receiver input circuit is tuned to match, at any moment of time, the frequency of the transmitter. The

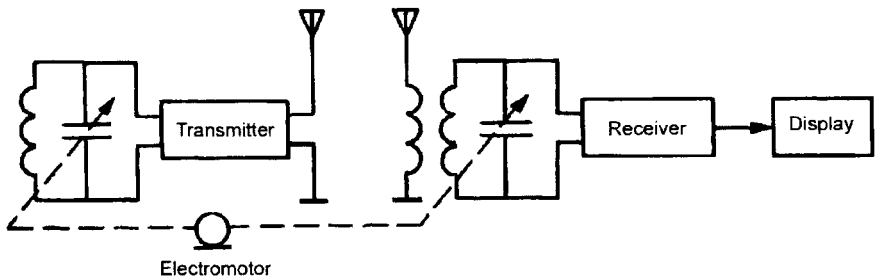

Figure 1.1 Block diagram of radio altimeter by Bentley.

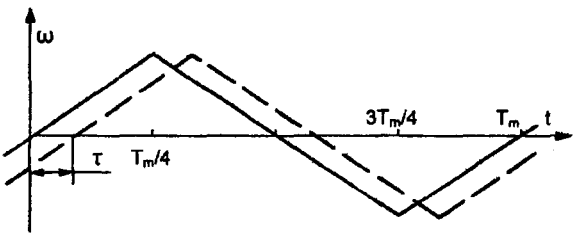

Figure 1.2 Instantaneous frequency of the radiated and reflected signals.

reflected signal frequency differs slightly from that of the transmission (Figure 1.2), being delayed by a time τ that is constant except for short intervals just after reversals of the slope of the transmitted frequency, which occur at times

$$(2n+1)\frac{T_m}{4}....(2n+1)\frac{T_m}{4}+\tau \text{ , where } n = 0,1,2, \ldots$$

The difference is much less than the passband of the receiver input circuit, which therefore accepts the reflected signal along with the transmitter leakage. The difference frequency Ω between these signals is formed by interaction of the two signals in a nonlinear receiver element (mixer or detector). The frequency Ω is directly proportional to the delay time (i.e., to range from the aircraft to the surface), except for the short time intervals following slope reversal. Measurement of Ω determines the aircraft altitude.

Industrial applications of this idea began only at the end of the 1930s, when the ultrahigh-frequency band was exploited. Mechanical frequency agility of the transmitter provided the necessary frequency deviation (~20 to 30 MHz). Signal processing after the mixer was performed in a very low-frequency band. The radar illustrated is very simple and hence reliable. This was the basic reason for wide application of FMCW radio altimeters in military aircraft before WW II, and subsequently in civil aircraft. At present a low-altitude FMCW radio altimeter is a necessary element of the avionics suite for most military and civil aircraft, and also for space vehicles during landing.

Most of the theoretical works on FMCW radar were published during a period from the late 1940s to the early 1960s [2-8]. In addition to radio altimetry, FMCW radars have been developed for applications such as merchant marine navigation.

The theory and engineering of pulse radar began to develop soon after the end of the 1930s. Most of the subsequent development in radar engineering was in pulse radars, which met most requirements of military and civil engineering and industrial applications. The FMCW radar art has found itself in the shadow of pulse radar. It has been largely "forgotten," and has been "recollected" only when requirements have appeared to measure very small ranges, from fractions of a meter to a few meters. Primary examples in military engineering are proximity fuzes

for artillery shells and missiles, and systems for detection of mobile targets. Major advances have been supported by development of the technology base in centimeter and millimeter waves and microelectronics.

FMCW radar has been developed and applied on a large scale in civil industry for measurement of levels of liquid, paste, or powder-like products in closed tanks. Such equipment is termed "level-measuring radar."

1.2 EXAMPLES OF USE OF FMCW RADAR

Before considering examples of FMCW radar applications, we will note the basic features of these radars. These are:

- Ability to measure small and very small ranges to the target, minimal measured range being comparable to the transmitted wavelength;
- Ability to measure simultaneously the target range and its relative speed;
- Small error of range measurement, which with some processing methods is within hundredths or even thousandths of a percent;
- Ability to measure small range changes (less than fractions of a percent of the wavelength);
- Ability to use various types of indicators (panoramic, plan-position etc.);
- Signal processing after mixing is performed in a range of frequencies, commensurable with the modulation frequency (i.e., in a frequency band from hundreds of hertz up to hundreds of kilohertz), considerably simplifying realization of the processing circuits;
- Safety from absence of pulse radiation;
- Compactness, the dimensions of a radar using modern technology being determined, basically, by the dimensions of the microwave block;
- Small weight and small energy consumption due to absence of high circuit voltages.

We should note in particular one more feature: the possible application of ultrasonic transmissions.

We will now consider several examples of FMCW radar applications.

1.2.1 Radio Altimeters

The application of FMCW radars as *radio altimeters* is well known in the radar community. There is a great deal of literature in which the theory of operation and practice for radio altimeters is discussed, and hence there is no need to dwell further on this issue.

1.2.2 Level-Measuring Radar

The device works in the following way. The entire device or its transceiver antenna is placed on the cover of the tank (Figure 1.3). The antenna beamwidth does not usually exceed 10 to 12 degrees. The antenna beam is pointed vertically toward the surface of the tank contents to which the range R is measured. As the range H from the antenna to the bottom of the tank is known, the level is determined as $L = H - R$.

The maximum measured range is the height of the tank, which in most cases does not exceed 50m (e.g., in oil tankers). The minimal measuring range R is about 0.5 to 1.0m. The frequency bands J or K are typically used to obtain a pencil-beam antenna pattern. The most important parameter in a level-measuring radar is the range error. For most devices the rms error is within fractions of one percent to a few percent of R. In some cases measurement is required in small-volume tanks (with small heights). In these cases, R does not exceed one or two meters, and it is most expedient to apply ultrasonic level-measuring radar.

In some manufacturing processes there is a two-layer liquid in the tank for which it is necessary to know only the level (layer thickness) of the lower liquid (for example, to pour out the bottom liquid and leave the top liquid). This problem can be solved with ultrasonic radar (Figure 1.4). The ultrasonic transducer is located on the bottom of the tank with its narrow beam directed vertically upwards. The radiated signal is reflected from the boundary between the two liquids, and thus the thickness of the bottom layer is measured. Part of the signal, of course, penetrates through the boundary and is reflected from the top surface of the liquid or gas (or air), passing again through the boundary of the liquids and entering the receiver. As a rule, however, this signal is strongly attenuated and easily filtered.

1.2.3 Navigational Radar

FMCW radar can be applied to navigation radars with ranges up to several kilometers. It should not be supposed that the operating range of FMCW radar is inher-

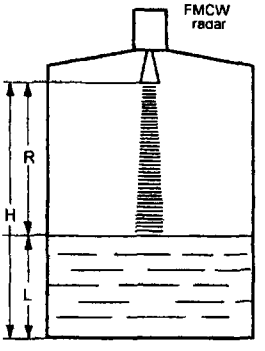

Figure 1.3 Tank with level-measuring radar.

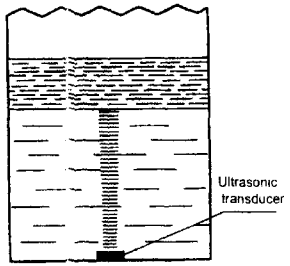

Figure 1.4 Ultrasonic radar in a tank with a two-layer liquid.

ently limited to several kilometers, as longer ranges are entirely feasible even though pulse radars are generally used in such cases. FMCW radar is most useful at short ranges, from tens to hundreds of meters (e.g., for surveillance of the sea or large river ports when vessels arrive under conditions of bad visibility). FMCW radar can be used not only to search the water surface of the port but also to measure range and relative speed of any targets within the port.

The ability to measure very short ranges, those within fractions of a meter, makes possible realization of one more very important function. When a vessel makes fast to the wall of a quay the captain may not be able to observe the range between the hull and the wall, especially with large sea-going ships. This greatly complicates docking. The same problem arises in passing through a lock chamber, where he must control not only the distance from his hull to the lock chamber, but also distance to the next vessel. *This problem is easily solved by placing FMCW radar at the bow and stern for measurement of distance to the wall. The small size, simplicity, and economy of FMCW radars suit them to these problems.*

1.2.4 Vehicle Collision Warning Systems

In the past several years vehicle collision warning systems (VCWS) have been developed in response to the substantial traffic growth in cities and on motorways. The design of these systems is very complex and difficult. For a brief description

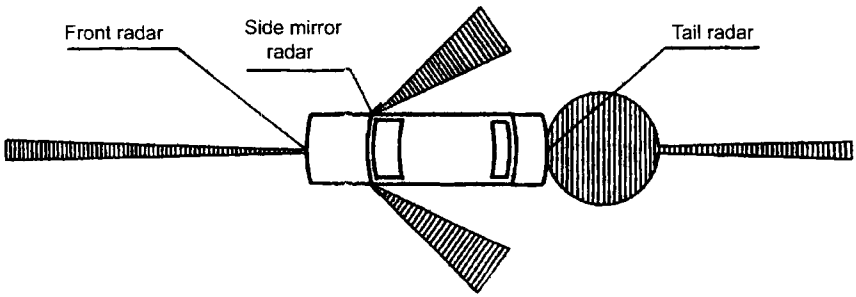

Figure 1.5 Coverage zones of vehicle collision warning system.

of one possible VCWS, we refer to Figure 1.5. The shading designates operating ranges of this system. These ranges are covered by four radars: front, tail, and two side mirrors. The front radar has a pencil-beam pattern several degrees wide. The range of this radar is about 300m, with a minimal range of 20 to 30 cm. The radar provides continuous measurement of range and relative velocity for targets ahead of the vehicle. This data appears on the display and in a computer that gives a danger signal based on this data, and if necessary activates the brake system.

The tail radar carries out the same operations as the front radar, but in a circular operating zone directly behind the automobile at ranges from ~ 20 or 30 cm to a maximum of ~2 to 3m. This operating zone is used for parking and backing.

The operating range of the side-mirror radar is ~10m, with a width of 10 to 20 degrees, depending on the design of the automobile. This radar gives a danger signal when the next automobile is within its coverage.

Comparing these VCWS specifications and the features of FMCW radars listed above, it is clear that these radars offer a good approach for VCWS.

1.2.5 Precision Range Meter for Fixed Targets

Methods of precision range measurement have long been known. Multifrequency CW radars using phase processing of the reflected signal are applied for this purpose. These radars allow us to measure range up to tens of kilometers with a relative error of the order 10^{-6} to 10^{-5}. Multifrequency CW radars have already been applied in a geodesy [7]. However, there is a disadvantage to this type of CW radar: the impossibility of range measurement to fixed targets. To measure range to a fixed target we must install on it an active reflector to simulate a Doppler shift, but this is inconvenient and not always possible. FMCW radar is free from this disadvantage [9], appreciably expanding its area of application, as shown by the following examples.

For measurements in a triangulation network it is not currently necessary to use active reflectors. It is sufficient to install passive reflectors (e.g., corner reflectors) at the appropriate points of this network.

Another example is monitoring the behavior of glaciers and snow avalanches in mountains. At present this monitoring is performed by theodolites. The deficiencies of this method are obvious: need for special crews for installation and operation; maintenance of these crews with appropriate housing and supplies; ability to make measurements only under conditions of good visibility; and the additional calculations required.

Using FMCW radar this task can be solved much more easily. On the surface of a glacier (or snow avalanche) we install corner reflectors or drop them from a helicopter or by parachute from an aircraft. An FMCW radar is installed on a slope or top of the next mountain to observe the glacier. This radar continuously or periodically measures range to the appropriate corner reflector. Thus it is possible to obtain a record of dynamics (changes) of glacier motion or snow avalanche. The radar can work automatically, data being transferred by radio circuit. Hence, there

is no necessity to mount expeditions. This substantially simplifies and reduces the price of monitoring glaciers and snow avalanches.

FMCW radars can also be used to measure displacement of walls of high buildings, towers, and other structures.

1.2.6 Measurement of Very Small Motions

A typical example of small motion measurement is the observation of vibrations of various components of machines and mechanisms. The most useful device for such measurements is contactness, meaning that there is no physical contact between the device and the vibrating component. Several devices for contactness vibration measurement are known, but all have one or another disadvantage (e.g., inability to perform measurement at high temperatures or in aggressive environments).

Attempts to apply continuous microwave signals for these measurements are also known. In this case the narrow beam of a microwave radiation with frequency ω is radiated toward a vibrating element and the phase difference between radiated and reflected signals is measured. If the delay of the reflected signal is τ, this phase difference is $\omega\tau$. Then a reflected signal phase shift of 360° corresponds to a range change of $\lambda/2$. For example, if $\lambda = 7.2$ mm, then a 10-μm change produces 1° of phase shift. This permits us to measure very small range changes.

As methods of direct measurement of phase differences of microwave signals are unknown, various indirect ways for such measurement have been developed. The resulting devices for vibration measurement using microwave signals are very complex and have not been widely applied. FMCW radar simply solves this problem [10]. The fact is that the information on the phase angle $\omega\tau$ appears in the low-frequency signal at the mixer output of the receiver. This considerably simplifies measurement of the phase angle $\omega\tau$ with the usual analog or digital phase detector. It is obvious that one area of application for FMCW radar is for measurement.

The list of examples of application of radars can be continued. However, from this list it can be seen that the area of application of these radars is wide. In the following chapters we will call FMCW radar short range radar (SRR) for brevity.

References

[1] Bentley, J. O., "Airplane Altitude Indicating System," U. S. Patent No. 2,011,392, issued August 13, 1935, application August 10, 1928.

[2] Luck, D. G. C., *Frequency Modulated Radar,* New York: McGraw-Hill Book Company, 1949.

[3] Ismail, M. A. W., *A Study of the Double Modulated FM Radar,* Zurich: Verlag Leemann, 1955.

[4] Horton, B. M., "Noise-Modulated Distance Measuring Systems," *Proc. IRE,* Vol. 47, May, 1959, pp. 823-828; reprinted in Barton, D. K., *Radars*, Vol. 7, *CW and Doppler Radar*, Dedham, MA: Artech House, 1978

[5] Saunders, W. K., "Post War Developments in Continuous-Wave and Frequency-Modulated Radar," *IRE Trans.,* Vol. ANE-8, March, 1961, pp. 7-19; reprinted in Barton, D. K., *Radars*, Vol. 7, *CW and Doppler Radar*, Dedham, MA: Artech House, 1978.

[6] Saunders, W. K., "Correction to 'Post-War Developments in Continuous-Wave and Frequency-Modulated Radar,'" *IRE Trans.,* Vol. ANE-8, October, 1961, p. 105; reprinted in Barton, D. K., *Radars*, Vol. 7, *CW and Doppler Radar*, Dedham, MA: Artech House, 1978.

[7] Skolnik, M. I., *Introduction to Radar Systems*, New York: McGraw-Hill Book Company, 1962.

[8] Fried, W. R., "An FM-CW Radar for Simultaneous Three Dimensional Velocity and Altitude Measurement," *IEEE Trans.,* Vol. ANE-11, March, 1964, pp. 45-57.

[9] Komarov, I. V., and S. M. Smolskiy, "FM Short-Range Radar – From Systems of Weapon to Precision Distance Meters," *Proc. 3rd Int. Symposium Sibconvers'99,* Tomsk, Russia, May 18-20, 1999, pp. 392-394.

[10] Smolskiy, S. M., et al., "FM Short-Range Radar – Vibrations and Pressure Meter," *3rd Int. Symposium Sibconvers'99,* Tomsk, Russia, May 18-20, 1999, pp. 395-396.

Chapter 2

Basic Theory of Short-Range FM Radar

2.1 PRINCIPLE OF OPERATION AND BASIC BLOCK DIAGRAM OF FM RADAR

The principle of operation of pulse radar is based on time separation between the transmitted and reflected signal and measurement of the time interval between transmitted and received pulses. In FM radar, because continuous radiation is used, separation of transmitted and reflected signals in time is impossible. Hence, reception of information about the range to a target is possible only when the transmission is modulated in amplitude or phase.

Amplitude modulation is not used because it is practically impossible to select the reflected signal against the interfering background of the transmission, the reflected signal from targets even a few meters from the radar being some tens of decibels less than the transmitted signal. Thus the only means to determine the reflected signal delay relative to the transmission is on the basis of the phase difference of these angular modulated signals. This operation can be easily carried out by multiplication of transmitted and reflected signals. After multiplication, two signals are formed, one with a phase equal to the difference of phases of the multiplied signals, and the other with a phase equal to the sum of these phases. The latter signal is easily filtered out, as its frequency is twice that of the radiated signal.

The basic block diagram of an FM radar is shown in Figure 2.1. The signal from the FM generator, controlled by the modulator, is radiated toward the target by the transmitting antenna. The expression for the transmission is:

$$u_p(t) = U_p(t)\cos\varphi_p(t) \tag{2.1}$$

where $U_p(t)$ is the signal amplitude and $\varphi_p(t)$ is its phase. A sample of the FM generator signal passes to the multiplier (mixer) as the heterodyne signal. This signal, which we will call the *direct* one, can be expressed as:

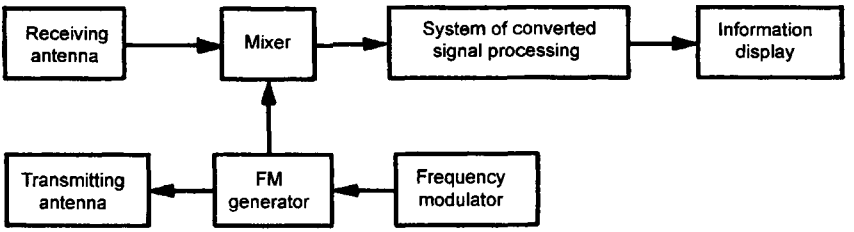

Figure 2.1 Basic block diagram of an FM radar system.

$$u_d(t) = U_d(t)\cos\varphi_d(t) \tag{2.2}$$

where $U_d(t)$ is the direct signal amplitude and $\varphi_d(t)$ is its phase. The time-dependence of amplitudes of the transmitted and direct signals is caused by the fact that the frequency modulation is practically always accompanied by parasitic amplitude modulation. Also, the amplitude of a signal from any generator always fluctuates.

The reflected signal from the receiving antenna also enters the mixer. In further analysis we will consider that the reflecting target introduces no further amplitude or phase fluctuations (i.e., it is a point target). Such a model of the reflected signal does not correspond completely to a real reflected signal, but it allows rather simple analysis of the mixer output signal as we consider processing methods and carry out necessary calculations. The theory of operation of FM radar, in view of parameters of the real reflected signal, is a subject of an extensive separate discussion. Thus, the reflected signal can be written as:

$$u_r = U_r(t,\tau)\cos\varphi_r(t,\tau) = k_1 U_r(t-\tau)\cos\left[\varphi_p(t-\tau)+\varphi_0\right] \tag{2.3}$$

where k_1 expresses the reduction in its amplitude, τ is its time delay relative to the transmission, and φ_0 is the phase shift caused by reflecting properties of the target.

As the reflected signal entering the mixer is much less than the direct signal, the mixer output signal can be written as

$$u_t(t) = k_2 U_r(t,\tau)\cos\left[\varphi_d(t)-\varphi_r(t,\tau)-\varphi_0\right] + k_3 U_d(t) \tag{2.4}$$

where the first term represents the result of conversion of the reflected signal, the second is the result of amplitude detecting the direct signal, and k_2 and k_3 are factors describing the mixer voltage gains in conversion and amplitude detection modes. We will call the mixer output signal the *converted signal*. In the literature it is frequently called an *intermediate frequency* (IF) signal (by analogy to the

intermediate frequency signal in a superheterodyne receiver), and also the *distance measuring signal.*

Only the first term in the converted signal (2.4) is useful, containing the information on target range and speed relative to the FM radar. The second term is a *parasitic signal.* This signal has no influence on the useful signal, but at the same time has a major influence on operation and technical parameters of FM radar, especially on short-range FM radar. The fact is that the intensity of this signal, as a rule, exceeds that of the useful signal by a ratio varying from a few to tens of decibels, and its spectrum overlaps that of the useful signal. The reduction of parasitic signal effects on the operation of FM radar is one of most important and difficult technical problems in design.

The converted signal from the mixer output passes to the system of processing, selection, and display of range and speed information. Thus, in further analysis of the useful signal we will consider that the transmitted, direct, and reflected signals have no amplitude modulation (i.e., $U_p(t) = U_p$, $U_d(t) = U_d$, and $U_r(t) = U_r$). Methods for decreasing of influence of parasitic amplitude modulation of the direct signal on operation of FM radar will be analyzed further in Chapters 4 and 5.

As we can see, the main feature of an FM radar is the multiplication of transmitted (direct) and reflected signals. Let us note also that this block diagram is rather close to that of the correlation receiver. This block diagram forms the basis of many block diagrams of FM radar. We now proceed to consideration of typical block diagrams of short-range FM radar.

2.2 TYPICAL BLOCK DIAGRAM OF SHORT-RANGE FM RADAR

2.2.1 System with Separate Transmitting and Receiving Antennas and Nonzero Intermediate Frequency

The block diagram of this radar, which is the most complex and ideal, is given in Figure 2.2. The main difference between this system and the basic one is that a central frequency shift is included in the direct signal path between the FM generator and mixer. In this block the central frequency is shifted to one side or the other by $\delta\omega$, and the parameters of modulation remain unchanged, as necessary for system operation. This shift is often implemented by amplitude modulation of the direct signal followed by selection of one sideband. The size of shift is determined by the transmitted spectral width, by parameters of the filter selecting the sideband, and by requirements for suppression of other parts of the signal spectrum. In a radar operating at centimeter wavelengths, the carrier frequency shift is usually between tens and several hundreds of MHz.

The basic purpose of the central frequency shift is the realization of classical heterodyne reception. As the central frequencies of direct and reflected signals are separated by $\delta\omega$, the converted signal spectrum will be grouped around that frequency. This permits the basic amplification of a received signal by an IF band-

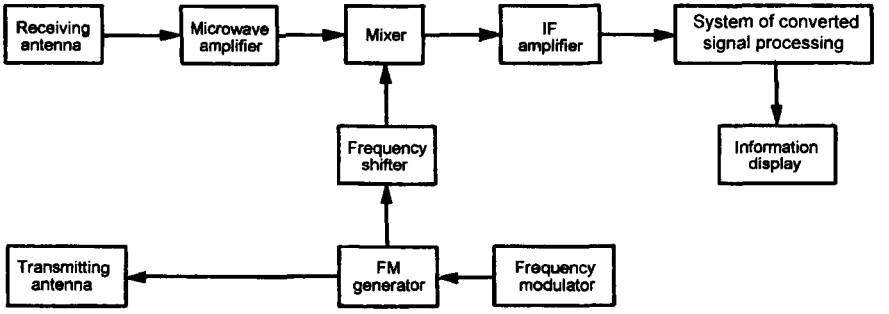

Figure 2.2 FM radar with nonzero intermediate frequency.

pass amplifier, as is done in typical superheterodyne receivers, and achieves decoupling between this signal and the parasitic amplitude modulation signal. An additional microwave amplifier can also be included between the receiving antenna and the mixer. In other respects this block diagram does not differ from the basic circuit of Figure 2.1.

This circuit is applied mainly in cases where high receiver sensitivity is necessary and there is an opportunity to ensure sufficient decoupling between receiving and transmitting antennas. With insufficient decoupling, an intense signal with frequency $\delta\omega$ will appear at the input to the IF amplifier as a result of leakage from the transmitting antenna into the receiving antenna, which can complicate amplifier operation and cause coupling between the useful signal and the parasitic amplitude modulation signal.

2.2.2 Circuit with Nonzero Intermediate Frequency and Complex Frequency Modulation

By applying certain complex types of modulation, the converted signal, whose spectrum occupies higher frequencies in comparison with modulation frequency, may be caused to have so-called dual-frequency modulation (i.e., modulation by the sum of two periodic functions). The appropriate block diagram of such radar is given in Figure 2.3. In this system there is no carrier frequency shift of the direct signal, and therefore the receiver here is called a *homodyne*. In other respects this

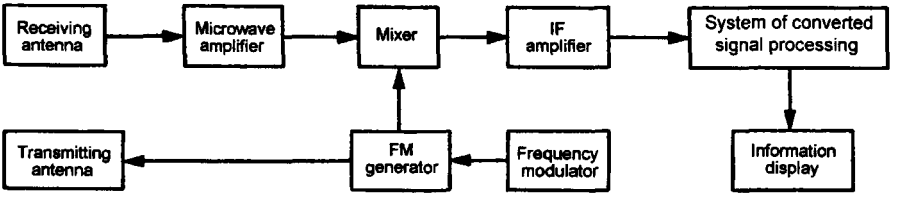

Figure 2.3 Homodyne FM radar (with nonzero intermediate frequency).

system does not differ significantly from the previous one.

This system has not found wide application, mainly due to the fact that it requires the application of complex modulation, complicating selection of the useful part of the converted signal spectrum, especially in cases where the range to the target varies very widely, and homodyne reception does not give the advantages inherent in the previous circuit. Homodyne reception is nevertheless applied in most short-range FM radars. Despite its disadvantages, homodyne reception has one very important advantage: it permits use of one antenna for both transmission and reception of a continuous signal.

2.2.3 System with a Single Transmitting-Receiving Antenna

This type of short-range FM radar is the most widely used, as it has minimum size and can be built as a single block. It differs from the previous one by the structure and circuit of the microwave block, and hence we show in Figure 2.4 not the full radar circuit but the only the diagram of that block.

As in the previous circuits, the FM generator can be modulated by one or by the sum of two or more modulating functions. The generated signal enters port 1 of the circulator. Almost all the energy of this signal (losses are typically tenths of a decibel) passes from port 2 to the transceiver antenna and is radiated toward the target. As the isolation between ports 1 and 3 is not infinite (usually no more than 20 to 30 dB), a small part of the signal power from port 1 appears at port 3, to which the mixer is connected. This leakage signal can serve two functions. On the one hand it can serve the function of a direct signal as the heterodyne signal for the mixer. On the other hand, it can simultaneously be harmful as a source of a parasitic signal at the mixer output, formed because of amplitude detection of the direct signal with parasitic amplitude modulation.

Which of these two functions applies to this signal depends on the mixer parameters (i.e., on the ratio of gain factors in conversion and detection modes, and also on the ratio of the reflected and direct signals: the more the first factor exceeds the second and the greater the ratio of signals, the greater the effect of the first function and vice versa). In most cases the leakage signal performs both functions. If the leakage signal power is insufficient for normal mixer operation, an

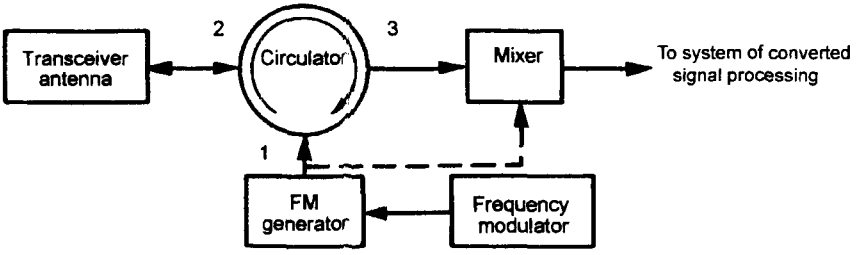

Figure 2.4 FM radar with single transmit-receive antenna.

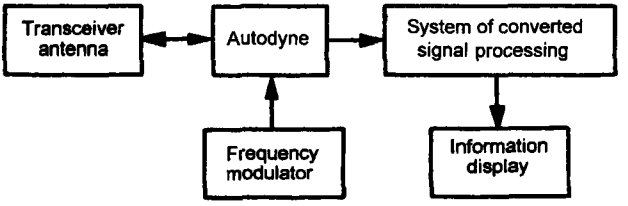

Figure 2.5 Autodyne FM radar with single transmit-receive antenna.

additional path can be provided connecting the direct signal to the mixer (shown by a dashed line in Figure 2.4).

The signal reflected enters port 2 of the circulator, passes to port 3 and on to the mixer. The converted signal from the mixer output passes to the processing and information selection system. As we can see, the microwave block is rather simple: for millimeter band operation its volume does not exceed several cubic centimeters. The basic disadvantage of this circuit is the difficulty of neutralization of the harmful effect of the parasitic amplitude modulation signal on the processing circuit, resulting from amplitude detection of the leakage signal. However, this does not prevent wide application of this circuit to short-range FM radar.

2.2.4 Autodyne System with a Single Antenna

The block diagram of this FM radar is given in Figure 2.5. The main difference between this system and the previous ones is the use of an *autodyne*. The autodyne is an oscillator that simultaneously carries out functions of generating the transmission and mixing the transmitted and reflected signals. There is no separate path for the direct signal in the autodyne, as the radiated and reflected signals exist at the same point of the autodyne circuit. It is obvious that the autodyne can operate only with one combined (transmitting-receiving) antenna. The main advantage of this circuit is the simplicity of its microwave part, compactness, and relative cheapness. Therefore this circuit is applied when these qualities are determining, for example, in widely applied small-sized onboard FM radars.

A specific feature of the autodyne is the fact that quasi-linear conversion is possible only up to a certain reflected signal level at which it has no appreciable influence on the mode of autodyne operations. However, operation with rather intense reflected signals at small target ranges is possible in short-range FM radar. The detailed theory of autodyne operation is given in the second part of this book.

2.3 GENERAL EXPRESSIONS FOR TRANSMITTED, REFLECTED, AND CONVERTED SIGNALS

For frequency modulation of the transmission, the expression for its frequency is

$$\omega_p(t) = \omega_c + \Delta\omega\gamma(t) \tag{2.5}$$

where ω_c is the central frequency; $\Delta\omega$ is the frequency deviation; and $\gamma(t)$ is the frequency modulating function. The phase of the transmitted signal is

$$\varphi_p(t) = \int_0^t \omega_p(t)dt = \omega_c t + \Delta\omega\int_0^t \gamma(t)dt = \omega_c t + \Delta\omega F_p(t) \tag{2.6}$$

Here, the initial phase is set equal to zero, and for simplification of formulas the integral in (2.6) is designated as:

$$F_p(t) = \int_0^t \gamma(t)dt \tag{2.7}$$

The function $F_p(t)$ by analogy with $\gamma(t)$ is the phase modulating function of the signal. If there is no the shift in the central frequency of the direct signal, its phase will be the same as that of the transmitted signal: $\varphi_d(t) = \varphi_p(t)$.

With shift of the central frequency, the phase of the direct signal will be

$$\varphi_d(t) = (\omega_c \pm \delta\omega)t + \Delta\omega F_p(t) \tag{2.8}$$

The additional phase shift in the direct signal path can also be considered zero, as it has no influence on radar operation.

With the provision that we consider the target as a point target, the phase of the reflected signal is

$$\varphi_r(t,\tau) = \omega_c(t-\tau) + \Delta\omega F_r(t,\tau) + \varphi_0 \tag{2.9}$$

where $F_r(t,\tau) = \int_\tau^t \gamma(t-\tau)dt = \int_0^{t-\tau} \gamma(t)dt$ is the phase modulating function of the reflected signal. The lower limit in the integral in this formula is equal to τ because the reflected signal has that time delay.

Substituting (2.6), (2.8), and (2.9) into (2.4), we obtain the expression for phase of the converted signal for the cases without and with central frequency shift, respectively:

$$\varphi_t(t,\tau) = \omega_c\tau + \Delta\omega\left[F_p(t) - F_r(t,\tau)\right] - \varphi_0 \tag{2.10}$$

$$\varphi_t(t,\tau) = \delta\omega t + \omega_c\tau + \Delta\omega\left[F_p(t) - F_r(t,\tau)\right] - \varphi_0 \tag{2.11}$$

The difference of the modulating functions in square brackets in these formulas is the phase modulating function of the converted signal and can be expressed as:

$$F_t(t,\tau) = \int_0^t \gamma(t)dt - \int_0^{t-\tau} \gamma(t)dt = \int_{t-\tau}^t \gamma(t)dt \tag{2.12}$$

For further analysis of the properties of the converted signal, let us assume that the delay of the reflected signal in time varies linearly:

$$\tau(t) = \tau_0 + \frac{2V_r}{C}t \tag{2.13}$$

where τ_0 is the initial value of delay; V_r is the relative radial speed between the radar and the target; and C is the speed of propagation of electromagnetic energy. In this case

$$\omega_c\tau(t) = \omega_c\tau_0 + \frac{2V_r}{C}\omega_c t = \varphi_\tau + \Omega_D t \tag{2.14}$$

where φ_τ is the initial phase shift and Ω_D is the Doppler frequency. Thus, the assumption is that the Doppler frequency caused by target motion is constant as is necessary to carry out the analysis of the converted signal spectrum. Such an assumption is reasonable for the following reason. The maximal time necessary for processing of the converted signal for most short-range FM radars does not exceed several tens of milliseconds. During this interval the motion of most targets is so insignificant that we may consider the relative radial speed constant. For example, at 100 km/h the target will move by only 30 cm in 10 ms.

Substituting (2.14) in (2.10) and (2.11), we obtain

$$\varphi_t(t,\tau) = \pm\Omega_D t + \Delta\omega F_t(t,\tau) + \varphi_\tau - \varphi_0 \tag{2.15}$$

$$\varphi_t(t,\tau) = (\delta\omega \pm \Omega_D)t + \Delta\omega F_t(t,\tau) + \varphi_\tau - \varphi_0 \tag{2.16}$$

Differentiating (2.15) and (2.16) with respect to time, we obtain expressions for the instantaneous frequency of the converted signal:

$$\Omega(t,\tau) = \left|\pm\Omega_D + \Delta\omega\frac{dF_t(t,\tau)}{dt}\right| \tag{2.17}$$

$$\Omega(t,\tau) = (\delta\omega \pm \Omega_D) + \Delta\omega\frac{dF_t(t,\tau)}{dt} \tag{2.18}$$

In (2.17) the absolute value is necessary because the converted signal frequency at different moments of time can have "negative" sense. The sign of Doppler frequency in (2.17) and (2.18) has symbolical meaning and serves as a reminder that the Doppler frequency shifts the spectrum toward higher frequencies for approaching targets, and toward lower frequencies for receding targets.

2.4 GENERAL RELATIONSHIPS FOR THE CONVERTED SIGNAL WITH MODULATION BY A PERIODIC FUNCTION

For periodic transmitter modulation we will define the frequency modulating function $\gamma(t)$ as a function with period T_m, having zero average value, varying from -0.5 to $+0.5$ and having a definite type of symmetry.

The normalization of limits of function $\gamma(t)$ is necessary because with different types of modulation the limits of frequency change are determined only by the frequency deviation $\Delta\omega$. It is otherwise impossible to compare parameters of the converted signal with various types of modulation. With periodic modulation, the modulating function of the converted signal phase, as follows from (2.12), is also periodic and hence the converted signal is a frequency-modulated signal.

For further analysis it is useful to consider the following. As the phase modulating function of the reflected signal is moved in time τ relative to the modulating function of the transmission, the modulating function of phase of the converted signal equal to their difference is asymmetric, because of a shift of $\tau/2$. In this connection, it is expedient for operations with this function to make a replacement of the variable, setting $t' = t - \tau/2$.

In short-range FM radar the relationship $T_m >> \tau$ is usually applicable. Actually, for an example at target ranges up to 150m and with a modulation frequency of 10 kHz, the ratio $T_m/\tau = 100$, and at smaller range this ratio will be even greater. In this case, using the known theorem for the average value of the integral, it is expedient to calculate the simple expression for the phase modulating function of the converted signal:

$$F_t(t,\tau) = \int_{t-\tau}^{t} \gamma(t)dt \approx \tau\gamma\left(t - \frac{\tau}{2}\right) = \tau\gamma(t') \tag{2.19}$$

Note that (2.19) is applicable only in the event that the function $\gamma(t)$ has no discontinuities in the interval from $t - \tau$ to t, as is true for most modulating functions.

Equation (2.19) is very convenient in calculation, as it avoids integration of the function $\gamma(t)$, and equally importantly, it allows us to see directly the relationship of the phase modulating function of the converted signal to the function $\gamma(t)$ (the type of modulation of the transmitter):

$$\varphi_t(t,\tau) = \pm\Omega_D t + \Delta\omega\tau\gamma(t') + \varphi_\tau - \varphi_0 \tag{2.20}$$

$$\varphi_t(t,\tau) = (\delta\omega \pm \Omega_D)t + \Delta\omega\tau\gamma(t') + \varphi_\tau - \varphi_0 \tag{2.21}$$

Using (2.17), (2.18), and (2.19) we also have simple expressions for the instantaneous frequency of the converted signal:

$$\Omega_t(t,\tau) = \left|\pm\Omega_D + \Delta\omega\tau\frac{d\gamma(t')}{dt}\right| \tag{2.22}$$

$$\Omega_t(t,\tau) = (\delta\omega \pm \Omega_D) + \Delta\omega\tau\frac{d\gamma(t')}{dt} \tag{2.23}$$

One of the major characteristics of the converted signal is its spectrum. It is obvious that the converted signal spectrum in the case of direct signal central frequency shift differs significantly from that without such a shift. In the first case the converted signal spectrum is concentrated in the band $\delta\omega$. The parameters of modulation of the transmission are selected in such a manner that the converted signal spectral width is much less than $\delta\omega$. Hence the converted signal spectrum in this case does not differ from that of an FM signal whose frequency is defined by (2.18) or (2.23). The procedure for calculation of the FM signal spectrum is described in detail in any textbook on the fundamentals of radio engineering, and it is therefore unnecessary to carry it out within the framework of this book.

In the second case the converted signal spectrum appears in the band of frequency of modulation, or equivalently in the region of "zero intermediate frequency." Often in the first case the converted signal is exposed to a second conversion with heterodyne frequency $\delta\omega$ and is moved into the region of "zero intermediate frequency." Thus, the calculation of a spectrum only for the second case represents the greater interest.

For calculation of its spectrum, we will write the converted signal from (2.10), (2.12), and (2.14) as:

$$\begin{aligned} u_t &= U_t \cos\left[\pm\Omega_D t + \Delta\omega F_t(t,\tau) + \varphi_\tau - \varphi_0\right] \\ &= U_t \left\{\begin{array}{l} \cos\left[\pm\Omega_D t + \varphi_\tau - \varphi_0\right]\cos\Delta\omega F_t(t,\tau) \\ \quad -\sin\left[\pm\Omega_D t + \varphi_\tau - \varphi_0\right]\sin\Delta\omega F_t(t,\tau) \end{array}\right\} \end{aligned} \tag{2.24}$$

The functions $\cos\Delta\omega F_t(t,\tau)$ and $\sin\Delta\omega F_t(t,\tau)$ are periodic by virtue of periodicity of the function $F_t(t,\tau)$ and can be presented as Fourier series. However, this only applies with one assumption: we consider τ constant in expansion of the specified functions. Otherwise these functions are not periodic and their expansion in a Fourier series is impossible. This assumption is justified by the fact that the delay time practically does not vary during the period of modulation. Actually, the period of modulation in most cases does not exceed milliseconds, but even at 100 km/h the range will change by only ~3 cm in 1 ms. The change of $\Delta\omega\tau$ will also be insig-

nificant. So for example, at ~10m range, the relative change will be ~0.3%. Besides, at a range of 10m targets do not move with relative speed of 100 km/h. Thus, the assumption is not only necessary but justified.

At the same time we note that if in (2.13) we accept the delay time as constant, then the Doppler effect is not taken into account in the analysis of the converted signal, which is obviously completely inadmissible. So, setting $t - \tau/2 = t'$, we obtain

$$\cos \Delta\omega F_t(t',\tau) = \frac{a_0(\tau)}{2} + \sum_{n=1}^{\infty} K_n(\tau) \sin\left[n\Omega_m t' + \psi_n(\tau)\right] \tag{2.25}$$

where

$$K_n(\tau) = \sqrt{a_n^2(\tau) + b_n^2(\tau)}$$

$$\psi_n(\tau) = \arctan \frac{a_n(\tau)}{b_n(\tau)}$$

$$a_n(\tau) = \frac{2}{T_m} \int_0^{T_m} \cos \Delta\omega F_t(t',\tau) \cos\left(n \frac{2\pi}{T_m} t'\right) dt'$$

$$b_n(\tau) = \frac{2}{T_m} \int_0^{T_m} \cos \Delta\omega F_t(t',\tau) \sin\left(n \frac{2\pi}{T_m} t'\right) dt'$$

and

$$\sin \Delta\omega F_t(t',\tau) = \frac{c_0(\tau)}{2} + \sum_{n=1}^{\infty} L_n(\tau) \sin\left[n\Omega_m t' + \chi_n(\tau)\right] \tag{2.26}$$

where

$$L_n(\tau) = \sqrt{c_n^2(\tau) + d_n^2(\tau)}$$

$$\chi_n(\tau) = \arctan \frac{c_n(\tau)}{d_n(\tau)}$$

$$c_n(\tau) = \frac{2}{T_m} \int_0^{T_m} \sin \Delta\omega F_t(t',\tau) \cos n \frac{2\pi}{T_m} t' dt'$$

$$d_n(\tau) = \frac{2}{T_m} \int_0^{T_m} \sin \Delta\omega F_t(t',\tau) \sin n \frac{2\pi}{T_m} t' dt'.$$

Substituting (2.25) and (2.26) into (2.24) and using the variable t, we obtain:

$$u_t = U_t \left\{ \begin{array}{l} e_0(\tau) \sin\left[\Omega_D t + \varphi_\tau - \varphi_0 + \zeta(\tau)\right] \\ \quad + \sum_{n=1}^{\infty} A_n(\tau) \sin\left[(\Omega_m - \Omega_D)t - \varphi_\tau + \varphi_0 - n\Omega_m \frac{\tau}{2} + \eta(\tau)\right] \\ \quad + \sum_{n=1}^{\infty} B_n(\tau) \sin\left[(\Omega_m + \Omega_D)t + \varphi_\tau - \varphi_0 - n\Omega_m \frac{\tau}{2} + \nu(\tau)\right] \end{array} \right\} \tag{2.27}$$

where: $U_t e_0(\tau) = 0.5\sqrt{a_0^2(\tau) + c_0^2(\tau)}$ is the amplitude of the spectral component with the Doppler frequency;

$\zeta(\tau) = \arctan\dfrac{a_0^2(\tau)}{c_0^2(\tau)}$ is the additional phase shift of the component with the Doppler frequency;

$U_t A_n(\tau) = 0.5\sqrt{K_n^2(\tau) + L_n^2(\tau) - 2K_n(\tau)L_n(\tau)\sin\left[\psi_n(\tau) - \chi_n(\tau)\right]}$ is the amplitude of a spectral component with frequency $n\Omega_m - \Omega_D$;

$U_t B_n(\tau) = 0.5\sqrt{K_n^2(\tau) + L_n^2(\tau) + 2K_n(\tau)L_n(\tau)\sin\left[\psi_n(\tau) - \chi_n(\tau)\right]}$ is the amplitude of a spectral component with frequency $n\Omega_m + \Omega_D$;

$\eta_n(\tau) = \arctan\dfrac{K_n(\tau)\sin\psi_n(\tau) - L_n(\tau)\cos\chi_n(\tau)}{K_n(\tau)\cos\psi_n(\tau) + L_n(\tau)\sin\chi_n(\tau)}$ is the additional phase shift of the spectral component with the frequency $n\Omega_m - \Omega$;

$\nu_n(\tau) = \arctan\dfrac{K_n(\tau)\sin\psi_n(\tau) + L_n(\tau)\cos\chi_n(\tau)}{K_n(\tau)\cos\psi_n(\tau) - L_n(\tau)\sin\chi_n(\tau)}$ is the additional phase shift of the spectral component with the frequency $n\Omega_m + \Omega$.

From (2.27) it follows that the converted signal spectrum includes a component with the Doppler frequency determined by the first term, and an infinite number of components with frequencies $n\Omega_m + \Omega$, and that the components with frequencies $n\Omega_m$ are absent. This implies that the converted signal belongs to a class of so-called almost periodic fluctuations.

The amplitudes and phases of each pair of components with frequencies $n\Omega_m + \Omega$ and $n\Omega_m - \Omega$ are related and depend on the range to the target, the type of modulation, and the frequency deviation of the transmission. If the range between the radar and the target is constant (i.e., Doppler effect is absent), each pair of spectral components merges into one with frequency $n\Omega_m$.

2.5 GENERAL RELATIONS FOR A CONVERTED SIGNAL WITH DUAL-FREQUENCY MODULATION

Modulation by the sum of two periodic functions is called *dual-frequency modulation.* The need to analyze the converted signal with this modulation is explained by several factors. First, such types of modulation are applied in SRR. The second modulation is intended to provide the necessary SRR parameters and performance (improvement of range resolution, generating a signal of "intermediate frequency"), for security of operation of automatic systems in the converted signal processing device, and so forth. Second, in some cases of modulation by a composite function it is convenient in the analysis of a converted signal to represent

the frequency modulating function of the transmission as the sum of two other functions that are more convenient for integration in evaluation of the Fourier series coefficients. In some cases such an approach may be the only feasible method for performing the necessary calculations.

Third, it is convenient in analyzing the effect of a nonlinear FM generator modulation characteristic to express this characteristic as the sum of linear and nonlinear parts. Thus an incidental dual-modulation appears even when single modulation is intended. With dual-modulation the frequency of the transmission can be expressed as

$$\omega_p(t) = \omega_c + \Delta\omega_1\gamma_1(t) + \Delta\omega_2\gamma_2(t) \tag{2.28}$$

where $\gamma_1(t)$ and $\gamma_2(t)$ are frequency modulating functions with periods T_{m1} and T_{m2} and varying within limits from −0 5 to 0.5. By analogy with previous calculations, the phase of the converted signal is

$$\varphi_t(t,\tau) = \pm\Omega_D t + \Delta\omega_1 F_{t1}(t,\tau) + \Delta\omega_2 F_{t2}(t,\tau) + \varphi_\tau - \varphi_0 \tag{2.29}$$

Further analysis can be carried out in two ways. The converted signal can be expressed as in (2.24), and the phase shift due to the second modulation is included as an addition to angles $\pm\Omega_D t + \varphi_\tau - \varphi_0$, for which we write (2.24) as:

$$\begin{aligned} u_t &= U_t \cos\left[\pm\Omega_D t + \Delta\omega_1 F_{t1}(t,\tau) + \Delta\omega_2 F_{t2}(t,\tau) + \varphi_\tau - \varphi_0\right] \\ &= U_t \left\{ \begin{array}{l} \cos\left[\pm\Omega_D t + \varphi_\tau - \varphi_0 + \Delta\omega_2 F_{t2}(t,\tau)\right]\cos\Delta\omega_1 F_{t1}(t,\tau) \\ -\sin\left[\pm\Omega_D t + \varphi_\tau - \varphi_0 + \Delta\omega_2 F_{t2}(t,\tau)\right]\sin\Delta\omega_1 F_{t1}(t,\tau) \end{array} \right\} \end{aligned} \tag{2.30}$$

and perform further calculations using (2.25) - (2.27). After that we view each spectral component of the converted signal with frequency $n\Omega_{m1} \pm \Omega_D$ as a phase-modulated oscillation whose phase varies according to $\Delta\omega_2 F_{t2}(t,\tau)$. Such an approach is expedient for applying the rule that there appear near each component of the converted signal spectrum one or two sidebands, for small phase modulation index of the second modulation, and if the periods of modulating functions $\gamma_1(t)$ and $\gamma_2(t)$ differ significantly the sideband spectra do not overlap.

A spectral analysis similar to that carried out for a single modulation (2.24) - (2.27) allows us to define the general regular dependence of the converted signal spectrum on phase (2.29).

Using known formulas of trigonometry, it is possible to express the converted signal as

$$u_t = U_t \left[\begin{array}{l} \cos x(\cos y\cos z - \sin y\sin z) \\ \quad -\sin x(\sin y\cos z + \cos y\sin z) \end{array} \right] \tag{2.31}$$

where $x = \pm\Omega_D t + \varphi_\tau - \varphi_0$, $y = \Delta\omega_1 F_{t1}(t,\tau)$, and $z = \Delta\omega_2 F_{t2}(t,\tau)$. Further functions $\sin y$, $\sin z$, $\cos y$, and $\cos z$ are represented as Fourier series similarly to (2.25) and (2.26). From comparison of (2.25), (2.26), and (2.31) it follows that the converted signal spectrum for dual-modulation consists of components with frequencies $\pm n\Omega_{m1} \pm k\Omega_{m2} \pm\Omega_D$, where $n = 0,1,2,3...$, $k = 0,1,2,3...$, whose amplitudes are determined by products of the form

$$a_{01}a_{02}, c_{01}c_{02}, a_{01}c_{01}, a_{01}c_{02}, a_{02}c_{01}, a_{02}c_{02},$$

$$a_{01}L_{k2}, a_{02}L_{n1}, c_{01}K_{k2}, c_{02}K_{n1}, K_{n1}K_{k2}, L_{n1}L_{k2}, K_{n1}L_{k2}, L_{n1}K_{k2}$$

in which the coefficients a, c, K, and L are determined from (2.25) and (2.26) for the first and second modulations. From this analysis at least two important deductions follow:

1. With dual-modulation the spectrum of the converted signal becomes considerably complicated, and hence filtration of this signal becomes complicated. Therefore dual-modulation, if applied, is auxiliary and its parameters are picked so that a Fourier series of functions $\sin z$ and $\cos z$ can be restricted to a small number of terms.

2. The dependence of the amplitude of any spectral component upon the product of the relevant coefficients of a Fourier series creates additional opportunities for forming the necessary converted signal spectrum.

2.6 GENERAL RELATIONS FOR A CONVERTED SIGNAL WITH MODULATION BY A MODULATED PERIODIC FUNCTION

In practice, for an SRR there are cases of intended double modulation, when the amplitude or angular modulation of the modulating function itself $\gamma(t)$ is applied. Such modulation is applied, for example, for security of operation of automatic radar systems or for obtaining the necessary performance of the converted signal. With amplitude modulation by the function $\gamma(t)$, the frequency modulating function of the transmission is:

$$\eta(t) = [1 + m\delta(t)]\gamma(t) \tag{2.32}$$

where $\delta(t)$ is the function defining the type of amplitude modulation, and m is the amplitude modulation index. The frequency of the transmission is

$$\omega_p(t) = \omega_c + \Delta\omega[1 + m\delta(t)]\gamma(t) \tag{2.33}$$

In the overwhelming majority of cases the period of function $\delta(t)$ differs considerably from the period of function $\gamma(t)$, and more often the period of the first is much greater than that of the second.

The analysis of the converted signal in this case is easily carried out, considering the function $\gamma(t)$ as unmodulated, and frequency deviation as modulated by $\Delta\omega[1 + m\delta(t)]$. Thus, calculation of the converted signal parameters is initially carried out using the procedure described in Section 2.4, on the assumption that the frequency deviation is fixed. After that the dependence of the relevant converted signal parameters (phase, instantaneous frequency, spectrum) upon the varying deviation is determined.

This approach can be applied also for the case in which the repetition periods of functions $\delta(t)$ and $\gamma(t)$ are commensurable, but in this case the calculations became significantly complicated because of spectrum overlapping of sidebands appearing near each component of the converted signal spectrum.

If the repetition period of function $\gamma(t)$ is modulated, that will occur much more slowly than the period of the function. Therefore here again it is possible to carry out all calculations assuming a constant period, and then inserting the relevant corrective amendments to the converted signal parameters, related to the period of the modulating function $\gamma(t)$ (for example, the value of instantaneous frequency or frequencies of spectral components of the converted signal).

2.7 BLOCK DIAGRAMS OF ULTRASONIC SRR AND FEATURES OF THE CONVERTED SIGNAL

As specified in Chapter 1, implementation of SRR is possible not only in radio frequency bands, but also at ultrasonic frequencies. In this case the transmitted signal is ultrasonic waves representing mechanical oscillations of the gas or fluid surrounding the SRR. These waves are generated by ultrasonic transducers that excite mechanical oscillations in the gas or fluid in response to an electrical signal. The principle of operation of these transducers is based on the piezoelectric effect or on magnetostriction. Thus, the ultrasonic transducer is the antenna of the ultrasonic SRR. As in the radio antenna, the ultrasonic transducer cannot only radiate ultrasonic waves, but also convert ultrasonic waves to an electrical signal, and as with the radio antenna, the ultrasonic transducer is characterized by a radiation pattern, gain factor, and sidelobe levels.

The range of operating frequencies of transducers lies between ~20 and 100 kHz for operation in a gas medium, and ~50 to 300 kHz for a fluid. The width of the radiation pattern varies from a few degrees up to two or three tens of degrees and depends on the geometrical size of the transducer and its construction. The power of the transmission is such as to provide an operating range up to several tens of meters in a gas medium and hundreds of meters in a fluid.

Ultrasonic waves are propagated much more slowly than radio waves. The velocity of sound in air is ~330 m/s, and in water ~1,500 m/s. Also, the velocity of

sound propagation depends on the temperature of the medium (for example propagation in air varies by ~0.5 m/s°C), the water vapor or dust content of the gas medium, the concentration of the weighed particles in a fluid, and so forth.

As we can see, the velocity of ultrasonic waves in air is approximately 10^6 times less than the velocity of propagation of an electromagnetic field. Thus, the wavelength of an ultrasonic wave in air at a frequency ~50 kHz is equal to the wavelength of radio-waves at a frequency ~50 GHz (~6 mm). The same ratio applies to the frequency deviation: a frequency deviation of ~1 kHz in an ultrasonic wave in air corresponds to a deviation of 1 GHz in a radio frequency, as the products $\Delta\omega\tau$ in both cases will be identical.

The reduced values and the parameters of ultrasonic transducers allow us to draw the conclusion that the ultrasonic SRR follows the same principles as for radio waves. Actually, ultrasonic SRRs are usually designed with the same block diagrams as radio-wave systems (Figures 2.2 to 2.5). Ultrasonic transducers are used instead of "antennas." Precisely the same variants with two and with one "antenna" - the ultrasonic transducer - are also possible. Certainly, in the scheme of Figure 2.4 there is no circulator, and the FM transmitter signal is passed to the same point: the ultrasonic transducer and mixer.

Principles and expedients of converted signal processing in an ultrasonic SRR are almost the same as for the radio frequency one. Some differences are caused by large values of delay time of the reflected signal, because of which it is difficult to ensure the validity of the relation $T_m >> \tau$ in some cases. For example, at a target range of 16m, the delay time of a reflected ultrasonic signal propagating in air is ~0.1s. Thus, even with frequency modulation at 10 Hz, $T_m \approx \tau$, and it is obvious that with target delay time equal to the modulation period there is an ambiguity in determination of range, as this situation is equivalent to absence of a delay (i.e., to zero target range).

With increase in the period of modulation it can appear that the frequency of modulation is commensurate with or even less than the Doppler frequency. Note that the Doppler frequencies for radio frequency and ultrasonic SRR are approximately identical, as the radiated wavelengths are approximately identical. With comparable frequency modulation and Doppler frequency there are difficulties in filtration and processing of the converted signal. Hence, with a change of Doppler frequency such converted signal parameters as its phase, instantaneous frequency, and spectral pattern vary considerably. For this reason ultrasonic SRR with continuous radiation can be most expediently applied to measuring of very small ranges (less than several meters), with small target velocities, especially when a simple, reliable, and mainly cheap measuring device is required.

Chapter 3

Characteristics of the Converted Signal with Different Transmitter Modulations

3.1 SINUSOIDAL MODULATION

Modulation by a sinusoidal function is often applied in SRR. It is explained by several considerations. First, it is relatively simple to produce such modulating voltage or current. The narrow bandwidth of the modulating process reduces requirements on the frequency response of the modulator. The frequency spectrum of the converted signal makes it suitable for processing and deriving of range data. Thus, the area of application of this modulation: simple and compact SRR, such as low-range altimeters, level measuring radar, and sensors of mobile targets in security systems.

3.1.1 Modulation by a Single Sinusoid

In this case the modulating function of transmitter frequency is defined as

$$\gamma(t) = \frac{\cos \Omega_m t}{2} \tag{3.1}$$

Note that the modulating function could be defined by a sine without changing the result.

According to (2.12), phase modulating function of the converted signal is

$$F_t(t,\tau) = \int_{t-\tau}^{t} \frac{\cos \Omega_m t}{2}\, dt = \left(\frac{\sin(\pi\tau / T_m)}{\pi\tau / T_m}\right)\frac{\tau}{2}\cos\Omega_m\left(t - \frac{\tau}{2}\right) \tag{3.2}$$

In most cases the term in brackets before the cosine differs little from unity because $T_m >> \tau$. However, in some cases this relationship is violated and it is impossible to neglect this term.

According to (2.17) and (2.18), we obtain expressions for instantaneous frequency of the converted signal accordingly for the case with no direct signal central frequency shift and with a shift:

$$\Omega_t(t,\tau) = \left| \pm\Omega_D - \left(\frac{\sin(\pi\tau / T_m)}{\pi\tau / T_m} \right) \frac{\Delta\omega\tau}{2} \Omega_m \sin\Omega_m \left(t - \frac{\tau}{2} \right) \right| \tag{3.3}$$

$$\Omega_t(t,\tau) = \delta\omega \pm \Omega_D - \left(\frac{\sin(\pi\tau / T_m)}{\pi\tau / T_m} \right) \frac{\Delta\omega\tau}{2} \Omega_m \sin\Omega_m \left(t - \frac{\tau}{2} \right) \tag{3.4}$$

It follows from (3.4) that with direct signal central frequency shift, the converted signal has sinusoidal frequency-modulation with a frequency deviation given by

$$\Delta\Omega_t(\tau) = \left(\frac{\sin(\pi\tau / T_m)}{\pi\tau / T_m} \right) \frac{\Delta\omega\tau}{2} \Omega_m \tag{3.5}$$

In this case deviation is understood as maximal shift of instantaneous frequency from a center frequency of the converted signal (note that the frequency deviation of the transmitted signal was defined as a frequency shift from its minimum to its maximum). From (3.5) it also follows that the maximum value of frequency deviation of the converted signal is $\Delta\omega$ at $\tau = T_m/2$.

For $T_m >> \tau$ the dependence of frequency deviation of the converted signal on echo signal delay is linear and, importantly, is continuous. This permits convenient use of this dependence for range measurement. From (3.4) it also follows that the center frequency of the converted signal is shifted in to one side or the other by the Doppler frequency. To which side the frequency is shifted depends on whether the target is receding from or approaching the SRR, and on whether the direct signal central frequency is below or above that of the transmitted central frequency.

Let us suppose that the target is approaching, producing a center frequency of the reflected signal $\omega_{cr} = \omega_c + \Omega_D$. If the direct signal central frequency is $\omega_{cd} = \omega_c - \delta\omega$, the center frequency of a converted signal is $\omega_{ct} + \Omega_D - (\omega_c - \delta\omega) = \delta\omega + \Omega_D$. If the direct signal central frequency is $\omega_{cd} = \omega_c + \delta\omega$, the center frequency of the converted signal is $\omega_{ct} + \delta\omega - (\omega_c + \Omega_D) = \delta\omega - \Omega_D$. For a receding target the situation will correspondingly be the opposite: the center frequency of converted signal for an approaching target will be shifted downwards by the Doppler frequency, and for a receding target will be shifted upwards. Thus, by the shift of center frequency of the converted signal it is possible to determine not only the relative (radial) speed of the target, but also whether it approaches or recedes.

Completely different time dependence of instantaneous frequency of the converted signal takes place in the absence of direct signal central frequency shift. In this case the converted signal is also frequency-modulated. Formally the "central" frequency of the converted signal is the Doppler frequency, and for fixed targets it is "zero" frequency. The frequency deviation is also determined by (3.5). Therefore, dependence of instantaneous frequency in this case is largely determined by the magnitude of Doppler frequency. If $\Omega_D > \Delta\Omega_t(\tau)$, the converted signal represents an FM signal with center frequency Ω_D and sinusoidal modulation. On the other hand, if $\Omega_D < \Delta\Omega_t(\tau)$, separate segments of instantaneous frequency values fall in area of "negative frequencies." However, as "negative" frequencies do not exist, the "negative" values of instantaneous frequency are folded to the area of positive frequencies, and a plot of instantaneous frequency from (3.3) has an inflection on the time axis [Figure 3.1(b), (c)].

For approaching targets, when the center frequency of reflected signal is increased, the plot of instantaneous frequency is shifted upwards by the Doppler frequency [Figure 3.1(b)], and for receding targets is shifted downwards by the same value of "negative" Doppler frequency [Figure 3.1(c)]. But, as we can see, one curve differs from other only in that it is shifted in time by a half-period of the modulating function. Therefore, it is impossible in this case to determine the "sign" of Doppler frequency from parameters of the converted signal, and from it

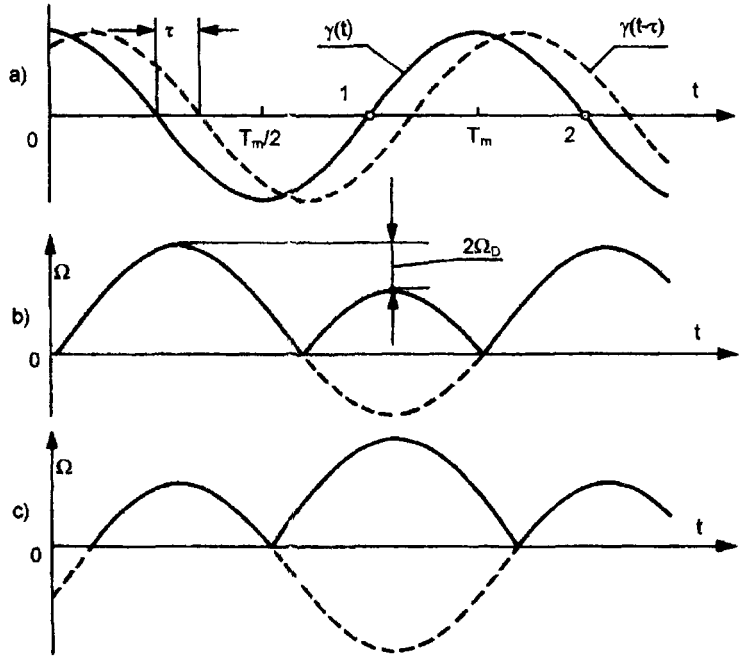

Figure 3.1 Modulating function and instantaneous frequency of the converted signal.

to determine whether the target is approaching or receding. That can be done only by comparing values of maximal instantaneous frequency to values of the derivative of the modulating function at its zero points [Figure 3.1(a)]. If the derivative is positive, we are at point 1, and if it is below zero, at point 2. Comparing values of instantaneous frequency at these time moments it is possible to determine whether the target is approaching or receding.

The spectrum of the converted signal in the case of direct signal central frequency shift, as noted in Section 2.4, differs not at all from the spectrum of a "usual" FM RF signal with sinusoidal modulation. The same spectrum will appear if $\Omega_D > \Delta\Omega_t(\tau)$. The difference is only that in the first case the center frequency of the converted signal is $\delta\omega \pm \Omega_D$, and in the second it is Ω_D. Therefore we shall calculate a spectrum only for a case of no direct signal central frequency shift, and supposing $\Omega_D < \Delta\Omega_t(\tau)$. For this derivation we use (3.2) and (2.24).

In this case it is not necessary to use (2.25) and (2.26), as it is easier to apply the well-known series from the theory of Bessel functions:

$$\cos(X\cos\theta) = J_0(X) + 2\sum_{n=1}^{\infty}(-1)^n J_{2n}(X)\cos 2n\theta \tag{3.6}$$

$$\sin(X\cos\theta) = 2\sum_{n=0}^{\infty}(-1)^n J_{2n+1}(X)\cos(2n+1)\theta \tag{3.7}$$

where $J_k(x)$ is a cylindrical Bessel function of the first type and order k.

Assuming $X = \left(\dfrac{\sin(\pi\tau/T_m)}{\pi\tau/T_m}\right)\dfrac{\Delta\omega\tau}{2}$, and $\theta = \Omega_m(t-\tau/2)$, and using (2.24), (3.6), and (3.7) we obtain, for the spectrum of the converted signal:

$$u_t = U_t\left\{\begin{aligned}
&J_0(X)\cos(\Omega_D t + \varphi_\tau - \varphi_0)\\
&\quad + \sum_{n=1}^{\infty}(-1)^n J_{2n}(X)\cos\left[(2n\Omega_m + \Omega_D)t + \varphi_\tau - \varphi_0 - n\Omega_m\tau\right]\\
&\quad + \sum_{n=1}^{\infty}(-1)^n J_{2n}(X)\cos\left[(2n\Omega_m - \Omega_D)t - \varphi_\tau + \varphi_0 - n\Omega_m\tau\right]\\
&\quad - \sum_{n=0}^{\infty}(-1)^n J_{2n+1}(X)\cos\left[\left[(2n+1)\Omega_m + \Omega_D\right]t + \varphi_\tau - \varphi_0 - (2n+1)\Omega_m\tau/2\right]\\
&\quad - \sum_{n=0}^{\infty}(-1)^n J_{2n+1}(X)\cos\left[\left[(2n+1)\Omega_m - \Omega_D\right]t - \varphi_\tau + \varphi_0 - (2n+1)\Omega_m\tau/2\right]
\end{aligned}\right\} \tag{3.8}$$

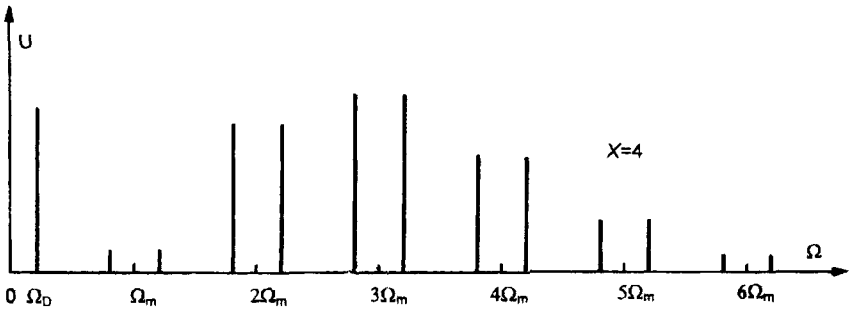

Figure 3.2 Spectrum of the converted signal.

It follows from (3.8) that the spectrum consists of components with frequencies $k\Omega_m \pm \Omega_D$, and the amplitudes of each pair of components are identical. A portion of the spectrum applicable to value $X = 4$ is shown in Figure 3.2.

In comparing this spectrum to the known spectrum of an FM signal at a center frequency $\delta\omega \pm \Omega_D$, it is easy to note that the former is obtained from the latter by a shift to zero frequency. Thus, the components of the spectrum that have appeared at "negative" frequencies are displaced to positive frequencies by "folding" of the spectrum about a vertical axis at zero frequency. As the amplitudes of spectral components with negative and positive frequencies are identical, and the entire spectrum is shifted to one or the other side by Doppler frequency, the illustrated spectrum is obtained. Notice also that the spectral structure will not vary with variation of "sign" of Doppler frequency, as each pair of components will change places.

The spectral structure shown in Figure 3.2 is valid if the relationship $\Omega_D < \Omega_m/2$ applies. If this relationship does not hold, the spectral components are changed such that the component with frequency $(n-1)\Omega_m + \Omega_D$ is situated on the frequency axis more to the right of the component with frequency $n\Omega_m - \Omega_D$. The extent of this change depends on how much the Doppler frequency exceeds half the modulation frequency.

The spectrum of the converted signal has no well-defined maxima. This is explained by the nature of Bessel functions, which decay slowly with increase in the argument. For fixed τ, with increase in τ/T_m up to value 0.5, the spectrum spreads in frequency because of increase in the frequency deviation of the converted signal. Then, with further increase in this ratio, the spectrum is again narrowed.

3.1.2 Dual Sinusoidal Modulation

The modulating function of a transmitter frequency in this case is given by

$$\gamma(t) = \frac{\cos\Omega_{m1}t}{2} + \frac{\cos\Omega_{m2}t}{2} \tag{3.9}$$

The modulating function of the converted signal phase is determined by (2.12), and its instantaneous frequency by (2.17). The particular aspect of dependence of these parameters upon time is determined by magnitudes of frequency deviations $\Delta\omega_1$ and $\Delta\omega_2$.

The calculation of the converted signal spectrum is made using (2.5), (3.6), and (3.7), resulting in:

$$
\begin{aligned}
u_t = U_t \cos\psi(t) \Bigg\{ & J_0(X_1)J_0(X_2) + 2\sum_{k=1}^{\infty}(-1)^k J_0(X_1)J_{2k}(X_2)\cos 2k\Omega_{m2}t' \\
& + 2\sum_{n=1}^{\infty}(-1)^n J_0(X_2)J_{2n}(X_1)\cos 2n\Omega_{m1}t' \\
& + 2\sum_{\substack{k=1\\n=1}}^{\infty}(-1)^{k+n} J_{2k}(X_2)J_{2n}(X_1)\cos(2k\Omega_{m2} \pm 2n\Omega_{m1})t' \\
& - 2\sum_{\substack{k=0\\n=0}}(-1)^{k+n} J_{2n+1}(X_1)J_{2k+1}(X_2)\cos\left[(2k+1)\Omega_{m2} \pm (2n+1)\Omega_{m1}\right]t' \Bigg\} \\
- U_t \sin\psi(t) \Bigg\{ & 2\sum_{n=0}^{\infty}(-1)^n J_0(X_2)J_{2n+1}(X_1)\cos(2n+1)\Omega_{m1}t' \\
& + 2\sum_{k=0}^{\infty}(-1)^k J_0(X_1)J_{2k+1}(X_2)\cos(2k+1)\Omega_{m2}t' \\
& + 2\sum_{\substack{k=0\\n=1}}^{\infty}(-1)^{n+k} J_{2k+1}(X_2)J_{2n}(X_1)\cos\left[(2k+1)\Omega_{m2} \pm 2n\Omega_{m1}\right]t' \\
& + 2\sum_{\substack{k=1\\n=0}}^{\infty}(-1)^{n+k} J_{2k}(X_2)J_{2n+1}(X_1)\cos\left[(2n+1)\Omega_{m1} \pm 2k\Omega_{m2}\right]t' \Bigg\}
\end{aligned}
\tag{3.10}
$$

where $X_1 = \left(\dfrac{\sin(\pi\tau/T_{m1})}{\pi\tau/T_{m1}}\right)\dfrac{\Delta\omega_1\tau}{2}$,

$X_2 = \left(\dfrac{\sin(\pi\tau/T_{m2})}{\pi\tau/T_{m2}}\right)\dfrac{\Delta\omega_2\tau}{2}$,

$\psi(t) = \Omega_D t + \varphi_\tau - \varphi_0$, and

$t' = t - \tau/2$.

As we can see, the spectrum of the converted signal is quite complicated, each spectrum component depending on parameters of both modulating functions.

Certainly, the number of spectrum components that should be taken into consideration to allow for parameters of filtering of the converted signal is significantly limited. It is reached by the applicable choice of deviations $\Delta\omega_1$ and $\Delta\omega_2$, and modulation frequencies Ω_{m1} and Ω_{m2}.

3.2 LINEAR FREQUENCY MODULATION

In SRR practice, this type of modulation is applied most frequently, especially in those SRRs using the schemes in Figures 2.3 and 2.4 (i.e., without direct signal central frequency shift). Therefore, further analysis of the converted signal will be conducted only for that case. The broad application of a linear frequency modulation is explained by several positive properties of the converted signal corresponding to this modulation, chiefly the constancy of its instantaneous frequency signal during all periods of modulation, or parts thereof, and its minimum spectral width.

Linear frequency modulation is carried out by three types of modulating functions: a non-isosceles sawtooth function [Figure 3.3(a)], symmetrical (or isosceles) sawtooth function [Figure 3.3(b)], and asymmetrical sawtooth function [Figure 3.3(c)]. Of these, the last is used most frequently.

3.2.1 Modulation with an Asymmetrical Sawtooth Function

In this case the modulating function of frequency of the transmitted signal is expressed by

$$\gamma_n(t) = \frac{t - nT_m}{T_m} \tag{3.11}$$

where T_m is the period of the sawtooth function and n is number of that period. The plot of this function is shown in Figure 3.4(a) (solid line). The frequency

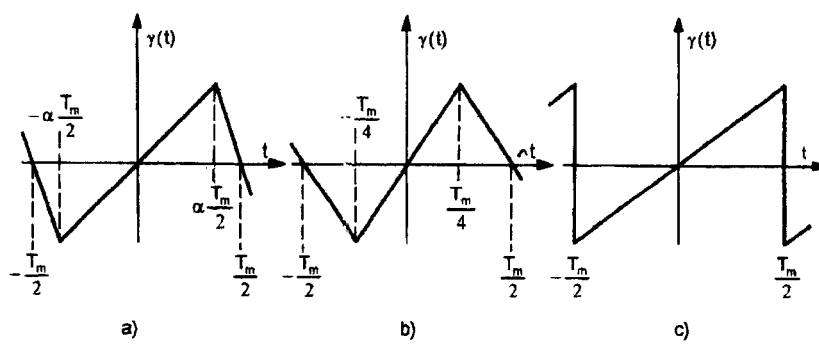

Figure 3.3 Modulating functions with linear modulation.

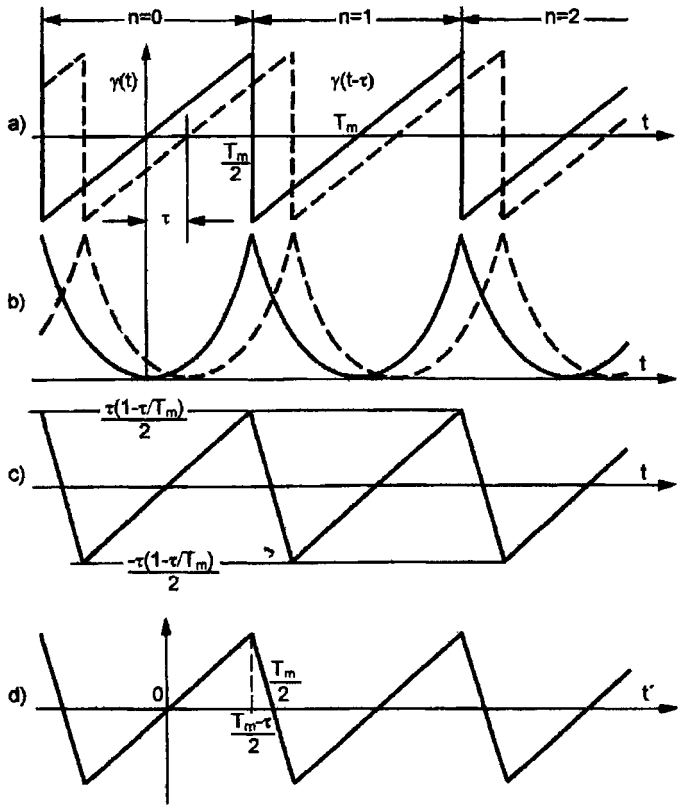

Figure 3.4 Modulating functions: (a) frequency and (b) phase of transmitted and reflected signals, and (c) and (d) phase of converted signal.

modulating function of a reflected signal is shown by the dashed line.

The modulating function of a radiated signal phase pursuant to (2.6) can be shown as:

$$F_{rn}(t) = \frac{(t - nT_m)^2}{2T_m} \tag{3.12}$$

The plot of this function is shown in Figure 3.4(b).

The modulating function of converted signal phase cannot be written as a single expression valid for any time instant. In segments from $(n - ½)T_m + \tau$ to $(n + ½)T_m$, this function, from (2.12), can be written as:

$$F_{tn}(t,\tau) = \frac{\tau}{T_m}t - \frac{\tau}{T_m}\left(\frac{\tau}{2} + nT_m\right) \tag{3.13}$$

In segments from $(n + ½)T_m$ to $(n + ½)T_m + \tau$, we have

$$F_{tn}(t,\tau) = \frac{\tau}{T_m} t - \frac{\tau^2}{2T_m} - n\tau - t + \tau + nT_m - \frac{T_m}{2} \tag{3.14}$$

A plot of the function $F_{tn}(t,\tau)$ is shown in Figure 3.4(c). As we can see, this function is piecewise linear, varying between the limits $-\tau(1 - \tau/T_m)/2$ and $\tau(1 - \tau/T_m)/2$, and symmetrical about the point $t = \tau/2$. Considering (2.17) and differentiating (3.13) and (3.14), we obtain expressions for instantaneous frequency of the converted signal in segments from $(n - ½)T_m + \tau$ to $(n + ½)T_m$:

$$\Omega_t(t,\tau) = \left| \pm\Omega_D + \Delta\omega \frac{\tau}{T_m} \right| \tag{3.15}$$

and in segments from $(n + ½)T_m$ to $(n + ½)T_m + \tau$:

$$\Omega_t(t,\tau) = \left| \pm\Omega_D + \Delta\omega \left(\frac{\tau}{T_m} - 1 \right) \right| \tag{3.16}$$

We see that the constancy of converted signal frequency on these segments is conditioned on linearity of its phase variations within each segment.

Thus, in this case the converted signal represents a frequency-shift keying oscillation, the frequencies of which are determined by (3.15) and (3.16). It is very convenient that the frequency of the converted signal in segments from $(n - ½)T_m + \tau$ to $(n + ½)T_m$ is fixed and depends linearly on the echo delay. All this permits deriving the range information. The signal in segments from $(n + ½)T_m$ to $(n + ½)T_m + \tau$, with frequency expressed by (3.16), can easily be filtered out in the processing, as its frequency differs little from that of the transmitted signal.

By virtue of periodicity of the modulating function, it is enough for calculation of the converted signal spectrum to consider the two segments of the function $F_{tn}(t,\tau)$ plot corresponding to $n = 0$ and $n = 1$. It is also expedient to change to a variable $t' = t - \tau/2$. Then we obtain

$$F_{t0}(t,\tau) = \frac{\tau}{T_m} t' \tag{3.17}$$

$$F_{t1}(t,\tau) = \left(\frac{\tau}{T_m} - 1 \right) t' + \frac{T_m - \tau}{2} \tag{3.18}$$

The plot of this function is shown in Figure 3.4(d).

The calculation of Fourier series coefficients is carried out using (2.25) and (2.26). The integration within limits 0 to $(T_m - \tau)/2$ is carried out with (3.17), and within limits $(T_m - \tau)/2$ to $T_m/2$ with (3.18). As in this case the function $\cos\Delta\omega F_t(t',\tau)$ is even, and the function $\sin\Delta\omega F_t(t',\tau)$ is odd, coefficients $b_n = c_n = d_0 = 0$. Omitting the intermediate calculations, we obtain the final expression for the converted signal spectrum:

$$u_t = U_t\left\{\begin{array}{l}\dfrac{\Delta f T_m \sin\left[\pi\Delta f\tau(1-\tau/T_m)\right]}{\pi\left[\Delta f(T_m-\tau)\Delta f\tau\right]}\cos(\Omega_D t+\varphi_\tau-\varphi_0)\\ +\displaystyle\sum_{k=1}^{\infty}\frac{\Delta f T_m \sin\left[\pi(\Delta f\tau+k)(1-\tau/T_m)\right]}{\pi\left[\Delta f(T_m-\tau)-k\right](\Delta f\tau+k)}\cos\left[(k\Omega_m-\Omega_D)t-\varphi_\tau+\varphi_0-k\Omega_m\frac{\tau}{2}\right]\\ +\displaystyle\sum_{k=1}^{\infty}\frac{\Delta f T_m \sin\left[\pi(\Delta f\tau-k)(1-\tau/T_m)\right]}{\pi\left[\Delta f(T_m-\tau)+k\right](\Delta f\tau-k)}\cos\left[(k\Omega_m+\Omega_D)t+\varphi_\tau-\varphi_0-k\Omega_m\frac{\tau}{2}\right]\end{array}\right\} \tag{3.19}$$

If the inequality $T_m >> \tau$ applies, then also $\Delta f T_m >> k$, and (3.19) is simplified:

$$u_t = U_t\left\{\begin{array}{l}\dfrac{\sin\pi\Delta f\tau}{\pi\Delta f\tau}\cos(\Omega_D t+\varphi_\tau-\varphi_0)\\ +\displaystyle\sum_{k=1}^{\infty}\frac{\sin\left[\pi(\Delta f\tau+k)\right]}{\pi(\Delta f\tau+k)}\cos\left[(k\Omega_m-\Omega_D)t-\varphi_\tau+\varphi_0-k\Omega_m\frac{\tau}{2}\right]\\ +\displaystyle\sum_{k=1}^{\infty}\frac{\sin\left[\pi(\Delta f\tau-k)\right]}{\pi(\Delta f\tau-k)}\cos\left[(k\Omega_m+\Omega_D)t+\varphi_\tau-\varphi_0-k\Omega_m\frac{\tau}{2}\right]\end{array}\right\} \tag{3.20}$$

Let us consider in more detail the last expression. The given spectrum has several relevant features (Figure 3.5). Consider the last line in (3.20). If in the

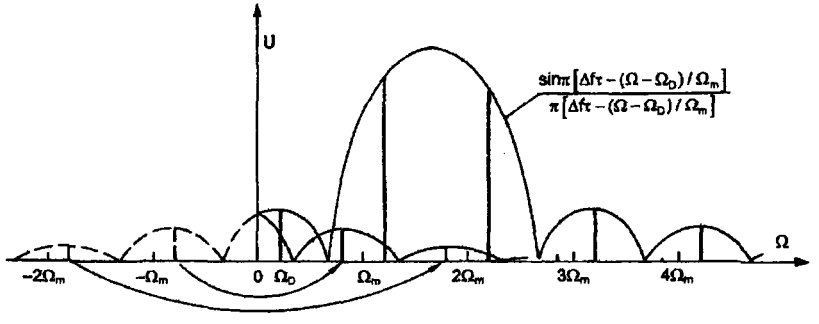

Figure 3.5 Spectrum of converted signal with modulation by an asymmetrical sawtooth function.

factor $\{\sin[\pi(\Delta f\tau - k)]\}/\pi(\Delta f\tau - k)$ the component number k corresponds to the current frequency rate (i.e., $k = (\Omega - \Omega_D)/\Omega_m$), we will obtain the spectral envelope formed by components with frequencies $k\Omega_m + \Omega_D$. The maximum of the major lobe of the envelope corresponds to frequency $\Delta\omega\tau/T_m + \Omega_D$, and its base width is equal to $2\Omega_m$. The maxima of the first sidelobes are −13.5 dB, and of the second −17.8 dB, relative to the major lobe.

As we can see, within the limits of a major lobe there can be no more than two spectral components, which contain ~ 85% of the converted signal energy. With variation of time delay the spectral envelope is displaced on the frequency axis, and with $\Delta f\tau = k$ only one component with frequency $k\Omega_m + \Omega_D$ remains in the spectrum. Consider in more detail the reason for this. As follows from (3.13) with $T_m >> \tau$ and $\Delta f\tau = k$, the phase of the converted signal within the limits of the modulation period is inflected linearly on $2\pi k$, and at the start of each period the phase values are identical. Thus, in the absence of motion the converted signal represents a continuous sine wave without phase jumps. The period of this sine wave equals T_m/k and the spectrum, as is known, consists of one component. With a constant relative target velocity [(2.13), (2.14)], the linear phase change $\Omega_D t$ is added and the spectral component is displaced by the Doppler frequency.

One more idiosyncrasy of the given spectrum is that the amplitudes of spectral component pairs with frequencies $k\Omega_m \pm \Omega_D$ are not identical. The reason for this can be easily explained. In essence the converted signal represents a succession of radio pulses with a rectangular envelope, the duration of which is equal to the recurrence interval. Therefore, the spectrum of the converted signal is the same as for a succession of such radio pulses. It is known that the envelope of a spectrum of rectangular pulses succession is described by a function $(\sin x)/x$, and the spectral envelope maximum is at the carrier frequency. Thus, in spite of the fact that the instantaneous frequency of the converted signal does not fall in the area of negative frequencies, a definite portion of its spectrum falls in this area (Figure 3.5). With folding of the spectrum about zero frequency, the components with negative frequencies are located near the corresponding components with positive frequencies. The second line in (3.20) indicates that spectrum components with negative frequencies "fold" to the area of positive frequencies.

Thus, there arises a question: on which side from the frequency $k\Omega_m$ are the larger and smaller spectrum components situated? In other words, is the frequency of the larger spectral components $k\Omega_m + \Omega_D$ or $k\Omega_m - \Omega_D$? It turns out that this depends not only on whether the target approaches or recedes (i.e., on the "sign" of Doppler frequency), but on the slope of the sawtooth modulating function.

To explain this we consider Figure 3.6. In Figure 3.6(a), the plots of converted signal phase changes $F_{in}(t,\tau)$ for a fixed target are shown, the sawtooth rising on the left and descending on the right. In Figure 3.6(b), the same plots are shown, but with an approaching target. The dashed line is the additional phase component originating from motion. The negative derivative of this line is determined by decrease in delay as the target approaches. As we can see, the steepness

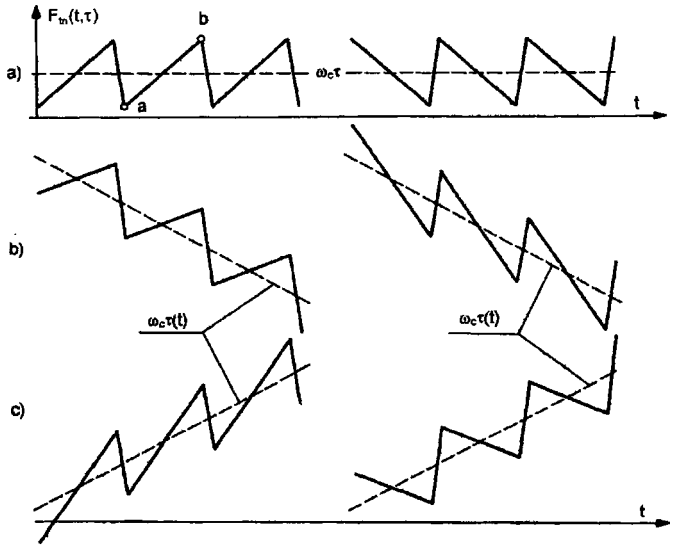

Figure 3.6 Graphs illustrating the influence of Doppler effect on a spectrum of converted signal.

of the segment a-b of function $F_{tn}(t,\tau)$ was reduced for the plot at the left and was increased for the plot on the right. Therefore, on the left, the frequency of the converted signal was decreased by the Doppler frequency and the larger spectral components have frequency $k\Omega_m - \Omega_D$. On the contrary, at the right, the frequency of the converted signal was increased and the larger spectral components have frequency $k\Omega_m + \Omega_D$. In Figure 3.6(c), the same plots are shown corresponding to receding targets. The situation here is reversed compared with the previous case. Thus, this property of the converted signal spectrum allows us to determine the relative velocity of the target and direction of its motion.

As was already stated, in real SRR the ratio $T_m >> \tau$ usually applies, and all calculations of parameters of the converted signal are based on this conjecture. For example, (3.20) was obtained from (3.19) in this manner. Actually, this means that we neglect the segments from $(n + ½)T_m$ to $(n + ½)T_m + \tau$ of the converted signal as being negligible compared with the period of modulation.

In this connection it is desirable to have a quantitative assessment of admissibility of ratio $T_m >> \tau$. This estimation is easy to perform using (3.19), which is valid for any ratio of τ/T_m. The criterion for assessment can be the extent of variation of the converted signal spectrum with the ratio τ/T_m.

For calculation we assume any fixed value $\Delta f\tau$, for example $\Delta f\tau = 10$. Then in the spectrum, according to (3.20), only the component with frequency $10\Omega_m + \Omega_D$ and relative amplitude of unity is present. The calculation of the spectrum from (3.19) with particular values τ/T_m permits us to judge the differences from those based on (3.20) and to determine acceptable values of τ/T_m, at which it is possible

to consider the inequality $T_m >> \tau$ to be valid. The results of the calculations are listed in Table 3.1, where k is number of the spectral component and $y = \tau/T_m$.

Table 3.1

Variation of Spectral Components with Ratio $y = \tau/T_m$

y	$k = 8$	$k = 9$	$k = 10$	$k = 11$	$k = 12$
0.01		–40	–0.09	–40	
0.05	–46	–26	–0.44	–26	–46
0.1	–20.4	–20	–0.9	–20	–22.5
0.2	–15	–14.4	–1.9	–14.9	–16.8

The values of amplitudes of the corresponding spectral components are given in decibels relative to unity. As we can see in the table, already for $y = 0.05$ the spectral components $k = 9$ and $k = 11$ are at a level –26 dB relative to the maximum. For $y = 0.1$, components $k = 9$ and 11 as well as $k = 8$ and 12 are significant.

Thus, it is possible to consider the inequality $T_m >> \tau$ valid if the period of modulation is greater than 10 times the maximum time delay of the echo signal. In radio-wave SRR this ratio is easily obtained, as a rule, in the absolute majority of cases. In ultrasonic SRR this ratio is obtained only with great difficulty, especially during operation in a gaseous medium.

The spectrum of the converted signal when $T_m >> \tau$ does not apply is subject to the same relationships as are established above. However, because of reduced duration of the converted echo in segments from $(n - \frac{1}{2})T_m + \tau$ to $(n + \frac{1}{2})T_m$, the major lobe of spectrum envelope is reduced and the spectral components applicable to frequency in segments $(n + \frac{1}{2})T_m$ to $(n + \frac{1}{2})T_m + \tau$ increase. The spectrum is distorted to the greatest degree when $\tau = T_m/2$.

3.2.2 Modulation with Non-Isosceles and Symmetrical Sawtooth Functions

For modulation with a non-isosceles sawtooth function [Figure 3.3(a)] the modulating function of transmitter frequency can be written as:

$$\gamma_n(t) = \frac{1}{(-1)^n - 1 + 2\alpha}\left(\frac{2}{T_m}t - n\right) \tag{3.21}$$

where n is the number of a segment on the time axis, within which lies the value of a current time t; and α is a coefficient between 0.5 and 1, such that for $\alpha = 0.5$ the non-isosceles function becomes symmetrical and for $\alpha = 1$ asymmetrical. We will perform analysis of the converted signal assuming that the condition $T_m >> \tau$ is satisfied. Then, on the basis of (2.19) we obtain at once

$$F_{tn}(t,\tau)=\frac{\tau}{(-1)^n-1+2\alpha}\left[\frac{2}{T_m}\left(t-\frac{\tau}{2}\right)-n\right] \tag{3.22}$$

Using (2.22), we obtain the expression for instantaneous frequency of the converted signal:

$$\Omega_{tn}(t,\tau)=\pm\Omega_D+\frac{\Delta\omega\tau}{T_m}\left(\frac{2}{(-1)^n-1+2\alpha}\right) \tag{3.23}$$

In this case the converted signal represents frequency-shift keyed oscillations, the frequency of which varies by jump and is equal to

$$\Omega_t=\left|\Omega_D+\frac{\Delta\omega\tau}{\alpha T_m}\right| \text{ in the segments with even } n \tag{3.24}$$

$$\Omega_t=\left|\Omega_D-\frac{\Delta\omega\tau}{(1-\alpha)T_m}\right| \text{ in the segments with odd } n \tag{3.25}$$

The spectrum of the converted signal is calculated in the same manner as with modulation using an asymmetrical sawtooth function. Neglecting subproducts, we write the final expression for converted signal spectrum:

$$\begin{aligned}u_t=&U_t\frac{\sin\pi\Delta f\tau}{\pi\Delta f\tau}\cos\left(\Omega_D t+\varphi_\tau-\varphi_0\right)\\&+U_t\sum_{k=1}^{\infty}\left\{\alpha\frac{\sin\pi\left(\Delta f\tau+k\alpha\right)}{\pi\left(\Delta f\tau+k\alpha\right)}+\left(-1\right)^k\left(1-\alpha\right)\frac{\sin\pi\left[\Delta f\tau-k\left(1-\alpha\right)\right]}{\pi\left[\Delta f\tau-k\left(1-\alpha\right)\right]}\right\}\\&\qquad\times\cos\left[\left(k\Omega_m-\Omega_D\right)t-\varphi_\tau+\varphi_0-k\Omega_m\tau/2\right]\\&+U_t\sum_{k=1}^{\infty}\left\{\alpha\frac{\sin\pi\left(\Delta f\tau-k\alpha\right)}{\pi\left(\Delta f\tau-k\alpha\right)}+\left(-1^k\right)\left(1-\alpha\right)\frac{\sin\pi\left[\Delta f\tau+k\left(1-\alpha\right)\right]}{\pi\left[\Delta f\tau+k\left(1-\alpha\right)\right]}\right\}\\&\qquad\times\cos\left[\left(k\Omega_m+\Omega_D\right)t+\varphi_\tau-\varphi_0-k\Omega_m\tau/2\right]\end{aligned} \tag{3.26}$$

As expected, there are two maxima in this spectrum (Figure 3.7) in the area of frequencies (3.24) and (3.25). As contrasted to the spectrum for modulation by an asymmetrical sawtooth function, the major lobes of the spectral envelopes in the area of these frequencies are broader. This is explained by the fact that the duration of segments of the converted signal with frequencies (3.24) and (3.25) is less than a period of modulation.

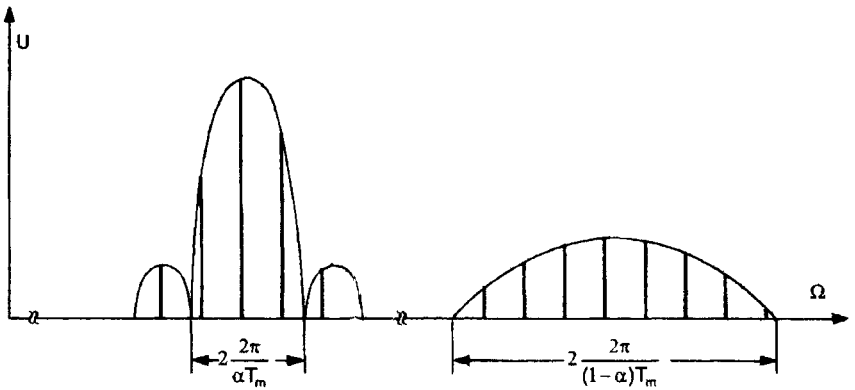

Figure 3.7 Spectrum of converted signal with modulation by a non-isosceles sawtooth function.

Assuming in (3.21) – (3.26) that $\alpha = 0.5$, we obtain similar expressions for modulation with an isosceles sawtooth function:

$$\gamma_n(t) = (-1)^n \left(\frac{2}{T_m} t - n \right) \tag{3.27}$$

$$F_{tn}(t,\tau) = (-1)^n \left[\frac{2}{T_m} \left(t - \frac{\tau}{2} \right) - n \right] \tag{3.28}$$

$$\Omega_{tn}(t,\tau) = \left| \Omega_D + (-1)^n \frac{2\Delta\omega\tau}{T_m} \right| \tag{3.29}$$

From (3.29) it follows that the frequency of the converted signal within the limits of one half-cycle is fixed and its values in adjacent half-cycles differ by $2\Omega_D$.

The spectrum of the converted signal can be written in the following way:

$$\begin{aligned} u_t = {} & U_t \frac{\sin \pi \Delta f \tau}{\pi \Delta f \tau} \cos\left(\Omega_D t + \varphi_\tau - \varphi_0 \right) \\ & + U_t \sum_{k=1}^{\infty} \left\{ \frac{\sin \pi (\Delta f \tau + k/2)}{2\pi (\Delta f \tau + k/2)} + (-1)^k \frac{\sin \pi [\Delta f \tau - k/2]}{2\pi [\Delta f \tau - k/2]} \right\} \\ & \times \cos\left[(k\Omega_m - \Omega_D) t - \varphi_\tau + \varphi_0 - k\Omega_m \tau / 2 \right] \\ & + U_t \sum_{k=1}^{\infty} \left\{ \frac{\sin \pi (\Delta f \tau - k/2)}{2\pi (\Delta f \tau - k/2)} + (-1^k) \frac{\sin \pi [\Delta f \tau + k/2]}{2\pi [\Delta f \tau + k/2]} \right\} \\ & \times \cos\left[(k\Omega_m + \Omega_D) t + \varphi_\tau - \varphi_0 - k\Omega_m \tau / 2 \right] \end{aligned} \tag{3.30}$$

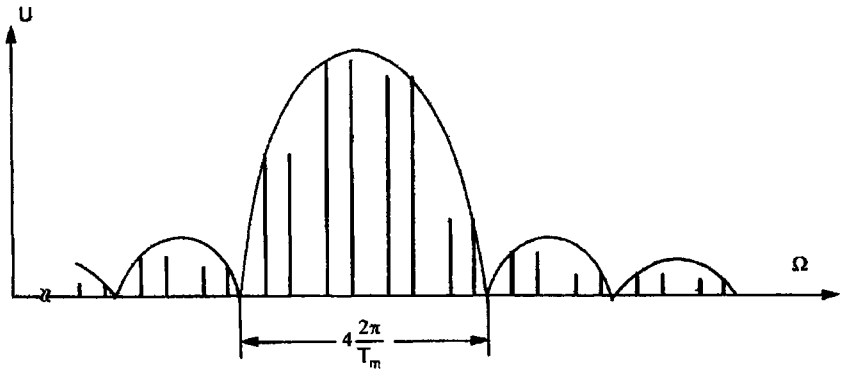

Figure 3.8 Spectrum of converted signal with modulation by an isosceles sawtooth function.

In Figure 3.8, this spectrum looks like the spectrum for modulation using an asymmetrical sawtooth function. However, the maxima of the spectrum corresponds to twice the smaller value of product $\Delta f\tau$. This is explained by the fact that the slope of a symmetric function is double that of an asymmetrical one. The amplitudes of spectrum component pairs with frequencies $k\Omega_m + \Omega_D$ and $k\Omega_m - \Omega_D$ are identical.

3.3 DISCRETE MODULATION

One of the major problems that should be solved in SRR design is that of deriving a more linear and stable modulation characteristic of the FM oscillator. One of the possible paths to the solution of this problem is applying a frequency synthesizer as the FM oscillator. Controlling in an appropriate way the frequency of the synthesizer output, it is possible to realize ideal precise frequency control for any modulation. For example, changing the frequency after a definite time period by a constant value makes it is possible to obtain ideal linear modulation. However, in this case the output signal appears quantized in frequency.

In Figure 3.9(a) there is a plot of synthesizer frequency against time, applicable to modulation with an asymmetrical sawtooth function. Here it is appropriate to point out that at transferring from one frequency to another there should not be phase discontinuity in the output of the synthesizer; otherwise there will be complete destruction of the converted signal. It is apparent that the same dependence will be obtained by modulating the usual oscillator with an ideal linear modulation characteristic for a "stepping" asymmetrical sawtooth function.

Thus, as discrete modulation is technically possible, it is necessary to consider properties and arguments of a converted signal for such modulation. We will conduct analysis of the converted signal using an example of asymmetrical sawtooth modulation.

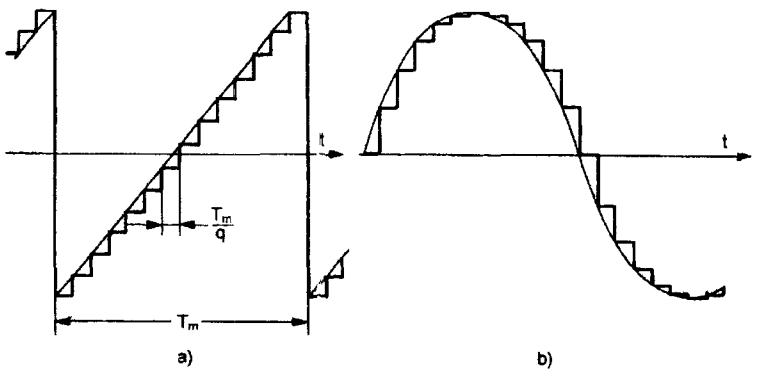

Figure 3.9 Discrete modulating function and section of the converted signal.

Let us assume that in a period of modulation T_m there must be q discrete values of frequency, and that the ratio $T_m/q >> \tau$ applies. Thus, a ratio $T_m >> \tau$ certainly applies. How will the converted signal appear in this case?

With the usual modulation the converted signal repeats sections of a sine wave of duration T_m. With discrete modulation, according to (2.20), the phase of the converted signal is changed by a modulating function. Therefore, the converted signal will appear as a stepping sine wave [Figure 3.9(b)]. If the sine wave with such digitization does not loose its shape (i.e., remains "on average" as a sine wave), the stepping is easily removed by appropriate filtering of the converted signal. This qualitative reasoning allow us to draw a conclusion about the necessity of deriving quantitative results.

In essence the problem is reduced to determination of an indispensable minimum number of quantization steps in the period of modulation, for which the converted signal distortion is within tolerance limits. Here it is important to note that the given problem has nothing in common with the problem described with the known Kotelnikov theorem. This theorem establishes the connection between the width of a continuous signal spectrum and the number of samples necessary for discrete representation of this signal. In other words, here the signal is already present and is introduced in analytical aspect.

In our case the discussion is about signal conditioning with admissible distortions. A discrete process is introduced in one signal (modulation), and the distortions are completely calculated for the other (converted) signal.

First of all, we note the clear fact that if the duration of each quantization step is commensurable with a period of the sine wave of the converted signal (not with a period of modulation!), there will be a significant distortion of the converted signal because of phase jumps. Thus, the following inequality should be met:

$$\frac{T_m}{k} > \frac{T_m}{q} \quad \text{or} \quad q > k \tag{3.31}$$

where k is the number of the spectral component with maximum frequency (i.e., applicable to the maximum measured range interval).

For further analysis, we will represent one period of a stepping modulating function t by the sum of two functions (Figure 3.10):

$$\gamma(t) = \gamma_1(t) + \gamma_2(t) = \frac{t}{T_m} - \left(\frac{t}{T_m} - n_2\right) \tag{3.32}$$

where n_2 is the period number of the second function, which is $T_{m2} = T_m/q$. If the limits of the variations in the definition of the first function are equal ±0.5, then for the second they are $\pm 0.5/q$.

With such definition of the modulating function, the spectrum of the converted signal is equal to the product of the spectra defined by (3.19) or (3.20), depending on whether the ratio $T_m >> \tau$ is valid or not. The fact is that with a large number of quantization steps this ratio can be valid for the first function and not for the second.

Let us note also that in calculating parameters of the second spectrum it is necessary to have the value of products $\Delta f_2 \tau = \Delta f \tau / q$, as the amplitude of the second modulating function is q times less than the first.

For calculation of the spectra we will take into account also the following circumstance. If the condition $q > k$ is always satisfied, for any value τ,

$$\Delta f_2 \tau = \frac{\Delta f \tau}{q} = \frac{k}{q} < 1 \tag{3.33}$$

Therefore, in the second spectrum the basic role is played by the first term, as all others are much less, and the spectrum of the converted signal is equal to the product of the first spectrum and the amplitude of the first member of the second spectrum.

Let us consider now two cases, when the condition $T_m/q >> \tau$ is valid and when it is not. Let us assume that condition $T_m/q >> \tau$ is satisfied. Then the amplitude of the first member of the second spectrum is determined by (3.20) and is equal to

Figure 3.10 Representation of the discrete modulating function by the sum of two sawtooth functions.

$$\frac{\sin(\pi\Delta f_2\tau)}{\pi\Delta f_2\tau} = \frac{\sin(\pi k/q)}{\pi k/q} \cong 1 - 0.166\left(\frac{\pi k}{q}\right)^2 \tag{3.34}$$

For approximation of this function we used the known relationship

$$\frac{\sin x}{x} = 1 - 0.166x^2 + 0.0076x^4 \quad \text{for } 0 < x < \frac{\pi}{2}$$

Assuming, for example, that in (3.32) $(\sin x)/x \le 0.95$, we obtain $q/k \ge 6$. Accordingly, for $(\sin x)/x = 0.99$, $q/k \approx 12$.

Now we assume that the condition $T_m/q >> \tau$ is invalid. The greatest departure from this condition is reached at $T_{m2} = T_m/q = 2\tau$. Having taken advantage of (3.19) and allowing (3.33), we obtain

$$\frac{\Delta f_2 T_{m2} \sin\left[\pi\Delta f_2\tau(1-\tau/T_{m2})\right]}{\pi\left[\Delta f_2(T_{m2}-\tau)\Delta f_2\tau\right]} = \frac{\sin(\pi k/2q)}{\pi k/2q} \cong 1 - 0.166\left(\frac{\pi k}{2q}\right)^2 \tag{3.35}$$

As we can see, in this case the requirements for the ratio q/k are half as strict as for the previous case. This is explained by the fact that in implementation of this ratio the converted signal consists of sections of a sine wave of duration $T_{m2}/2$ and frequency Δf_2. The phase of sine waves in adjacent sections differs by 180°, and this is equivalent to twice the number of quantization steps.

From these calculations the deduction follows that the digitization of a modulating function does not practically change the parameters of the converted signal, if the number of quantization steps in a modulation period is at least an order of magnitude greater than the maximum number of the spectral component of the converted signal (i.e., $q/k \ge 10$).

3.4 EFFECTS OF TRANSMITTER MODULATION NONLINEARITY ON CONVERTED SIGNAL PARAMETERS

The modulation characteristics of all known FM oscillators are nonlinear to some extent. The typical modulation characteristic is a curve whose derivative decreases with increasing frequency (Figure 3.11). The magnitude of the nonlinearity is usually defined as a ratio of maximum error in modulation characteristic to its width (i.e., to a tuning frequency range). This ratio is expressed as a percentage.

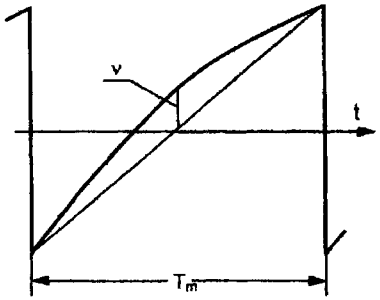

Figure 3.11 Typical modulation characteristic.

In some cases, especially for oscillators with large tuning ranges (a few GHz), the modulation characteristic represents a log-log curve with a set of short segments, between which the derivative changes not only in magnitude but also in sign. The departure from its average value can then reach a few percent of the oscillator tuning range.

To elaborate any general theory of the effects of nonlinear modulation characteristic on the converted signal makes no sense for several reasons. First, it is very difficult to obtain an analytical expression describing a real modulation characteristic. Second, even if that can be done, it is very difficult to calculate the converted signal, for this case, and most importantly, this effort makes no sense at all, as the oscillator modulation characteristic varies during operation.

At the same time, there is definite interest in making an estimate of the effect of modulation characteristic nonlinearity on the converted signal. We will make this estimate as follows. Let us consider the modulation characteristic of the oscillator as ideally linear, and to the linear modulation function we will add a term representing nonlinearity. Then the calculation of the converted signal will be reduced to calculating this signal with dual modulation. The method of conducting this calculation is particularized in Section 2.5.

As a linear modulation function it is most convenient to use an asymmetrical sawtooth function. With this modulation, as was shown above, the converted signal has the most compact spectrum, considerably easing calculation. As the error term we may use any monotonic even function. The choice of this function is determined primarily by convenience and by the possibility of a solution.

Let us use as the accessory term the half-period of a cosine. Then the modulating function of oscillator frequency can be introduced as

$$\gamma(t) = \frac{t}{T_m} + \nu \cos \frac{\pi}{T_m} t \quad \text{for} \quad -T_m/2 \le t \le T_m/2 \tag{3.36}$$

where ν is a coefficient describing nonlinearity of the modulation characteristic.

As we can see, a dual modulation takes place in this case. For further calculation let's assume that the ratios $T_m >> \tau$ and $\Delta f\tau = k$ are valid, so that, as was established above, there is only one component with frequency $k\Omega_m + \Omega_D$ in the spectrum of the converted signal. Thus, the calculation will be considerably simplified and distortion of the spectrum of the converted signal will be most obvious. Let us assume also that $\Omega_D t + \varphi_\tau - \varphi_0 = 0$. This is acceptable, as the given problem is not to obtain a precise expression for the spectrum, but only an estimate of possible distortions. It also will simplify calculation.

Using (2.22) and (3.36), we obtain the expression for instantaneous frequency of the converted signal

$$\Omega_t(t,\tau) = \Omega_m \left|\Delta f\tau - \nu\pi\Delta f\tau \sin(\pi t / T_m)\right| \tag{3.37}$$

For calculation of the spectrum we use (2.31), (3.6), (3.7), and (3.20). Skipping intermediate, elementary enough calculations, we produce a final output:

$$u_t = U_t\left\{J_0(\nu\Delta\omega\tau)\cos n\Omega_m t + \sum_{n=1}^{\infty}(-1)^n J_{2n}(\nu\Delta\omega\tau)\cos\left[(k\pm n)\Omega_m\right]t\right\} \tag{3.38}$$

Let us perform calculations with these formulas. We assume that the modeled nonlinearity of the modulation characteristic is ~0.02 (i.e., only 2%). Then $\nu = 0.02$. From (3.37) we find that the relative variation of instantaneous frequency at the ends of the modulation period is

$$\frac{\Omega_m \nu\pi\Delta f\tau}{\Omega_m \Delta f\tau} = \nu\pi \approx \pm 6\% \tag{3.39}$$

As we can see, even the small nonlinearity of modulation characteristic results in considerable variation of instantaneous frequency of the converted signal.

The spectrum of the converted signal is also exposed to considerable distortion. From (3.38) it follows that with an ideal modulating characteristic ($\nu = 0$) there is one component in the spectrum with frequency $k\Omega_m$, applicable to the assumed condition $\Delta f\tau = k$.

In Figure 3.12 the results of calculation with (3.38) are shown. On the abscissa is the number of the individual spectral component for a linear modulation characteristic. On the ordinate the relative amplitude of spectral components is plotted. The curves shown in this plot naturally are determined by the assumed approximation. However, it is not details of the curves but the tendency of their variations that are relevant in this case.

As we can see, with an increase in k the basic component is reduced and near it there are two components whose frequencies are $(k \pm 1)\Omega_m$. The magnification of spectral distortion with increasing instantaneous frequency of the converted signal is explained by increase in the absolute value of instantaneous frequency

change. So for $k = 1$ the instantaneous frequency will vary by $\sim 0.06\,\Omega_m$, and for $k = 20$ by $\sim \Omega_m$.

This calculation allows us to draw the conclusion that the modulation characteristic of the transmitter is one of its major parameters. The linearity of this characteristic and its stability depend on the structure of the converted signal processing block, the measuring error of range and speed, the required magnitude of frequency deviation, and many other SRR parameters.

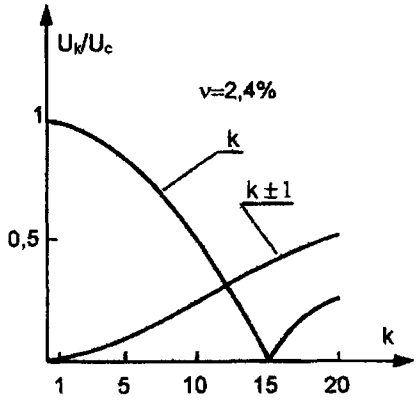

Figure 3.12 Distortion of the spectrum of the converted signal.

Chapter 4

Integrated Methods of Converted Signal Processing

4.1 GENERAL DESCRIPTION

Integrated methods of converted signal processing are defined to be methods in which all signal parameters (i.e., amplitude, frequency, and phase) will be utilized for processing.

As follows from material in Chapter 2, the information on range and relative velocity of the target is contained in the phase, and therefore in the frequency of the converted signal. It is impractical to utilize the amplitude of the converted signal for deriving range, as this depends not only on range but also on the magnitude of the reflected signal, which, in turn, depends on the effective cross section of the target.

Use of the range dependence of the instantaneous frequency of the converted signal is the most commonly used method of the signal processing in SRR. This is because range finding by measuring a frequency difference between transmitted and reflected signals is straightforward, though it has not always been implemented correctly. For many years the theory and the practice of FM SRR was developed on the basis of this method of processing, achieving significant success, although not without errors and unexpected peculiarities.

For example, the author of one patent based his invention on the fact that the instantaneous frequency of the converted signal depends on range continuously and linearly (evident from the drawing). Therefore a "simple and effective" method of range finding was proposed: to pass the converted signal through a narrowband filter with a bandpass much less than the modulation frequency. This filter was offset from the instantaneous frequency of the converted signal by an amount depending on the target range. As the filter was narrowband it was possible to relate the instantaneous frequency to the range with great fidelity. The mistake of the author of this patent is obvious. It is enough to consider the converted

signal spectrum: the signal at the output of the filter will occur only when it is tuned to frequencies of the target spectral component. At the same time the idea of the author is not lacking in common sense; it is necessary only to apply another method of converted signal processing (which will be discussed in Section 4.4.2).

For a long time in many scientific publications, the problem of an ostensible inherent granularity of range readout in FM SRR and a resulting error bound was considered. However, the appearance of this error is conditioned on rather coarse methods of processing the converted signal. Hence, this error can be considered as dependent on the processing method, but inherent in some cases.

Phase-frequency processing of the converted signal has one very relevant and fundamental feature: with this method of processing it is impossible to realize resolution of targets in range. Therefore this method can be applied only in cases where (a) it is known that there is only one target in the beam, or (b) it is unnecessary to resolve targets in range.

It is widely known that FM SRR is used in radio altimeters and liquid-level meters, in systems for collision avoidance in transportation facilities, in parking or mooring, and in measuring distances to walls of buildings or artificial reflectors (for example, corner reflectors). The need for range resolution often precludes the application of FM SRR in security systems.

Let us consider this problem in more detail. Assume that there are two targets, which are at random ranges from the radar within its operating zone. In this case three signals (Figure 4.1) act on the mixer: a direct signal U_d, and reflected signals U_{r1} from the first target and U_{r2} from the second. The vector of the direct signal is considered fixed. Then the angles $\varphi_{t1}(t,\tau_1)$ and $\varphi_{t2}(t,\tau_2)$ are given by (2.10). The total vector is

$$U_\Sigma^2 = (U_d + U_{r1}\cos\varphi_{t1} + U_{r2}\cos\varphi_{t2})^2 + (U_{r1}\sin\varphi_{t1} + U_{r2}\sin\varphi_{t2})^2 \qquad (4.1)$$

or

$$U_\Sigma = \sqrt{U_d^2 + U_{r1}^2 + U_{r2}^2 + 2U_dU_{r1}\cos\varphi_{t1} + 2U_dU_{r2}\cos\varphi_{t2} + 2U_{r1}U_{r2}\cos(\varphi_{t1} - \varphi_{t2})} \qquad (4.2)$$

Assuming that $U_d >> U_{r1,2}$ and that the mixer consists of a nonlinear element and lowpass filter, we obtain the converted signal at the output of the mixer:

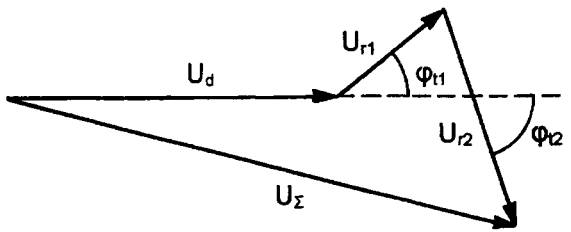

Figure 4.1 Phasor signals from direct component and two targets.

$$U_t \cong U_{r1} \cos \varphi_{t1} + U_{r2} \cos \varphi_{t2} \tag{4.3}$$

From (4.3) it follows that the principle of superposition of the converted signals is applicable (i.e., the voltage output of the mixer is the sum of the voltages of the converted signals of the individual targets). As these signals exist simultaneously, it is possible to distinguish them only through differences in their spectra.

Let us consider the possibilities of using the converted signal parameters for measuring range and velocity. For this purpose we will refer to the formulas of Chapter 2. First, we notice that there appears in all formulas defining parameters of the converted signal the product of a frequency deviation of the transmission and target-echo delay time $\Delta\omega\tau$. Therefore, two methods of using the converted signal parameters are possible.

The first method assumes that the deviation is fixed. Then it is possible to utilize dependence on τ of the converted signal frequency deviation, its instantaneous frequency, or phase shift for a modulation period.

The second method is that with variation in τ, some parameter of the converted signal is maintained constant by varying the frequency deviation. Hence the magnitude of the deviation (technically the magnitude of a modulating voltage or current) is a measure of the delay time (i.e., target range). In this it is naturally assumed that the modulation characteristic of the transmitter is stable.

A discriminator sensitive to the applicable parameter is necessary for operation of a deviation feedback system. The simplified block diagram of an SRR with this method of processing is shown in Figure 4.2.

Instantaneous frequency and, accordingly, phase shift also depend on relative velocity (i.e., from the Doppler effect). On the one hand this allows us simultaneously to obtain range and velocity. But, on the other hand, it can produce an additional error in range measurement if we fail to apply the applicable measures for the separation of Doppler effect from range measurement.

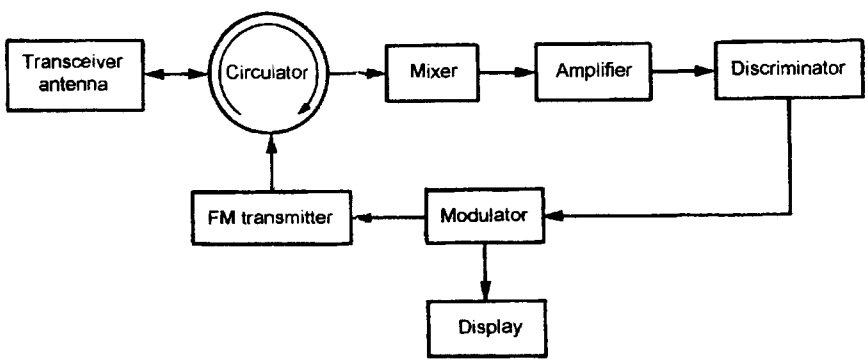

Figure 4.2 Block diagram of SRR with deviation feedback system.

4.2 EFFECT OF PARASITIC AMPLITUDE MODULATION OF THE TRANSMISSION ON OPERATION OF THE SRR RECEIVER

4.2.1 General Description

As was noted in Chapter 2, one of features of the FM SRR receiver is use as a heterodyne signal of a part of energy of the transmission. Even in dual-antenna systems, part of the transmission couples directly between the transmitting and receiving antennas. This has been termed transmitter spillover. The presence in the receiver of these signals creates definite problems in receiver operation. As W. K. Saunders notes in Skolnik's *Radar Handbook* [1] "the history of CW radar shows a continuous attempt to devise ingenious methods to achieve the desired sensitivity in spite of spillover."

More recently the seriousness of this problem has been significantly reduced. Nevertheless, it had previously been one of the most relevant problems affecting SRR design. Therefore, before considering different methods of converted signal processing, it is necessary to analyze the influence on receiver operation of transmitter spillover.

At first we will consider the dual-antenna version of the block diagram with a shift of the direct signal center frequency (Figure 2.2). Here, because of poor decoupling between antennas, a part of the transmission enters the receiving antenna. As spacing between antennas is insignificant, this signal is equivalent to a target echo from zero range. If there were no frequency shift of this spillover it would not introduce any special hazard into the receiver. It could only, being added to the direct signal, change the operating point of the mixer. But the mixer operating point can be always corrected, taking into account the level of spillover.

If there is frequency shift, two FM signals with in-phase modulation act on the mixer, and the center frequencies of these signals differ by the magnitude of an offset $\delta\omega$. As a result, a sinusoidal signal with frequency $\delta\omega$ appears at the mixer output. This signal can seriously affect receiver operation. Obviously, this signal cannot be filtered, as it is at intermediate frequency. It is possible only to cancel it, using for this purpose a signal with frequency $\delta\omega$ available in the block providing frequency shift of the direct signal.

In all events, the decoupling between antennas should be of the same order of magnitude as target echo attenuation. Inevitably this is a major deficiency of this SRR version.

The signal of any unmodulated or FM oscillator is always accompanied by parasitic fluctuating amplitude and phase modulation. Because of an incidental phase modulation, the frequency of the oscillator fluctuates, but this does not have any influence on SRR operation.

Nor does fluctuating amplitude modulation cause noticeable effects on receiver operation, in spite of the fact that there is amplitude detection of the direct signal in the mixer. This can be explained as follows. The spectral density of an amplitude fluctuating modulation spectrum for the majority of oscillators is

approximately −150 to −160 dB/Hz. The attenuation of a target echo relative to the transmission varies for SRR approximately from 50 up to 110 dB. The direct signal is reduced relative to the transmission by approximately 30 dB. The equivalent noise bandwidth of the receiver usually does not exceed 10 kHz. Let us consider that the transmission factor of the mixer in its conversion and detection regimes are identical. It is actually not but for an estimation this is adequate. Thus, the noise power at the mixer output, relative to power of the radiated signal is −150 − 30 + 40 = −140 dB, or 30 dB less than the power of the converted signal.

A much more serious danger for the receiver is introduction of parasitic amplitude modulation (PAM), which tracks with frequency modulation. The coefficient of this PAM can reach several percent. Thus, the PAM signal power is 30 to 40 dB less than the power of the direct signal, or some 50 to 60 dB less than the power of the transmission. Hence the PAM signal can exceed a useful signal by 40 to 50 dB. Obviously, a parasitic signal with such level above a useful one will completely destroy the normal operation of the receiver if necessary actions to prevent this are not taken. It is necessary to note that the above-mentioned data is referring to the worst case.

The PAM signal structure is defined by the amplitude-frequency characteristic of the FM transmitter. A typical amplitude-frequency characteristic is shown in Figure 4.3(a). As we can see, it is a domed curve with a maximum at the center frequency and with a large degree of symmetry about that frequency. The signal power reduction at the edges of tuning range usually does not exceed 5% to 7 % of the maximum. A more variable amplitude characteristic is shown on Figure 4.3(b). It has a random nature and is characterized by fluctuations of the oscillator regime. The level of these fluctuations is usually 30 to 40 dB below the regular PAM component.

The characteristics of the PAM signal are defined by both the shape of the transmitter amplitude characteristic and its modulating function. Relative smoothness and good symmetry of the amplitude characteristic cause the overwhelming part of the PAM signal energy (90% to 95%) to be concentrated in the first three or four harmonics of its spectrum. The remaining fraction of signal energy will be distributed rather uniformly among a large number of higher harmonics.

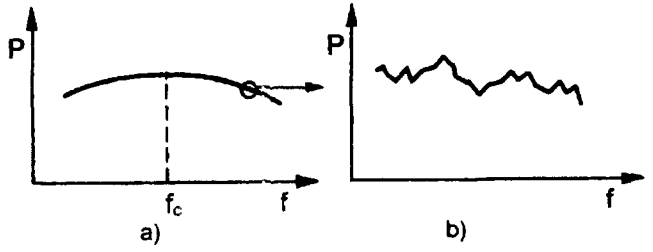

Figure 4.3 Typical amplitude-frequency characteristic.

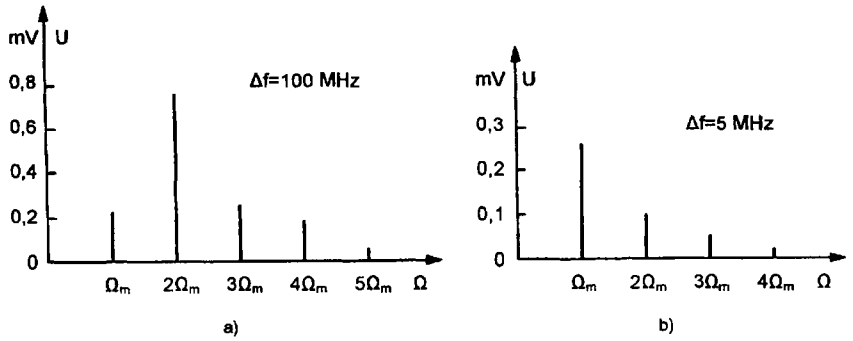

Figure 4.4 Typical PAM spectra at mixer output.

As an illustration, the real spectrum of the PAM signal at the mixer output of a radio-frequency block of an SRR is shown in Figure 4.4. The SHF block was based on the standard single-antenna version (Figure 2.4). The FM generator is a Gunn diode operating at 8-mm wavelength, a horn antenna is used with half-power beamwidth 6°, the mixer is one-stage with diodes, and asymmetrical sawtooth voltage modulation was used.

As we can see, the second harmonic of the PAM spectrum is maximum at a frequency deviation of 100 MHz, because of symmetry of the oscillator amplitude characteristic. Also, the spectrum in the area of the first harmonics is slightly wider than that of modulating signal. The voltage of higher harmonics does not exceed 100 μV.

For a frequency deviation of 5 MHz, the nature of a spectrum changes. With such deviation it is possible to consider the modulation characteristic linear, and therefore the PAM signal reproduces the shape of a modulating signal (i.e., an asymmetrical sawtooth). Accordingly, the spectrum of the incidental signal to some extent reproduces the shape of the modulating signal spectrum. The largest harmonic now becomes the first, and the voltage of harmonics beyond the third does not exceed 10 μV.

For estimating the levels of converted and PAM signals we will show the results of measuring signals obtained at the mixer output of the same UHF block. The converted signal was measured for the following targets:

(a) Reflection from a smooth metallic sheet, at 2m range from the antenna aperture, producing a converted signal voltage of approximately 70 mV;

(b) Reflection from a reinforced-concrete wall, 10m range, 15 mV;

(c) Reflection from a brick building, 80m range, 0.8 mV.

The frequency deviation in these cases was 150, 30, and 5 MHz, respectively.

4.2.2 Methods of Decreasing PAM Signal Effects on Receiver Operation

Methods of reducing PAM signal influence can be divided into two categories: direct and indirect. Direct methods are defined as those that reduce the PAM level

of the oscillator output or the direct signal. SHF signal power-level limiting devices or automatic power-level stabilization may be used for this purpose However, as a rule, these methods do not give the desired result but only complicate the SHF unit. Limiting devices react only slightly to minor variations of power and decrease the PAM factor by such small factors that they are completely inadequate in most cases.

Automatic power-level stabilization systems require very large amplification in the feedback circuit because of the low error signal. It is thus difficult to provide system stability. Besides, even if the oscillator were to have no PAM at all, it would arise with FM because of the resonant-frequency behavior of the direct signal channel.

Indirect methods of reducing PAM influence are most effective. Because the useful and parasitic signals are present at the mixer output simultaneously, they can only be separated by using differences in their spectra. The best approach in this respect is the system with frequency shift of the forward signal (Figure 2.2). In this version the spectrum of the PAM signal at the mixer output is in the region of the modulation frequency, while the spectrum of the useful signal is in the region of frequency $\delta\omega$. Therefore it is possible to provide good separation of these signals with a simple filter. The main danger for the receiver in this version is the spillover between the transmitting and receiving antennas.

The easiest way to reduce the level of the parasitic signal is to suppress several first spectrum components of the converted signal, where the basic energy of the PAM signal is concentrated. So, for example, for a signal consisting of an isosceles sawtooth, 99% of energy is concentrated in the first three harmonics of its spectrum. Therefore this simple method appears quite effective in most cases. Obviously in this approach there is a dead band, the extent of which is defined by the magnitude of the frequency deviation and the number of saturated components. If the dead band is too great, it is possible to divide the operation of the receiver into two regimes: short ranges, where the ratio of a useful to parasitic signals is large enough without suppression of the first components, and longer ranges at which suppression is required. The reduction of PAM signal can be made effective enough by applying an irregular frequency response curve to the converted signal amplifier.

As is known, for an irregular target the power of its echo varies inversely with the fourth power of range. The maximum of the converted signal spectrum is displaced in frequency by an amount that is directly proportional to range. Therefore it is necessary to increase the gain of the converted signal amplifier by 12 dB per octave to maintain the converted signal level more or less constant. For this purpose its frequency response should be appropriately reshaped. This is equivalent to the sensitivity time control used in pulse radar.

For short-range radar systems, a reduction of the effective target cross section often accompanies reduction in range. This is explained by reduction in the area of the illuminated surface, especially with narrow antenna patterns. In this case, the

power of a target echo varies approximately in inverse proportion to the third power of range, and the gain of the amplifier is increased by 9 dB per octave.

As the gain of the amplifier is reduced with decreasing frequency, there is a suppression of the most intense harmonics of the PAM signal spectrum. It is possible to judge performance of this suppression with simple calculations. Let us assume that the power of a target echo varies inversely with the third power of range. Then the normalized frequency response of the converted signal amplifier is written as

$$K = \left(F/F_{\max}\right)^{3/2} \tag{4.4}$$

where $F_{\max}$ is the frequency applicable to the last component of the converted signal spectrum. In terms of the modulation frequency

$$K = \left(k/n\right)^{3/2} \tag{4.5}$$

where k is the number of the current component and n is the number of the largest component of the converted signal spectrum.

Let us assume that the amplitude characteristic of the oscillator is linear and that the modulation takes the form of an asymmetrical sawtooth function. This is the worst case, in which the largest parasitic signal is received. The attenuation of the parasitic signal is

$$A = \frac{\sqrt{\sum_{k=1}^{n} U_k^2}}{U_m} \tag{4.6}$$

where U_k is the effective voltage of the kth harmonic of the parasitic signal spectrum at the output of an amplifier with an irregular amplitude-frequency characteristic, and U_m is the effective voltage of the parasitic signal at the amplifier output with a flat amplitude-frequency characteristic. This voltage is equal to the rms voltage of a sawtooth signal with unit amplitude, which is $1/\sqrt{3}$.

As is known, the Fourier-series expansion of a sawtooth function with unit amplitude is expressed as

$$y = \frac{2}{\pi}\sum_{k=1}^{\infty}\frac{1}{k} \tag{4.7}$$

Then, with allowance for (4.5), the effective voltage of kth harmonic of the parasitic signal spectrum at the amplifier output is

$$U_k = \frac{2k^{3/2}}{\sqrt{2}\pi k n^{3/2}} = \frac{\sqrt{2k}}{\pi n^{3/2}} \tag{4.8}$$

Substituting (4.8) in (4.6), we obtain

$$A = \frac{\sqrt{3(n+1)}}{\pi n} \tag{4.9}$$

Figure 4.5 shows as curve 1 a plot of the coefficient A, based on (4.9). A similar calculation for modulation using an isosceles sawtooth function gives the following expression for the coefficient A

$$A \approx \frac{0.4\sqrt{2+0.5\ln\left[(n+1)/2\right]}}{n^{3/2}} \tag{4.10}$$

The resulting plot is shown as curve 2 in Figure 4.5. As we can see, the amplifier with an irregular frequency response decreases the parasitic signal by 20 dB or more.

With a linear oscillator amplitude characteristic the available decrease is not so large (curve 1), but a linear amplitude characteristic corresponds to a small frequency deviation, for which the PAM coefficient is small. With large values of frequency deviation the amplitude characteristic is more or less symmetrical, and therefore the PAM waveform even with modulation by asymmetrical tooth voltages comes nearer to an isosceles sawtooth. A large reduction of the parasitic signal (curve 2) can be reached in this case.

A rather effective method of reducing the PAM signal is to use rejection filters attenuating the first, most intensive harmonics of the PAM spectrum. However, up until the present time this method has not found wide application because of serious engineering difficulties in its realization. First, the rejection band should be as small as possible. Otherwise, at small Doppler frequencies there will be suppression of the converted signal. Therefore, the Q-factor of filter resonant elements

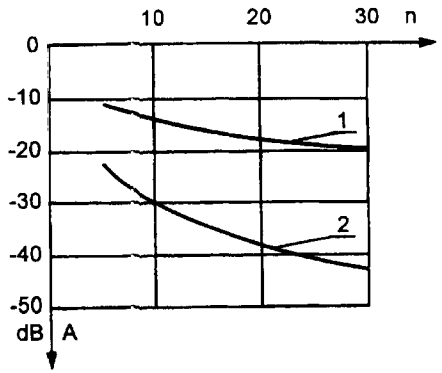

Figure 4.5 Attenuation of parasitic signal.

should be rather high – about several hundreds or greater. In the range of customary modulation frequencies, from hundreds of hertz up to tens of kilohertz, it is very difficult to realize such Q-factors.

Second, when the rejection band is narrow, rigid requirements are placed on mutual stability of filter resonance frequency and modulation frequency. Of course, these requirements can be satisfied with crystal filters and quartz-crystal control of the modulation frequency. However, such filters are very cumbersome and expensive.

The so-called synchronous rejection comb filter, based on switched capacitors, is free of all these deficiencies. The detailed theory of synchronous filters based on switched capacitors is explained in the special literature of the theory of active filters, and is not considered here. High stability of the comb-rejected frequencies, with a Q-factor of some thousands and simplicity of realization, favorably distinguish these filters from analog and digital rejection filters.

In Figure 4.6 the block diagram of one of the optional versions of such a filter is shown. The principle of operation of this filter is as follows. The sum of the useful signal and a periodic disturbance is applied to the input of the sample-and-hold block. From the output of this block, the voltage, sampled in time and fixed at a level, passes to the synchro-switched RC-filter composed of N identical capacitors, controlled with switches, and thereafter to resistor R. The operation of the filter is controlled by a pulse distributor, to the input of which a clock signal generator reference voltage is applied. The pulse repetition frequency of this oscillator exceeds by the factor N the rejection frequency for the first harmonic of a disturbance. The number of rejection channels N_r of such filters depends on the number of switched capacitors and is set to $N_r \leq N/2$. The rejection band at the –3 dB level is identical in all rejection channels and is $\Delta f \approx 1/\pi NRC$. For example, with $N = 16$, $R = 100$ kΩ, and $C = 10$ nF, $\Delta f \approx 20$ Hz. The depth of rejection is about 60 dB. In Figure 4.7 the sample normalized amplitude-frequency characteristic of the filter is shown. This characteristic is practically unchanged when the clock signal

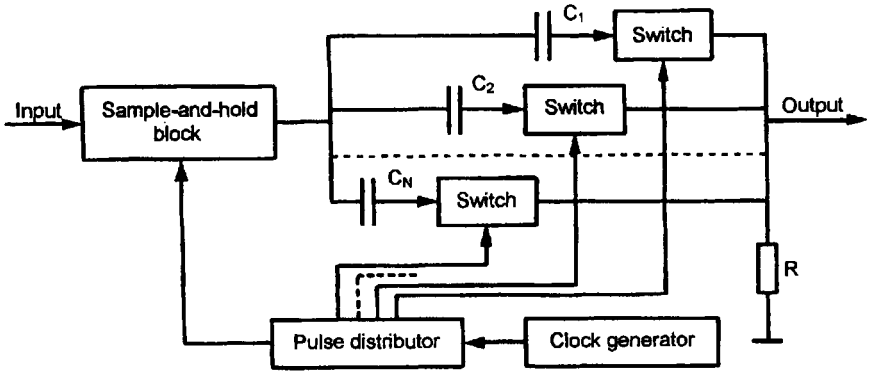

Figure 4.6 Synchronous rejection comb filter based on switched capacitors.

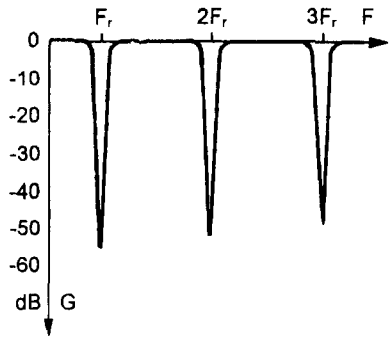

Figure 4.7 Frequency response of synchronous comb filter.

generator frequency changes by a reasonable factor. Accordingly, the frequency of each rejection channel is changed by that same factor.

Hence, if the clock signal generator is synchronized to a modulating signal or if the clock pulses are reshaped from a modulating signal, the frequencies of rejection channels will correspond precisely to frequencies of harmonics of the PAM signal spectrum.

As we can see, the application of a synchronous rejection filter enables effective suppression of a PAM signal by rather simple means. Certainly, together with the PAM signal, the applicable harmonics of the spectrum of the useful signal from fixed reflective targets are suppressed. Thus, the radar becomes "blind" to fixed targets at specific ranges. As the first harmonics are suppressed, as a rule the station will become "blind" to the nearest targets, as those go into the blind range regions. In some cases this can be useful, as selection of moving targets in a background of nearby clutter is obtained.

If this is inadmissible, it is possible to imitate Doppler shift by applying a dual modulation to the transmission. The frequency of the additional modulation is selected to equal a cloned Doppler frequency. The deviation of additional modulation is selected such that at the greatest measured range the maximum of the first harmonic of the converted signal spectrum from this modulation is reached. Thus, we conclude that there are adequate methods of receiver protection from PAM signals. In other words, the devil is not so terrible as he is painted!

4.3 STABILIZATION OF THE FREQUENCY DEVIATION

As was noted earlier the majority of converted signal parameters which will be used for ranging depend on product $\Delta\omega\tau$. During SRR operation a modulating voltage (or current) as well as the modulation characteristic of the transmitter can vary, and hence the deviation will not correspond to the nominal value. Obviously, this will lead to an additional measuring error in range.

If the allowable relative range error is level 5% to 10%, it is not necessary in most cases to undertake any special measures for stabilizing the nominal value of deviation. Otherwise, it is necessary either to stabilize the deviation or to measure the true value of the deviation and apply a correction to the measured result.

It is possible to solve a problem of stabilizing the nominal value of frequency deviation by two methods. The first method is to apply a frequency synthesizer (see Section 3.3).

The second method is inclusion of a special channel, similar to a measuring channel, for calibration of the frequency deviation (Figure 4.8). The signal delay is provided by a delay line. The operating principle of the calibration channel is as follows. The signal delay in the delay line is known, and therefore parameters of the signal at the output of the processing unit, applicable to a nominal value of a frequency deviation, also are known. With a departure of these parameters from the nominal value, an error signal is obtained, which either adjusts the amplitude of the modulating voltage or the readings of the range finder.

The processing unit of the converted signal in the calibration channel can be the same as or different from that in the measuring channel. All depends on the specifications of the SRR parameters. The quality of operation of this system is controlled by its operating principle and by the parameters of the processing unit of the converted signal in the calibration channel.

For example, the first harmonic in the spectrum of the converted signal in the calibration channel (Figure 4.9) can be used for calibration. The signal delay in a delay line τ_d is chosen such that the rated value of a deviation $\Delta\omega_r$ corresponds to first null of the selected harmonic of the spectrum. For example, with modulation by an asymmetrical sawtooth it corresponds to the product $\Delta f_r \tau_d = 2$, while with sinusoidal modulation it is $\Delta f_r \tau_d = 1.22$. The first harmonic of the signal is passed to a phase detector. A voltage with the modulation frequency, produced from the modulating voltage, is used as a reference signal for the phase detector. The phase shifter is included for compensation of the phase shift between voltages at the input to the phase detector. The voltage output of the phase detector is used in the modulator for adjusting the modulating voltage. Upon passing through the null, the

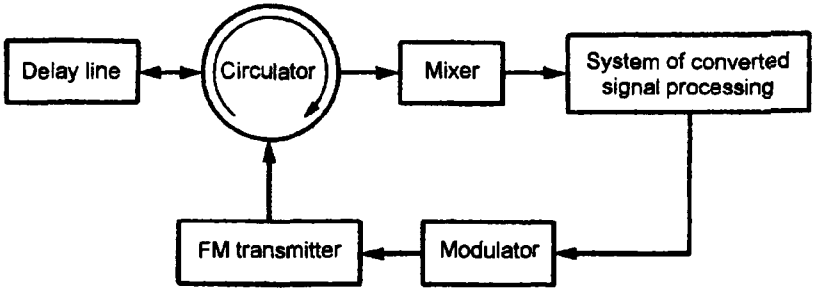

Figure 4.8 Calibration of frequency deviation.

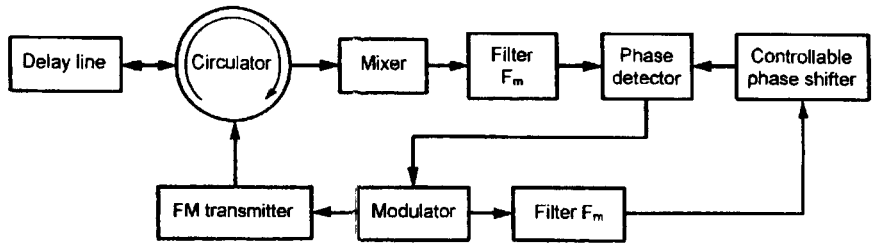

Figure 4.9 Block diagram of the calibration channel.

phase of the harmonic varies by 180°, and the sign of the output voltage of the phase detector varies accordingly. Thus, it is a typical feedback control system.

A more complex system of using a phase-locked loop (PLL), in which the converted signal of the calibration channel will be used, enables not only maintaining a nominal value of frequency deviation, but also simultaneous compensation of the nonlinearity of the oscillator frequency modulating function. The applicable block diagram of the calibration channel is shown in Figure 4.10. Let us consider the operation of this unit.

Let us assume that FM is carried out using an asymmetrical sawtooth function. In this case the converted signal represents samples of a sine wave with duration and recurrence interval T_m (see Section 3.3). This signal is applied to a phase detector, along with the reference signal with frequency $\Omega = \Delta\omega_r\tau_d/T_m$ where $\Delta\omega_r$ is the nominal frequency deviation and τ_d is the signal delay time in a delay line. The delay time can be always selected so that $\Omega = n\Omega_m$.

As we can see, the frequency of the reference signal is equal to that of the converted signal in the calibration channel with nominal deviation. The output voltage of the phase detector is added to the modulating voltage. If the frequency deviation does not correspond to the nominal value, the amplitude of modulating voltage is changed. Simultaneously there is distortion of the modulating voltage compensating the nonlinearity of the modulating function.

This can be shown by a simple calculation. Let us refer the nonlinearity of the modulating characteristic of the oscillator to a modulating voltage (i.e., consider the modulation characteristic theoretically linear, and the modulating voltage

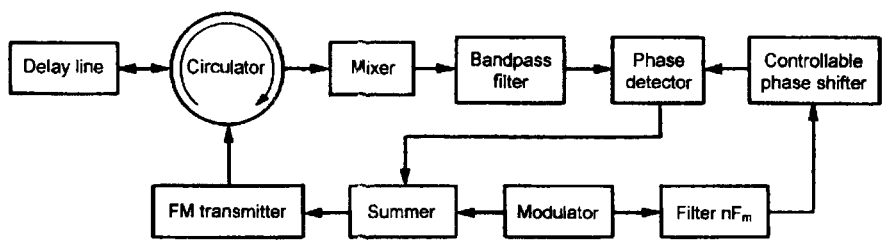

Figure 4.10 Calibration channel using PLL.

distorted). Then the modulating voltage will be written as:

$$U_m = k_1 \frac{t}{T_m} + k_2 \psi(t) - U_0(t) \tag{4.11}$$

where $\psi(t)$ is the function defining nonlinearity of the modulating voltage, $U_0(t)$ is the output voltage of the phase detector, and k_1, k_2 are constants of proportionality. The phase of the converted signal is:

$$\varphi_t(t, \tau_d) = \frac{\Delta\omega\tau_d}{T_m} t + k_3 \Delta\omega\tau_d \psi(t) - k_4 \Delta\omega\tau_d U_0(t) + \varphi_0 \tag{4.12}$$

and the voltage at the output of phase detector is

$$U_0 = S\left[\varphi_t(t, \tau_d) - \frac{\Delta\omega_r \tau_d}{T_m} t\right] \tag{4.13}$$

where S is the slope of the linear part of the phase detector detection characteristic. Substituting (4.13) in (4.12), and solving it for $U_0(t)$, we obtain

$$U_0(t) = S\left[\frac{\Delta\omega\tau_d t}{(1 + Sk_4\Delta\omega\tau_d)T_m} + \frac{k_3\Delta\omega\tau_d\psi(t)}{1 + Sk_4\Delta\omega\tau_d} + \frac{\varphi_0}{1 + Sk_4\Delta\omega\tau_d} - \frac{\Delta\omega_r\tau_d t}{(1 + Sk_4\Delta\omega\tau_d)T_m}\right] \tag{4.14}$$

Substituting (4.14) in (4.12), we obtain finally the expression for phase of the converted signal at the mixer output to the calibration channel

$$\varphi_t(t, \tau_d) = A\left(\frac{\Delta\omega\tau_d t}{T_m} + k_3\Delta\omega\tau_d\psi(t) + \varphi_o\right) + \left(\frac{Sk_4\Delta\omega\tau_d}{1 + Sk_4\Delta\omega\tau_d}\right)\frac{\Delta\omega_r\tau_d t}{T_m} \tag{4.15}$$

where $A = 1 - \dfrac{Sk_4\Delta\omega\tau_d}{1 + Sk_4\Delta\omega\tau_d} = \dfrac{1}{1 + Sk_4\Delta\omega\tau}$.

As follows from (4.15), the difference between $\Delta\omega_r$ and $\Delta\omega$ is decreased by the factor $1 + Sk_4\Delta\omega\tau_d$, and the nonlinearity of modulation is decreased by the same factor. As is known, the increase of product $Sk_4\Delta\omega\tau$ is limited only by the stability of operation of the automatic deviation control system. That stability is ensured with known methods applied in PLL systems.

4.4 FREQUENCY PROCESSING OF THE CONVERTED SIGNAL

The oldest and most common method of processing the converted signal exploits the relationship between its frequency and the target range.

4.4.1 Range Finding by Counting the Number of Zero Points of the Converted Signal for a Modulation Period

This method was the first realized method of range measurement and has been used for many years. There are several reasons for its wide use: the simplicity and obvious application to SRR, its ability to measure very small ranges, and the simplicity of signal processing. The latter, in the "tube epoch" of radio engineering, had decisive importance. That is why this method of signal processing has systematically been used, primarily in low-altitude radio altimeters. In this application there are very strict requirements for reliability, mass, and overall dimensions.

A large body of scientific research and articles is dedicated to the study of this method of processing. The theoretical analysis of the method is founded on such concepts as "difference frequency," "beat frequency," and "number of beats." In other words, the theory establishes the dependence of the instantaneous frequency of the converted signal on range. Certainly the number of zero crossings of the converted signal directly depends on its instantaneous frequency. But this method is not in any way connected to *measuring* of instantaneous frequency and use of measured results for range finding. Therefore it can best be referred to as one of the varieties of phase processing.

The important issue is that the difference frequency is not determined, but the number of cycles of converted signal phase, modulo π, per modulation period is determined. Confusion was introduced in this problem, apparently, because of the simple and visual explanation of the operation principle, as a meter for difference frequency. Let us consider this problem in more detail, for which we will refer to the SRR block diagram of the single-antenna SRR version with this type of processing, shown in Figure 4.11.

As we can see, the converted signal from the mixer output passes to a limiting amplifier. The frequency response of this amplifier increases with frequency, providing suppression of parasitic amplitude modulation signals and leveling of output amplitude with variation of target range. The limiting device changes the converted signal into a square wave, completely eliminating dependence between its output and input amplitudes. The square wave is then differentiated, and the resulting short pulses are applied to a counter that produces a voltage proportional to the number of pulses in a modulation period. This voltage is proportional to measured range.

One of the interesting features of this circuit for processing the converted signal is its invariance to the applied modulation waveform. It is possible to apply any of the periodic modulations discussed above. The result will be same, in that only the number of impulses for a modulation period will vary: with sinusoidal

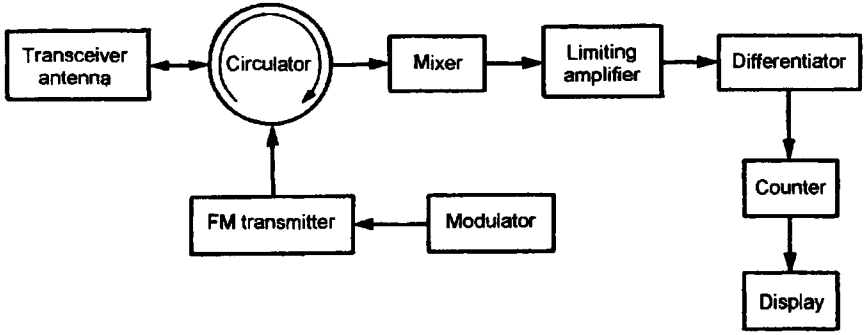

Figure 4.11 Block diagram of single-antenna SRR with pulse counter.

modulation or modulation by an isosceles sawtooth it will be twice that obtained with modulation by a non-isosceles sawtooth. This is easily explained if we consider the phase of the converted signal.

As was shown in Chapter 2, the phase of a converted signal is defined as

$$\varphi_t(t,\tau) = \omega_c\tau + \Delta\omega\tau\gamma(t') - \varphi_0 \tag{4.16}$$

Let us determine a phase shift of a converted signal for a period between two maxima of the modulating function, which by definition are equal to +0.5 and –0.5.

$$\Delta\varphi_t(t,\tau) = \omega_c\tau + 0.5\Delta\omega\tau - \varphi_0 - \omega_c\tau + 0.5\Delta\omega\tau + \varphi_0 = \Delta\omega\tau \tag{4.17}$$

If the maxima of the modulating function are situated at the beginning and end of its period, this will be the phase shift for a modulation period. This case in particular corresponds to modulation using an asymmetrical sawtooth function. With sinusoidal modulation or modulation by an isosceles sawtooth, this phase shift is reached in half the period.

At the same time, as follows from (4.17), the phase shift does not depend on the modulation waveform. It is important only that the values of phase of the converted signal are fixed at the moments of the minimum and maximum of the modulating function. Now it is clear why this method of processing is invariant to the modulating waveform. Accordingly, with this method there are less rigid requirements for linearity of the transmitter modulation characteristic, a clear advantage for this method of processing. But, on the other hand, it is clear that rather coarse processing of the converted signal is applied. The phase shift of converted signal with a resolution of π is, in fact, measured. Therefore the range measuring error is found from equating $\Delta\omega\Delta\tau = \pi$ to obtain

$$\Delta r = C/4\Delta f \tag{4.18}$$

This formula appears in many articles where difference frequency is counted, or number of beats, and so the deduction of this formula appears to be much more difficult.

Even in the first experiments with these radars it was noted that with range variations of about $\lambda/4$, the number of impulses varied by ± 1. This phenomenon is also easily explained. For this purpose we will refer to Figure 4.12, where the plot of the formula for the converted signal phase is shown. In cases a, b, and c the value of $\Delta\omega\tau$ is identical, with $5\pi < \Delta\omega\tau < 6\pi$. In case a the number of impulses is equal to 5. If the range is increased by $\approx\lambda/8$, the number of pulses immediately becomes equal to 6, as in case b. With further increase in range the number of impulses is again equal to 5, as in case c. This applies as long as $\Delta\omega\tau$ does not become more than 6π. Then the number of pulses will oscillate between 6 and 7, and so on. Because of this there is a granularity in range measurement.

Some time ago, when a frequency deviation of 30 to 50 MHz was considered large and the transmitted frequency was not greater than 300 to 500 MHz, this phenomenon necessarily resulted in large inaccuracies in range measurement, especially at small ranges where the relative error reached several tens of percents.

Different methods of "averaging" for the detecting instrument were therefore proposed. For example, it was proposed to input into the direct signal channel a modulated phase shifter, which modulated the initial phase of the converted signal. Due to this, the observations of the detecting instrument were averaged. Currently the urgency of this problem has been considerably reduced. With deviations of 200 to 300 MHz the measuring error at ranges from 10m to 15m amounts to 2% to 3%. This is reasonable in the majority of applications. Also, in the cm wave band, averaging is obtained due to movement and heterogeneity of reflective surface.

4.4.2 Measuring of the Instantaneous Frequency

In some SRR applications, range measurement to immobile (slow-moving) targets is required (for example, in liquid-level-measuring radar, meters for ranging to unapproachable fixed targets, and meters for small movements of various targets). The basic requirement presented in the characteristics of such SRRs is relative simplicity and minimum measuring error.

In this case it is convenient to apply the method of range determination by measuring the instantaneous frequency or period of the converted signal. In the

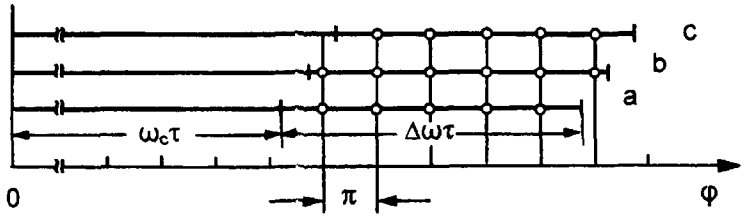

Figure 4.12 Typical converted signal phase versus time plots.

final analysis the matter is again reduced to determination of the magnitude of the converted signal phase shift $\Delta\omega\tau$ for a modulation period. This case differs from the previous method of processing only in that the time interval between nulls of the converted signal (i.e., the duration of its half-period) is measured instead of the number of zero crossings.

As there is no necessity for determination of speed or adjusting of measurement in connection with the Doppler effect, the most convenient modulation to apply is the asymmetrical sawtooth function. Well known methods of measurement technology are applied for measuring of time interval, and therefore here it is not necessary to consider this problem. It is important only to note that existing methods allow us to measure time intervals with errors not more than hundredths of one percent. Accordingly, the phase shift $\Delta\omega\tau$ is measured with the same inaccuracy. However, this is correct only in the case when the FM is ideally linear.

With departure of modulation from linearity the duration of adjacent periods of the converted signal is unequal. Therefore the mean value of the converted signal period is determined for range measurement. The deviation of the mean value of the period from its true value, corresponding to the theoretical modulation, is controlled by two factors: the nonlinearity factor of the modulating function and its shape (see Section 3.4).

The nonlinear component of the modulating function is often nearly symmetrical with respect to the middle of the modulation period. We can then use (3.36) and (3.37) for calculation. From (3.37) it is at once visible that the mean frequency rate of the converted signal is equal to $\bar{\Omega}_t = \Delta\omega\tau / T_m$ (i.e., is equal to its nominal value). This is easily explained by the fact that for the first half of the modulation period the instantaneous frequency is slightly less, while for the second it is greater by exactly the same value.

We utilize the same approximation for a maximum asymmetry of modulating function,

$$\gamma(t) = \frac{t}{T_m} + \nu \sin \frac{\pi}{2T_m}\left(t + \frac{T_m}{2}\right) \quad \text{and} \quad \bar{\Omega}_t(t,\tau) = \frac{\Delta\omega\tau}{T_m}(1+\nu) \tag{4.19}$$

The applying of another approximation (for example, a parabola) gives the same result.

Thus we find that inaccuracy of phase shift determination in this case is no greater than the nonlinearity factor of the modulation function. A combination of a calibration channel and PLL to control the deviation permits this method of converted signal processing to measure the range with relative error not more than tenths of one percent. Certainly, no granularity in readout of range is present.

4.4.3 Fixing the Instantaneous Frequency of the Converted Signal

The circuit of a calibration channel with PLL control of transmitter frequency deviation was reviewed above. Precisely the same circuit can be utilized as well for implementing a measurement channel. The applicable block diagram of single-antenna SRR version is shown in Figure 4.13.

The parameter that is maintained constant is the instantaneous frequency of the converted signal. The modulation is an asymmetrical sawtooth function. A phase detector is used as the discriminator. The applicable harmonics of the modulating voltage are used to generate a reference signal for the phase detector. The voltage output of the phase detector is applied to the modulator to vary the modulating voltage.

The converted signal is applied to a bandpass amplifier that uses automatic gain control (AGC). The bandpass of this amplifier should be wider by a factor of two or three than the major spectral lobe of the converted signal (i.e., about $10F_m$). The normalization of the converted signal amplitude is essential here to ensure stability of the automatic frequency deviation control system. If necessary, the signal can be limited after amplification. The modulating voltage appears as the output signal of the processing unit, which is applied to a range indicator. The amplitude of the modulating voltage is inversely proportional to target range.

Frequency locking must occur for normal operation of the automatic control. However, it cannot take place if the instantaneous frequency of the converted signal is not equal to a fixed frequency at radar turn-on. To ensure locking, a special search unit is provided. When there is no signal at the phase detector output, the frequency deviation is slowly swept by this unit from minimum value up to maximum (or vice versa). As soon as locking occurs, the unit is turned off. If for any reason the automatic system breaks lock, the search unit is again actuated. The search time depends on the response rate of the automatic control system and usually exceeds a period of modulation T_m by one or two orders of magnitude. As the discriminator, it is possible to apply the usual frequency detector, in which case there is no need for a reference signal.

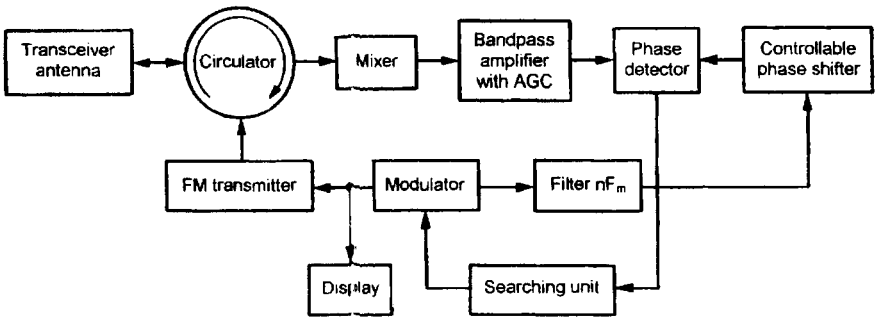

Figure 4.13 Block diagram of an FM SRR with fixed instantaneous converted signal frequency.

The stabilized value of instantaneous frequency of the converted signal depends on several factors: on the ranges to be measured, the possible tuning frequency range of the transmitter, the parasitic amplitude modulation signal level at the mixer output, and the magnitude of Doppler frequency.

The latter is explained by dependence of instantaneous frequency not only upon target range, but also upon its velocity. Therefore, the range measurement system is subject to an error depending on speed. This is certainly a deficiency of this processing method. For reduction of this error it is necessary to increase as much as possible the stabilized instantaneous frequency of the converted signal.

To eliminate influence of the Doppler effect, it is possible to apply sweep-frequency modulation by a symmetrical sawtooth function. As in this case the instantaneous frequency in adjacent half-cycles differs by $2\Omega_D$ (see 3.29), and the signal at the phase detector output has the shape of a symmetrical sawtooth. For normal operation of the automatic control system it is necessary to derive from this voltage its average value using a simple lowpass filter. The variable component can be used for determination of the relative velocity of the target. The inaccuracy of range finding in this case is caused primarily by instability of the modulation characteristic of the transmitter.

4.4.4 Use of the Frequency Deviation of the Converted Signal

Use of the frequency deviation of the converted signal is one of the most effective methods for simultaneous measurement of range and relative velocity. This method was designed originally as a method of eliminating a granularity in range finding [2]. As follows from (3.3), (3.4), and (3.5), the frequency deviation of the converted signal varies linearly and continuously with delay time of the target echo over range delays from zero up to $\tau \approx 0.1T_m$.

It is most convenient in this case to use the SRR version with frequency shift of the direct signal (Figure 2.2) and sinusoidal modulation of the transmission. The application of other SRR types, reviewed in Chapter 2, with use of dual sinusoidal modulation is sometimes possible.

The simplified SRR block diagram is shown in Figure 4.14. It differs from the circuit in Figure 2.2 only in that the contents of the unit "system of converted signal processing" is rendered more concretely. As was already noted, the converted signal in this case represents an FM signal with central frequency $\Delta\omega \pm \Omega_D$ and sinusoidal modulation. Therefore the preferred circuit for FM signal processing (a limiting device and frequency detector) is connected to the output of the IF amplifier. The transition frequency of the discriminator curve is $\delta\omega$.

It is evident that the voltage at the output of the discriminator represents a sine wave, the amplitude of which is proportional to range. The constant component of the discriminator output is proportional to the offset of the converted signal center frequency by the Doppler shift.

However, this circuit is only an illustration of the SRR operating principle with this version of converted signal processing. To realize such a simple processing

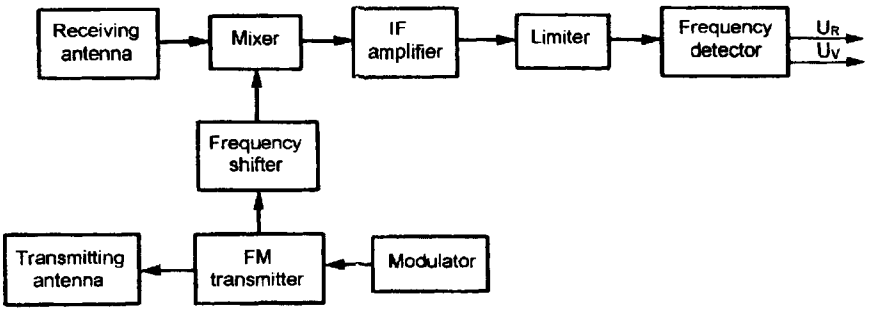

Figure 4.14 Simplified block diagram FM SRR with frequency detector.

circuit in practice is unrealistic for the following reasons. As was already mentioned, the frequency shift of the forward signal and accordingly the center frequency of the converted signal, is about 100 MHz. The frequency deviation of the converted signal can be greater than the modulation frequency by two or three orders of magnitude. Even if the modulation frequency were rather high, for example 1 kHz, the deviation does not exceed several hundreds of kilohertz. At a transmitted wave length of ~8 mm and relative velocity up to 100 km/h, the Doppler frequency does not exceed ~20 kHz.

At frequencies of 100 MHz or more it is very difficult to make a discriminator with a bandwidth of some hundreds of kilohertz. The characteristic of the discriminator with such large bandwidth has, accordingly, reduced slope. It is, in general, impossible to ensure frequency stability in the discriminator characteristic and the shift frequency to the accuracy of hundreds or even of tens of hertz, as is necessary for precise measurement of Doppler frequency.

For this reason it is necessary to apply multiple conversions of the frequency of the converted signal to a value that does not exceed several hundreds of kilohertz. The applicable block diagram is shown in Figure 4.15. Here the FM transmitter (1) is modulated sinusoidally by the modulator (2). Part of the transmitter power (the direct signal) arrives at mixer No. 1 (3), to which an unmodulated signal with frequency $\delta\omega$ from the supplementary oscillator (4) is also applied. At the output of mixer No. 1 there is a single-sideband filter (9), which selects the signal with frequency $\omega_d = \omega_c - \delta\omega + (\Delta\omega\cos\Omega_m t)/2$. This signal is applied to mixer No. 2 as a direct signal. The converted signal with frequency

$$\Omega_t(t,\tau) = (\delta\omega \pm \Omega_D) + \Delta\Omega_t(\tau)\sin\Omega_m t'$$

is input to the IF bandpass amplifier (13).

For realization of multiple down-conversion of the signal frequency, two signals, one from oscillator (4) and another from oscillator (6) with frequency ω_1 are applied to Mixer No. 3 (5), such that $\omega_1 < \delta\omega$. As a result, the signal at the output of filter (10) is at the frequency $\delta\omega - \omega_1$. This signal arrives at mixer No. 4 (14). The subsequent filter and IF amplifier select a signal with frequency

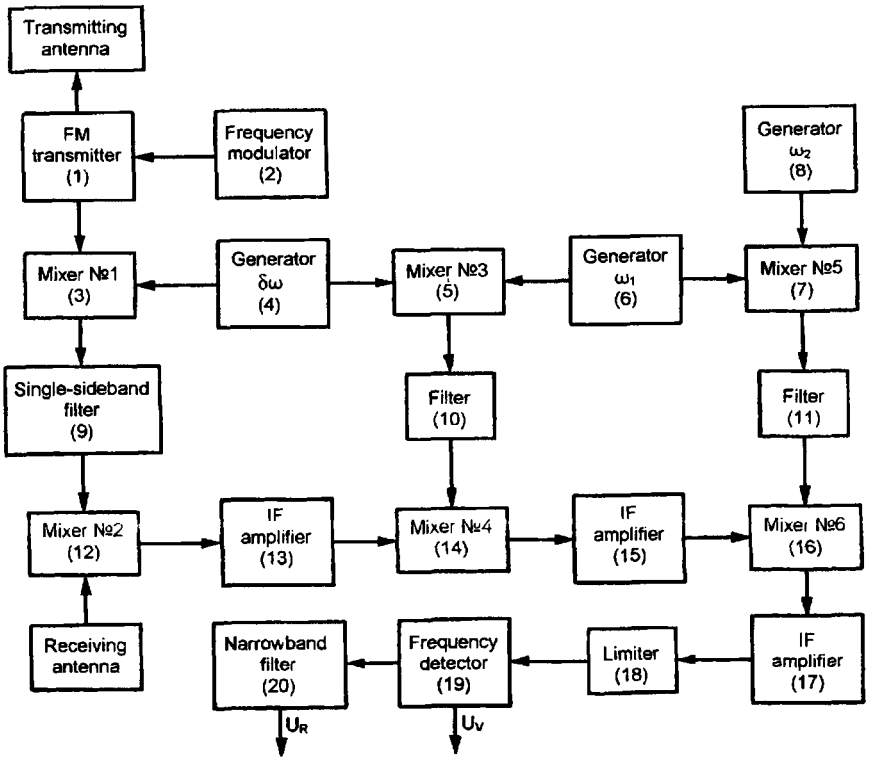

Figure 4.15 Complete block diagram FM SRR with frequency detector.

$$\omega_1 \pm \Omega_D + \Delta\Omega_t(\tau)\ \sin\Omega_m t'$$

The further transformations of the signal are clear from the block diagram. In this case two stages of downconversion are used as an example, but more stages can be used. It is important that the frequency of the last supplementary oscillator should be made low and stable enough. The transition frequency of the discriminator characteristic is equal to the frequency of the last supplementary oscillator (8). This also achieves high stability of the converted signal center frequency and the transition frequency of the discriminator characteristic. The constant component of output voltage of the discriminator is proportional to relative target velocity, and its sign indicates the direction of movement. The variable component, selected by a narrowband filter (20), is proportional to target range.

Other circuits for deriving the direct signal frequency shift are also possible, for example that shown in Figure 4.16. Here a supplemental FM generator is used for deriving the direct signal with shifted frequency. This oscillator is connected to the FM transmitter by a phase-lock circuit. The signal frequency of the reference

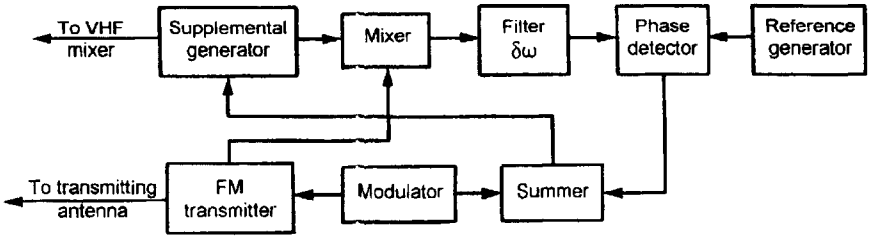

Figure 4.16 Block diagram of the frequency shifter.

generator in the PLL system is equal to $\delta\omega$. This frequency can be made reasonably small (i.e., equal to the frequency of oscillator (8) of the previous circuit). Accordingly, the frequency stability of this oscillator can also be made high enough. Thus, the SRR receiver is simplified at the cost of some complicating of the direct signal channel.

Here it is convenient, if necessary, to apply cancellation of the intermediate frequency signal originating from spillover of the radiated signal into the receiving antenna. For this purpose a signal from the reference oscillator is summed with the parasitic signal (Figure 4.17). An attenuator and phase shifter are used to ensure equal and antiphase summing of these signals.

4.4.5 Applying Dual Sinusoidal Modulation

It was noted in Chapter 2 that one possible method of deriving a converted signal with nonzero intermediate frequency when using homodyne reception is to apply dual modulation. In this case it is most convenient to apply dual sinusoidal modulation. Parameters of the basic modulation (which we will call for brevity "first") are selected as in the previous case.

The frequency of supplementary ("second") modulation is selected much higher than the frequency of the first, but no more than the frequency of the supplementary oscillator (8) of the previous circuits. The frequency deviation of the second modulation is usually selected smaller (i.e., such that even at maximum range there will be no more than one or two components in the spectrum of the

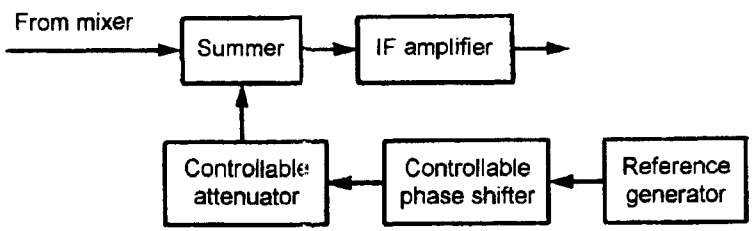

Figure 4.17 Spillover cancellation circuit.

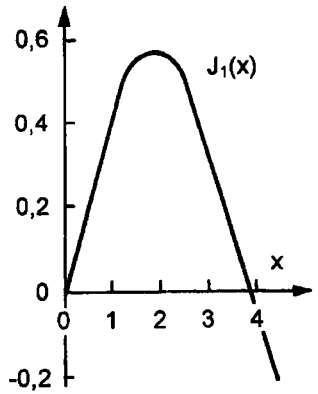

Figure 4.18 Graph of a cylindrical Bessel function of the first type and order 1.

second converted signal). It is also necessary that within the limits of measured ranges the component of the spectrum used have no nulls.

Referring to the profiles of cylindrical functions (Bessel functions) of the first kind (Figure 4.18), it is evident that this requires that the first component correspond to a Bessel function argument within a maximum range $X \approx 1.5$ to 1.7. Supposing $X = 1.57$, we obtain a simple relationship between the second deviation and maximal delay time

$$\Delta f_2 = 1/2\tau_{max} \tag{4.20}$$

If the delay time is measured in microseconds, we obtain a deviation in megahertz.

The basic difficulty in applying a dual modulation consists in separation of the necessary part of the entire spectrum of the converted signal. Figure 4.19 shows the spectrum of the converted signal.

We can see that, except for a low frequency portion of the spectrum dependent upon the frequency of the first modulation, there are lines clustered around of frequencies Ω_{m2} and $2\Omega_{m2}$. Let us consider in more detail the composition of these spectrum components. Rewriting (2.29) in more compact form:

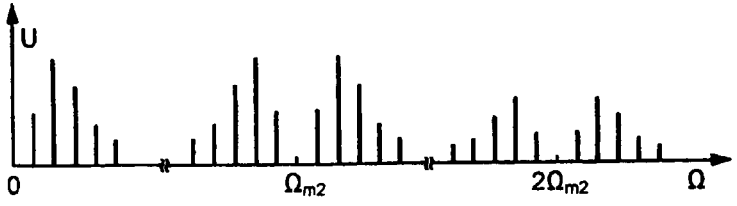

Figure 4.19 Spectrum of converted signal with dual modulation.

$$\begin{aligned}\varphi_t(t,\tau) &= \underbrace{\pm\Omega_D t + \varphi_\tau - \varphi_0 + \Delta\omega_1 F_{t1}(t,\tau)}_{\psi(t,\tau)} + \Delta\omega_2 F_{t2}(t,\tau) \\ &= \psi(t,\tau) + \Delta\omega_2 F_{t2}(t,\tau)\end{aligned} \tag{4.21}$$

then (2.30) can be rewritten in the form

$$u_t = U_t\left\{\cos\psi(t,\tau)\cos\Delta\omega_2 F_{t2}(t,\tau) - \sin\psi(t,\tau)\sin\Delta\omega_2 F_{t2}(t,\tau)\right\} \tag{4.22}$$

As we can see, the multiplicands $\cos\psi(t,\tau)$ and $\sin\psi(t,\tau)$ are generated only by the first modulation and the Doppler effect. Accordingly, multiplicands $\cos\Delta\omega_2 F_{t2}(t,\tau)$ and $\sin\Delta\omega_2 F_{t2}(t,\tau)$ are generated only by the second modulation and can be expressed by a Fourier series.

Then, supposing $T_{m2} >> \tau$ and using (3.2), (3.6), (3.7), we obtain

$$\cos\Delta\omega_2 F_{t2}(t,\tau) = J_0(X_2) - 2J_2(X_2)\cos 2\Omega_{m2}(t-\tau/2) \tag{4.23}$$

$$\sin\Delta\omega_2 F_{t2}(t,\tau) = 2J_1(X_2)\cos\Omega_{m2}(t-\tau/2) \tag{4.24}$$

After expansion only the first three components of spectrum are necessary, as the amplitudes of remaining components are very small and it is possible to neglect them. Finally, we obtain

$$u_t = U_t\left\{\begin{matrix} J_0(X_2)\cos\psi(t,\tau) - 2J_1(X_2)\cos\Omega_{m2}(t-\tau/2)\sin\psi(t,\tau) \\ -2J_2(X_2)\cos 2\Omega_{m2}(t-\tau/2)\cos\psi(t,\tau)\end{matrix}\right\} \tag{4.25}$$

The useful component of the spectrum is the second, which is located in the region of frequency Ω_{m2}. It is easily selected with a bandpass filter, as the spectrum generated by the first modulation is significantly narrower than that of the second modulation frequency. Thus, on the output of the bandpass filter with unity gain we have

$$\begin{aligned}U_{out} &= U_t 2J_1(X_2)\cos\Omega_{m2}(t-\tau/2)\sin\psi(t,\tau) \\ &= U_t J_1(X_2)\left\{\begin{matrix}\sin\left[\Omega_{m2}(t-\tau/2)+\psi(t,\tau)\right] \\ -\sin\left[\Omega_{m2}(t-\tau/2)-\psi(t,\tau)\right]\end{matrix}\right\}\end{aligned} \tag{4.26}$$

As we can see, the suppressed-carrier AM signal is present at the output of the filter, and there is no FM on this signal. This signal consists of two signals, the spectra of which are overlapped, and it is impossible to separate them with filters.

It is possible to apply, for suppression of one signal, the well-known phase-compensation method of deriving an SSB signal. For this it is necessary to obtain a second converted signal with 90° phase shift, namely the signal

$$u_t = U_t \sin\left[\psi(t,\tau) + \Delta\omega_2 F_{t2}(t,\tau)\right] = U_t \left\{ \begin{array}{l} \sin\psi(t,\tau)\cos\Delta\omega_2 F_{t2}(t,\tau) \\ \quad + \cos\psi(t,\tau)\sin\Delta\omega_2 F_{t2}(t,\tau) \end{array} \right\} \tag{4.27}$$

For this purpose there must be a second SHF mixer, to which the direct signal with a phase shift of 90° is applied. Further, from the spectrum of the second converted signal we obtain the applicable signal

$$U_{out} = U_t 2J_1(X_2)\cos\Omega_{m2}(t-\tau/2)\cos\psi(t,\tau) = U_t J_1(X_2)\left\{ \begin{array}{l} \cos\left[\Omega_{m2}(t-\tau/2)+\psi(t,\tau)\right] \\ \quad + \cos\left[\Omega_{m2}(t-\tau/2)-\psi(t,\tau)\right] \end{array} \right\} \tag{4.28}$$

One of the signals U_{out} is shifted in phase by 90°, then is added to the other signal U_{out}. The result is a single sideband FM signal with a central frequency Ω_{m2}. The appropriate block diagram is shown in Figure 4.20.

As in the version with shift of the forward signal central frequency, this SRR receiver is rather complicated. As two phase shifters for the direct signals are required, the application of the single-antenna version is precluded. Phase-shifting of signals by 90° does not introduce significant engineering difficulties, as these signals are narrowband. At the same time, the receiver requires careful alignment.

These methods of processing the converted signal certainly have many positive qualities. These include linearity and continuity of range readout with simultaneous speed measurement, the absence of Doppler influence on range measurement,

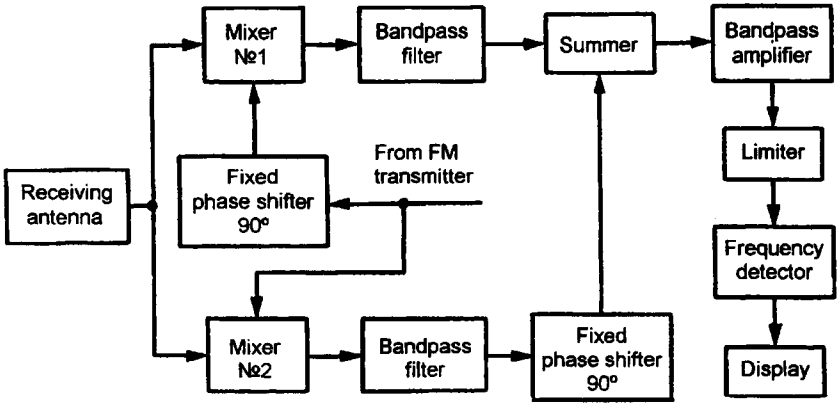

Figure 4.20 Block diagram of single-sideband processor.

and the possibility of measuring of very small ranges (1m or less), with rather small frequency deviation. Certainly, a large disadvantage is the necessity of using two antennas, and of ensuring high decoupling between them. Also, the complication of the circuit may be excessive relative to its performance. Therefore these methods have not received widespread use.

4.4.6 Single-Antenna Version with Zero Intermediate Frequency

Consider a converted signal with sinusoidal modulation applied to a lowpass filter with linearly increasing frequency response (we will call this a "shaping filter") (Figure 4.21). Let us assume that the frequency of the converted signal varies slowly and the quasi-stationary representation for passing of the FM signal through the reshaping filter is possible (the condition of applicability of this representation is shown below). Then an AM-FM signal will appear at the output of this filter, the envelope of which is proportional to the instantaneous frequency of the converted signal. It is sufficient to detect this signal with an amplitude detector, and from the resulting voltage to select with a filter a voltage with frequency $2F_m$. The amplitude of this voltage is proportional to the frequency deviation of the converted signal (i.e., to target range) and does not depend on the Doppler effect. The frequency deviation in adjacent half-cycles differs by $2\Omega_D$ (see Figure 3.1), and the average voltage is selected by filtering. This apparently very simple solution cannot be realized for the following reason: clearly, the output voltage of this circuit depends not only on range, but also on the amplitude of the converted signal. To apply amplitude limitation to the converted signal in this case is impossible because this signal is broadband. Hence it is impossible to filter higher harmonics originating in the limiter.

Therefore in this case it is necessary to apply an amplifier with AGC instead of the limiting device for normalization of converted signal amplitude. The frequency response of this amplifier should be constant in the entire frequency range of the converted signal spectrum, except for the first several components. It is necessary to eliminate these first components because the frequency of the envelope

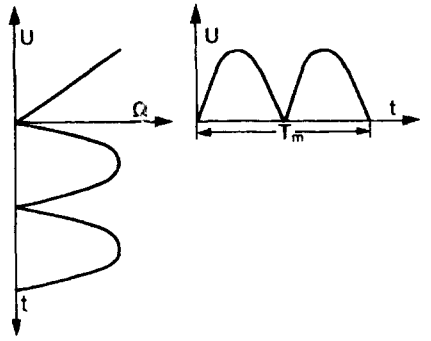

Figure 4.21 Conversion of frequency to voltage.

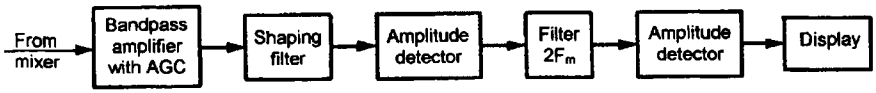

Figure 4.22 Processing of single-antenna signal using AGC.

of the received AM signal is equal to $2F_m$ and is commensurable with a low frequency part of the instantaneous frequency range of the converted signal. Therefore, normal detection of targets in this band of frequencies is impossible. After that, the normalized signal arrives on the shaping filter, and so forth (Figure 4.22).

Let us consider the condition for applicability of the quasi-stationary representation for passing the FM signal. In theoretical publications on this problem, it is shown that this representation is applicable if the following condition is satisfied:

$$B >> 2\sqrt{\Delta\omega\Omega} \tag{4.29}$$

where B is the filter passband, $\Delta\omega$ is the frequency deviation of affecting FM signal, and Ω is the modulation frequency. The most difficult condition for applicability takes place when the frequency deviation of the converted signal is commensurable with the bandpass of the reshaping filter. Taking into consideration that in this case $\Omega = 2\Omega_m$, we obtain a simple relationship linking the modulation frequency to the frequency deviation

$$\Omega_m << 0.1\Delta\Omega_t \tag{4.30}$$

Technically this condition is easily met. For example, with a maximum range $\Omega_m = 100\Delta\Omega_t$ it corresponds to the product $\Delta f\tau \approx 30$ (i.e., to a deviation of 30 MHz at a range of 150m, or 300 MHz at 15m).

The range measuring error in this version depends basically on the quality of normalization of the converted signal and the quality of the frequency response of the reshaping filter.

4.4.7 Fixing the Frequency Deviation of the Converted Signal

The method of fixing one of the parameters of the converted signal can be realized by fixing the frequency deviation of this signal. The basic engineering problem that must then be solved is the design of the applicable discriminator. As we will show, it is rather simple to make such a discriminator. To show the possibility of deriving discrimination performance, we will consider the character of variation of amplitude of the first spectrum harmonic of some periodic function $y(t)$. For this purpose we refer to Figure 4.23.

As we can see, the function $y = f(x) = 1$ in segment $x_1 \le x \le x_2$ and monotonically decreases to 0 for $x > x_2$. Let us assume also that function $\varphi(t)$ is a periodic even function monotonically descending from 1 to 0 as t varies from 0 to $T/2$.

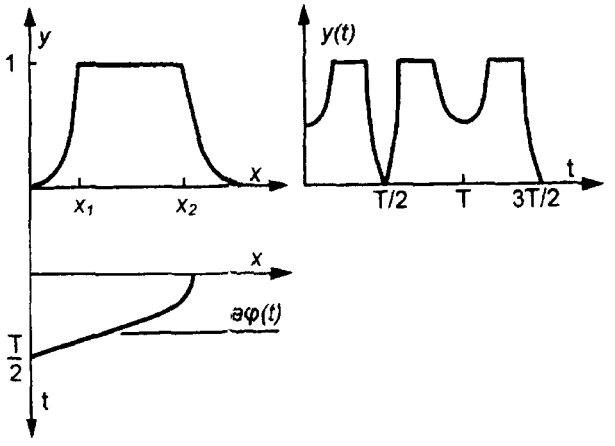

Figure 4.23 Plot for calculation of the discriminator.

Supposing $x = a\varphi(t)$, we form a function $y(t) = f[a\varphi(t)]$, where a is a factor dependent neither on x nor on t.

Let us consider the dependence of function $y(t)$ on the factor a. Note that the function $y(t)$, as well as $\varphi(t)$, is periodic and even. We see that $x_1 \le a \le x_2$ for $y(t) = 1$. With increase in a beyond x_2 at times $t = nT$ ($n = 0, 1, 2, \ldots$), the function $y(t)$ has a minimum, which decreases with increase of a. Thus the region for which $y(t)$ = maximum is displaced to times $t = (2n + 1)T/2$.

Having clarified the regularity of variation of function $y(t)$ with factor a, we consider dependence of the first spectral harmonic of $y(t)$ on that same factor. By virtue of the even nature of $y(t)$, the first harmonic of its spectrum is found as

$$y_1 = \frac{4}{T}\left[\int_0^{T/4} y(t)\cos\frac{2\pi}{T}t \;\; dt + \int_{T/4}^{T/2} y(t)\cos\frac{2\pi}{T}t \;\; dt\right] \tag{4.31}$$

With variation in a within limits from x_1 to x_2, we see that $y_1 \approx$ const. With further increase of a, the amplitude of the first harmonic drops because of a decrease of the first integral, and at reaching equality

$$\int_0^{T/4} y(t)\cos\frac{2\pi}{T}t \;\; dt = -\int_{T/4}^{T/2} y(t)\cos\frac{2\pi}{T}t \;\; dt \tag{4.32}$$

it goes to zero. The increase in factor a results in a further decrease of the first integral in (4.32), because of which the amplitude of the first harmonic becomes negative (i.e., the phase of the harmonic is reversed at 180°).

We will obtain particular variations of the first harmonic amplitude for particular functions $f(x)$ and $\varphi(t)$. Assuming that $f(x) = 1$ for $x_1 \le x \le x_2$, and $f(x) = 0$ for $x \le x_1$, $x \ge x_2$, we find

$$\varphi(t) = \cos\frac{\pi}{T}t \quad \text{for} \quad -\frac{T}{2} \le t \le \frac{T}{2}. \tag{4.33}$$

In this case amplitude of the spectrum first harmonic is described by the following expressions:

$$y_1 = 0 \quad \text{for } a \le x_1 \tag{4.34}$$

$$y_1 = \frac{4x_1}{\pi a}\sqrt{1-\left(\frac{x_1}{a}\right)^2} \quad \text{for } x_1 \le a \le x_2 \tag{4.35}$$

$$y_1 = \frac{4}{\pi}\left[\frac{x_1}{a}\sqrt{1-\left(\frac{x_1}{a}\right)^2} - \frac{x_2}{a}\sqrt{1-\left(\frac{x_2}{a}\right)^2}\right] \quad \text{for } a \ge x_2 \tag{4.36}$$

A plot of the variation of the first harmonic amplitude with the ratio a/x_2, provided that $x_1 = 0.5x_2$, is shown in Figure 4.24. As we can see, it is the typical discriminator characteristic.

It is possible to realize particular proportions, physically, having realized functions $f(x)$ and $a\varphi(t)$. In a context of this description it is seen that the function $a\varphi(t)$ describes the instantaneous frequency of a converted signal with sinusoidal modulation, and the factor a is proportional to the frequency deviation. Then the function $f(x)$ can be realized using a serial connection of a bandpass filter with the

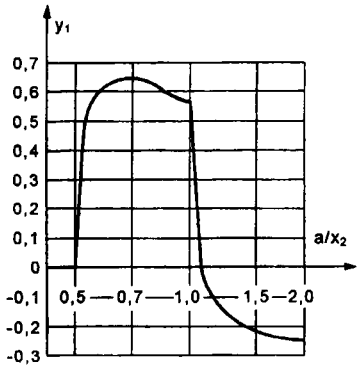

Figure 4.24 Magnitude of first harmonic as a function of a/x_2.

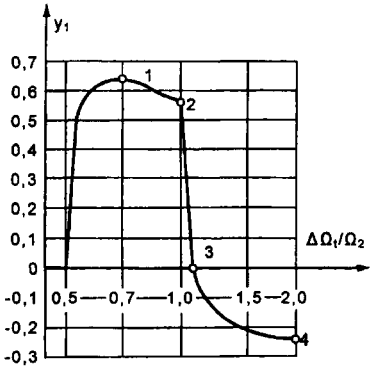

Figure 4.25 Discriminator characteristic.

applicable frequency response and an amplitude detector (we will call this filter, as well as that in the previous paragraph, a shaping filter). To separate the first harmonic of the output signal spectrum of an amplitude detector it is passed through a narrowband filter with a resonant frequency $2\Omega_m$.

Supposing that the frequency response of the shaping filter is ideally rectangular in the frequency range from Ω_1 to Ω_2, (4.35) and (4.36) now take the form

$$y_1 = \frac{4}{\pi}\frac{\Omega_1}{\Delta\Omega_t}\sqrt{1-\left(\frac{\Omega_1}{\Delta\Omega_t}\right)^2} \quad \text{for } \Omega_1 \le \Delta\Omega_t \le \Omega_2 \tag{4.37}$$

$$y_1 = \frac{4}{\pi}\left[\frac{\Omega_1}{\Delta\Omega_t}\sqrt{1-\left(\frac{\Omega_1}{\Delta\Omega_t}\right)^2} - \frac{\Omega_2}{\Delta\Omega_t}\sqrt{1-\left(\frac{\Omega_2}{\Delta\Omega_t}\right)^2}\right] \quad \text{for } \Delta\Omega_t \ge \Omega_2 \tag{4.38}$$

where $\Delta\Omega_t$ is the frequency deviation of the converted signal defined in (3.5). In Figure 4.25 we show the profile of the discriminator characteristic described by (4.37) and (4.38) for $\Omega_2/\Omega_1 = 2$. The coordinates of characteristic points of this characteristic are given by the following formulas:

Point of maximum positive response (1):
$$y_1 = \frac{2}{\pi}, \quad \frac{\Delta\Omega_t}{\Omega_2} = \frac{\Omega_1}{\Omega_2}\sqrt{2} \tag{4.39}$$

Inflection point (2):
$$y_1 = \frac{4}{\pi}\frac{\Omega_1}{\Omega_2}\sqrt{1-\left(\frac{\Omega_1}{\Omega_2}\right)^2}, \quad \frac{\Delta\Omega_t}{\Omega_2} = 1 \tag{4.40}$$

Null point of the characteristic (3):
$$y_1 = 0, \quad \frac{\Delta\Omega_t}{\Omega_2} = \sqrt{1+\left(\frac{\Omega_1}{\Omega_2}\right)^2} \tag{4.41}$$

Point of maximum negative response (4):
$$y_1 \approx \frac{4}{\pi}\left[-\frac{1}{2} - \frac{1}{\sqrt{2}(\Omega_2/\Omega_1 + \Omega_1/\Omega_2)}\right], \quad \frac{\Delta\Omega_t}{\Omega_2} = \sqrt{2+2\left(\frac{\Omega_1}{\Omega_2}\right)^2} \tag{4.42}$$

The simplified formulas correspond to an idealized discriminator characteristic.

The formula for the significant characteristic is connected first of all with the problem of passing of FM oscillations through linear quadripoles. In general this problem consists of determination of the law of signal amplitude and frequency variations at the output of a quadripole, given an FM signal as its input. A full

solution of this problem has not yet been obtained, and there are only separate proprietary results.

In this case we must solve a simpler problem. Ignore here the frequency shift of the output signal, as it will be applied to an amplitude detector. With respect to amplitude variation only one part, the gap in amplitude, is of interest, because of which there is a reversal of phase of the first harmonic. But the solution of this problem becomes complicated by the fact that the instantaneous frequency of the input signal may necessarily exceed the limits of band pass of the quadripole (shaping filter). Therefore the quasi-stationary method is inapplicable. This leaves only the method of stationary phase [3]. This method does not give a precise solution, but does give a good approximation.

As the frequency deviation of the converted signal is generated at frequency Ω_2, the problem is reduced to calculation of the modulation frequency at which the zero point of the discriminator characteristic is shifted to the right of its allowable magnitude, compared with the ideal characteristic. In other words, how rapidly can the instantaneous frequency of the converted signal be changed?

Omitting the rather cumbersome calculations, we will produce a final result, the formula for calculation of modulation frequency:

$$\Omega_m \le \Omega_2\left(1-\frac{\Omega_1}{\Omega_2}\right)\left(0.2-\frac{1}{2\pi\beta_1\sqrt{1+(\Omega_1/\Omega_2)^2}}\right), \tag{4.43}$$

where $\beta_1 \ge 1.2$ is a coefficient describing the null shift of the real discriminator characteristic as contrasted with the theoretical one. For example, for $\beta_1 = 1.2$, $\Omega_2/\Omega_1 = 2$, $\Omega_m \le \Omega_2/25$ it corresponds to a product $\Delta f\tau = 25/\pi \approx 8$. Thus, at 15m range a deviation of 80 MHz is required.

It is also possible to evaluate precisely the influence of a trapezoidal filter frequency response on the shift of the zero point of the discriminator characteristic. As shown by calculations, the high-frequency lobe of this characteristic exercises primary influence over the shift of the null. The applicable profile for a similar coefficient β_2 is shown in Figure 4.26.

The shift of the null of the discriminator characteristic is influenced, of

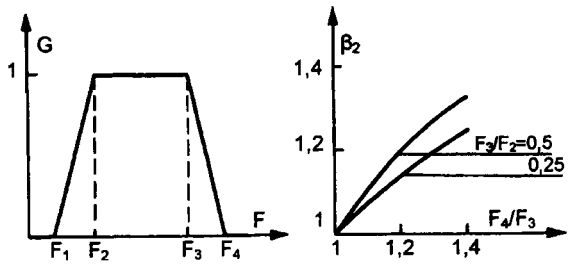

Figure 4.26 Plot of the coefficient β_2.

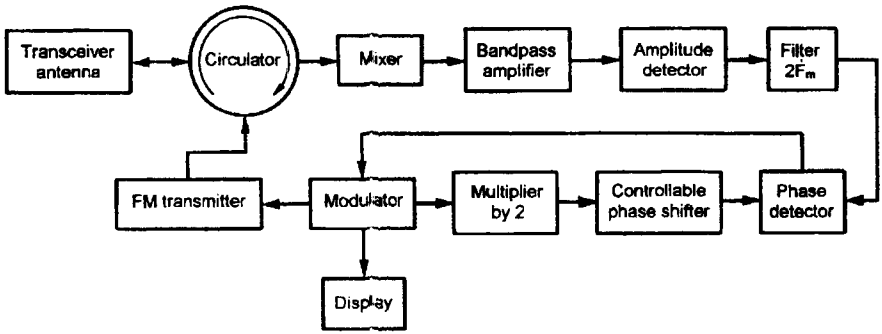

Figure 4.27 SRR using fixed frequency deviation of converted signal.

course, by Doppler effect. But this influence can be reduced to an acceptable minimum by increasing the modulation frequency, and, accordingly the upper boundary frequency of the frequency response of the filter. The block diagram of an SRR with this discriminator is shown in Figure 4.27. It in many respects is similar to the circuit that fixes the instantaneous frequency (Figure 4.13) and does not require further special explanation. The phase shifter in the reference signal circuit is included for cancellation of the phase shift generated in passing the signal through the processing unit. The search unit is omitted here, as it is always possible to establish an initial value of frequency deviation such that the instantaneous frequency of the converted signal will be in the filter passband, following which the automatic control system will lock.

4.5 PHASE PROCESSING OF THE CONVERTED SIGNAL

Strange as it may seem, phase processing of the converted signal has not found broad application, though the elements of the theory were obtained more than a half-century ago. Apparently, this is explained by the fact that 30 to 40 years ago technical factors did not allow realization of this type of processing. In particular, it was impossible to construct a sufficiently compact arithmetic-logic unit to perform the calculations necessary for phase processing. There was also probably no practical need for its realization. The key feature of phase processing is that its application allows us to measure short ranges, from fractions of a meter up to hundreds of meters, with an error no more than one-tenth of one percent. Naturally, such precise measurement can be realized only with definite technical characteristics both in the SRR and the target.

In particular, if the frequency deviation of the oscillator is varied during operation even as much as one percent, a range error less than one percent cannot be provided. Also, for example, a range of 10m can be measured with error of some millimeters. But the reflecting surface is usually rough, with amplitude of surface irregularities of some centimeters. Obviously, applying phase processing in this

case makes little sense. Thus, phase processing is most useful for application in high-precision fluid-level meters in closed tanks, and measuring displacement of various targets and constructions.

The principle of phase processing and the resulting small measuring error are based on the following calculations. As already shown, the phase shift of the converted signal in the interval between two maxima of the modulating function, which are equal to +0.5 and –0.5, is given by

$$\Delta\varphi_t(t,\tau) = \omega_c\tau + \Delta\omega\tau 0,5 - \varphi_0 - \omega_c\tau + \Delta\omega\tau 0,5 + \varphi_0 = \Delta\omega\tau. \qquad (4.44)$$

If the maxima of the modulating function are at the beginning and end of a period, this will be the phase shift for a modulation period. This case, in particular, corresponds to modulation with an asymmetrical sawtooth function. At the same time, as follows from (4.44), the phase shift does not depend on the modulation waveform. It is important only that the values of the converted signal phase are fixed at the moments of the minimum and maximum of the modulating function. From (4.44), it follows that by measuring a phase shift $\Delta\varphi_t(t,\tau)$ and knowing a frequency deviation, it is easy to determine echo delay (i.e., target range).

Let us assume that $\Delta\varphi_t(t,\tau)$ =1,000° and that the inaccuracy of phase shift measurement is equal to 1°. Then the relative inaccuracy of range measurement is equal to 10^{-3}. The measuring of a phase shift with such a small error does not introduce any engineering difficulties in this case, as it is made with a modulation frequency that one can set low enough (for example, 100 to 1,000 Hz).

For example, if the range is 15m and frequency deviation is 100 MHz, then $\Delta\varphi_t(t,\tau)$ = 360° × 10 = 3,600°, and if the inaccuracy of the phase shift measurement is 1°, the range error is ≈4.2 mm. Let us note that with a deviation of 100 MHz, the range error from counting number of nulls or maxima of the converted signal for a modulation period is 180 times greater, or 75 cm. Thus, it is possible to arrive at the conclusion that phase processing is very effective as well as simple. But many factors prevent realization of such simple processing. First, the initial phase of the converted signal at the start of the modulation period, as well as phase values in the final parts of the period, are obscure. Obviously, without determination of these phases it is impossible to determine the phase shift $\Delta\omega\tau$.

Second, measurement of the phase shift $\Delta\varphi_t(t,\tau)$ is complicated by the fact that the phase varies nonlinearly in time because of nonlinearity of the modulation characteristic of the FM oscillator and nonlinearity of the modulating voltage. Third, to achieve measurement of fractions of one percent, it is necessary to maintain the magnitude of the frequency deviation with the same fidelity.

Let us consider possible ways of overcoming these difficulties in realization of phase processing. At first we will consider how to determine the phase shift $\Delta\varphi_t(t,\tau) = \Delta\omega\tau$. For determination of this phase shift it is most convenient to use linear frequency modulation (for example, an asymmetrical sawtooth function). If the frequency of the FM oscillator were modulated ideally under the linear law, the

measuring of a phase shift would be unnecessary: it would be sufficient to measure a period of the converted signal T, then

$$\Delta\varphi_t(t,\tau) = 2\pi T_m / T \tag{4.45}$$

Such an algorithm of calculation is possible when using a frequency synthesizer as the FM oscillator, where it is possible to derive an ideally linear modulation characteristic (Section 3.4).

For more usual oscillators the modulation characteristic is nonlinear, and therefore the converted signal represents a sample of a sine wave with a variable period. The variation of the period is no more than several percent of its average value, but the inaccuracy of calculating the phase shift in (4.45) will also cause an error of some percent. If such inaccuracy of measurement in the given particular case is allowable, the problem is resolved.

If it is not allowable, more complex methods for determination of $\Delta\varphi_t(t,\tau)$ rather than those under (4.45) are required.

Let us consider these calculations, for which we will refer to Figure 4.28, where a converted signal with variable frequency is shown.

In essence, the problem is reduced to determination of the phase shift of the converted signal in time periods $t_0 \ldots t_1$ and $t_4 \ldots T_m$. In the time interval $t_1 \ldots t_4$, the integer number of half-cycles of the converted signal is retained, and therefore the phase shift in this time period is obtained by multiplying the number of half-cycles by 180°.

For determination of phase shift in time intervals $t_0 \ldots t_1$ and $t_4 \ldots T_m$, it is convenient to compare the duration of these intervals with adjacent half-cycles, as it is possible to consider a phase change in two adjacent half-cycles linear enough. Then

$$\Delta\varphi_{0-1} = \pi \frac{t_1 - t_0}{t_2 - t_1} \tag{4.46}$$

and

$$\Delta\varphi_{4-T_m} = \pi \frac{T_m - t_4}{t_4 - t_3} \tag{4.47}$$

after which

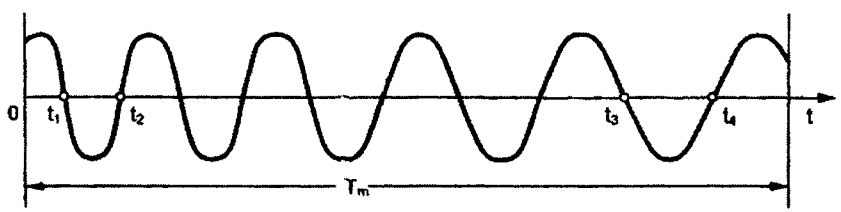

Figure 4.28 Plot of converted signal with variable frequency.

$$\Delta\varphi_t(\tau) = \pi k + \Delta\varphi_{0-1} + \Delta\varphi_{4-T_m}, \tag{4.48}$$

where k is the integer number of half-cycles of the converted signal in a period of modulation.

For estimation of utility of this algorithm we will estimate the measurement error of a phase shift with real nonlinearity of the FM oscillator modulation characteristic. It is most simple and convenient to approximate a working section of modulation characteristic by the sum of a linear function and quadratic (parabolic) function [Figure 4.29(a)]. The shape of the modulation characteristic using this approximation corresponds to the most frequently encountered real modulation characteristics.

In this case, the phase of the converted signal with linear-frequency modulation also varies in time under the same law [Figure 4.29(b)] and can be expressed as

$$\varphi_t(t,\tau) = \Delta\omega\tau a - 4\delta\varphi(a^2 - a) + \varphi_0 \tag{4.49}$$

where $\delta\varphi = q\Delta\omega\tau$ is the factor that determines the magnitude of nonlinearity of the modulation characteristic, $a = (t - t_0)/T_m$, and φ_0 is the initial phase.

The greatest error in determination of phase shift is when for a period of modulation an almost integer number of half-cycles of the converted signal will be received (i.e., the phase shift in time intervals $t_0 \ldots t_1$ and $t_4 \ldots T_m$ will differ from 180° by fractions of one degree). Therefore for calculation it is expedient to put this shift equal to 180° (or π), and φ_0=0.

For calculation of the phase shift in the interval $t_0 \ldots t_1$ it is necessary to determine intervals of time $t_0 \ldots t_1$ and $t_1 \ldots t_2$, and then determine the phase shift from (4.48) [Figure 4.29(c)]. The difference of the computed result from 180° will determine the error.

Equating (4.49) to π, assuming $\Delta\omega\tau = k\pi$, and solving the resulting equation with for $(t_1 - t_0)/T_m$, we find

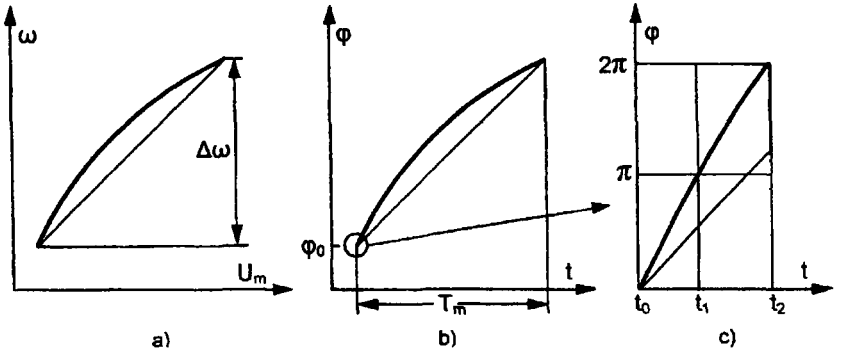

Figure 4.29 Illustration of the phase calculation.

$$(t_1 - t_0)/T_m = z\left(1 - \sqrt{1-x}\right) \tag{4.50}$$

where $x = 16q/(1 + 4q)^2k$ and $z = (1 + 4q)/8q$. Similarly, equating (4.49) to 2π, we find

$$(t_2 - t_0)/T_m = z(1 - \sqrt{1-2x}) \tag{4.51}$$

Substituting (4.50) and (4.51) in (4.46), we obtain

$$\Delta\varphi_{0\text{-}1} = \pi \frac{1 - \sqrt{1-x}}{\sqrt{1-x} - \sqrt{1-2x}} \tag{4.52}$$

Carrying out similar calculus for $\Delta\varphi_{4\text{-}T_m}$, we obtain

$$\Delta\varphi_{4\text{-}T_m} = \pi \frac{1 - z\left(1 - \sqrt{1-x(k-1)}\right)}{z\left(\sqrt{1-x(k-2)} - \sqrt{1-x(k-1)}\right)}. \tag{4.53}$$

Subtracting π from (4.52) and (4.53) and adding the results, we obtain the error of calculating the phase shift $\delta(\Delta\varphi_i)$. The results of these calculations are shown in Figure 4.30.

As we can see, even for small numbers of half-cycles (15 ... 20) the inaccuracy of the phase shift measurement does not exceed fractions of one percent. Thus, the method of calculation described allows us to determine a phase shift with an obscure initial phase and nonlinear FM oscillator modulation characteristic.

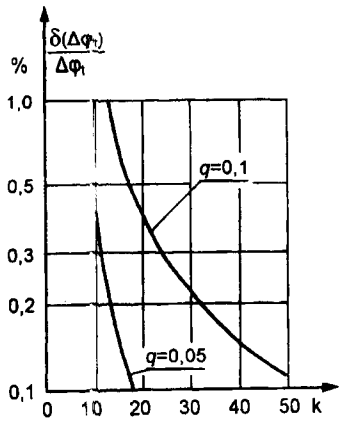

Figure 4.30 Phase error versus number of half-cycles in modulation period.

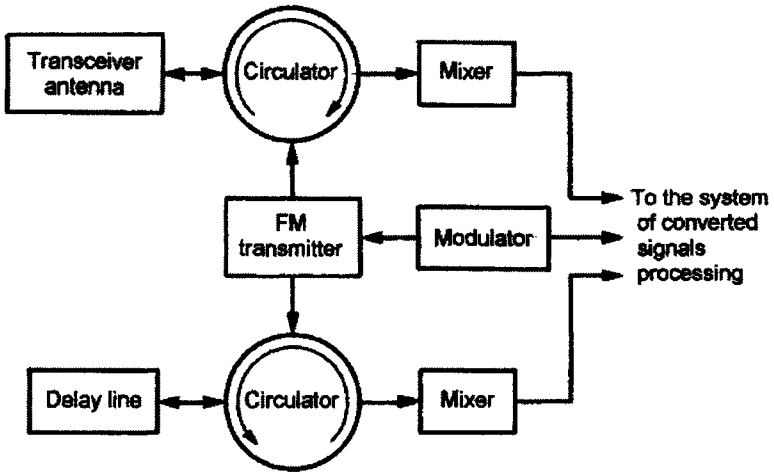

Figure 4.31 Range measurement using calibration channel.

Now we proceed to a problem of stabilizing the frequency deviation of the oscillator. As already stated, one method is use of a frequency synthesizer or calibration channel. The second method is for the frequency deviation of the oscillator to remain unstabilized relative to its nominal value. Through a calibration channel, the true value of the deviation is determined and the applicable correction in calculation of target range is entered. In many cases this method can appear as simpler and sufficiently effective.

As an example we will consider one possible realization of this method. This was applied in combination with the previously mentioned phase processing of the converted signal in development of a high-precision SRR for liquid level measurement in a closed tank [4]. The block diagram of the radio-frequency unit that includes the calibration channel is shown in Figure 4.31.

As we can see, the signal from the FM oscillator branches, one part of it arriving at the measuring channel circulator and one part at the calibration channel circulator. The transceiving antenna is connected to the measuring channel circulator. The delay line, short-circuited at the end, is connected to the calibration channel circulator. The modulation is an asymmetrical sawtooth voltage.

For an explanation of the algorithm of calibrating and measuring channel interaction we refer to Figure 4.32, which shows the waveforms of the radiated signal frequency change (a) and the limited converted signals of calibrating (b) and measurement (c) channels.

At time t_b, when the instantaneous value of the calibration channel converted signal passes through zero in a positive direction, the readout of phase shift for both calibrating and measurement converted signals starts. The process of measuring phase shift stops at t_e when a definite number of periods of the calibrating

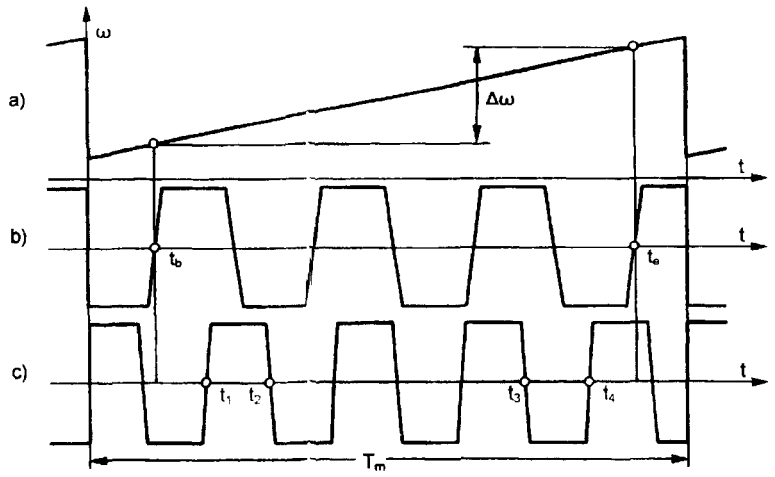

Figure 4.32 Plots of frequency of transmission and limited converted signals.

converted signal, constant for the given instrument, (three periods in Figure 4.32) will have passed. Obviously, the phase shift of the calibrating converted signal is

$$\Delta\varphi_c = \Delta\omega\tau_d = 2\pi n, \tag{4.54}$$

where $\Delta\omega$ is the magnitude of frequency change of the FM oscillator during the period from t_b to t_e, τ_d is the delay time of the signal in the delay line, and n is the number of periods of the calibrating converted signal.

The nonlinearity of the FM oscillator modulation characteristic does not influence the magnitude of the phase shift $\Delta\varphi_c$, as during measurement an integral number of periods of the calibrating converted signal has passed. The phase shift of the measuring converted signal is

$$\Delta\varphi_t(\tau) = \Delta\omega\tau = \pi\left(k + \frac{t_1 - t_b}{t_2 - t_1} + \frac{t_e - t_4}{t_4 - t_3}\right) \tag{4.55}$$

where k is an integral number of half-cycles in the period $t_b \ldots t_e$. Substituting $\Delta\omega$ from (4.54) in (4.55) and solving for τ, we obtain

$$\tau = \tau_d \frac{\Delta\varphi(t)}{2\pi n} = C\Delta\varphi_t(\tau), \tag{4.56}$$

where $C = \tau_d/2\pi n$ = const, a coefficient defined only by parameters of the delay line and the number of periods n, which are known for the given instrument.

Instability of the center frequency and slope of the modulation characteristic of the FM oscillator do not influence the error in measurement of delay time of the target echo. Let us estimate the effect of target motion on measurement error. For this purpose assume that as a result of motion the phase shift is shifted to magnitude $\delta\varphi$ for a modulation period. Then $\delta\varphi = \Delta\omega\delta\tau$, where $\delta\tau$ is the variation of time delay for a modulation period. From the last formula it is easy to obtain the expression for the allowable speed of the target

$$V = \frac{\delta\varphi C F_m}{720\Delta f} \tag{4.57}$$

where $\delta\omega$ is determined in degrees, and C is the velocity of light.

For example, if $\delta\omega = 0.1°$ and $F_m = 1$ kHz, $V = 0.4$ m/s. For targets requiring such precise measurement (for example, in liquid-level measurement in wrap-around tanks), such speed is not experienced. For example, variation of gasoline level with such speed in the reservoir of a filling station with the surface space 3m × 6m corresponds to speed of fill in (or draining) 7.2 m^3/s, which is completely unrealistic.

References

[1] Skolnik, M. I. (ed.) *Radar Handbook*, 2nd ed., New York: McGraw-Hill Book Company, 1990, p. 14.1.

[2] Ismail, M. A. W., *A Study of the Double Modulated FM Radar*, Zurich: Verlag Leemann, 1955.

[3] Jones, D. S., and M. Kline, "Asymptotic Expansion of Multiple Integrals and the Method of Stationary Phase," *J. Math. and Phys.*, 1958, XXXVII, 1.

[4] Komarov, I. V., and V. I. Pleshcheev, "High Precision Radar Gauge for Measuring Levels of Liquid and Powder Products in Closed Containers," *Konversia*, No. 8, 1996, pp. 49-51.

Chapter 5

Spectral Methods of Processing the Converted Signal

5.1 GENERAL DESCRIPTION

As indicated by its name, this processing method uses the parameters of the converted signal spectrum to obtain information on target range and radial velocity. These target parameters are measured by:

- Dependence of the amplitudes of spectral components on target range;
- Doppler frequency shift of spectral components;
- Phase of spectral components.

Spectral processing is most easily applied in SRRs using the block diagrams Figures 2.3 or 2.4 (see Chapter 2). In these circuits, the spectrum of the converted signal is in the range of frequencies that are multiples of the modulation frequency (i.e., rather low frequencies), substantially simplifying realization of the processing circuits. We will therefore examine the methods of spectral processing only with reference to such circuits.

The major advantage of spectral processing is the opportunity for the SRR to resolve several targets. As was shown in Section 4.1, the converted signal in this case represents the sum of the converted signals from each target. From spectral analysis theory it follows that the spectrum of the sum of the signals is equal to the sum of the spectra of each of them. Thus, using distinctions between signal spectra, it is possible to identify them separately.

Let us consider briefly the opportunities for use of the listed parameters of the converted signal spectrum. As follows from the analysis of Chapter 2, the dependence on target range of spectral component amplitudes of the converted signal is defined by the transmitted signal modulation waveform and the reflected signal level. This dependence is shown most distinctly in the case of asymmetrical

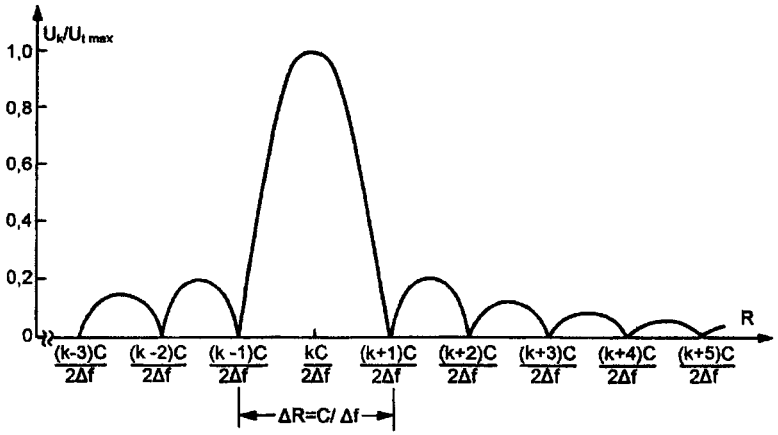

Figure 5.1 Variation of the *k*th component amplitude with range.

sawtooth modulation. In the following, unless noted otherwise, we examine the spectrum for this type of modulation.

To derive this dependence we express τ as a function of R in (3.20), obtaining the range dependence of the amplitude of the *k*th component. A diagram of this dependence is shown in Figure 5.1, for the larger component of the *k*th pair in the spectrum, whose amplitude given by

$$U_t \frac{\sin \pi(\Delta f \tau - k)}{\pi(\Delta f \tau - k)} = U_t \frac{\sin \pi\left(\Delta f \dfrac{2R}{C} - k\right)}{\pi\left(\Delta f \dfrac{2R}{C} - k\right)} \tag{5.1}$$

The range corresponding to the maximum amplitude of the *k*th component is determined by k and by the frequency deviation of the transmitted signal. At the same time, the range resolution ΔR, corresponding to the base width of the main response lobe, is determined only by the frequency deviation. Figure 5.2 shows a three-dimensional plot of the dependence on target range of the spectral component amplitudes. As we can see each spectral component reaches a maximum only for a particular value of range. We can measure range with a certain error using the number (or in practice the frequency) of the largest spectral component.

To obtain a spectral plot of echoes from a single target we take a section of Figure 5.2 in a plane perpendicular to the abscissa at a point corresponding to the target range. For example, in Figure 5.2, $R \approx 3.3C/2\Delta f$.

If there are two or more targets located at different ranges and within the antenna beam, we make two or more projections (Figure 5.3). As we can see, it is possible to resolve these objects and to measure the range of each. Note also that it

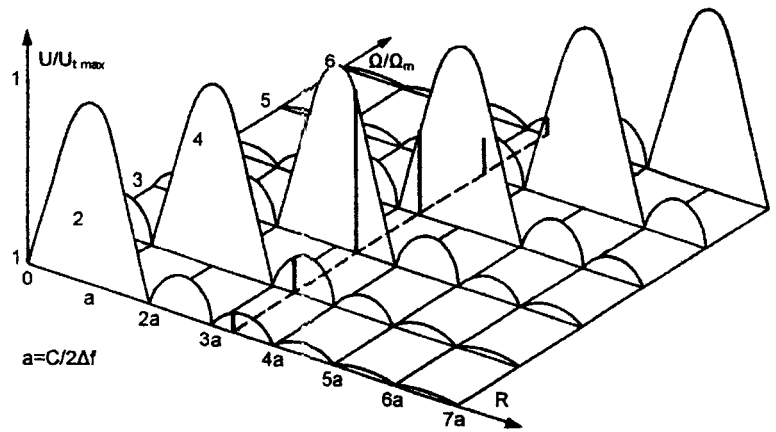

Figure 5.2 Spectral component amplitude dependence on target range.

is possible to use combinations of spectral components on the basis of dependence of their amplitudes on target range in realizing processing algorithms.

Consider now the phases of spectral components of the converted signal. In this case, as follows from the analysis in Chapter 2, the phases of spectral components do not depend on the frequency modulation waveform. For any modulation the phase of the kth component with frequency $k\Omega_m + \Omega_D$ is

$$(k\Omega_m + \Omega_D)t + \varphi_\tau - \varphi_0 - k\Omega_m \frac{\tau}{2} + \eta(\tau) \tag{5.2}$$

and for components with frequency $n\Omega_m - \Omega_D$,

$$(n\Omega_m - \Omega_D)t - \varphi_\tau + \varphi_0 - n\Omega_m \frac{\tau}{2} + \nu(\tau) \tag{5.3}$$

Thus the information on target range and radial velocity is present in the phase of any spectral component. The phase angles $\varphi_\tau = \omega_c\tau_0$ and $k\Omega_m\tau/2$ contain the range information, while angles $\eta(\tau)$ and $\nu(\tau)$ are equal or to zero or $\pi/2$ for the usual modulation waveforms. It is also useful to note that the kth component pair with frequencies $k\Omega_m + \Omega_D$ and $k\Omega_m - \Omega_D$ has phase angles φ_τ and φ_0 with different signs. As will be shown below, this permits cancellation of these angles. For range measurement it is also possible to use the phase angle $k\Omega_m\tau/2$, but for this a particular relationship of the modulation period to the reflected signal delay time is necessary.

On the basis of this brief review, we conclude that the use of the converted signal spectrum provides ample opportunities for design of various signal processing

algorithms and circuits. To work with a spectrum we must have it physically, but a mixer output contains the converted signal rather than its spectrum. Hence, we must process the converted signal in such a way as to extract its spectral parameters. Let us review this question in more detail.

In Chapters 2 and 3 the analysis of the converted signal spectrum was carried out to obtain its essential characteristics. In this case the spectral analysis of a *function* (the converted signal), given by its *analytical* expression, was carried out. Accordingly the spectrum was calculated *analytically*. In this chapter there is an analysis of a spectrum of a *physical* process (the converted signal) as it appears (i.e., in real time). Clearly this analysis must be only *physical*, and a corresponding circuit block, which we name the *analyzer*, is necessary for processing the converted signal.

Thus, spectral processing the converted signal depends on an analyzer whose output is a signal representing the converted signal spectrum in an appropriate form. This signal passes to the input of the spectral processing block, which as a rule exchanges information with the modulator and the output display. The processing block is in essence a special computer that processes the input information and produces the appropriate signal on the display. The program on which this computer works is defined by many SRR technical parameters.

Hence, the end result of spectral processing of the converted signal depends not only on its spectral parameters but also on properties of the analyzer and the processing block. An important feature of spectral processing is its ability to measure radial velocity of the target, including the sign of this velocity as well as its magnitude, simultaneously with range measurement. This ability depends on the Doppler shift of spectral components relative to frequencies that are multiples of the modulation frequency (see Chapter 3). Technically, measurement of speed is reduced to measurement of Doppler frequency. Methods of measurement of signal

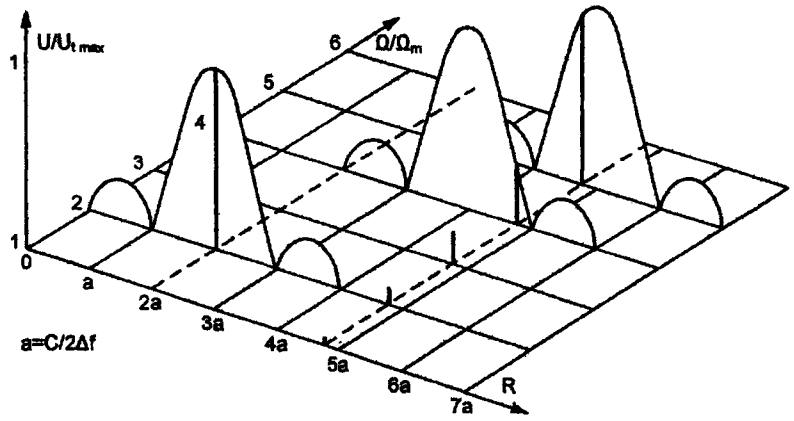

Figure 5.3 Spectrum component amplitude dependence on target range (two or more targets).

frequency and selection of its sign are well known, and therefore are not discussed in this chapter.

5.2 RANGE RESOLUTION

It is worth considering the question of SRR resolution, assuming that asymmetrical sawtooth modulation is used. Let us consider first an idealized picture of target arrangement.

We assume that there are two point targets in the main lobe of the SRR antenna pattern. The reflected signals from these targets are identical. The signal delays of the targets are τ_1 and τ_2, and the quantities $\Delta f\tau_1 = k$ and $\Delta f\tau_2 = n$ are equal, where k and n are integers. In this case the spectra of the target signals consist of unique components with frequencies $k\Omega_m$ and $n\Omega_m$ respectively, and the spectrum analyzer can identify these components as belonging to two targets. The minimal radial distance between the targets that can be resolved corresponds to $k \pm 1 = n$ [i.e., components appear as in Figure 5.4(a)]. Then from (3.20) it follows that $\Delta f\Delta\tau = 1$ and the minimal resolvable radial distance between the two targets is

$$\Delta R_{\min} = \frac{C}{2\Delta f} \tag{5.4}$$

Clearly this arrangement of targets is improbable. However, (5.4) defines the maximum possible range resolution of an FM SRR that serves as a reference for the actual range resolution.

Now let us assume that the targets are located such that $\Delta f\Delta\tau_1 = k \pm 0.5$ and $\Delta f\Delta\tau_2 = n \pm 0.5$ are equal, the most adverse condition for target resolution. In this case, two components located in the main lobe of the spectrum are produced by each object and the sidelobe components are maximal [Figure 5.4(b)]. If the maximal spectra components are adjacent, then $\Delta f\Delta\tau = 2$, and accordingly

$$\Delta R = 2\Delta R_{\min} = \frac{C}{\Delta f} \tag{5.5}$$

Certainly, for more reliable resolution between the maximal components there should be at least a minimal separation of one spectral component [Figure 5.4(c)], in which case

$$\Delta R = 3\Delta R_{\min} = 1.5\frac{C}{\Delta f} \tag{5.6}$$

The value of ΔR given by (5.5) or (5.6) is actually the theoretical optimal range resolution. Formally, we may draw the conclusion from (5.6) that ΔR is

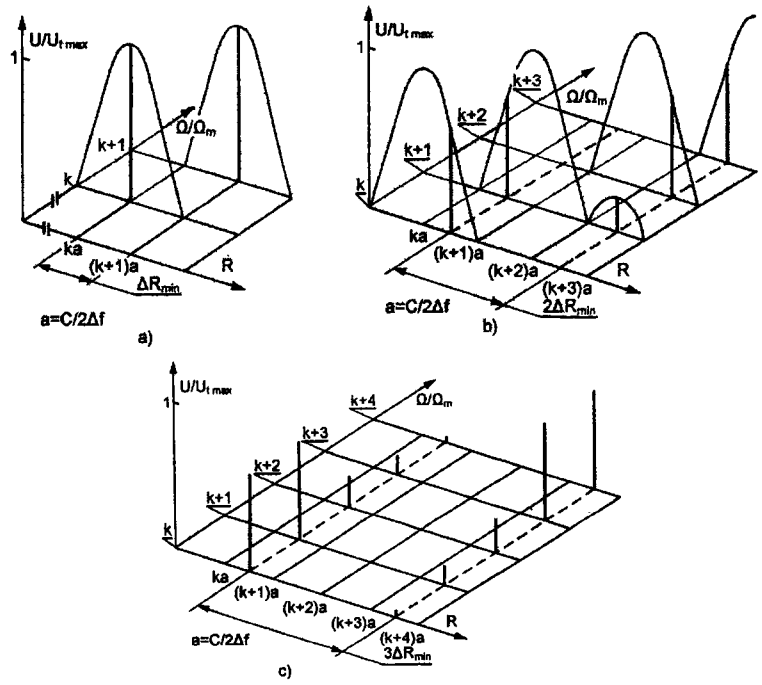

Figure 5.4 Illustration of range resolution for a fixed target.

limited only by the frequency deviation, but this is not absolutely true. This conclusion is applicable to SRRs operating at rather small ranges (e.g., several tens of meters) where very high resolution is required. For example, for ΔR = 1.5m a deviation near 300 MHz is required. At greater ranges (e.g., hundreds of meters or a few kilometers) resolution is limited also by the number of detectable spectral components. For given values of frequency deviation and target range the number of the largest spectral component is

$$n = \Delta f \frac{2R}{C}. \tag{5.7}$$

Determining from (5.6) a frequency deviation and substituting it into (5.7), we obtain

$$n = \frac{3R}{\Delta R}. \tag{5.8}$$

From (5.8) it follows, for example, that with R = 1500m and ΔR = 15m, then n = 300 and the required value of deviation is not too large: 30 MHz. Processing

of such numbers of components demands very high linearity in the modulation characteristic of the FM transmitter, as well as in the modulating signal (see Section 3.5). Therefore, it is more usual to have

$$\frac{\Delta R}{R} \sim 0.05 \ldots 0.1 \tag{5.9}$$

The analysis of spectra and range resolution becomes significantly more complicated if the reflected target signals are unequal and the targets are moving, corresponding to most real situations. The sidelobes of one spectrum may then be larger than the main lobe of the other [Figure 5.5(a)]. Thus resolution of two targets is possible only when the main spectral lobe of the smaller signal exceeds by a certain ratio the sidelobes of the larger signal. The distance between objects at which this condition is satisfied is the resolution appropriate to these conditions [Figure 5.5(b)].

Consider an example (Figure 5.6) in which the first target signal exceeds by 10 dB that of the second. We will assume that for reliable resolution of the second target we need a 5-dB ratio of components in the main lobe of its spectrum to those in the sidelobes of the first target. Let us calculate an allowable level of sidelobes in the spectrum of the first signal. This level should be no more than the sum of

−10 dB	(the difference between the first and second signals)
−4 dB	(the worst-case reduction of components in the main lobe envelope of the second signal spectrum)
−5 dB	(the ratio of components in the main lobe envelope of the second signal above components in sidelobes of the first)
= −19 dB	(allowable sidelobe level).

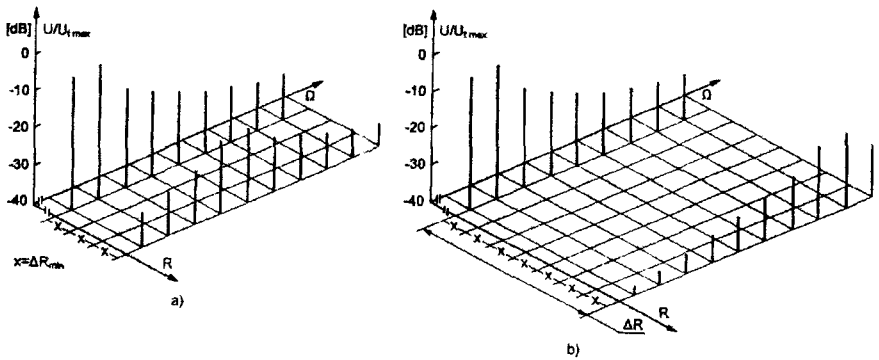

Figure 5.5 Illustration of range resolution for unequal reflected target signals.

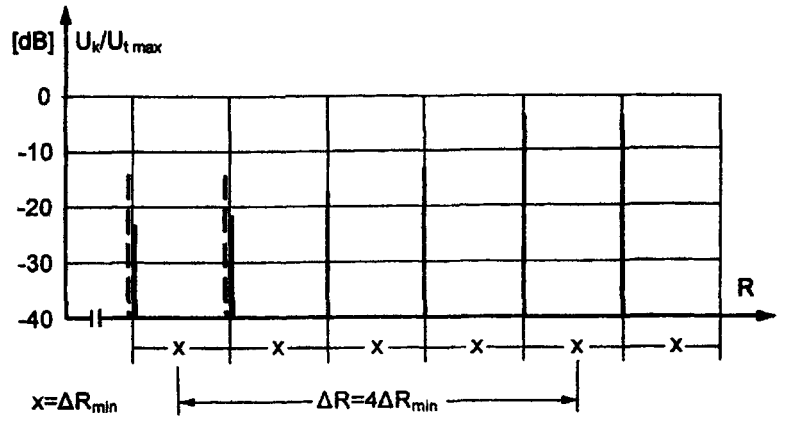

Figure 5.6 Range resolution for targets of different amplitudes.

In Figure 5.6 it is easily established that the main lobe of the second signal spectrum may be near the third and fourth sidelobes of the first signal spectrum. Thus

$$\Delta R = 4\Delta R_{min} = 2\frac{C}{\Delta f} \tag{5.10}$$

In Figure 5.7 results of similar calculations (dashed curves) are shown. The abscissa is the ratio of the two signals P_1/P_2 and the ordinate is the ratio of actual

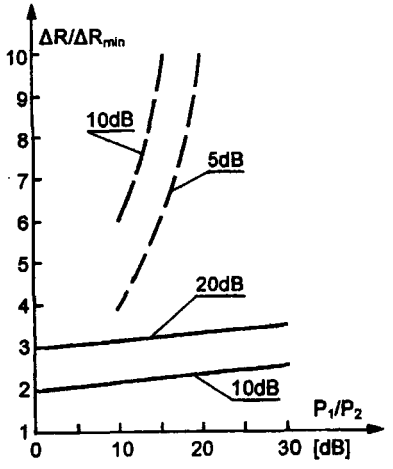

Figure 5.7 Ratio of range resolution to optimum value with weighting (solid line) and without (dashed line).

range resolution to maximum range resolution. The parameter of the curves is the ratio of components in the main lobe envelope of the smaller signal to those in the sidelobe envelope of the larger signal.

As we can see, the SRR resolution decreases sharply with increase in the ratio of one signal to the other. The main reason for reduction of resolution is the slow reduction of sidelobes of the converted signal spectrum.

As noted in Chapter 3, the sidelobes result from phase discontinuities at the ends of the modulation period. Therefore, it is logical to propose that for sidelobe reduction the converted signal should be amplitude modulated so that its amplitude drops to zero at the ends of the period. This reduction in amplitude should occur smoothly, without a break of the envelope near the end of the period (i.e., the derivative of the envelope at the ends of the period should go to zero). This method has been known for a long time and is usually termed *weighting* [1].

We can show that the most suitable modulation function (*weighting function*) for the converted signal envelope is $\cos^2(\pi/T_m)$. Since

$$\cos^2\left(\frac{\pi}{T_m}\right)=\frac{1}{2}\left[1+\cos\left(\frac{2\pi}{T_m}\right)\right] \tag{5.11}$$

it follows that the optimum converted signal is amplitude modulated with a cosine envelope. According to (2.24) and (5.11), this signal is

$$u_t = U_t\frac{1}{2}\left[1+\cos\left(\frac{2\pi}{T_m}\right)\right]\cos\left[\pm\Omega_D t+\Delta\omega F_t(t,\tau)+\varphi_\tau-\varphi_0\right] \tag{5.12}$$

Then, according to (2.27), each component of the converted signal spectrum is also an AM waveform, and the sidebands of each are summed with the adjacent components. The amplitude of the kth component is

$$U_n=\frac{U_t}{2}\left\{\frac{\sin\left[\pi(\Delta f\tau-k)\right]}{\pi(\Delta f\tau-k)}+\frac{\sin\left[\pi(\Delta f\tau-k+1)\right]}{2\pi(\Delta f\tau-k+1)}+\frac{\sin\left[\pi(\Delta f\tau-k-1)\right]}{2\pi(\Delta f\tau-k-1)}\right\} \tag{5.13}$$

It is easy to explain the effect of sidelobe suppression if we consider a spectrum, taking into account the "sign" of the amplitudes of its components.

In Figure 5.8(a) the components of the spectrum are shown for $\Delta f\tau = k \pm 0.5$ without multiplication by a weighting function. Upon multiplication of each component by the weighting function, two sidebands appear that are in an antiphase with the next components (except for two components in the main lobe numbered 3 and 4). So, in (b) the right sideband of 1 is in an antiphase with 2. In (c), the sidebands of 2, in turn, are in an antiphase with 1 and 3, while in (d), the sidebands of 3 are in an antiphase with those of 2 and in-phase with those of 4, and so forth.

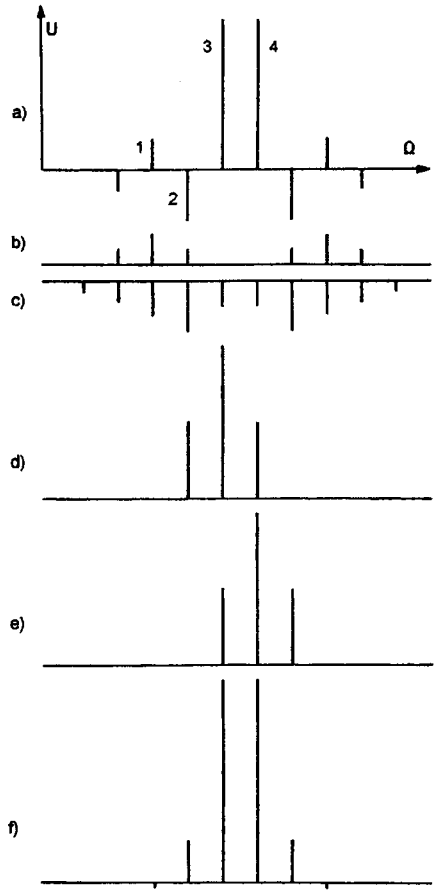

Figure 5.8 Explanation of weighting processing.

As a result of the addition of all spectral components in (f) components 3 and 4 are increased and all others considerably decreased.

Figure 5.9 shows the spectral envelopes with and without weighting. The left side of the envelope is not shown, as the envelope is symmetrical about the center of the main lobe. The two first rows of numbers above the sidelobes show the ratio of sidelobe to main lobe in decibels, the top line without weighting and the center row with weighting. The bottom row shows by how many decibels the appropriate lobe has been decreased by weighting. We can see that multiplication by the weighting function broadens the main lobe while significantly decreasing the sidelobes. It is especially important that the nearest sidelobes have decreased by 14-25 dB.

Results of range resolution calculations with weighting are shown in Figure 5.7 (solid line). We can see that with increasing ratio of one signal to the other

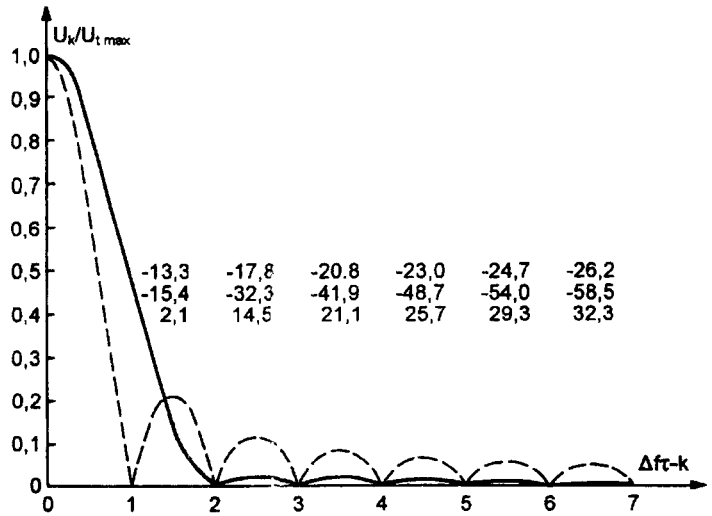

Figure 5.9 The fragments of a spectral envelope.

the range resolution changes only slightly, and is approximately two to three times worse than the maximum. Thus, the application of weighting of the converted signal is quite effective.

Technically it is simple to weight the converted signal. The weighting function is formed from the first harmonic of the modulating signal spectrum. Modern technology also permits very simple multiplication of the converted signal by the weighting function.

5.3 RADAR SCAN OF RANGE

As in pulse radar, it is possible in SRR to use displays such as A, B, or J type, on which target range is presented. In SRR, the range data displayed on the indicator is derived from analysis of the converted signal spectrum. We note that here the term *analysis* is understood in a completely different sense from that used in Chapters 2 and 3. In this case analysis of the spectrum is defined by the operating algorithm of the processing block, and the result of this analysis is a range estimate presented in an appropriate way on the indicator. Thus, for realization of range estimation it is necessary first of all to obtain at the output of the analyzer a signal representing the converted signal spectrum.

There are two methods of generating such signals: simultaneous analysis and sequential analysis. In the first the analyzer is implemented as a bank of bandpass filters with resonant frequencies $n\Omega_m$ and passbands $2\Omega_{D\max}$ (Figure 5.10). The converted signal is applied to all filters simultaneously, and the signal corresponding to the nth component of the converted signal spectrum appears at the output of

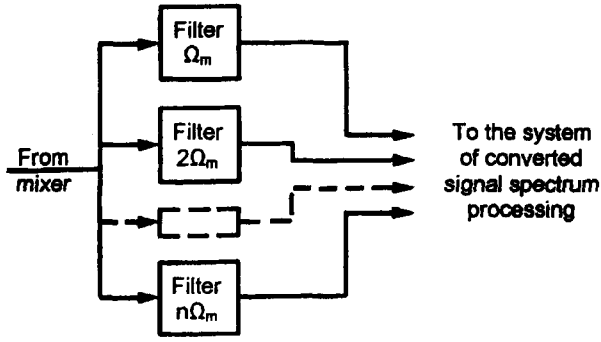

Figure 5.10 The simultaneous analyzer.

filter n. Signals from the filter outputs are applied simultaneously and continuously to the input of the processing block.

In the second method a single bandpass filter with variable resonant frequency is used. The resonant frequency of this filter is scanned to cover sequentially the frequencies of spectral components. As the resonant frequency of the filter scans past each of the n components, a signal corresponding to this component appears at the filter output. This method is termed sequential analysis.

Simultaneous analysis certainly has advantages over sequential: the information on amplitude of every spectral component is present at all times at the analyzer output and may be extracted at any moment. It is also very important that it is possible with simultaneous analysis to neglect transients from moving targets, because the time for a change in amplitude of the moving target component is much greater than the transient time of the filters. This is easily shown in an example.

The buildup time of a signal at the output of a bandpass filter after input of a sinusoidal signal at the filter's resonant frequency is $t_b \approx 0.8/B$, where B is the passband of the filter. In this case

$$t_b \approx \frac{0.8}{2F_D} = \frac{0.8C}{4f_cV} \tag{5.14}$$

The time over which the amplitude of a spectral component may change from zero to its maximum (see Figure 5.1) is

$$\Delta t = \frac{\Delta R}{V} = \frac{C}{\Delta f\, V} \tag{5.15}$$

Since $f_c >> \Delta f$ then $t_b << \Delta t$.

Simultaneous analysis has a major disadvantage in that the analyzer circuit is very bulky. This results from the need for large numbers of filters, as can be shown by an elementary calculation. Assuming that the ratio of the maximal to minimal

range is q, and the number of the spectral component appropriate to the minimal range is n, then the number of filters is $qn - n = n(q - 1)$. For example, if $q = 10$, and $n = 5$ there must be 45 filters. Reduction of n is not always possible for two reasons: (a) because of the need to filter out of the signal any parasitic amplitude modulation, and (b) because of the required range resolution (when the frequency deviation is large the range resolution is better, and large frequency deviation requires large n).

It is possible to reduce the number of filters by dividing the range coverage into two or more subbands. It is the most convenient if these subbands have identical ratios $q' = \sqrt[k]{q}$, where k is the number of subbands. Accordingly, the frequency deviation of the transmitted signal should decrease by the factor q' at each transition to the next sub-band. Only then will it be possible to use the same complete bank of analyzer filters in all subbands. Because of deviation reduction, the extent of each successive subband is increased by q' and the range resolution is worsened by q', but the ratio of resolution size to subband size remains constant.

Let us proceed to consider the operation of an analyzer performing sequential analysis. Despite its apparent simplicity, realization of this analyzer involves some technical difficulties. First, we note that if frequency agility is used a certain time is necessary to observe each set of spectral components. The speed of frequency agility cannot be more than a certain value, as otherwise the amplitude-frequency characteristic of the filter will be distorted, with resulting distortion of the analysis. Thus, while for simultaneous analysis we use "by default" the *static* amplitude-frequency characteristics of the analyzer filters, for sequential analysis we must consider the *dynamic* amplitude-frequency characteristic of the agile filter. The resulting difficulties are connected with the realization of filter agility over a wide range of frequencies and especially with maintaining invariance of its amplitude-frequency characteristic. Therefore, it is best to apply analyzer designs that do not require filter agility. There are two possible methods.

The first method is to transfer the converted signal spectrum to another frequency range and periodically scan the narrowband filter. This analyzer circuit is equivalent to the conventional superheterodyne receiver (Figure 5.11). The heterodyne (local oscillator) sweep is a sawtooth function and its frequency deviation equals the instrumented extent of the converted signal spectrum. The receiver is thus periodically tuned to all frequencies in this portion of the converted signal spectrum, while the narrowband filter is tuned to the intermediate frequency and

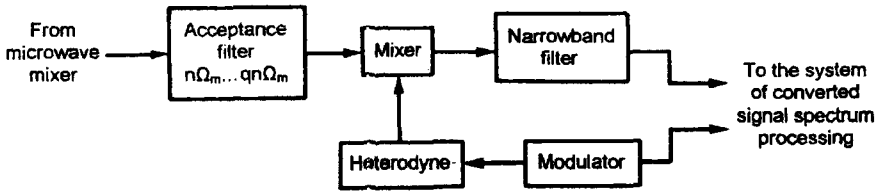

Figure 5.11 The sequential analyzer.

Figure 5.12 Frequency relationships in the sequential analyzer.

does not need agility. The acceptance filter of the receiver is a fixed, broadband LPF filter. To obtain good image-channel rejection while passing the desired signal, the intermediate frequency is chosen higher than the highest frequency of the instrumented extent of the converted signal spectrum. The relationships among this spectrum, the range of heterodyne frequencies, and the intermediate frequency are shown in Figure 5.12.

Thus, the filter does not scan across the frequencies of the converted signal spectrum, but rather the spectrum is scanned across the fixed filter bandpass.

The moving spectrum entering the filter generates a transient resulting from the influence on the filter of the linearly varying frequency. Thus, the amplitude-frequency characteristic of the filter is distorted: there is a shift of its maximum and a broadening of its passband. The more rapid the signal frequency variation the more strongly distorted is the amplitude-frequency characteristic. In Figure 5.13 the amplitude-frequency characteristics of the filter are shown for (a) static and (b) dynamic conditions, as a function of the normalized detuning

$$\xi = \frac{\omega - \omega_0}{\Delta\Omega} \tag{5.16}$$

Where ω_0 is the resonant frequency of the filter and $\Delta\Omega$ is half its 3-dB bandwidth.

There are many theoretical works devoted to analysis of varying-frequency signals in selective circuits. In this case, it is best to estimate the allowable rate of

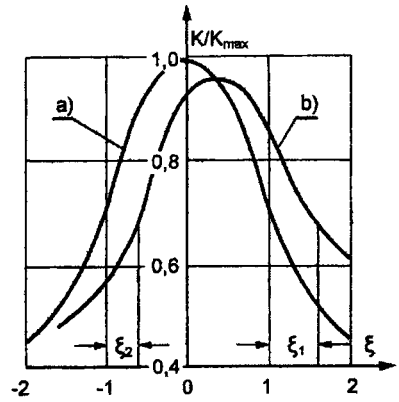

Figure 5.13 Amplitude-frequency characteristics under (a) static and (b) dynamic conditions.

change of the heterodyne frequency using works where simple formulas for engineering calculation of amplitude-frequency characteristic distortions are given. Such formulas are found, for example, in [2], which we will use to estimate the allowable rate of heterodyne frequency change of the analyzer. Let the heterodyne frequency vary linearly:

$$\omega = \omega_1 + \alpha t \tag{5.17}$$

where α is the rate of frequency change. It is obvious that the spectrum moves with the same rate relative to the fixed filter. For further calculations a parameter proportional to the speed of heterodyne frequency change is defined as

$$\mu = \alpha / (\Delta\Omega)^2 \tag{5.18}$$

where $\Delta\Omega$ is half the passband of the narrowband filter. In our case $\Delta\Omega = \Omega_{D\max}$. Parameters of the dynamic characteristic of the filter are determined by μ.

In particular in [2] it is shown that a flat amplitude-frequency characteristic (e.g., the characteristic of a double-tuned filter) is distorted to the greatest degree. Broadening of the passband (in terms of normalized detuning) is

$$\Delta\xi = \xi_1 - \xi_2 = 25\mu^2 \tag{5.19}$$

The average displacement of the characteristic is

$$\frac{\xi_1 + \xi_2}{2} = 2.1\mu = 0.42\sqrt{\Delta\xi} \tag{5.20}$$

from which we obtain

$$\alpha = 0.2\Omega_{D\max}^2 \sqrt{\Delta\xi} \tag{5.21}$$

Given the allowable rate of change of analyzer heterodyne frequency, it is possible to determine the minimal analysis time for the entire converted signal spectrum or the minimal period of modulation of the heterodyne frequency

$$T_{mh} = \frac{(q-n)\Omega_m}{\alpha} = 5\frac{(q-n)\Omega_m}{\Omega_{D\max}^2 \sqrt{\Delta\xi}} \tag{5.22}$$

where q and n are numbers of the highest and lowest spectral components, respectively.

To estimate T_{mh} consider the following example. Let $F_{D\max}$ = 10 kHz (the Doppler frequency observed in I- or K-band with a radial velocity ~ 100-150 km/h). The ratio $\Omega_m/\Omega_{D\max}$ does not usually exceed 10. Assume $(q - n) = 20$, and

$\xi = 0.01$ (a value so small that the dynamic characteristic does not differ significantly from the static). Shift of the characteristic is also negligibly small: $\xi = 0.042$. Substituting this data in (5.22), we find $T_{mh} = 0.16$s. Varying the initial data shows that the time to scan this range interval does not exceed fractions of a second.

Let us proceed to consideration of the second method of realizing a single-filter analyzer. This method is based on the fact that the amplitude of any spectral component depends on the product $\Delta f\tau$. Hence, dependence of amplitude of the nth component on delay time, for constant deviation, or on size of the deviation, for constant delay, are identical. Actually, if the filter is tuned to frequency $n\Omega_m$ and the delay of the reflected signal is τ, there is some value of deviation at which the product $\Delta f\tau = n$ applies and the output signal is maximal. Hence, for periodic display of the entire range interval we must change the value of frequency deviation periodically, smoothly and within the certain limits.

The block diagram of such an analyzer is given in Figure 5.14. The narrowband filter is tuned to frequency $n\Omega_m$ and has a passband $2\Omega_{D\max}$. The number of the selected spectral component depends on the size of parasitic amplitude modulation signals and the required SRR resolution. In most cases the value of n does not exceed 10 to 20.

A block is included between the modulator and the FM generator to apply sawtooth amplitude modulation. This block is controlled by a signal periodic at $T_{m\Delta f}$ generated in the control signal generator, from which signals also go to the processing block and the display. To obtain a linear scale of range on the display, we must change the frequency deviation according to a certain law, for which we refer to Figure 5.15.

Figure 5.15(a) shows the display sweep signal. For a linear range scale the dependence of the indicated range on sweep time [Figure 5.15(b)] should be also linear:

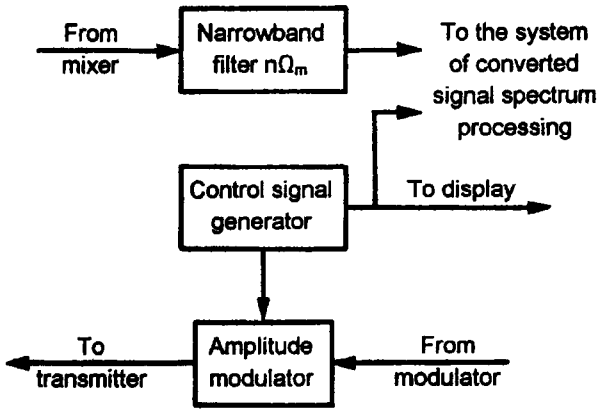

Figure 5.14 The sequential analyzer.

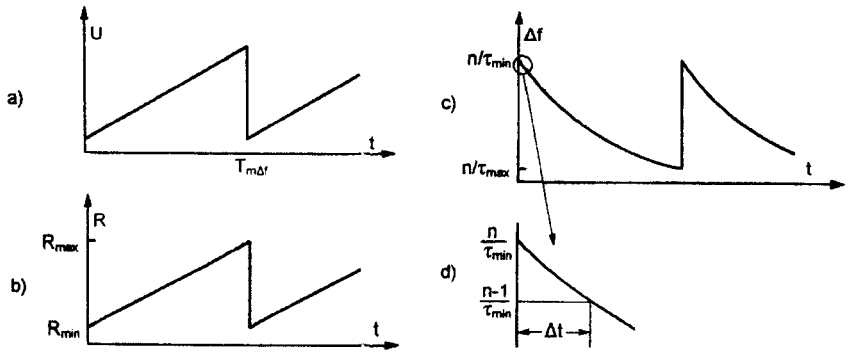

Figure 5.15 Derivation of the look time: (a) display sweep signal, (b) range sweep, (c) change in transmitted frequency deviation, and (d) time for change from one spectral component to the next.

$$R = R_{\min} + \left(R_{\max} - R_{\min}\right)\frac{t}{T_{m\Delta f}} \quad \text{or} \quad \tau = \tau_{\min} + \delta\tau\frac{t}{T_{m\Delta f}} \tag{5.23}$$

where $\delta\tau = 2(R_{\max} - R_{\min})/C$. Using the ratio $\Delta f\tau = n$, we obtain

$$\Delta f(t) = \frac{nT_{m\Delta f}}{\tau_{\min}T_{m\Delta f} + \delta\tau t} \tag{5.24}$$

Hence, for the period of range estimation the frequency deviation of the radiated signal [Figure 5.15(c)] should vary on a hyperbola from $n/\tau_{\min}$ to $n/\tau_{\max}$.

To determine the minimal duration of the sweep period $T_{m\Delta f}$, note first that only the amplitude of the appropriate spectral component varies with a change of deviation. Therefore the transient process is characterized by the transient time of the filter output signal as it responds to change of the input signal. Transient time was given by (5.14), and this time needs to be compared to the time for change from zero to maximum value of the nth spectral component. We designate this time as Δt [Figure 5.15(d)]. This spectral component changes from zero to its maximum with a change of frequency deviation from n/τ to $(n - 1)/\tau$ (i.e., by an amount $1/\tau$). The time in which the deviation will change by this amount is determined by the rate of change of the frequency deviation. In Figure 5.16(c) we see that the greatest deviation rate corresponds to its value at $t = 0$. Differentiating (5.24) with respect to t and setting $t = 0$, we obtain

$$\frac{d\Delta f}{dt} = -\frac{n\delta\tau}{\tau_{\min}^2 T_{m\Delta f}} \tag{5.25}$$

Then, from Figure 5.15(d), we have

$$\Delta t = \tau_{\min} \frac{T_{m\Delta f}}{n(\tau_{\max} - \tau_{\min})} \tag{5.26}$$

Assuming that $\Delta t = 10t_b = 4/F_D$, we have

$$T_{m\Delta f} = \frac{4n}{F_D}\left(\frac{\tau_{\max}}{\tau_{\min}} - 1\right) \tag{5.27}$$

The sweep period $T_{m\Delta f}$ for $n = 20$, $\tau_{\max}/\tau_{\min} = 10$, and $F_D = 10$ kHz is found to be $T_{m\Delta f} = 72$ ms. Thus, even with such hard constraints, when the transient time in the filter is an order less than the time of selected spectral component change, the sweep time does not exceed several tens of milliseconds.

In this case, however, we must estimate the period $T_{m\Delta f}$ on a completely different basis. With a change of deviation there is a change in the converted signal spectrum (i.e., we must deal with the current spectrum, although strictly speaking the spectra of physical processes are always current because the spectra obtained mathematically are true only as $t \to \infty$). A spectral change in a physical process requires a certain time to observe. For the case considered this means that the rate of change of frequency deviation must be limited, or else the spectrum of the converted signal will differ considerably from that calculated in Chapter 3.

Strict calculation of the current spectrum of the converted signal with change in frequency deviation is very complex. However, an approximate calculation of the necessary sweep period $T_{m\Delta f}$ is simple to perform, assuming that in time Δt [Figure 5.15(d)] the nth component of the spectrum can be successfully generated. Thus, the problem is reduced to calculation of the current spectrum of a sinusoid in the time Δt and, further, to calculation of $T_{m\Delta f}$ depending on the necessary degree of formation of the converted signal spectrum. To perform this approximate calculation we will consider again the current spectrum of a sinusoid.

By definition of the current spectrum, if $f(t) = \sin\Omega t$, then the current spectrum is determined as

$$s_t = \int_0^t e^{-j\omega t} \sin\Omega t \quad dt = \frac{\Omega}{\Omega^2 - \omega^2}\left[1 - e^{-j\omega t}\left(\cos\Omega t + j\frac{\omega}{\Omega}\sin\Omega t\right)\right] \tag{5.28}$$

This equation can be significantly simplified by considering values of spectral density for discrete moments of time

$$t = t_k = k\frac{\pi}{\Omega} = k\frac{T}{2} \quad . \tag{5.29}$$

Having substituted (5.29) in (5.28), we obtain

$$s_t = \frac{1}{\Omega} \frac{1}{1-\left(\frac{\omega}{\Omega}\right)^2} \left[1-(-1)^k e^{-jk\pi\frac{\omega}{\Omega}}\right] \tag{5.30}$$

and the current spectrum is

$$S(t) = |s_t| = \frac{1}{\Omega} \frac{1}{1-\left(\frac{\omega}{\Omega}\right)^2} \begin{matrix}\sin \\ \cos\end{matrix}\left(k\frac{\pi}{2}\frac{\omega}{\Omega}\right) \tag{5.31}$$

In (5.31) the sine function corresponds to even k, and the cosine function to odd k. The uncertainty of (5.31) at $\omega = \Omega$ can be easily resolved:

$$S_{t\ \omega=\Omega} = k\frac{T}{4} = \frac{t}{2} \tag{5.32}$$

Thus, the spectral density at frequency $\omega = \Omega$ increases linearly with time.

From (5.31) it follows first that the spectrum is homogeneous, as is the spectrum of any short-term process. Further, the spectral lobing shown in Figure 5.16 is gradually formed. The envelope's main lobe is eventually increased and becomes more and more narrow, and only in a limit as $t \to \infty$ does the lobe turn into a discrete line.

In our case the degree of spectrum formation is easiest to estimate based on the width of the spectral envelope's main lobe. Let us determine this width as a function of the factor k. The values ω/Ω corresponding to $\sin[(k\pi/2)(\omega/\Omega)] = 0$ are determined from

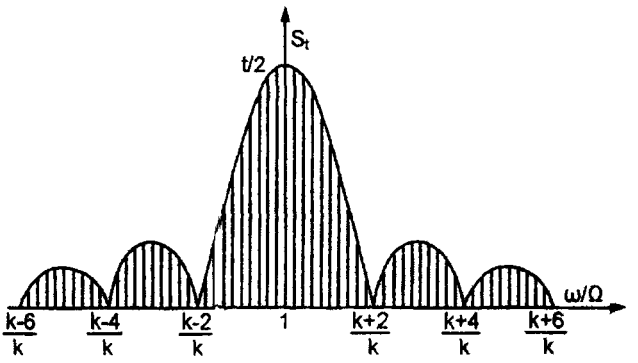

Figure 5.16 Current spectrum of a sinusoid.

$$k\ \frac{\pi}{2}\left(\frac{\omega}{\Omega}-1\right)=q\pi \tag{5.33}$$

where $q = 0, \pm1, \pm2, \pm3, \ldots$

The value $q = 0$ corresponds to the maximum of the spectrum main lobe and the values $q = \pm1$ to the first nulls, for which we obtain

$$\left.\frac{\omega}{\Omega}\right|_0=\frac{k\pm2}{k} \tag{5.34}$$

Thus, for the current spectral envelope of a sinusoid, the null-to-null width of the main lobe is

$$\frac{\Delta\omega_0}{\Omega}=\frac{4}{k} \tag{5.35}$$

As we can see (5.35) relates the width of the spectral main lobe to time through (5.29). Defining k from (5.35) and substituting it in (5.29), we obtain

$$t=\frac{4\pi}{\Delta\omega_0} \tag{5.36}$$

As the criterion for formation of the spectrum we use the ratio of mainlobe width to half the passband of the analyzer filter (i.e., we assume that $\Delta\omega \le \gamma\Omega_D$, and $\gamma << 1$). Then, equating (5.26) and (5.36), we obtain

$$T_{m\Delta f}\ge\frac{2n\left(\frac{\tau_{max}}{\tau_{min}}-1\right)}{\gamma F_D} \tag{5.37}$$

As we can see, the values of $T_{m\Delta f}$ determined by (5.27) and (5.37) have the same order. Usually values of $T_{m\Delta f}$ are between several tenths and units of seconds. The limit to increase in the analysis time depends also on the requirement that there be no serious distortion of the spectrum caused by target motion during the analysis, as may occur for high target speeds at small ranges.

One more method of realization of sequential analysis of the converted signal spectrum is possible. In this method the modulation frequency is changed while the frequency deviation remains constant. With change in the modulation frequency, the spectrum of the converted signal is stretched or compressed on the frequency axis. There will always be a modulation frequency such that the frequency of the nth spectrum component will coincide with the frequency of the

analyzer filter. This method has no advantages in comparison with those considered above, and hence details of this method are not considered here.

In conclusion, we consider the problem of normalization of the converted signal for use in the spectral processing methods discussed above. In Chapter 4 (see Section 4.2.2), a method of signal normalization with simultaneous suppression of parasitic amplitude modulation signals was described, using an amplifier with a nonuniform amplitude-frequency characteristic. Such an amplifier may also be included between the mixer and the analyzer in the simultaneous or sequential analyzer. For improved normalization we may also include an AGC circuit in this amplifier, which will be followed by the weighting block. Inclusion of such an amplifier in the analyzer using change of frequency deviation is obviously not meaningful. Actually, for $\Delta f\tau = n$, the basic part of the spectrum concentrates around the nth component, where n is fairly high (in most cases between 10 and 20). This provides adequate selectivity with respect to parasitic amplitude modulation signals.

5.4 SPECTRAL PROCESSING USING THE PARASITIC AM SIGNAL

In some cases (e.g., for SRRs used in security systems) we must detect targets at short range. In this case the spectrum of the converted signal overlaps that of the parasitic amplitude modulation signal (see Section 4.2). To extract the useful signal against the background of parasitic amplitude modulation we may certainly apply a rejection filter (as in Section 4.2), but another method is possible that may be preferable. For consideration of this method we address Figure 5.17. Here the components of the converted signal spectrum together with the spectrum of a parasitic signal are shown for (a) sinusoidal modulation and (b) asymmetrical sawtooth modulation. The spectral components of the parasitic signal are shown by dashed lines. As we can see, the three spectral components (the parasitic signal and spectral components of the converted signal located near it) are formally similar to the spectra of (a) an AM signal or (b) an AM-PM signal.

Thus, it is possible to extract the spectral components with a bandpass filter and detect them with an amplitude detector. Such detection produces a Doppler signal whose amplitude varies with range, according to the law of change of ampli-

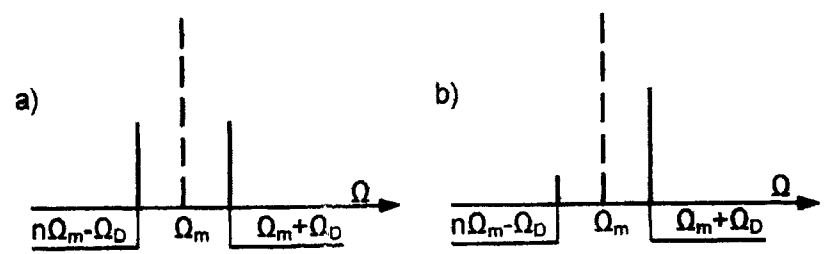

Figure 5.17 Spectral components of converted and parasitic signals.

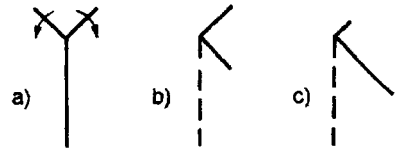

Figure 5.18 Phasor diagrams: (a) AM signal, (b) detected signal for sinusoidal modulation, and (c) detected signal for asymmetrical sawtooth modulation.

tude of the nth spectral component of the converted signal. This signal may be further processed in the same way as the nth component of a signal with frequency $n\Omega_m \pm \Omega_D$.

The nth component signal at the bandpass filter output is, however, only formally an AM signal, as the phase relationships peculiar to an AM signal are not present. In an AM signal the sidebands are always located symmetrically about the carrier frequency, as in Figure 5.18(a). In our case the arrangement of "sidebands" with respect to the "carrier" is arbitrary, being defined by the phase of the carrier and angles φ_τ and φ_0 of sidebands. In particular, the vector diagram of this signal may appear as shown in Figure 5.18(b), corresponding to a PM signal with very small AM rather than to an AM signal. Therefore, in applying this processing method it is best to apply asymmetrical sawtooth modulation. In this case, because of the inequality of sidebands, the necessary amplitude modulation holds for any arbitrary position of the sidebands relative to the carrier, as shown in Figure 5.18(c).

A block diagram of this type of processing system is shown in Figure 5.19. The principle of operation and structure of the Doppler signal processing block is determined by the assigned function of the SRR and its technical parameters.

We must note that this SRR responds only to moving targets. It is a major advantage of this processing method that it allows very simple selection of moving targets against a fixed background.

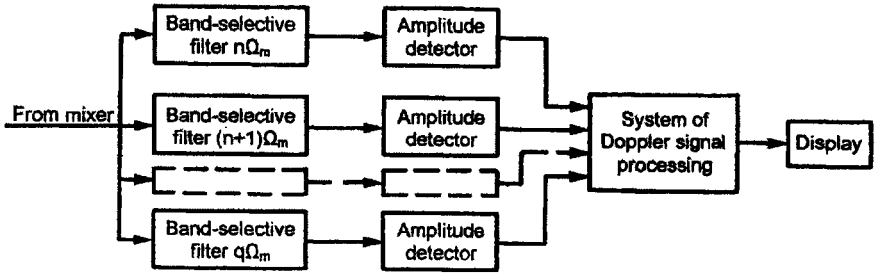

Figure 5.19 Block diagram of the processing system using a parasitic AM signal.

5.5 SIGNAL PROCESSING ON SEPARATE COMPONENTS OF THE CONVERTED SIGNAL SPECTRUM

It is obvious from the previous discussion that the entire spectrum of the converted signal is used for coverage of space by an SRR with spectral processing. Thus the target range is determined rather coarsely, usually with an error of a few percent of that range. The individual spectral components must be used for more exact measurement of range and velocity.

5.5.1 Formation of the Discriminator Characteristic

The target range is estimated during a scan of range and azimuth with an error approximately equal to the SRR target resolution. There is often a requirement for more exact measurement of range to individual targets. It is possible to do this using the fixed frequency deviation method described above with a suitable discriminator characteristic (see Section 4.4.3). Such a characteristic can easily be obtained for asymmetrical sawtooth modulation by subtracting the amplitudes of two adjacent spectral components of the converted signal. The appropriate circuit of this discriminator is shown in Figure 5.20. Here the components n and $n + 1$ are extracted from the spectrum by bandpass filters. The filter output signals are detected by amplitude detectors and applied to the subtraction block.

In the absence of weight processing the equation for the discriminator characteristic is

$$U(\Delta f, \tau, n) = U\left(\left|\frac{\sin \pi(\Delta f \tau - n)}{\pi(\Delta f \tau - n)}\right| - \left|\frac{\sin \pi(\Delta f \tau - n - 1)}{\pi(\Delta f \tau - n - 1)}\right|\right) \tag{5.38}$$

or

$$U(\Delta f, R, n) = U\left(\left|\frac{\sin \pi\left(\frac{\Delta f R}{150} - n\right)}{\pi\left(\frac{\Delta f R}{150} - n\right)}\right| - \left|\frac{\sin \pi\left(\frac{\Delta f R}{150} - n - 1\right)}{\pi\left(\frac{\Delta f R}{150} - n - 1\right)}\right|\right) \tag{5.39}$$

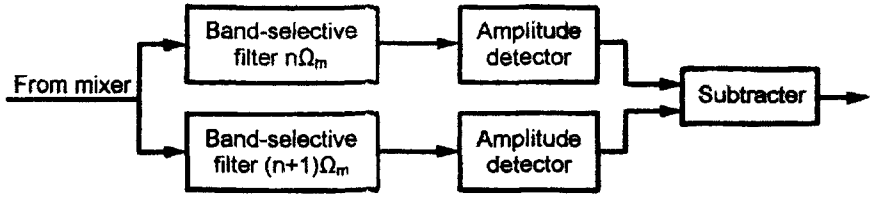

Figure 5.20 Block diagram of the discriminator.

where frequency deviation is in megahertz and range is in meters. A similar equation can also be written for weighted processing. Figure 5.21 shows the discriminator characteristics for unweighted and weighed processors.

To find the slope of the characteristic near its null, we differentiate (5.39) with respect to R and substitute the appropriate value of R, obtaining for (a)

$$S = 1.27\frac{2n+1}{R} \tag{5.40}$$

Similarly, for (b)

$$S = \frac{2n+1}{2R} \tag{5.41}$$

An important parameter of the discriminator characteristic is its sidelobe level. With a strong reflected signal there may be an automatic false lock on a sidelobe of the discriminator characteristic. In this respect characteristic (b) is preferable, since the level of its first sidelobe is more than 14 dB less than that of (a).

The range error depends on many parameters of the automatic frequency deviation control system and on error in measurement of the deviation. It is possible, however, to estimate the error using the discriminator characteristic. Assume that in the established mode an error signal at the discriminator output is k times less than the maximal value of the output signal. Then we find for characteristic (a) $\delta R = 1/kS$ and $\delta R/R = 1/[1.27k(2n - 1)]$ and for (b) $\delta R/R = 2/[k(2n + 1)]$ or $\delta R/R \approx 1/2kn$.

Note also that the discrimination characteristic does not depend upon Doppler shift, which is an advantage of this discriminator.

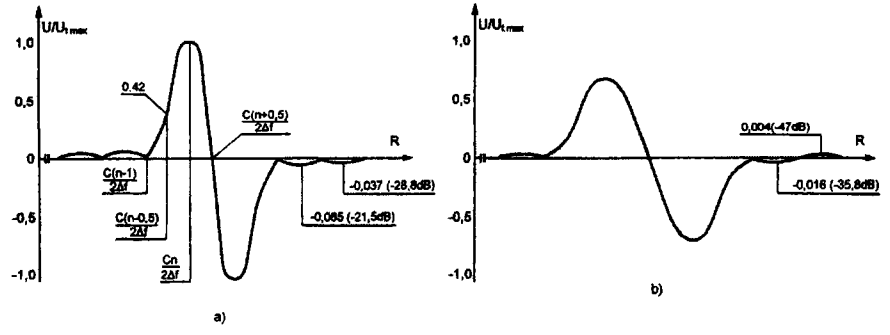

Figure 5.21 Discriminator characteristics for (a) unweighted and (b) weighted processing.

5.5.2 Phase Processing of Separate Components of the Converted Signal Spectrum

5.5.2.1 Use of an FM Signal Instead of a Multiple-Frequency Signal

It has been shown [3] that phase processing of the reflected signal permits measurement of target range with very small error. Thus, a multiple-frequency transmitted signal consisting of several sinusoidal waves with different frequencies can be used instead of a modulated signal. Such a radar is described in [3]. For convenience in further discussions, we will give a brief description of this radar, whose block diagram is shown in Figure 5.22.

The transmitter consists of n oscillators with frequencies

$$\omega_1 = \omega_0, \omega_2 = \omega_0 + \delta\omega_1, \omega_3 = \omega_0 + \delta\omega_2, \ldots \omega_n = \omega_0 + \delta\omega_{n-1}$$

where $\delta\omega_1 < \delta\omega_2 \ldots < \delta\omega_{n-1} << \omega_0$. The oscillator signals are summed and applied to the transmitting antenna. Signals from each oscillator are also applied to the appropriate mixer as a heterodyne signal. All mixers are fed from the receiving antenna. It is assumed that the decoupling between antennas is sufficient that leakage of the radiated signal between transmitter and receiver can be neglected. Use of a single antenna may be possible because $\delta\omega_k << \omega_0$.

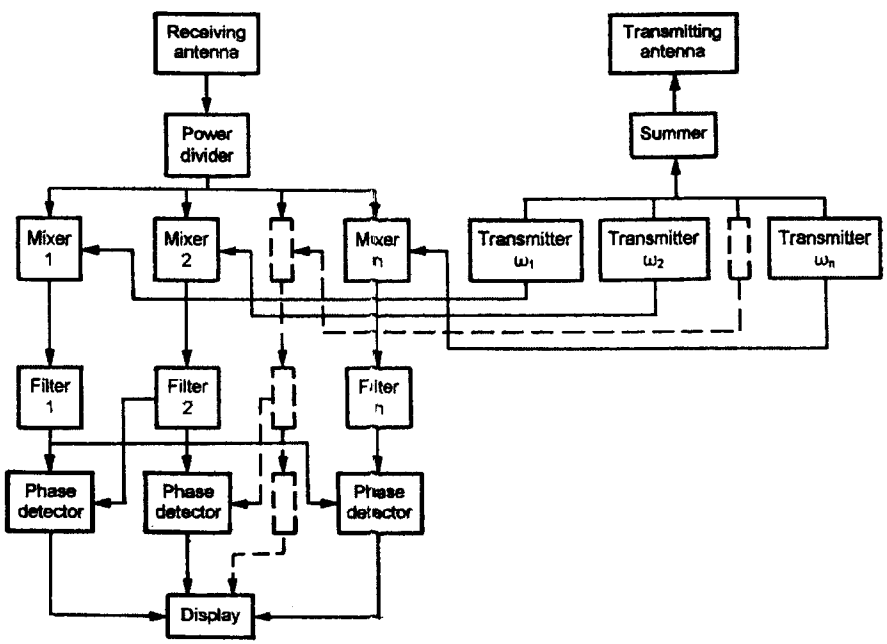

Figure 5.22 Block diagram of the multifrequency radar.

A Doppler filter is included at the output of each mixer. If $\delta\omega_k >> \Omega_{D\max}$, it is possible to consider that each mixer will pass only that echo signal whose frequency corresponds to the frequency of "its own" heterodyne signal. We assume further that the target moves at a constant radial speed corresponding to the Doppler shift Ω_D. Then, using (2.10) and (2.14) and assuming that $\Delta\omega = 0$, we obtain expressions for the phases of mixer outputs

$$\begin{aligned}
&\varphi_{t1}(t,\tau) = \Omega_{D1}t + \omega_0\tau_0 - \phi_{01} \\
&\varphi_{2}(t,\tau) = \Omega_{D2}t + \omega_1\tau_0 - \phi_{02} \\
&\varphi_{t3}(t,\tau) = \Omega_{D3}t + \omega_3\tau_0 - \phi_{03} \\
&\ldots \\
&\varphi_{tn}(t,\tau) = \Omega_{Dn}t + \omega_n\tau_0 - \phi_{0n}
\end{aligned} \tag{5.42}$$

Because differences between signal frequencies are very small (as will be shown below) we may assume that

$$\Omega_{D1} = \Omega_{D2} = \Omega_{D3} = \ldots = \Omega_{Dn} \quad \text{and} \quad \varphi_{01} = \varphi_{02} = \varphi_{03} = \ldots = \varphi_{0n}$$

Then, for example, the phase difference between signals from mixers 1 and 2 is

$$\Delta\varphi_{1\text{-}2}(\tau) = \varphi_{t1}(t,\tau) - \varphi_{t2}(t,\tau) = (\omega_1 - \omega_2)\tau_0 = \delta\omega_1\tau_0$$

and between mixers 2 and 3 is

$$\Delta\varphi_{2\text{-}3}(\tau) = \varphi_{t2}(t,\tau) - \varphi_{t3}(t,\tau) = (\omega_2 - \omega_3)\tau_0 = (\delta\omega_2 - \delta\omega_3)\tau_0$$

Target range can be measured by determining this phase difference with a phase detector. Thus, a limit of unambiguous measurement of range, restricted by the size of phase difference $\Delta\varphi_{1\text{-}2}(\tau) = 2\pi$, is

$$R_{\max} = \frac{\pi c}{\delta\omega_1} \tag{5.43}$$

The measurement error depends on the frequency separation and the error of phase measurement. If we can measure a phase difference with an error of 1° the measurement error at maximal range will be ~ 0.3%. By increasing the frequency separation by a factor of ten we can reduce the error to ~ 0.03%, but then there will be an ambiguity in measurement of range.

Thus there are two opposing requirements on the frequency separation: to reduce error the frequency separation should be increased, while for elimination of

measurement ambiguity it should be reduced. To satisfy both of these requirements, the number of frequencies transmitted is usually increased to three, four, or more. For example, with three frequencies the separation between the first two is made small enough for unambiguous range measurement, while separation of the third is large enough to provide the required accuracy of range measurement and is a multiple of the separation of first two frequencies. If the required accuracy is not provided by this, the number of frequencies can be increased.

Thus, by rather simple means, it is possible to realize the measurement of range with an error no more than 0.001% or even 0.0001%. At the same time there is a disadvantage to this method of measurement: the impossibility of range measurement on fixed targets. To measure range to a fixed target we must install a reflector on it to simulate a Doppler shift, but this is inconvenient and not always possible. This disadvantage is avoided by application of FM to the transmission.

To establish the validity of this statement, we compare (5.42) with (2.27). As we can see for $\Omega_D = 0$ in (2.27) these formulas coincide except for phase shifts $n\Omega_m\tau/2$, $\eta(\tau)$ and $\nu(\tau)$. Thus, the role of Doppler frequency is played by the modulation frequency. The phase shifts $n\Omega_m\tau/2$, $\eta(\tau)$, and $\nu(\tau)$ are identical for signals of all channels, and therefore are subtracted in measuring the phase differences.

However, comparing (5.42) with (2.27), we notice the following significant difference. Each spectral component of the converted signal in (2.27), for any modulation waveform, is formed by two signals: one in the positive frequency domain and the other in the "negative" domain but moved to the domain of positive frequencies. The amplitudes of these signals are identical for sinusoidal and symmetrical sawtooth modulations [(3.8) and (3.30)], while for asymmetrical sawtooth modulation they are different (3.20). But phase angles $\varphi_\tau = \omega_c\tau_0$ and φ_0 have different signs. The vector diagram for equal signal amplitudes is shown in Figure 5.23(a). We can see that for change of angles $\varphi_\tau = \omega_c\tau_0$ and φ_0, the signal vectors rotate in different directions, but the phase of the total signal remains constant: only its amplitude varies. Hence, sine wave and symmetrical sawtooth modulation are unacceptable in this case.

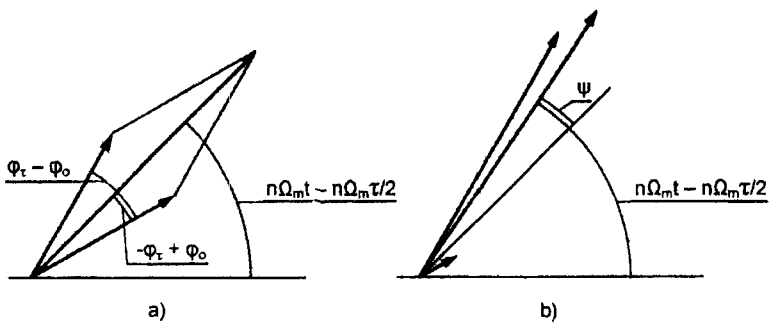

Figure 5.23 Vector diagrams for (a) sinusoidal and symmetrical sawtooth modulation, and (b) symmetrical sawtooth modulation.

The necessary phase relationships may be obtained with asymmetrical sawtooth modulation. In this case the vector diagram is shown in Figure 5.23(b). Here the phase of the total vector is defined mainly by the vector with the greater amplitude, and phase of this vector is

$$n\Omega_m t + \psi - n\Omega_m \frac{\tau}{2} \tag{5.44}$$

But $\psi = \varphi_\tau - \varphi_0$ only for $\Delta f\tau = n$, when the small vector is zero.

The angle ψ is easy to determine, using known formulas for the amplitude and a phase of the sum of two sine waves

$$\tan\psi = \frac{A_1 \sin\varphi_1 + A_2 \sin\varphi_2}{A_1 \cos\varphi_1 + A_2 \cos\varphi_2} \tag{5.45}$$

Assuming that

$$A_1 = \frac{\sin\pi(\Delta f\tau - n)}{\pi(\Delta f\tau - n)}$$

$$A_2 = \frac{\sin\pi(\Delta f\tau + n)}{\pi(\Delta f\tau + n)} \text{ and}$$

$$\varphi_1 = \varphi_\tau - \varphi_0,\ \varphi_2 = \varphi_\tau + \varphi_0$$

we obtain

$$\psi = \arctan\left[\frac{n}{\Delta f\tau}\tan(\varphi_\tau - \varphi_0)\right] \tag{5.46}$$

Using this formula, we may determine the difference between the angles ψ and $\varphi_\tau - \varphi_0$. The appropriate diagrams are given in Figure 5.24, where the ordinate is the angle $\Delta\psi = \varphi_\tau - \varphi_0 - \psi$. The angle $\Delta\psi = 0$ at $n/\Delta f\tau = 1$, increasing for deviation from unity. This angle decreases with increased n because the ratio of the smaller vector to the larger decreases. For example, $n/\Delta f\tau = 0.66$ when $n = 1$ and $\Delta f\tau = 1.5$, and $n/\Delta f\tau = 0.95$ when $n = 10$ and $\Delta f\tau = 10.5$.

Hence, for example, if the spectral component $n \geq 10$ is chosen to avoid a parasitic amplitude modulation signal, then there are no special requirements for stability of frequency deviation. If it is necessary to maintain the frequency deviation at a constant level we may apply a very simple method (see Figure 5.25). A small auxiliary sinusoidal amplitude modulation (e.g., a few percent) is applied to the sawtooth modulating voltage. Because of the deviation modulation the selected spectral component also appears modulated in amplitude. The envelope phase for $\Delta f\tau > n$ differs by 180° from that for $\Delta f\tau < n$, is detected by the amplitude detector,

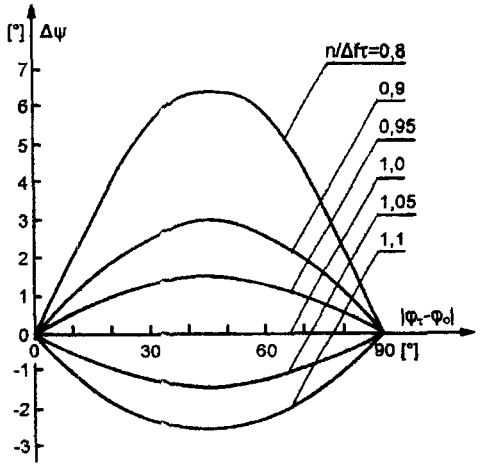

Figure 5.24 Graphs of phase measurement error.

and applied to the phase detector. The output voltage of the phase detector is used to control the frequency deviation and to maintain $\Delta f\tau \cong n$.

Thus, to realize this method of converted signal processing, we must replace, in circuit Figure 5.22, unmodulated oscillators by FM oscillators with appropriate central frequency separations, and Doppler filters by filters tuned to the frequency of selected spectral components of the converted signal. In other respects the circuit remains as shown. Realization of this circuit is not difficult. The bulkiest part of this SRR is the microwave block, including the transmitter. It is simple to obtain a small number of FM signals with separated central frequencies and in-phase modulation, using a circuit similar to Figure 4.16. We may make other technical choices, such as using a synthesizer as the transmitter exciter.

This SRR will also work for moving targets, but can be significantly simplified for measurement of range to fixed targets by omitting the simultaneous radia-

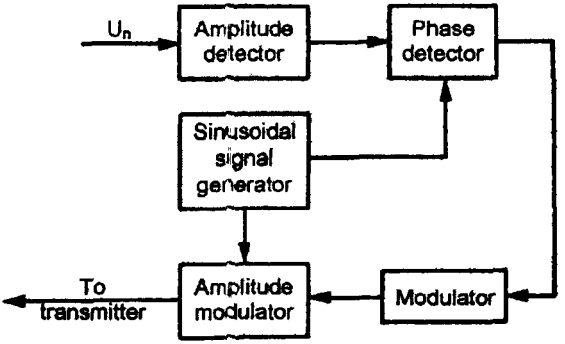

Figure 5.25 Block diagram of the control deviation system.

tion of the several FM signals with different central frequencies, in the following way. During a particular time interval, a signal with central frequency ω_c is radiated, and the output of filter $n\Omega_m$ is stored. During the next time interval, a signal with central frequency $\omega_c + \delta\omega_1$ is radiated, the filter output is again stored, and so on. The stored signals are recovered from memory and the appropriate phase differences between them are measured.

It is obvious that the standard transceiver-antenna microwave block may be used in this case. The transmitter becomes simpler, as there is no need to radiate simultaneously several signals with different central frequencies. Application of a frequency synthesizer as the exciter permits very simple frequency switching and provides the necessary stability of these frequencies. The time interval during which the signal with one or another central frequency is radiated should be about $100T_m$. This time will be sufficient to form the signal spectrum.

It is not necessary to store all the filter output signals (i.e., the sinusoid with frequency $n\Omega_m$). It is enough to measure and remember the initial phase of this sinusoid. As its frequency is known, a measurement of an initial phase is sufficient. It is obvious that the phase difference between two signals is equal to the difference between their initial phases. Modern digital technology permits us to carry out all necessary calculations.

5.5.2.2 Use of the Phase Angle $\omega_c\tau$ [4]

Presence of a phase angle $\omega_c\tau$ in the phase of each spectral component of the converted signal permits us to measure increments of ranges with errors measured in micrometers, a property that is certainly unique to FM SRR. For an illustration of this statement consider an elementary calculation. Assume that a continuous unmodulated signal with wavelength λ is radiated toward a target. Then a reflected signal phase shift of 360° is produced by a range change of $\lambda/2$. If, for example, $\lambda = 7.2$ mm, then a 10-μm change produces 1° of phase shift.

Methods of phase difference measurement on continuous unmodulated signals in centimeter and millimeter bands are well known, but they are so difficult that they have not seen practical application. In FM SRR, the phase shift information as the angle $\omega_c\tau$ is contained in any component of the converted signal spectrum. *Thus, there is an opportunity to measure the phase difference between transmitted and received microwave signals using a low-frequency signal: the modulation frequency.* This permits us to simplify considerably the actual phase meter and to increase the measurement accuracy.

The SRR being considered uses the standard single-antenna transceiver approach, for which the converted signal spectrum processing system follows the block diagram of Figure 5.26.

The reference signal for the phase detector is derived from the modulating signal. The phase shifter in the reference signal circuit cancels the angles φ_0 and $n\Omega_m\tau/2$, and shifts the phase detector characteristic working point to its linear region. The number of selected spectral components depends on target range, the

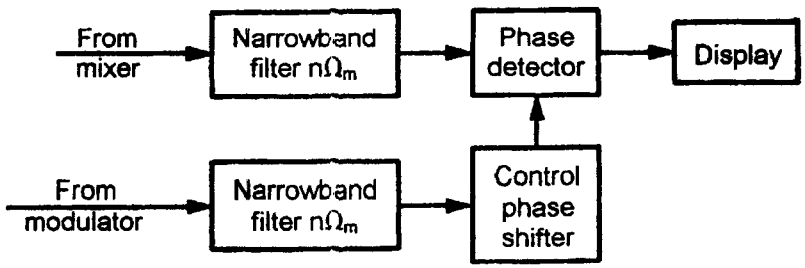

Figure 5.26 Block diagram of the phase processing system.

size of the parasitic amplitude modulation, and the frequency deviation of the transmission.

The main thing to which we must pay attention here is the modulation waveform of the transmission. Sinusoidal modulation and symmetrical sawtooth modulation are completely unacceptable, for reasons detailed in the previous section. Only asymmetrical sawtooth modulation is applicable. The adjustment of frequency deviation can be made to obtain $\Delta f\tau \cong n$, using the circuit Figure 5.25. It must be emphasized, however, that this type of SRR is not applicable to measurement of moving targets at ranges of tens or hundreds meters. It can be used very effectively to measure small target motions at ranges from fractions of a meter to several meters. As an example of application of such an SRR, we will give a brief description of an instrument for measuring the vibration levels and steam pressures inside steam turbines [5].

The standard single-antenna transceiver is used, but the propagation of electromagnetic energy to the target (reflecting surface) and back is in a waveguide whose open end is placed 2 to 3 mm from the vibrating element. This ensures a minimum illuminated area, which in turn, reduces measurement errors. Measurements of continuous vibrations of turbine components can be achieved during operation using a waveguide projecting into the turbine case. Heating the waveguide will not affect measurement, as the radio unit is outside the turbine case.

Measurement of steam pressure inside a turbine case is currently made by placing a metal membrane on the case. Pressure bends the membrane, and the amount of bending, proportional to pressure, is measured using a strain gauge. Strain gauges require cooling, and it is impossible to measure pressure inside the turbine case in this way because the steam temperature reaches 500°C at pressures up to 200 atmospheres.

The problem of pressure measurement is solved by using a radar measuring instrument in the following way. We insert a waveguide through the turbine case, terminating it with a horn covered by a membrane. Deformation of the center of the membrane is measured. Steam pressure measurement is possible at almost any location inside the turbine case by appropriate bending of the waveguide.

5.5.2.3 Use of the Phase Angle $n\Omega_M\tau/2$

The method of range measurement using the phase angle $n\Omega_m\tau/2$ is based on the fact that this angle appears in the phase of all spectral components of the converted signal. Hence, we must extract the nth spectral component and apply it to the phase detector. As a reference signal for the phase detector we use the nth harmonic of the modulating signal. Then, at the output of the phase detector we obtain a voltage directly proportional to the target range. However, the use of phase angle $n\Omega_m\tau/2$ in ranging requires observance of several conditions:

(1) We must cancel the angles $\Omega_D t$, φ_τ and φ_0;
(2) We must ensure $T_m > 2\tau_{max}$ to obtain unambiguous readout of range;
(3) The selected component of a converted signal spectrum must have no zero values in the interval of measured range.

Let us consider possible ways of obtaining these conditions. A method of canceling angles $\Omega_D t$, φ_τ, and φ_0 is known and applied in communication systems for restoration of the carrier in a balance-modulated AM signal. It is based on applying the signal to a square-law multiplier (squarer), after which a bandpass filter extracts the usual AM signal with unity modulation factor. As is known, the spectrum of a signal with balanced sine wave AM consists of two components

$$U\cos(\omega_0 t - \Omega_m t - \varphi) \quad \text{and} \quad U\cos(\omega_0 t + \Omega_m t + \varphi) \tag{5.47}$$

If this signal is applied to the square-law multiplier whose output goes through a filter passing frequencies in the vicinity of $2\omega_0$, we obtain

$$\begin{aligned} &\frac{1}{2}U^2\cos(2\omega_0 t - 2\Omega_m t - 2\varphi) \\ &+U^2\cos 2\omega_0 t \\ &+\frac{1}{2}U^2\cos(2\omega_0 t + 2\Omega_m t + 2\varphi) \end{aligned} \tag{5.48}$$

As we can see, there are no angles $2\Omega_m\tau$ and φ in the phase of the second term in (5.48). Hence, to cancel angles $\Omega_D t$, φ_τ, and φ_0, we must use a modulation such that the converted signal spectrum consists of pairs of the components with identical amplitudes and phase angles $\Omega_D t$, φ_τ, and φ_0, but having opposite signs. The spectra of converted signals with sinusoidal or symmetrical sawtooth modulation have such properties (see Sections 3.1 and 3.3.2).

As follows from (3.8) and (3.30), we may represent any pair of components of the converted signal spectrum as

$$\begin{aligned} &\pm U_n \cos\left(n\Omega_m t + \Omega_D t + \varphi_\tau - \varphi_0 - n\Omega_m \frac{\tau}{2} \right) \\ &\pm U_n \cos\left(n\Omega_m t - \Omega_D t - \varphi_\tau + \varphi_0 - n\Omega_m \frac{\tau}{2} \right) \end{aligned} \tag{5.49}$$

If this pair is applied to a square-law multiplier, the output of a bandpass filter will be

$$\begin{aligned} &\frac{U_n^2}{2} \cos\left[2\left(n\Omega_m t + \Omega_D t + \varphi_\tau - \varphi_0 - n\Omega_m \frac{\tau}{2} \right) \right] \\ &\pm U_n^2 \cos\left(2n\Omega_m t - n\Omega_m \tau \right) \\ &+ \frac{U_n^2}{2} \cos\left[2\left(n\Omega_m t - \Omega_D t - \varphi_\tau + \varphi_0 - n\Omega_m \frac{\tau}{2} \right) \right] \end{aligned} \tag{5.50}$$

The resulting filter output is an AM signal with modulation frequency $2\Omega_D$ and unity modulation factor. From this it is clear that the filter must reject spectral sidelobes in order to obtain a signal, represented by the second term in (5.50), that is free of angles $\Omega_D t$, φ_τ, and φ_0. Otherwise, the signal at the phase detector output will be modulated in amplitude, and measurement of phase difference becomes impossible. We notice that it is best to use the phase detector – lowpass filter system to obtain the signal $U_n^2 \cos(2n\Omega_m t - n\Omega_m \tau)$. A block diagram of the appropriate processing system is shown in Figure 5.27.

From this analysis, it also follows that the method is applicable only to moving targets. If $\Omega_D = 0$ and $\varphi_\tau + \varphi_0 = \pm\pi$, the signal at the phase detector input is zero. Additionally, the last equality repeats with changes of target range by multiples of half the transmitted wavelength.

In the absence of target motion, the Doppler effect can be simulated by use of dual modulation (see Sections 3.2 and 4.5.2), sinusoidal modulation being the most convenient.

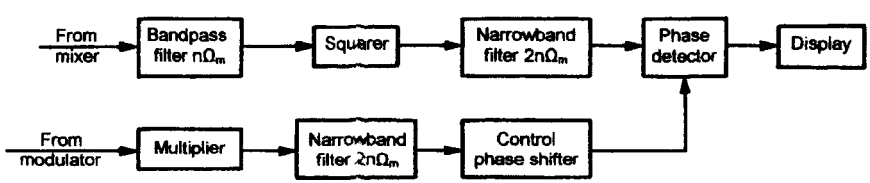

Figure 5.27 Block diagram of second type of phase processing system.

References

[1] Skolnik, M. I. (ed.), *Radar Handbook,* New York: McGraw-Hill Book Company, 1970.

[2] Turbovitch, I. T., "Dynamic Frequency Characteristics of Selectivity Systems," *Radiotechnika,* Vol. 12, No. 11, 1957, pp. 39-49.

[3] Skolnik, M. I., *Introduction to Radar Systems*, New York: McGraw-Hill Book Company, 1962.

[4] Komarov, I. V., and S. M. Smolskiy, "FM Short-Range Radar – From Systems of Weapon to Precision Distance Meters," *Proc. 3rd Int. Symposium Sibconvers'99,* Tomsk, Russia, May 18-20, 1999, pp. 392-394.

[5] Smolskiy, S. M., I. V. Komarov, et al., "FM Short-Range Radar – Vibrations and Pressure Meter," *3rd Int. Symposium Sibconvers'99,* Tomsk, Russia, May 18-20, 1999, pp. 395-396.

Part II

Chapter 6

Analysis of Constant Frequency Oscillators

The signals used in radio systems are usually sinusoidal:

$$u(t) = U\cos(\omega t + \varphi) \tag{6.1}$$

and the transmitted information is contained in modulation of the amplitude U, the radian frequency ω, or the phase φ. In most cases (even with pulse modulation), amplitude, frequency, and phase vary slowly during the period of the carrier:

$$\frac{1}{U}\frac{dU}{d\omega t} << 1, \quad \frac{d\varphi}{d\omega t} << 1 \tag{6.2}$$

On the basis of these assumptions initially formulated by Van der Pol [1], it is possible to decrease the order of the initial differential equations by reducing them to so-called "abbreviated" equations for slowly varying amplitude and phase, to facilitate study. Using this approach, called the method of slowly varying amplitudes (SVA), it is possible to describe a wide variety of tasks in the theory of oscillations [2].

In formulating the abbreviated equations the researcher proceeds from the complete differential equations usually expressed in time or in operator form. The procedure for obtaining the abbreviated equations in the time form appears tedious and leads to the goal only for simple systems (e.g., for second or third orders). Simplifications in the analysis can be achieved by use of the operator method, which allows us to formalize writing of the abbreviated equations. The method of symbolic abbreviated equations (SAE), developed by S. Evtianov, is based on this idea, being one of most convenient from the engineering point of view [3]. It is especially attractive for systems of high order or for complex systems subject to external effects, such as autodynes for short-range radar systems.

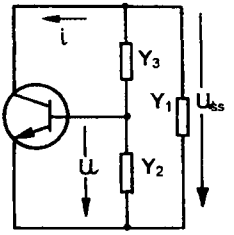

Figure 6.1 Basic circuit of single-tuned oscillator.

In this chapter a substantiation of the SAE method is first given, and elementary examples of its application are carried out and then applied to cases of multiple-order oscillator systems based on complex active bandpass elements.

6.1 RULE FOR OBTAINING THE ABBREVIATED EQUATIONS

Let us consider the single-tuned oscillator with an *inertialess* active element, say, a bipolar transistor in the range of frequencies where it is possible to neglect its inertial properties (Figure 6.1). Neglecting the entrance current of the transistor, the differential equation of the oscillator connecting the time-varying values of the input voltage $u(t)$, and collector current $i(t)$, is possible to write in a symbolic form:

$$y(j\omega)\ u = i(u) \tag{6.3}$$

Here $y(j\omega) = y_{ss}(j\omega)/\boldsymbol{k}_{fb}$ is the *control admittance*,
$y_{ss}(j\omega)$ is the admittance of the selective system (load),
$\boldsymbol{k}_{fb} = -\dot{U}/\dot{U}_{ss}$ is the complex feedback factor of the oscillator, and
$j\omega = d/dt$ is the symbolic operator of differentiation.

Examples of single-tuned oscillator circuits are given in Figure 6.2.

Equation (6.3) is correct for oscillators with inertialess two-pole active elements (AE) as well (e.g., for tunnel diodes). In this case for $y(j\omega)$ the admittance

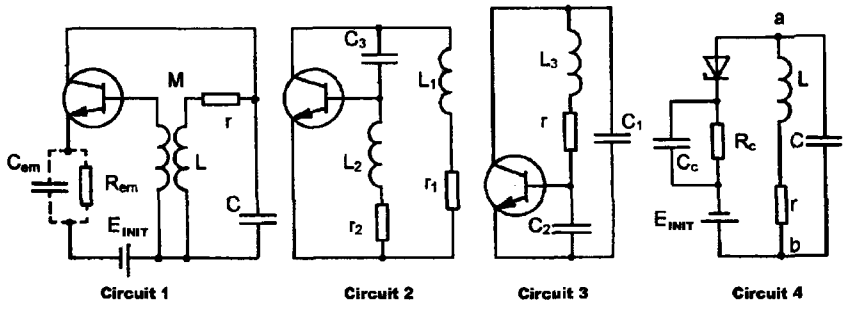

Figure 6.2 Examples of single-tuned oscillators.

between connection points of the two-pole AE (points a-b in Figure 6.2, Circuit 4) is understood.

Let us consider as a concrete example the circuit with transformer feedback (Figure 6.2, Circuit 1), for which by the usual rules of circuit theory we find:

$$y_{ss}(j\omega) = \frac{(j\omega)^2 LC + j\omega CR + 1}{j\omega L + r} \; ; \quad \boldsymbol{k}_{fb} = \frac{j\omega M}{j\omega L + r}$$

Having entered the *natural resonant frequency of the circuit* $\omega_0 = 1/\sqrt{LC}$, its *attenuation* $\delta = \omega_0 CR$ and the *control resistance* at a resonance $R = M/CR$, we obtain:

$$y\left(\frac{j\omega}{\omega_0}\right) = \frac{y_{ss}}{k_{fb}} = \frac{(j\omega/\omega_0)^2 + \delta j\omega/\omega_0 + 1}{\delta R j\omega/\omega_0} \tag{6.4}$$

Considering $j\omega/\omega_0$ as the operator of differentiation $p = d/d\tau$ in dimensionless time $\tau = \omega_0 t$, we will write on the basis of (6.3) and (6.4) the differential equations of the oscillator in operator form

$$\left(p^2 + \delta p + 1\right) u = \delta R p i(u) \tag{6.5}$$

or in time form

$$\frac{d^2u}{d\tau^2} + \delta\frac{du}{d\tau} + u = \delta R \frac{di}{d\tau} \tag{6.6}$$

Before explaining the essence of the SAE method, we will obtain from (6.6) the abbreviated equations using the well-known Van der Pol method [1]. Thus we find a solution as:

$$u(\tau) \approx U(\tau)\cos\left[\tau + \varphi(\tau)\right] \tag{6.7}$$

where U and φ are slowly varying functions of time, that is,

$$\frac{1}{U}\frac{dU}{d\tau} \sim \delta, \quad \frac{1}{U}\frac{d^2U}{d\tau^2} \sim \delta^2, \quad \frac{d\varphi}{d\tau} \sim \delta, \quad \frac{d^2\varphi}{d\tau^2} \sim \delta^2$$

The circuit attenuation δ is assumed here to be small.

The current i is represented by a Fourier series and we keep only the first harmonic component:

$$i_1(\tau) \approx I_1(\tau)\cos\left[\tau + \varphi(\tau)\right] \tag{6.8}$$

Let us differentiate (6.7) and (6.8) with respect to τ and substitute the expressions for derivatives in (6.6). Equating the coefficients for $\sin(\tau + \varphi)$ and at $\cos(\tau + \varphi)$, we have:

$$-2\frac{dU}{d\tau}\left(1+\frac{d\varphi}{d\tau}\right)-U\frac{d^2\varphi}{d\tau^2}-\delta U\left(1+\frac{d\varphi}{d\tau}\right)=-\delta RI_1\left(1+\frac{d\varphi}{d\tau}\right)$$

$$\frac{d^2U}{d\tau^2}-U\left(1+\frac{d\varphi}{d\tau}\right)^2+\delta\frac{dU}{d\tau}+U=\delta R\frac{dI_1}{d\tau}$$

Neglecting the terms of order δ^2, we obtain the system of abbreviated equations

$$\frac{2}{\delta}\frac{dU}{d\tau}+U=RI_1 \tag{6.9}$$

$$d\varphi/dt=0 \tag{6.10}$$

Let us now carry out the following formal procedure. Consider expression (6.4) near to the resonant frequency (i.e., assume $\omega = \omega_0 + \Delta\omega$, where $\Delta\omega/\omega_0 \approx \delta$ is a small frequency disturbance). Replacing ω/ω_0 in (6.4) with $1 + \Delta\omega/\omega_0$ and keeping only the first-order terms, we obtain the approximate expression $Y(j\Delta\omega)$ describing the behavior of admittance $y(j\omega)$ near the resonant frequency:

$$Y\left(j\Delta\omega\right)=\frac{\delta+2j\Delta\omega/\omega_0}{\delta R} \tag{6.11}$$

Considering that *abbreviated admittance* (6.11) relates the complex amplitudes of a current $\dot{I}_1 = I_1 e^{j\varphi}$ and voltage $\dot{U} = Ue^{j\varphi}$, and that the term $j\Delta\omega/\omega_0$ corresponds to the differentiation operator $p = d/d\tau$, from

$$Y\left(j\Delta\omega/\omega_0\right)\ \dot{U}=\dot{I}_1 \tag{6.12}$$

it is possible to obtain directly the abbreviated operating equations. Actually, from (6.12) we have:

$$\left(\delta+2\frac{d}{d\tau}\right)Ue^{j\varphi}=\delta RI_1e^{j\varphi}$$

or

$$U+\frac{2}{\delta}\frac{dU}{d\tau}+j\frac{2}{\delta}U\frac{d\varphi}{d\tau}=RI_1$$

Dividing the real and imaginary parts, we obtain the system of equations (6.9) and (6.10).

Thus, it is possible to formulate the following rule for drawing up the abbreviated equations according to the S. Evtianov method:

1) We enter complex slowly varying amplitudes of signals (complex envelopes) written using the resonant frequency ω_0;

2) We enter a small frequency disturbance and simplify the expression for symbolic admittance (or impedance) in the vicinity of the resonant frequency;

3) Replacing in the symbolic equation (6.12) for complex envelopes the small frequency disturbance $j\Delta\omega/\omega_0$ by the differentiation operator $p = d/d\tau$ and dividing the real and imaginary parts, we obtain the abbreviated equations in time form.

Though this rule is formulated here on a basis of a rather simple example (a single-tuned oscillator with fixed bias voltage), it can be applied as well to the analysis of more complex circuits. Let us show it first for autonomous non-modulated systems.

6.2 SUBSTANTIATION OF THE SAE METHOD

Let us consider the symbolic equation

$$y(p)\, u = i(u) \tag{6.13}$$

A feature of the selectivity systems commonly used is that in the denominator of the expression for admittance it is always possible to allocate a small parameter δ at least in the first degree:

$$y(p) = \frac{Q(p,\delta)}{\delta\, P(p,\delta)} \tag{6.14}$$

Having substituted (6.14) in (6.13), we obtain the symbolic equation of the oscillator:

$$Q(p,\delta)\, u = \delta P(p,\delta)\, i(u) \tag{6.15}$$

Free oscillations of a conservative system are described by the equation (6.15) at $\delta = 0$ (i.e., by the equation $Q(p,0)u = 0$). By virtue of system conservatism the characteristic polynomial $Q(p,0)$ can have only imaginary conjugated roots, if the polynomial degree is even. If the degree is odd, a zero root is added to the imaginary roots, and the solution looks like:

$$u = -\left(E - E_{init}\right) + \sum_{k=1}^{n} U_k \cos\left(\omega_k t + \varphi_k\right) \tag{6.16}$$

where: ω_k are the roots of the equation $Q(j\omega,0) = 0$ with $2n$ or $2n + 1$ degrees;
E, U_k, and φ_k are arbitrary constants, dependent upon the initial conditions; and
E_{init} is the initial bias voltage of the active element (amplifying device).

According to the SVA method we will find the solution of equation (6.15) as (6.16), assuming that arbitrary constants E, U_k, and φ_k are slowly varying functions of time. Among natural frequencies ω_k, two or more can differ from each other by amounts near δ. It is possible to replace the sum of such components in (6.16), having chosen as the natural frequency $\omega_{0k} \approx \omega_k$, by one component with a new amplitude and phase, still slowly varying. The total number of components in the sum in (6.16) will decrease and be equal to the number of nonoverlapped passbands of the selective system. The required solution will be of the form:

$$u = -(E - E_{init}) + \sum_{k=1}^{l} U_k(t)\cos\left[\omega_{0k}t + \varphi_k(t)\right] \tag{6.17}$$

Let us substitute (6.17) in the right part of (6.15) and expand as a Fourier series the current $i[u(t)]$ as a function of time. Assuming that the frequencies ω_{0k} are not harmonically related, we will keep in the decomposition only the basic components with frequencies ω_{0k}

$$i = I_0(E,U_1,...,U_l) + \sum_{k=1}^{l} I_k(E,U_1,...,U_l)\cos(\omega_{0k}t + \varphi_k) \tag{6.18}$$

Here the components I_k are functions of a bias voltage E and of amplitudes U_k. The precondition about slowly changing E and U_k allows us in the spectral analysis to consider them constant during the period of oscillation.

Having substituted (6.17) and (6.18) in (6.15), we obtain one equation for $E(t)$:

$$-Q(p,\delta)\ (E - E_{init}) = \delta\, P(p,\delta) I_0 \tag{6.19a}$$

and l equations for amplitudes of the form:

$$Q(p,\delta)\dot{U}_k\, e^{j\omega_{0k}t} = \delta\, P(p,\delta)\dot{I}_k\, e^{j\omega_{0k}t} \tag{6.19b}$$

where $\dot{U}_k = U_k e^{j\varphi_k}$, $\dot{I}_k = I_k e^{j\varphi_k}$ are complex amplitudes or complex envelopes of signals ($k = 1, 2, \ldots l$).

The system (6.19) is simplified in comparison with the complete equation (6.15) due to neglecting the combinative components of a spectrum. This is possible because the linear part of the system has highly selective properties near the

resonant frequencies. Let us notice that it is impossible to reduce (6.19b) by the exponential multiplier $e^{j\omega_{0k}t}$, as it stands under the differential operator. In order to carry it out, we apply the theorem of displacement for operational polynomials. Instead of (6.19b) we shall write:

$$Q(p+j\omega_{0k},\delta)\dot{U}_k = \delta\, P(p+j\omega_{0k},\delta)\dot{I}_k \tag{6.19c}$$

This result can be treated as the introduction of the *displaced operator*, $p_1 = -j\omega_{0k}$ working on complex envelopes of signals, instead of the operator p working on instant values. Actually, equation (6.19c) is obtained from (6.19b) after formal replacement $p = p_1 + j\omega_{0k}$ with the subsequent rejection of an index at the new displaced operator.

The equations in the form (6.19a) and (6.19c) are convenient for the simplified realization used in the SVA method. The slowness of change $E(t)$ and $\dot{U}_k(t)$ means that derivatives of order n from E, U_k, and φ_k are the sizes that have nth order of smallness

$$p^n E \sim \delta^n\ , \quad \left|p^n \dot{U}_k\right| \sim \delta^n U_k \tag{6.20}$$

This allows us to consider the operator p as having the order δ and to formalize sorting the components in the order of their smallness.

Let us consider the procedure of abbreviation in detail, using as an example one of the system equations (i.e., we will fix an index k). The results obtained for $k = 0$ will apply to equation (6.12).

Upon sorting the members according to their order of smallness we will take into account that $Q(j\omega_{0k}+p,\delta)$ and $P(j\omega_{0k}+p,\delta)$ are polynomials in p and δ (that is, they can be expanded in double Taylor series in p and δ near the point $(j\omega_{0k},0)$ with the number of terms

$$Q(j\omega_{0k}+p,\delta) = \sum_{m=0}^{M}\sum_{n=0}^{N}\frac{1}{m!}\frac{1}{n!}\frac{\partial^{m+n}Q(j\omega_{0k},0)}{\partial p^m \partial\delta^n}p^m\delta^n \tag{6.21a}$$

$$P(j\omega_{0k}+p,\delta) = \sum_{m=0}^{M}\sum_{n=0}^{N}\frac{1}{m!}\frac{1}{n!}\frac{\partial^{m+n}P(j\omega_{0k},0)}{\partial p^m \partial\delta^n}p^m\delta^n \tag{6.21b}$$

Having substituted these decompositions in equation (6.19b), we will write it as:

$$\sum_{m=0}^{M}\sum_{n=0}^{N}\frac{1}{m!}\frac{1}{n!}\left[\frac{\partial^{m+n}Q}{\partial p^m\partial\delta^n}\right]p^m\delta^n\dot{U}_k = \delta\sum_{m=0}^{M}\sum_{n=0}^{N}\frac{1}{m!}\frac{1}{n!}\left[\frac{\partial^{m+n}P}{\partial p^m\partial\delta^n}\right]p^m\delta^n\dot{I}_k \tag{6.22}$$

Here, the sizes calculated at $p = j\omega_{0k}$ and $\delta = 0$ are given in square brackets (i.e., for conservative systems).

Let us now obtain from (6.22) the *equations of the first approximation*. For this purpose it is necessary to equate on the left and on the right the terms of one (initially the first) order of smallness. If in this equation there appears an identity such as $0 = 0$, it is then necessary to keep the terms of the second order of smallness, and so forth.

Let us take into account that the order of terms in the left part is equal to a total degree $p^m\delta^n$, and in the right to $m + n + 1$ because of the presence of the multiplier δ before the double sum. Keeping the components not higher than the first order of smallness, we obtain the required equation in symbolic form:

$$\left\{\left[\frac{\partial Q}{\partial p}\right]p+\left[\frac{\partial Q}{\partial \delta}\right]\delta+[Q]\right\}\dot{U}_k=\delta[P]\dot{I}_k \tag{6.23}$$

Here $[Q] = Q(j\omega_{0k},0)$. Let us remember that the basic frequency ω_{0k} is generally near, but not equal to, ω_k, one of the resonant frequencies of the conservative system, and consequently $Q(j\omega_{0k}) \neq 0$. Let us consider at first the case of exact equality of frequencies $\omega_{0k} = \omega_k$, when $[Q] = 0$.

In (6.23), as was mentioned, there can appear an identity such as $0 = 0$, that is,

$$\left[\frac{\partial Q}{\partial p}\right]=[Q]=\left[\frac{\partial Q}{\partial \delta}\right]=[P]=0 \tag{6.24}$$

that is characteristic for systems with two degrees of freedom, when the difference between the natural frequencies has the order δ. Such systems are, to a first approximation, described by a *symbolic abbreviated equation of the second order*. To obtain it, we will leave in (6.22) members of the order δ^2:

$$\left\{\frac{1}{2}\left[\frac{\partial^2 Q}{\partial p}\right]p^2+\left[\frac{\partial^2 Q}{\partial p\partial \delta}\right]p\delta+\frac{1}{2}\left[\frac{\partial^2 Q}{\partial \delta^2}\right]\delta^2\right\}\dot{U}_k=\delta\left\{\left[\frac{\partial P}{\partial p}\right]p+\left[\frac{\partial P}{\partial \delta}\right]\delta\right\}\dot{I}_k \tag{6.25}$$

This equation, in turn, for systems with three or more degrees of freedom and close resonant frequencies, appears as an identity. Thus all terms in square brackets in (6.25) are equal to zero. Continuing the process, it is possible to show that the order of the symbolic abbreviated equation is equal to the number of resonant frequencies lying in the appropriate passband of the selectivity system. Let us notice that the symbolical abbreviated equations can be written in a form similar to the complete equation:

$$Y(p)\dot{U}_k=\dot{I}_k \tag{6.26}$$

Here, $Y(p)$ is the abbreviated admittance and p is the differential operator.

So, for reception of the abbreviated equations it is enough to proceed from instantaneous values of voltages and currents to their complex envelopes and to find the expressions for symbolic admittance near the resonant frequencies. It is easy to do this by consideration of specific auto-oscillatory systems. Moreover, the simplified expressions for admittance are familiar to radio engineers and are widely used in practice. So, the symbolic simplified admittance in (6.23) corresponds to a single-tuned oscillatory circuit, and in (6.25) to double-tuned systems with closely spaced individual frequencies.

Let us return to the complete system of the abbreviated equations. In accordance with (6.19), it consists of $l + 1$ equations, where l is the number of non-overlapping passbands of the selective system. One more equation following from (6.19a) corresponds to slowly varying bias voltage:

$$-Q(p,\delta)(E-E_{inv}) = \delta P(p,\delta) I_0(E,U_1, \ldots U_l) \tag{6.27}$$

When we refer to (6.27) as about the abbreviated one, we mean that the operator p in it works on constant components of a control voltage E and current I_0. The order of this equation is defined by inertial properties of the automatic bias circuit and is equal to the number of roots of the equation $Q(p,\delta) = 0$, located within δ of the origin of coordinates in the complex plane of roots.

We study mainly single-frequency oscillations where it is assumed that the selective system has a single passband, or that the conditions for self-excitation at other frequencies are not present. Under these preconditions the oscillator is described by two abbreviated equations such as (6.23) for the complex envelope of high-frequency voltage and (6.27) for an automatic bias circuit (if it is present).

6.3 EXAMPLES OF DERIVING THE ABBREVIATED EQUATIONS

6.3.1 Single-Tuned Oscillator with Fixed Bias Voltage

Let us consider an oscillator using, for example, a tunnel diode (Figure 6.2, Circuit 4). The active element (diode) is considered as the noninertial device with a monotonic voltage-current characteristic $i(u)$. Let us neglect the nonlinear property of the p-n junction, the inductance of the wire leads, and other parasitic parameters.

The symbolic equation for the oscillator is in the form (6.13), where the admittance between the anode and cathode of the diode is

$$y(p) = \frac{p^2LC + pCR + 1}{pL + r} \tag{6.28}$$

Neglecting the losses (considering $r = 0$), we find the resonant frequency of the oscillatory system: $\omega_0 = \sqrt{LC}$. Having entered the attenuation of an oscillatory

circuit $\delta = r/(\omega_0 L)$ and the resonant resistance $R = \omega_0 L/\delta$ of the circuit, we shall write (6.28) as:

$$y(p) = \frac{1}{\delta R} \frac{(p/\omega_0)^2 + \delta(p/\omega_0) + 1}{(p/\omega_0) + \delta} \tag{6.29}$$

According to the SAE method it is necessary to find the symbolic admittance $Y(j\omega_0 + p)$ displaced in frequency. Replacing p in (6.29) with $j\omega_0 + p$ and grouping the terms according to their orders of smallness, we have

$$Y(j\omega_0 + p) = \frac{1}{\delta R} \frac{2j(p/\omega_0) + j\delta + (p/\omega_0)^2 + \delta(p/\omega_0)}{j + (p/\omega_0) + \delta} \tag{6.30}$$

Keeping only members of first-order smallness concerning small attenuation (we consider formally $p/\omega_0 \approx \delta$), we obtain the expression for abbreviated admittance:

$$Y(p) = \frac{\delta + 2p/\omega_0}{\delta R} \tag{6.31}$$

or

$$Y(p) = G_{ss}(1 + pT) \tag{6.32}$$

where: $G_{ss} = 1/R$ is the resonant conductivity of the selective system, and
$T = 2/\omega_0\delta$ is its time constant.

The substitution (6.32) in (6.26) gives the symbolical abbreviated equation in the complex form:

$$(pT + 1)\dot{U} = R\dot{I}_1$$

Taking into account that $\dot{U} = Ue^{j\varphi}$, $\dot{I}_1 = I_1 e^{j\varphi}$, and replacing p with d/dt, we have:

$$e^{j\varphi} T\left(\frac{dU}{dt} + jU\frac{d\varphi}{dt}\right) + Ue^{j\varphi} = RI_1 e^{j\varphi} \tag{6.33}$$

After reduction by the multiplier $e^{j\varphi}$ and allocation of real and imaginary parts in (6.33), we obtain two equations in the time form:

$$T\frac{dU}{dt} + U = RI_1(U), \quad T\frac{d\varphi}{dt} = 0 \tag{6.34}$$

Similar equations apply for all single-tuned oscillators with noninertial AE. The formulas for the account of parameters ω_0, k_{fb}, R_{ss}, and R of Circuits 1-4 in Figure 6.2 are given in Table 6.1.

Table 6.1

Formulas for Calculation of Parameters of Single-Tuned Oscillators

Parameter	*Circuit Number in Figure 6.2*			
	1	*2*	*3*	*4*
ω_0	$\frac{1}{\sqrt{LC}}$	$\frac{1}{\sqrt{(L_1+L_2)C_3}}$	$\sqrt{\frac{C_1+C_2}{L_3C_1C_2}}$	$\frac{1}{\sqrt{LC}}$
k_{fb}	M/L	L_2/L_1	C_1/C_2	1
R_{ss}	$\frac{(\omega_0 L)^2}{r}$	$\frac{(\omega_0 L_1)^2}{r}$	$\frac{1}{r(\omega_0 C_1)^2}$	$\frac{(\omega_0 L)^2}{r}$
R	$\frac{\omega_0^2 ML}{r}$	$\frac{(\omega_0 L_2)^2}{r}$	$\frac{1}{r(\omega_0 C_2)^2}$	I_0

The first part of (6.34) describes the transient process of oscillation amplitude U, while the second part determines frequency of fluctuations $\omega = \omega_0 + d\varphi/dt$. As we see, in the case of noninertial AE $d\varphi/dt = 0$, the frequency (as a first approximation) is constant at $\omega = \omega_0$ and does not depend on amplitude either in the transient or steady-state mode. Such oscillators are called *isochronous*. Basically all oscillators are *anisochronous*; however, in a case of noninertial AE the frequency change is proportional to δ^2 and can be found from the abbreviated equations of the second approximation.

The first part of (6.34a) assumes simple physical treatment, for which we will write it as:

$$\frac{T}{K}\frac{dU}{dt} = I_1(U) - \frac{U}{R} \tag{6.35}$$

For an active element, the dependence of the first harmonic of a current upon the amplitude of oscillations $I_1(U)$ is referred to as the *oscillatory characteristic of an active element*. The choice of an operating point on the voltage-current characteristic $i(u)$ determines the type of the oscillatory characteristic [Figure 6.3(a, b)]. In Figure 6.3 the direct lines U/R, called *feedback straight lines*, are also shown. In accordance with (6.35), the difference between the oscillatory characteristic and feedback lines is proportional to derivative dU/dt [Figure 6.3(c, d)]. The points of crossing of the oscillatory characteristic and feedback lines, in which $dU/dt = 0$ and, accordingly, the amplitude U is constant, determine the steady-state modes of the oscillator

$$I_1(U) = U/R \tag{6.36}$$

The function $I_1(U)$ describes a high-frequency current delivered by the AE to an oscillatory circuit, and U/R is the high-frequency current consumed by a circuit.

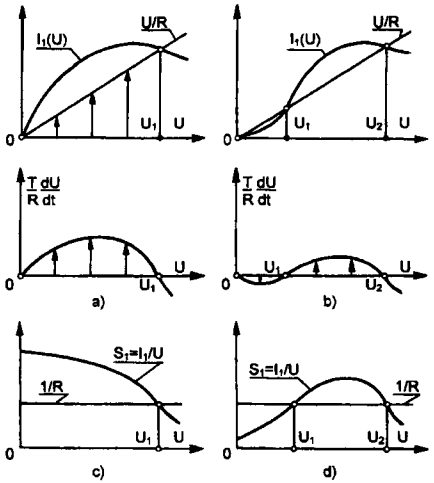

Figure 6.3 Operating points for different oscillator circuits.

When the generated and consumed currents are equal there is a *stationary mode of oscillations*. If the generated current is more than consumed: $I_1(U) > U/R$, $dU/dt > 0$ (i.e., the amplitude of oscillations increases), while if $I_1(U) < U/R$, $dU/dt < 0$ and the amplitude falls. This permits judging the *stability of the stationary modes*.

From Figure 6.3(a) we can see that the oscillator has stationary modes at two points: $U = 0$ and $U = U_1$. The point of rest $U = 0$ is unstable. The amplitude of oscillations, since small values increase, approaches U_1. Such a mode of oscillation excitation is referred to as *soft*. If under the influence of any of external or internal effect the amplitude exceeds U_1, the derivative dU/dt becomes less than zero and the amplitude will return to the value U_1. This means that the stationary mode of oscillations is stable.

In Figure 6.3(b) (for an oscillatory characteristic of another type) there are three stationary mode points: $U = 0$, $U = U_1$, and $U = U_2$. The point of rest is locally stable: if $U < U_1$, $dU/dt < 0$ and in the course of time $U \to 0$ (i.e., small increments around a point of rest fade and the operating point comes back to a point $U = 0$). If under influence of a large input (for example, a shock excitation), the amplitude U becomes more than U_1, the fluctuations will increase, approaching an amplitude U_2. With further increase of amplitude (for any reason), the operating point returns to a point U_2. Hence, the stationary mode at a point $U = U_2$ appears locally stable. Such a mode of oscillation excitation is referred to as *rigid*.

Let us write the conditions of local stability of stationary modes in analytical form. From Figure 6.3 we can see that the stationary modes are stable if $dI_1/dU < 1/R$. Let us transform this expression for a stable point. Here $U \to 0$ and $I_1 = SU$, where S is the *slope* of the voltage-current characteristic $i(u)$ at the operating

point. Hence, $dI_1/dU = S$ and the *conditions of self-excitation* of oscillations take the form

$$S > 1/R \text{ or } SR > 1 \tag{6.37}$$

For points of a stationary mode with final amplitude we will enter an average *slope* S_1 of the *oscillatory characteristic* $I_1 = S_1(U)U$. Calculating from this derivative $dI_1/dU = S_1 + UdS_1/dU$ and taking into account that in the stationary mode $S_1(U) = 1/R$, we obtain for the condition of stability:

$$dS_1 / dU < 0 \tag{6.38}$$

The geometrical interpretation of conditions (6.37) and (6.38) is shown in Figure 6.3(c, d). For monotonic dependence of $S_1(U)$ only one stationary point with nonzero amplitude [Figure 6.3(c)] exists that appears stable for soft self-excitation. For nonmonotonic dependence of $S_1(U)$ we have two stationary points with nonzero amplitude: the point with the greater amplitude is locally stable, and that with smaller amplitude is locally unstable. No point of a stationary mode has global stability. The self-excitation here appears rigid.

6.3.2 Single-Tuned Oscillator with Automatic Bias

If *automatic bias* is used in the oscillator, the mode of an active element will be determined not only by the value of the oscillation amplitude, but also by the value of a *bias voltage* E at the operating point. The abbreviated equation for a slowly varying bias voltage should be added to the abbreviated equations for complex slope of the control voltage in this case. Consider that in the equations for the first approximation it is usually possible to neglect any reduction in the constant voltage in the high-frequency circuit. Equating the voltage of an *initial bias source* E_{init} to the sum of the voltage on the autobias circuit and the input of the AE, we obtain the symbolic abbreviated equation for a bias voltage E:

$$E_{init} = \frac{I_0(E,U)}{Y_{bi}(p)} + E \tag{6.39}$$

Here: $I_0(E,U)$ is the *constant component of current* of an active element dependent both on amplitude and on bias voltage, and
$Y_{bi}(p)$ is the *admittance of the autobias circuit.*
For the usual RC circuits of autobias (Figure 6.2, Circuits 1 and 4)

$$Y_{bi}(p) = \frac{1 + pT_{em}}{R_{em}} \tag{6.40}$$

where $T_{em} = R_{em}C_{em}$ is the time constant of the autobias circuit.

Recall that p is here the differentiation operator applied to constant components of signals E and I_0. Substituting (6.40) in (6.39) and replacing p with d/dt we obtain the abbreviated equation for the autobias circuit in time form. Combining it with (6.34), we write the complete system of the abbreviated equations for an oscillator with autobias circuit:

$$\begin{cases} T\dfrac{dU}{dt} + U = RI_1(U,E), \\ \dfrac{d\varphi}{dt} = 0, \\ T_{em}\dfrac{dE}{dt} + E = E_{init} - R_{em}I_0(U,E) \end{cases} \tag{6.41}$$

The second equation, as before, concerns the isochronous feature of the oscillator (as a first approximation). For study of transients in the circuit it is necessary to solve the first and last parts of (6.41) simultaneously, as both parts include nonlinear functions (I_1 and I_0) of E and U.

Having put in (6.41) $dU/dt = 0$ and $dE/dt = 0$, we obtain the system of the equations determining stationary modes of the oscillator:

$$\begin{aligned} U &= RI_1(U,E) \\ E &= E_{init} - R_{em}I_0(U,E) \end{aligned} \tag{6.42}$$

Notice that the approach using the oscillatory characteristics (effective in study of oscillators with fixed bias $E = E_{init} = \text{const}$) cannot directly be used in this case. For the solution of system (6.42), two approaches can be used.

First, it is possible to calculate or measure experimentally the so-called dynamic oscillatory characteristics - the dependence of $I_1(U)$ on bias voltage E, determined by (6.42b). The amplitude U is set, and (6.42b) yields the appropriate bias voltage, where the values of E and U define the first harmonic of current $I_1(E,U)$. Experimental values may be measured similarly. An active element (for example, diode in Circuit 4, Figure 6.2) may be considered together with an auto bias circuit (i.e., concerning points 1, 2). To these points, a variable voltage with slowly varying amplitude U is supplied and the first harmonic of the AE current is measured. If the amplitude U varies so slowly that at each value of U the stationary value of auto bias voltage E has time to be established, the result of the experiment is the dynamic oscillatory characteristic $I_1(E,U)$. The points of its crossing a feedback line U/R define stationary modes of the oscillator.

Such an approach allows us to judge correctly the transients and stability of stationary modes, provided that the processes in the auto bias circuit occur much

faster than in an oscillatory circuit ($T_{em} << T$). This is called the case of non-inertial autobias.

Generally with comparable T_{em} and T it is expedient to use the approach of cutoff and bias diagrams. The dependence of $U(E)$, following the first part of (6.42), is referred to as the cutoff diagram, and dependence of $E(U)$, in the second part, as the bias diagram.

Physically, the cutoff diagram determines the dependence of oscillation amplitude U on bias voltage E for fixed parameters of the high-frequency circuit of the oscillator (control resistance R, feedback factor, etc.). The bias diagram determines a voltage E, established in the autobias circuit of the oscillator for a given amplitude U and constant parameters of the autobias circuit. The points of crossing of the cutoff and bias diagrams correspond to stationary modes of the oscillator.

Moreover, the plane (E,U) can be considered as the *phase plane* of an oscillator with autobias circuit. The term "phase" does not imply that the phases of signals are examined on a plane. The phase plane method was used for the first time in the theory of nonlinear fluctuations for consideration of the phase condition in mechanics, from which the name was derived. On the phase plane each point corresponds to specific values of oscillation amplitude and bias voltage, and movement on the phase plane corresponds to the laws of change in time of these parameters. The phase plane method (or the more general method of phase space) is very convenient for qualitative studies of nonlinear dynamic systems, to which autodyne signal converters belong.

Having solved equations (6.41) for the derivative and having divided the first equation by the second (i.e., having excluded time), we obtain the differential equation for *phase trajectories:*

$$\frac{dU}{dE} = \frac{T_{em}}{T} \frac{RI_1(E,U) - U}{E_{init} - R_{em} I_0(E,U) - E} \tag{6.43}$$

The application of the phase plane for study of transients in oscillators is discussed in detail in [3]. Here we consider two elementary cases:

(1) $T_{em} << T$;

(2) $T_{em} >> T$.

Notice that on the cutoff diagram the numerator of the fraction in (6.43) goes to zero (i.e., the cutoff diagram on a plane (E,U) is the *isoclinal line of horizontal tangent* (ILHT) to phase trajectories: $dU/dE = 0$). On the contrary, in points of the bias diagram the denominator in (6.43) goes to zero, meaning that the bias diagram is the *isoclinal line of vertical tangent* (ILVT) to phase trajectories: $dU/dE \to \infty$.

In the first case ($T_{em} \to 0$), in accordance with (6.43), $dU/dE \to 0$ at all points (E,U), except for the bias diagram. This means that for any point in the phase plane the corresponding point on the bias diagram moves horizontally (at constant

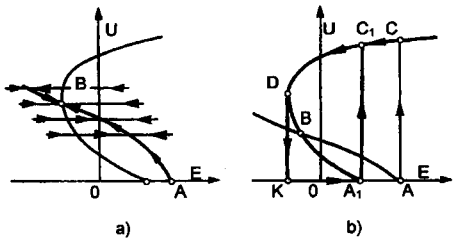

Figure 6.4 Phase portraits for (a) extra-low T_{em} and (b) extra-large T_{em}.

amplitude U) and further in the bias diagram moves to a point of a stationary mode [Figure 6.4(a)]. The direction of movement in the bias diagram is determined from the equation (6.41a): $dU/dt > 0$ "inside" the cutoff diagram and $dU/dt < 0$ outside of it. From the phase portrait in Figure 6.4(a) we can see that the point of rest A is unstable, the fluctuations increase softly, and the stationary mode in a point B is stable.

Another picture appears for significant inertiality of the bias circuit ($T_{em}/T \to \infty$). In this case, in accordance with (6.43), $dU/dE \to \infty$ at any point outside of the cutoff diagram. Physically, it means that the processes in the oscillating circuit occur much faster than in the autobias circuit, and the representing point from any point on a plane (E,U) moves vertically in the cutoff diagram [Figure 6.4(b)]. The movement in the cutoff diagram is determined by (6.41b) for an autobias circuit: $dE/dt < 0$ for points laying more to the right of the bias diagram and, on the contrary, $dE/dt > 0$ for points to the left of it. As a result both the point of rest A and the point of the stationary mode B appear unstable. From the point of rest, the representing point quickly passes to a point C on the cutoff diagram, and then slowly (at the rate of the time constant T_{em}) to a point D, where the tangent to the cutoff diagram is vertical. From here the point can move only to the left or downwards. The movement downward prevails (i.e., the amplitude U falls rapidly to zero at the rate of the time constant of a contour T). Further, condenser C_{em} is uncharged (voltage E grows) so long as conditions of self-excitation of oscillations are again executed. This occurs at point A_1, the amplitude here increases up to value at the point C_1, and then the process repeats. There is a limiting cycle A_1C_1DK, appropriate to faltering generation.

6.4 GENERAL ABBREVIATED AND CHARACTERISTIC EQUATIONS OF ANISOCHRONOUS OSCILLATORS

Studies of low-frequency oscillators usually take into account only one nonlinear parameter of an active element - the slope of the output current averaged on the first harmonic, assuming that it is a real function. It is equivalent to the replacement of the active element by an inertialess one-port network.

It is impossible in most cases to consider active elements of modern microwave diode oscillators used in autodyne SRRs as inertialess, and they should be frequently represented at high frequency by a unique but complex parameter. This complicates the study. It is even more difficult to study processes in high-frequency transistor oscillators. The basic feature of transistors as active elements of high-frequency oscillators is the need to represent them by two-port networks, all four characteristic parameters of which are nonlinear and complex.

The purpose of this section is to derive general abbreviated and characteristic equations for high-frequency transistor oscillators. At the same time a unique restriction can be applied to the inertia of an active element: the rather weak frequency dependence of its parameters within the passband of the oscillatory system, though the delay time of a signal in an active element can be significant. The majority of microwave amplifying devices satisfies these conditions, and therefore their general equations can be used for the analysis of single-frequency modes of oscillators using transistors, klystrons, tunnel diodes, Gunn and Reed diodes, and so forth.

6.4.1 Abbreviated Equations of Anisochronous Oscillators

The generalized so-called *three-port* circuit of the oscillator studied is given in Figure 6.5(a). For analysis it can be reduced to the circuit with an ideal transformer shown in Figure 6.5(b), which is more convenient for study. The active element in the circuit is represented by a two-port network with common, input, and output electrodes. The circuit with an ideal transformer is characterized by the transformation factor k_t, admittance of dispersion y_σ, and output admittance Y_{ss} of the oscillatory system. The relation between these parameters and the elements of the three-terminal circuit is determined by the following formulas:

$$k_t = \frac{\dot{U}}{\dot{U}_{ss}}\bigg|_{\dot{I}_{in}=0} = \frac{Y_3}{Y_2+Y_3}, \qquad y_\sigma = \frac{\dot{I}_{in}}{\dot{U}}\bigg|_{\dot{U}_{ss}=0} = \frac{(Y_2+Y_3)Y_4}{Y_2+Y_3+Y_4}$$

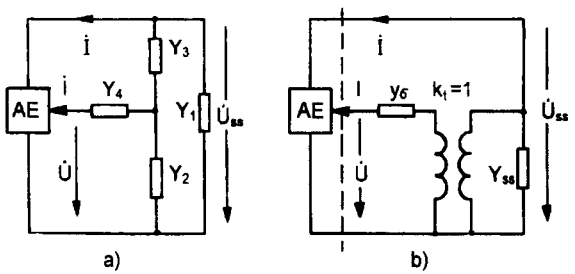

Figure 6.5 Generalized three-port oscillator circuits.

$$Y_{ss} = -\left.\frac{\dot{I}_{out}}{\dot{U}_{ss}}\right|_{\dot{I}_{in}=0} = Y_1 + \frac{Y_2 Y_3}{Y_2 + Y_3}, \qquad \dot{k}_{fb} = -\frac{\dot{U}}{\dot{U}_{ss}} = \frac{Y_{12} - k_t y_\sigma}{Y_{11} + y_\sigma}$$

Let us consider the circuit of the oscillator as a parallel connection of two two-port networks: active element (AE) and feedback circuit (FB) [the division is shown in Figure 6.5(b) by a dashed line]. Let us assume that due to the filtering properties of the FB circuit, the voltages in the circuit are close to sinusoidal. Having chosen as a reference the resonant frequencies of the oscillatory system ω_0 or close to it, we write

$$u(t) = \mathrm{Re}\dot{U} e^{j\omega_0 t}, \quad u_{ss}(t) = \mathrm{Re}\dot{U}_{ss} e^{j\omega_0 t}$$

where $\dot{U} = Ue^{j\phi}$ and $\dot{U}_{ss} = U_{ss}e^{j\varphi}$ are the complex envelope of voltages.

This assumption allows us to characterize the AE by the averaged first harmonic *Y*-parameters, which are generally complex and nonlinear:

$$\dot{I}_{in} = Y_{11}\dot{U} + Y_{12}\dot{U}_{ss}, \quad \dot{I}_{out} = Y_{21}\dot{U} + Y_{22}\dot{U}_{ss} \tag{6.44}$$

Having entered currents $\dot{I}'_{in}$ and $\dot{I}'_{out}$ flowing in an FB circuit, and having determined the *Y*-parameters, we obtain:

$$\dot{I}'_{in} = y_\sigma \dot{U} - k_t y_\sigma \dot{U}_{ss}, \quad \dot{I}'_{out} = -k_t y_\sigma \dot{U} + (Y_{ss} + k_T{}^2 y_\sigma)\dot{U}_{ss} \tag{6.45}$$

Combining equations (6.44) and (6.45) in pairs and taking into account that $\dot{I}_{in} + \dot{I}'_{in} = 0$ and $\dot{I}_{out} + \dot{I}'_{out} = 0$, we write in the symbolical form the system of abbreviated equations determining the influence of voltages $\dot{U}$ and $\dot{U}_{ss}$ on oscillatory system:

$$\dot{U}_{ss} = N(E,U)\dot{U} \tag{6.46a}$$

$$Y(E,U)\dot{U}_{ss} = Y_{ss}(p)\dot{U}_{ss} \tag{6.46b}$$

Here: $N = -1/k_{fb} = \dot{U}_{ss}/\dot{U}$ is a function opposite to the FB factor,

$$N(E,U) = -1/\boldsymbol{k}_{fb} = -(Y_{11} + Y_\sigma)/(Y_{12} - k_t y_\sigma), \tag{6.47}$$

$Y(E,U)$ is the *equivalent output admittance* of the oscillator referred to points of connection of the oscillatory system,

$$Y(E,U) = \frac{(Y_{12} - k_t y_\sigma)(Y_{21} - k_t y_\sigma)}{Y_{11} + y_\sigma} - Y_{22} - k_t^2 y_\sigma, \tag{6.48}$$

$Y_{ss}(p)$ is the abbreviated admittance of the oscillatory system at break on an AE input, and

$p = d/dt$ is the differential operator applied to complex signal envelopes.

In (6.46) it is shown that the nonlinear functions N and Y depend on the amplitude of the input voltage U and on the bias voltage E. This assumption is adequate for the so-called understressed mode [4], when the influence of the collector voltage and the Y-parameters of the transistor on the first harmonic can be neglected.

The system (6.46) describes processes in the fixed-bias oscillator ($E = E_{init}$ = const). These equations are complex, corresponding actually to four differential equations, the solution of which is quite difficult. However, for many practical oscillator circuits it is possible with the correct choice of common and input electrodes to make the transition from the practical circuit to one with an ideal transformer while achieving independence of function N from p. Then the two equations following from (6.46a), become algebraic, simplifying the study.

If we neglect the nonlinearity of input admittance Y_{11} and admittance of return reaction Y_{12} of the active element (i.e., consider k_{fb} as constant), (6.46a) is reduced to trivial form and it can be ignored in the analysis. This case is equivalent to representation of the AE by an inertial one-port network.

If automatic bias is used in the oscillator, (6.46) should be supplemented by the abbreviated equation for the autobias circuit, which can be found from Figure 6.6, where it is assumed that the autobias circuit as well as in the input electrode of AE are in the common electrode circuit:

$$E + I_{in0} / Y_{in}(p) + I_{com0} / Y_{com}(p) = E_{init} \tag{6.49}$$

where: I_{in0} and I_{com0} are constant components of currents of input and common electrodes,

E_{init} is the voltage of the external bias source, and

$Y_{in}(p)$ and $Y_{com}(p)$ are symbolical admittances of the autobias circuits.

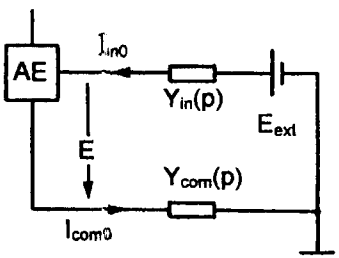

Figure 6.6 Oscillator circuit with autobias.

In considering (6.49) as with the abbreviated one, it is necessary to interpret the abbreviation of admittance $Y_{in}(p)$ and $Y_{com}(p)$ near "zero" frequency (i.e., to consider p as the differential operator applied to constant components of signals).

Equations (6.46) and (6.49) form a system of general abbreviated equations describing in the single-frequency approach processes in the anisochronous oscillator with a complicated oscillatory system and automatic bias circuits.

6.4.2 Stationary Modes of the Oscillator

To calculate the stationary modes of the oscillator, it is necessary in the abbreviated equations (6.46) and (6.49) to put $p = j\lambda$, where $\lambda = \omega - \omega_0$:

$$N(E,U)U = U_{ss} \tag{6.50a}$$

$$Y(E,U) = Y_{ss}(j\lambda) \tag{6.50b}$$

$$E + I_{in0}/Y_{in}(0) + I_{com0}/Y_{com0}(0) = E_{init} \tag{6.51}$$

Equation (6.50b) can be divided in two, having shared the real and imaginary parts:

$$G(E,U) = Y_{re}(\lambda), \tag{6.52a}$$

$$B(E,U) = Y_{im}(\lambda), \tag{6.52b}$$

where $G = \mathrm{Re}Y$, $B = \mathrm{Im}Y$, $Y_{re}(\lambda) = \mathrm{Re}(j\lambda)$, $Y_{im}(\lambda) = \mathrm{Im}(j\lambda)$. From (6.52b), we can see that generally $B \neq 0$, and it is impossible to determine the change of oscillation frequency λ irrespective of amplitude U and bias voltage E (anisochronity) that was possible in the analysis of oscillators using electronic lamps. For this reason, oscillators with inertial AE are called anisochronous.

Four equations of a stationary mode (6.50a), (6.51), (6.52a), and (6.52b) determine four unknown parameters: U, E, λ, and U_{ss}. Note that (6.51) and (6.52) do not depend upon U_{ss}, and hence it is possible at first from these equations to find U, E, and λ, and then from (6.50a) to determine U_{ss}. Therefore, the stationary state of the oscillator is completely determined by a point in *three-dimensional phase space* U, E, and λ, and (6.51), (6.52) establish surfaces crossed in points of a stationary mode.

Graphic methods are often applied for a solution to the equations. Let us assume at first that in the oscillator a fixed bias is used ($E = E_{init}$). Then it is necessary to solve simultaneously the equations (6.52) for E = const:

$$G(U) = Y_{re}(\lambda), \quad B(U) = Y_{im}(\lambda) \tag{6.53}$$

We see that even in this elementary case for the isochronous oscillator it is impossible to apply the approach of the oscillatory characteristics, as the right parts of the equations (6.53) depend on λ. However, the system (6.53) can be solved by the *method of hodographs*. For this purpose on a plane *B, G* we can plot the hodographs of equivalent admittance of the oscillator using (6.19b)

$$Q(p,\delta)\dot{U}_k e^{j\omega_{0k}t} = \delta P(p,\delta)\dot{I}_k e^{j\omega_{0k}t}$$

and of the oscillatory system Y_{ss}. The first, the hodograph of an active element, is derivable from the equation $Y(U) = G(U) + jB(U)$, where the oscillation amplitude is considered as a parameter. The second hodograph can be plotted from the equation $Y_{ss}(\lambda) = Y_{re}(\lambda) + jY_{im}(\lambda)$ with parameter λ. The points where the hodographs cross define stationary values of amplitude and frequency.

With automatic bias it is also possible to apply the method of hodographs, having modified it a little. The hodograph of the oscillatory system remains the same. The hodograph of the AE can be plotted in this way: we set the amplitude U from (6.51), find the appropriate value of E, and at these values we define components G, B, belonging to the AE hodograph. By analogy to the dynamic oscillatory characteristics it is possible to call this hodograph the *dynamic hodograph of AE*.

6.4.3 General Characteristic Equation of the Anisochronous Oscillator

The processes in oscillators are described by the nonlinear differential equations. In accordance with Liapunov, it is possible to determine the local stability of stationary states based on the behavior of a *linearized system*. Let us proceed to drawing up the linearized equations, considering for simplicity the case of single autobias.

First, note the following. The stationary-state equations determine the value of frequency change $\lambda_i = \omega_{osc} - \omega_0$ of oscillation frequency ω_{osc} relative to reference frequency ω_0. Therefore, in a stationary state the phases φ and ϕ are linear functions of time: $\varphi(t) = \lambda_i t + \varphi_i$, $\phi(t) = \lambda_i t + \phi_i t$. Thus, before linearization of the abbreviated equations it is also necessary to shift all operators by $\lambda = \omega_{osc} - \omega_0$, which is equivalent to abbreviation of admittance $Y_{ss}(p)$ concerning the frequency of stationary oscillations. In this case, abbreviated equations (6.46) will take the form:

$$\dot{U}_{ss} = N(E,U)\dot{U} \tag{6.54a}$$

$$Y(E,U)\dot{U}_{ss} = Y_{ss}(p + j\lambda)\dot{U}_{ss} \tag{6.54b}$$

Together with (6.39) for the bias circuit these form the complete system of the abbreviated equations of the oscillator. To find the equations of a stationary mode, it is necessary to put in this system $p = 0$.

Let us apply small increments to values determining a stationary mode: $U = \mathring{U} + \xi$, $E = \mathring{E} + \varepsilon$, $U_{ss} = \mathring{U}_{ss} + \eta$, and $\varphi = \mathring{\varphi} + \alpha$, where the circle above designates values of functions calculated at a stationary point. Let us now expand the functions $U_{ss}e^{j\varphi}$, NU, $YU_{ss}e^{j\varphi}$, in Taylor series in the vicinity of a stationary mode with small increments ξ, ε, η, and α. Neglecting terms of second and higher orders, we obtain:

$$U_{ss}e^{j\varphi} = \mathring{U}_{ss}\, e^{j\mathring{\varphi}} + e^{j\mathring{\varphi}}(\eta + j\mathring{U}_{ss}\,\alpha)$$

$$NU = \mathring{N}\mathring{U} + (\mathring{N} + \mathring{U}\frac{\partial \mathring{N}}{\partial U})\xi + \mathring{U}\frac{\partial \mathring{N}}{\partial E}\varepsilon$$

$$YU_{ss}e^{j\varphi} = \mathring{Y}\mathring{U}_{ss}\, e^{j\mathring{\varphi}} + e^{j\mathring{\varphi}}\left\{\mathring{Y}\eta + \mathring{U}_{ss}\frac{\partial \mathring{Y}}{\partial U}\xi + \mathring{U}_{ss}\frac{\partial \mathring{Y}}{\partial E}\varepsilon + j\mathring{Y}\mathring{U}_{ss}\,\alpha\right\}$$

Substitution of these decompositions in the initial equations (6.54), (6.39) and exclusion of the equations for a stationary mode give the *system of linearized equations*:

$$\eta - \mathring{N}(1+\mathring{n})\xi - \mathring{U}\frac{\partial \mathring{N}}{\partial E}\varepsilon = 0 \tag{6.55a}$$

$$(\mathring{Y} - Y_{ss})\eta + \mathring{U}_{ss}\frac{\partial \mathring{Y}}{\partial U}\xi + \mathring{U}_{ss}\frac{\partial \mathring{Y}}{\partial E}\varepsilon + j\mathring{U}_{ss}(\mathring{Y} - Y_{ss})\alpha = 0 \tag{6.55b}$$

$$\frac{\partial \mathring{I}_{com0}}{\partial U}\xi + \left[\frac{\partial \mathring{I}_{com0}}{\partial E} + Y_{com}(p)\right]\varepsilon = 0 \tag{6.55c}$$

where $n = (U/N)(\partial N/\partial U)$.

The second equation is complex; therefore the system actually includes four linearized equations relative to four variations. To simplify the problem, we will exclude from the system a variation of the phase α. For this purpose we will divide in the equation (6.55b), to look like: $A\eta + B\xi + C\varepsilon + jD\alpha = 0$, the real and imaginary parts:

$$\eta\,\mathrm{Re}\,A + \xi\,\mathrm{Re}\,B + \varepsilon\,\mathrm{Re}\,C - \alpha\,\mathrm{Im}\,D = 0 \tag{6.56}$$

$$\eta\,\mathrm{Im}\,A + \xi\,\mathrm{Im}\,B + \varepsilon\,\mathrm{Im}\,C + \alpha\,\mathrm{Re}\,D = 0 \tag{6.57}$$

Multiply (6.56) by ReD, (6.57) by ImD, and combine the resulting equations:

$$\eta \mathrm{Re}(AD^*) + \xi \mathrm{Re}(BD^*) + \varepsilon \mathrm{Re}(CD^*) = 0 \tag{6.58}$$

Hereafter, the symbol * designates the conjugate complex.

Substituting in (6.58) the values of A, B, C, and D from (6.55b), we obtain instead of (6.57) and (6.58) a single linearized equation

$$|\overset{\circ}{Y} - Y_{ss}|^2 \left\{ \eta + \xi \mathrm{Re} \frac{\hat{U}_{ss}(\partial \overset{\circ}{Y}/\partial U)}{\overset{\circ}{Y} - Y_{ss}} + \varepsilon \mathrm{Re} \frac{\overset{\circ}{U}_{ss}(\partial \overset{\circ}{Y}/\partial E)}{\overset{\circ}{Y} - Y_{ss}} \right\} = 0 \tag{6.59}$$

Let us note that it is impossible to reduce (6.59) using $\left|\overset{\circ}{Y} - Y_{ss}\right|^2$, as in this case the equation loses sense at $p = 0$, as $\overset{\circ}{Y} - Y_{ss}(j\lambda_i) = 0$, in accordance with (6.50b).

Equations (6.55a), (6.59), and (6.55c) describe the behavior of the linearized system for small disturbances around the stationary mode. The operator p thus is considered as a *parameter of exponential solutions*. The condition of nontrivial solutions of system of linearized equations results in the general characteristic equation:

$$\left|\overset{\circ}{Y} - Y_{ss}\right|^2 \begin{vmatrix} 1 & -\hat{N}(1+\hat{n}) & -\overset{\circ}{U}(\partial \hat{N}/\partial E) \\ 1 & \mathrm{Re}\dfrac{\overset{\circ}{U}_{ss}(\partial \overset{\circ}{Y}/\partial U)}{\overset{\circ}{Y} - Y_{ss}(p+j\lambda)} & \mathrm{Re}\dfrac{\overset{\circ}{U}_{ss}(\partial \overset{\circ}{Y}/\partial E)}{\overset{\circ}{Y} - Y_{ss}(p+j\lambda)} \\ 0 & \partial \hat{I}_{com0}/\partial U & \partial \overset{\circ}{I}_{com0}/\partial E + Y_{com}(p) \end{vmatrix} = 0 \tag{6.60}$$

Having expanded the determinant on elements of the first column and reduced first line by N, we will write the characteristic equation as:

$$\left|\overset{\circ}{Y} - Y_{ss}\right|^2 \begin{vmatrix} 1 + \overset{\circ}{n} + \mathrm{Re}\dfrac{\overset{\circ}{U}(\partial \overset{\circ}{Y}/\partial U)}{\overset{\circ}{Y} - Y_{ss}} & \dfrac{\overset{\circ}{U}}{N}\dfrac{\partial \overset{\circ}{N}}{\partial E} + \mathrm{Re}\dfrac{\overset{\circ}{U}(\partial \overset{\circ}{Y}/\partial E)}{\overset{\circ}{Y} - Y_{ss}} \\ \partial \overset{\circ}{I}_{com0}/\partial U & \partial \overset{\circ}{I}_{com0}/\partial E + Y_{com}(p) \end{vmatrix} = 0 \tag{6.61}$$

Here $Y_{ss} = Y_{ss}(p + j\lambda)$ and all derivatives are calculated at the point of a stationary mode.

With combined emitter and base autobias circuits, the third line of the characteristic determinant becomes complicated and expression for it can be simply derived from (6.49).

For oscillators with inertial one-port networks (Gunn diodes, klystrons, Reed diodes) or for inertial two-port networks, the admittances Y_{11} and Y_{12} of which do not depend on mode parameters, the characteristic equation turns out from (6.61) at $n = 0$ and $\partial N/\partial E = 0$. If the AE is also inertialess (electronic lamp, transistor at low frequencies), the characteristic equation becomes even simpler - the complex nonlinear function $Y(U)$ is replaced by the real $G(U)$.

The derivation of general abbreviated and characteristic equations is of interest from two points of view. First, the procedure of derivation of the equations for the specific circuits becomes much simpler, allowing us to concentrate attention directly on the analysis of systems. Second, it is possible to reveal some general properties of autooscillatory systems, which we will now describe.

6.4.4 Condition of Self-Excitation of Oscillators with Inertial Active Elements

To obtain the conditions of self-excitation of oscillators (i.e., to study stability of an initially stationary point, or point of rest), it is necessary in the characteristic equation (6.61) to put $\lambda = 0$, $U = 0$, $U_{ss} = 0$ and to take values of nonlinear functions in the point $U = 0$. Having done this, we will write the result as the product of two coefficients:

$$\left[\partial \mathring{I}_{com0}/\partial E + Y_{com}(p)\right]\cdot\left|Y(0) - Y_{ss}(p)\right|^2 = 0 \tag{6.62}$$

The first coefficient characterizes the stability of a point establishing a constant current, and the second to excitation of oscillations with frequency $\omega \approx \omega_0$.

In transistor and lamp oscillators, the equation

$$\partial I_{com0}/\partial E + Y_{com}(p) = 0 \tag{6.63}$$

as a rule, has roots with a negative real part, as usually $\partial \mathring{I}_{com0}/\partial E > 0$, and $Y_{com}(p)$ is the symbolical admittance of the passive circuit. The situation in diode oscillators is different. In this case, for excitation the working point of high-frequency oscillations on the volt-ampere characteristic of the AE always gets out on a site with negative resistance, so $\partial \mathring{I}_{com0}/\partial E = \partial i/\partial u\,|_{u=E} = -1/R_- < 0$. At the same time the working point should be stable for a constant current. For example, for the simple RC autobias circuit

$$Y_{com}(p) = (1 + pT_{com})/R_{com}$$

where $T_{com} = R_{com}C_{com}$ the equation (6.63) takes the form:

$$pT_{com} + 1 - (R_{com} / R_{-}) = 0$$

From this it follows that the working point is stable with a constant current, if $R_{com} < R_{-}$, and is unstable if $R_{com} > R_{-}$. Both these cases are shown in Figure 6.7. In the second case (the straight line 2 in the figure) three steady-state regimes are present and the working point at a falling site of the characteristic $i(u)$ is unstable, and the system, depending on the initial conditions, passes to one of two steady-state conditions with a constant current. However, here $\partial i/\partial u > 0$ and the opportunity to excite oscillations (at least, softly) at high frequency vanishes.

The stability of a point of rest to excitation of high-frequency fluctuations is determined by the following characteristic equation with order $2m_{ss}$, where m_{ss} is the order of symbolical admittance Y_{ss}:

$$|Y(0) - Y_{ss}(p)|^2 = \{Y(0) - Y_{ss}(p)\}\{Y(0) - Y_{ss}(p)\}^* = 0 \qquad (6.64)$$

As the polynomials with complex conjugate factors have complex conjugate roots, the real parts of the roots of the equations $Y(0) - Y_{ss}(p) = 0$ and $[Y(0) - Y_{ss}(p)]^* = 0$ coincide. Therefore, in the analysis of stability of a point of rest, it is possible to proceed from the characteristic equation (6.64) with the real factors, to the complex characteristic equation

$$Y(0) - Y_{ss}(p) = 0 \qquad (6.65)$$

for which the order is less by two. It simplifies the analysis of self-excitation conditions of the concrete circuits.

6.4.5 Order of the Characteristic Equation and the Sign of the Factor at the Upper Derivative

For definition of the order of the characteristic equation we will open the characteristic determinant (6.61), being the algebraic multinomial of p. The senior

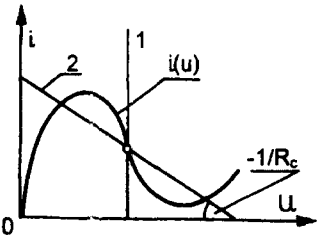

Figure 6.7 Operating characteristic of the oscillator.

member of the determinant is included in expression

$$(1+n)Y_{com}(p)\left|Y_{ss}(p+j\lambda)\right|^2 \tag{6.66}$$

Recall that the order of symbolical admittance is equal to the maximal degree p of its numerator or denominator. For oscillatory systems such as a parallel contour forming *quasi-sinusoidal signal* of voltage, the degree of the numerator $Y_{ss}(p)$ is greater than or equal to the degree of the denominator, and therefore the order of admittance is equal to the degree of the numerator. The same applies to symbolical admittances of autobias circuits.

Let us designate through m_{ss} and m_{com} the orders of the oscillatory system and the autobias circuit. Then the order of the characteristic determinant (6.61) is equal to $2m_{ss} + m_{com}$. However, the order of the characteristic equation m is reduced by one, as the free member of the characteristic determinant, which can be obtained from (6.61) at $p = 0$, is identically equal to zero, as $\overset{\circ}{Y} - Y_{ss}(j\lambda) = 0$ in accordance with (6.50b). Thus, $m = 2m_{ss} + m_{com} - 1$. It is obvious that with combined autobias (where the autobias circuits are included in a common and an input circuit) the order of the characteristic equation will increase and will be equal to $2m_{ss} + m_{com} + m_{in} - 1$.

Let us consider how we can define the sign of factor a_0 in the upper term of the characteristic equation. In accordance with (6.66), a_0 is equal to the product of the coefficient $(1 + n)$ in the upper term of the product $Y_{com}(p)|Y_{ss}(p + j\lambda)|^2$. As $Y_{com}(p)$ and $Y_{ss}(p + j\lambda)$ are the admittances of the passive circuits, all factors of polynomials in the numerator and denominator of expressions for $Y_{com}(p)$ and $|Y_{ss}(p + j\lambda)|^2$ are positive, and the sign of the factor a_0 agrees with the sign of the efficient $(1 + n)$. For stability factor a_0 to be positive $(1 + n) > 0$. This condition is a general condition of stability and is sometimes referred to as the condition of singular stability. The violation of it results in occurrence of special unstable modes such as stochastic relaxational automodulation of amplitude and frequency. Similar modes are characteristic for any dynamic system described by the abbreviated equations, of which the factor in the upper derivative can pass through zero with change of parameters.

References

[1] Van der Pol, B., *Nonlinear Theory of Electrical Oscillations* (in Russian), Moscow: Svyaz, 1937.

[2] Kapranov, M. V., V. N. Kuleshov, and G. M. Utkin, *Nonlinear Fluctuations in Radio Engineering* (in Russian), Moscow: Nauka, 1984.

[3] Bogachev, V. M., V. G. Lysenko, and S. M. Smolskiy, *Transistor Generators and Autodynes* (in Russian), Moscow: Publishing House of MPEI, 1993.

[4] Evtianov, S. I., *Lamp Generators* (in Russian), Moscow: Svyaz, 1967.

Chapter 7

Analysis of FM Systems Using Symbolical Abbreviated Equations

Modern short-range radars, including those with autodynes, use frequency modulation to increase the noise stability and reliability of operation, as has been noted in the previous chapters. The analysis of autodynes is complicated and strictly speaking we cannot apply the common radio engineering approach of symbolical abbreviated equations. Nor do quasi-static methods produce desirable conclusions, as with the *quasi-static approach* we cannot investigate the *dynamic properties* of the system, where the autodyne signal represents a particular variation of the stationary parameters.

There is also the problem of extending the method of symbolical abbreviated equations to FM generators (i.e., to systems with variable parameters). This new problem has not been examined earlier but will be carried out in this chapter. Thus, the general equations of systems with constant parameters will be derived again, as in Chapter 6, but in a more complex form applicable when diverse control signals (low-frequency, high-frequency asynchronous, high-frequency synchronous, control, stabilizing, etc.) operate on the autodyne. The method of symbolical abbreviated equations is then applied to FM autodynes. Examples of this approach are given at the end of the chapter.

7.1 SYMBOLICAL ABBREVIATED EQUATIONS FOR CONTROLLED SELF-OSCILLATORY SYSTEMS OF ANY KIND

A large amount of scientific and technical research has been devoted to analysis of various self-oscillatory systems (SOS), beginning with the classic theory of oscillations and extended in many modern studies. Especially in short-range radar, the constantly growing requirements for technical and operational characteristics of SOS operation, emergence of new types of active microwave devices, new microwave circuit design, intensive development and expansion of SOS functionality, and development of new mode control facilities require consideration of qualita-

tively new and significantly more complicated problems, demanding modernization of existing methods and development of new analysis methods.

The purpose of this chapter is the development of a general technique for analysis of the stationary modes and transients for autodyne SRRs with the various types of control signals that may be applied for diversified purposes.

In developing a general approach to analysis of *multielement SRRs* using SOS, an important step is to develop a physical and mathematical model that describes the phenomena encountered in such systems. The authors have studied the influence of signals of various types on the multipurpose SOS. Analysis of published models and the authors' operational experience have allowed them to develop a generalized model of the multielement SRR, one structure of which is shown in Figure 7.1.

The complex active element (CAE) of the SOS is shown in Figure 7.1 as a *multiport circuit*. High-frequency CAE inputs and outputs designated from 1 to n are connected (generally through an element with delay τ_{hf}) to a selective system (SS) that provides necessary signal filtration, and also to the high-frequency (HF)

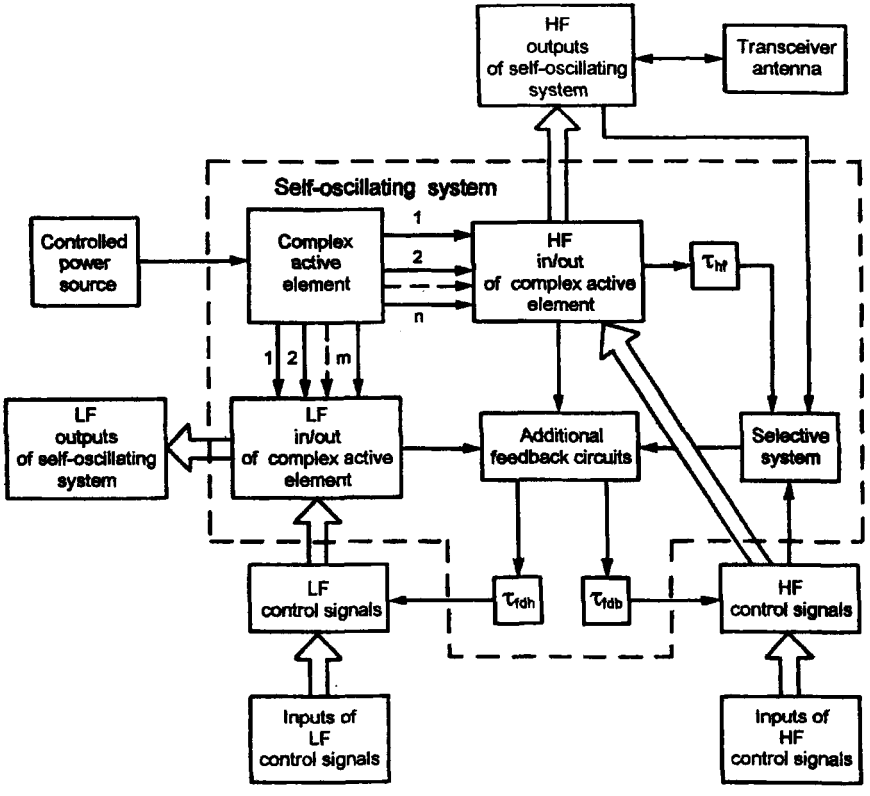

Figure 7.1 Structure of one cascade generalized model for a multielement short-range radar system.

output to the transceiver antenna. HF control signals from the appropriate inputs are applied to the HF inputs of the CAE and to the signal reflected into the antenna by the target. Low-frequency (LF) CAE inputs and outputs, marked 1 to *m*, connect to the low-frequency radar outputs. LF control signals (e.g., modulations, stabilization, control, etc.) are applied to the LF CAE inputs and to the SS.

Additional feedback (AFB) circuits that are often used to give specific properties to the SOS are shown in Figure 7.1. The LF and HF signals generally may be inputs to these circuits, and output signals of the AFB circuits may be applied both to LF and HF CAE inputs, through elements with delay τ_{fb}. The controlled power supply providing necessary voltages to the CAE and to separate SS elements (e.g., varicaps, varactors, or pin-diodes) is controlled by LF control signals. Multielement SRRs may use various configurations of the cascades shown in Figure 7.1, connected through HF and LF inputs and outputs or through space.

As the CAE in the circuit we may use inertialess and *inertial double-pole active elements*, which include tunnel diodes, avalanche diodes, Gunn diodes, negatrons (artificially created elements with negative resistance or conductivity) and their combinations, *two-port networks* (bipolar and field-effect transistors, transistor-diode circuits), and also *compound amplifying devices* (amplifiers of various types, multiport microcircuits and microassemblies, and also complex combinations of active and passive elements, including those using various physical principles of operation).

Oscillatory circuits in the system of Figure 7.1 may also be varied: concentrated and distributed elements; operating in reflection or transmission modes (or combined); with constant or controlled parameters; with selective circuit structures that generate the *quasi-sinusoidality* of the necessary (input and output) voltages or currents (so-called *Y*, *H*, *Z*, and *G*-circuits [1]); with special structures providing the necessary functioning of multielement SRRs (e.g., for creation of the self-oscillatory *autodyne phased antenna array*).

The structure of the CAE circuit also may vary depending on the task required. It may be a system to maintain constant oscillation amplitude, to maintain *modulation characteristic linearity* for the frequency-controlled generator, or to stabilize the autodyne detector potential; a *phase-locked loop* (PLL) system for frequency trim or automatic adjustment of phase, a system for *frequency restoration* on the received monopulse, or a device for expansion of stability zones or the synchronism band of the SOS.

The model presented is general enough to allow theoretical study of various SRRs that generate and process radio signals on the basis of self-oscillatory systems. The main preconditions of the generalized SOS analysis are the following:

- The oscillatory system has a large *Q-factor* (for the chosen voltage or current), that allows using the method of slowly changing amplitudes;
- The inertial CAE properties do not vary in the SS passband (i.e., the CAE does not contain within its structure any frequency-selective parts tuned near the operating frequency).

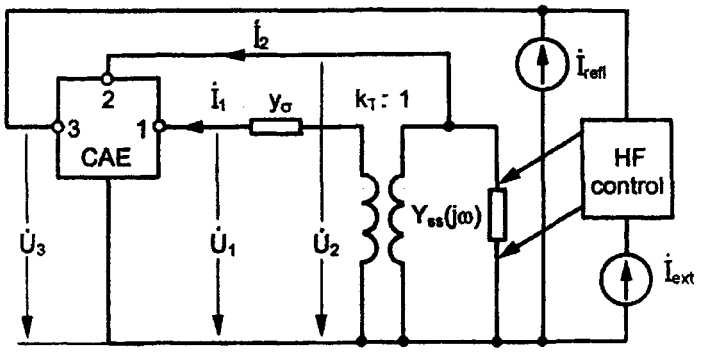

Figure 7.2 Self-oscillatory system on a three-input active element with an HF control circuit.

These assumptions apply in the majority of practical cases. We will consider again the case in which the operating frequency is unmodulated and the SOS contains a three-input CAE (Figure 7.2) with an HF control circuit. The following circuit parameters are designated: the complex amplitudes of the first harmonics of CAE voltages and currents, the current bearing the information from a reflected signal I_{refl}, and an external synchrosignal current I_{ext}. The oscillatory system in the case studied is used in the transmission mode: it is included between output 2 and input 1 electrodes of the CAE and is characterized, as usual, by its coupling factor k_T, the conductivity of dispersion y_σ, and the SS output conductivity Y_{ss}. For concreteness we will consider that the oscillatory system provides a *parallel resonance* at the operating frequency (i.e., it forms, from the nonsinusoidal output current i_2, the sine wave voltages u_1 and u_2).

We can obtain from this diagram the following subsystems: (a) the usual autodyne circuit, synchronized by an external signal, by excluding from the circuit the HF control block and input 3 of the CAE; (b) the circuit of an independent (unsynchronized) autodyne, by setting $I_{ext} = 0$; or (c) the usual oscillator circuit, by setting $I_{ext} = 0$ and $I_{refl} = 0$.

Let us represent the CAE by a system of complex parameters averaged at the first harmonic, as in Chapter 6:

$$\dot{I}_i = \sum_{j=1}^{3} Y_{ij} \dot{U}_j \tag{7.1}$$

where Y_{ij} are complex functions of amplitudes and phases of CAE input voltages.

The SS and HF circuits are described by the following equations:

$$\begin{cases} -\dot{I}_1 = y_\sigma \dot{U}_1 - k_T y_\sigma \dot{U}_2 \\ -\dot{I}_2 - \ddot{I}_2 = -k_T y_\sigma \dot{U}_1 + \left(Y_{ss} + k_T^2 y_\sigma\right)\dot{U}_2 + \dot{I}_{ext} \end{cases}, \quad \begin{cases} -\dot{I}_1 = Y_{32} \dot{U}_2 + Y_{33} \dot{U}_3 \\ -\ddot{I}_2 = Y_{22} \dot{U}_2 + Y_{23} \dot{U}_3 \end{cases} \tag{7.2}$$

where Y_{22}, Y_{23}, Y_{33}, and Y_{32} are parameters of the HF control circuit. Current sources I_{refl} and I_{ext} are also referred to the oscillatory system and the HF control circuit.

Excluding the currents from (7.1) and (7.2) and passing from complex amplitudes to amplitudes and phases of signals, we obtain three complex equations:

$$\begin{cases} U_2 e^{j\omega} = \dot{N}_1\left(U_1, U_2, U_3, I_{ext}, \varphi, \phi\right) U_1 e^{j\omega}, \\ U_2 e^{j\omega} = \dot{N}_3\left(U_1, U_2, U_3, I_{ext}, \varphi, \phi\right) U_3 e^{j\Omega t\omega}, \\ \dot{Y}\left(U_1, U_2, U_3, I_{ext}, \varphi, \phi\right) U_2 e^{j\varphi} = Y_{SS}\left(p + j\lambda\right) U_2 e^{j\varphi} + \dot{I}_{ext} \end{cases} \tag{7.3}$$

where N_1, N_3 and Y are nonlinear complex functions of amplitudes and phases, Ω is the frequency difference of a synchrosignal, and Y_{SS} is a complex function of the differential operator p. If it is necessary to use an automatic bias circuit for maintenance of the necessary mode of the amplifying devices included in CAE, we must add to (7.3) the differential equation for an autobias circuit having the following structure:

$$Y_{bi}(p)E + J_0(U_1, U_2, E) = E_{init} / R_{bi} \tag{7.4}$$

where $Y_{bi}(p)$ is the symbolical admittance of the autobias circuit, E and E_{init} are the resulting and initial bias voltages, and J_0 is the nonlinear direct current flowing through the active part R_{bi} of the admittance. In the presence of autobias the functions N_1, N_3, and Y in (7.3) will depend on the bias voltage E. The system (7.3), (7.4) forms the seven real nonlinear differential equations describing the processes in the self-oscillatory system to be analyzed. For $p = 0$ the general equations of SOS stationary modes follow from (7.3).

Local stability of single-frequency modes is determined by the general characteristic equation that may be obtained from (7.3) and (7.4) through linearization. We will omit these calculations as they are similar to those used in Chapter 6. So, for the synchronized generator with an HF control circuit without autobias, the characteristic equation is of the form:

$$\Delta = P_1 Q_2 - P_2 Q_1 = 0 \tag{7.5}$$

where Δ is a characteristic determinant of the linearized equation system.

On the basis of the described approach, we have obtained the general abbreviated and characteristic equations for the nonisochronous autonomous oscillator [2] and the synchronized oscillator [3], and the general abbreviated and linearized equations for transistor autodynes [4] of various types (Y, H, Z, and G). Using

these equations, many concrete problems in the analysis, calculation, and design of various autodyne self-oscillatory systems for SRR can be solved.

7.2 METHOD OF SYMBOLICAL ABBREVIATED EQUATIONS FOR FM SYSTEMS

Let us proceed to construction of a mathematical model of the self-oscillatory system with time-varying parameters, for which the method of the symbolical abbreviated equations cannot be directly used. The appeal of this method for radio engineers and science officers is obvious, as it allows them to use the classical approach of nonlinear oscillation theory, operating with complex amplitudes familiar to the engineer. To extend the method of symbolical abbreviated equations to FM generators and autodynes, with the objective of simplifying the calculations and discussions, we will consider an equivalent circuit of FM self-oscillatory system, Figure 7.3, containing a negatron (a two-pole active network with a nonlinear characteristic $i(u)$, where i and u are time signals of current and voltage). The symbolical conductivity $Y_{SS}(j\omega,\mu)$ of the oscillatory system depends not only upon the differential operator $j\omega$ but also upon a *modulation parameter* μ (or set of parameters) and has a polynomial form:

$$Y_{ss}(j\omega,\mu) = R(j\omega,\mu)/Q(j\omega,\mu) \tag{7.6}$$

The full differential equation of the FM generator will become

$$R(j\omega,\mu)u(t) = Q(j\omega,\mu)i(t) \tag{7.7}$$

Let us now perform *truncation* of (7.7) in general aspect. For this purpose we represent the required signals in a quasi-harmonic form:

$$u(t) = \dot{U}\exp(j\int\omega_{ss}dt)\ ,\ i(t) = \dot{I}\exp(j\int\omega_{ss}dt) \tag{7.8}$$

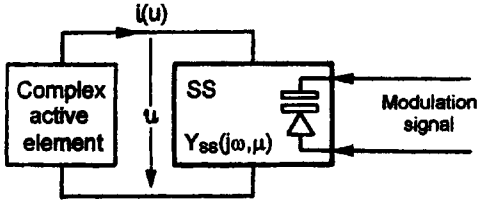

Figure 7.3 Equivalent circuit of an FM self-oscillatory system on a two-pole negatron.

where $\dot{U} = U\exp(j\varphi)$, $\dot{I} = I\exp(j\phi)$ are complex amplitudes of signals and ω_{SS} is the modulated circuit frequency. Now (7.7) will become:

$$R(j\omega,\mu)\dot{U}\exp(j\int\omega_{ss}dt) = Q(j\omega,\mu)\dot{I}\exp(j\int\omega_{ss}dt) \tag{7.9}$$

Let us now expand (7.9) polynomials R and Q of the current frequency of order l and n in a Taylor series:

$$R(j\omega,\mu) = \sum_{m=0}^{l}\alpha_m(\mu)(j\omega)^m\ ,\ Q(j\omega,\mu) = \delta\sum_{m=0}^{n}\beta_m(\mu)(j\omega)^m \tag{7.10}$$

Here it should be noted that factors of polynomial decomposition in series α_m and β_m may depend on the parameter μ, depending on time according to the modulation type. It is also taken into account that, for the usual oscillatory systems providing a parallel resonance near the working frequency, we may assume in the denominator of the symbolical polynomial $Y_{SS}(j\omega,\mu)$ that the attenuation δ is a *small parameter of the problem*. Now we will rewrite (7.9) as:

$$\begin{aligned}&\left[\exp\left(j\int\omega_{ss}dt\right)\right]\sum_{m=0}^{l}\sum_{i=0}^{m}\binom{m}{i}\left[(j\omega)^i\alpha_m\dot{U}\right]\left[(j\omega)^{m-i-1}\,j\omega_{ss}\right]\\ &=\delta\left[\exp\left(j\int\omega_{ss}dt\right)\right]\sum_{m=0}^{n}\sum_{i=0}^{m}\binom{m}{i}\left[(j\omega)^i\beta_m\dot{I}\right]\left[(j\omega)^{m-i-1}\,j\omega_{ss}\right]\end{aligned} \tag{7.11}$$

Here the operators $j\omega$ act only on those time functions that appear with them in square brackets.

Equation (7.11) is a complex and difficult equation, but it is possible to carry out in it a reduction of the rapidly oscillating members $\exp\left(j\int\omega_{ss}dt\right)$ as they are already removed from under the operator p. This will simplify a problem, but will not result in the abbreviated equations because for truncation it is necessary to carry out the sorting of members according to their order of smallness, for the measure of which we will use the attenuation δ of the oscillatory system. Considering as usual that changes of amplitude and phase of oscillations during the period are small, as well as the rate of frequency modulation, we will sort terms of (7.11) in order of smallness, having first expanded α_m and β_m in MacLaurin series in δ:

$$\alpha_m(\mu) = \sum_{i=0}^{\infty}\alpha_{mi}(\mu)\delta^i\ ,\ \beta_m(\mu) = \sum_{i=0}^{\infty}\beta_{mi}(\mu)\delta^i$$

After sorting the terms of (7.11) in order of smallness and rejection of high-order terms, we obtain the required abbreviated differential equations of the first approximation:

$$\begin{aligned}\delta\alpha_{01}\dot{U}+j\alpha_{10}\dot{U}\Delta\omega+j\delta\omega_0\alpha_{11}\dot{U}+j\alpha_{20}\dot{U}(j\omega\Delta\omega)+\left(j\omega\alpha_{10}\dot{U}\right)\\ +2j\omega_0\left(j\omega\alpha_{20}\dot{U}\right)=\delta\beta_{00}\dot{I}+j\delta\omega_0\beta_{10}\dot{I}\end{aligned} \tag{7.12}$$

Recall that $j\omega$ is the differential operator that operates on slowly varying complex amplitudes of signals $\dot{U}$ and $\dot{I}$ (i.e., on their amplitudes U, I, and phases φ,ϕ), as well as on the frequency difference $\Delta\omega$ and factors α_{ij} and β_{ij} that vary with modulation frequency. Equation (7.12) is complex and therefore its real and imaginary parts can be divided into two real equations. Having added this system to the equations connecting amplitude and phase of the first harmonic of current and voltage $\dot{U}$ (the connection being defined by the active element used in the generator), we will obtain two real equations describing the transients of amplitude U and phase φ of frequency-modulated oscillations.

In case (7.12) transforms into an identity such as 0 = 0, this means that the equations of the first approximation do not describe the practical case and it is necessary to complicate the problem, by using equations including the second approximation, whose members have the second order of smallness in attenuation δ. These equations follow from (7.11), taking into account terms of the second order, and take the form:

$$\begin{aligned}&j\delta\alpha_{11}\dot{U}\Delta\omega+j\delta^2\alpha_{12}\dot{U}\omega_0+j\delta\alpha_{21}\dot{U}(j\omega\Delta\omega)+j\alpha_{30}\dot{U}\left[(j\omega)^2\Delta\omega\right]\\ &+\delta\left(j\omega\alpha_{11}\dot{U}\right)+2j\Delta\omega\left(j\omega\alpha_{20}\dot{U}\right)+2j\omega_0\delta\left(j\omega\alpha_{21}\dot{U}\right)+3\left(j\omega\alpha_{30}\dot{U}\right)(j\omega\Delta\omega)\\ &+(j\omega)^2\left(\alpha_{20}\dot{U}\right)+3j\omega_0\left[(j\omega)^2\alpha_{30}\dot{U}\right]\\ &\quad=\delta\beta_{01}\dot{I}+j\delta\beta_{10}\Delta\omega\dot{I}+j\delta\beta_{20}\dot{I}(j\omega\Delta\omega)+\delta\left(j\omega\beta_{10}\dot{I}\right)+2j\delta\omega_0\left(j\omega\beta_{20}\dot{I}\right)\end{aligned} \tag{7.13}$$

Here also the differential operator $j\omega$ acts only on those slowly varying functions of time that are in the bracket with the operator.

Thus, the algorithm for using this procedure to obtain the abbreviated SOS equations for systems with modulated parameters is the following. We write the expression for the symbolical admittance Y_{SS} of the oscillatory system, allocate the

polynomials of its numerator and denominator, and determine the order of smallness of the terms. We then determine the expressions for the factors α_{10}, α_{01}, α_{11}, α_{20}, β_{00}, β_{10} and substitute them in (7.12). Further substituting in (7.12), as we did for systems with constant parameters, expressions for the complex amplitudes of voltage and current, we perform differentiation and separation of the real and imaginary parts, writing the abbreviated equations in the obvious form. If (7.12) then yields an identity (as, for example, in the case of a coupled-circuit oscillatory system with nearly equal individual frequencies), we must use equations of the second approximation (7.13) for analysis.

The proposed approach to the analysis of the frequency-modulated self-oscillatory systems is expanded in our works to more complex cases, when, in addition to a low-frequency (modulating) influence on the oscillatory system, other types of influence [5] apply as well.

Let us consider some concrete examples of deriving the abbreviated equations for FM systems.

7.3 DIFFERENTIAL EQUATIONS OF SOME FM SYSTEMS

In this section we will obtain the full and abbreviated differential equations of elementary frequency-modulated systems.

7.3.1 Differential Equations of a Parallel Conservative LC Circuit with Variable Capacitance and an Active Two-Pole

The basic circuit of the system is shown in Figure 7.4(a). The nonlinear element is represented as a source of current $i(u)$. Equating the sum of the currents flowing into unit "a" of the circuit, we obtain the integral-differential equation:

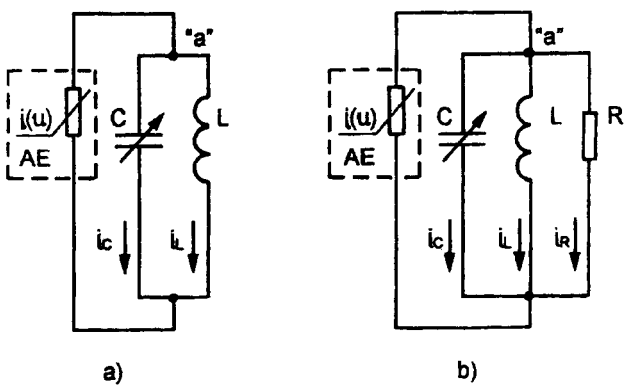

Figure 7.4 Basic conservative (a) and dissipative (b) tuned circuits with variable capacity and an active two-pole.

$$i(u) = i_L + i_C = \frac{1}{L}\int u(t)dt + \frac{d}{dt}(Cu) \tag{7.14}$$

where it is assumed that the capacitance $C(t)$ depends upon a time for realization of frequency modulation.

Differentiating (7.4) with respect to time

$$\frac{d}{dt}i(u) = \frac{1}{L}u + \frac{d^2}{dt^2}(Cu) \tag{7.15}$$

We take the second derivative:

$$\frac{d^2}{dt^2}(Cu) = \frac{d}{dt}\left[C\left(\frac{du}{dt}\right) + u\left(\frac{dc}{dt}\right)\right] = C\frac{d^2u}{dt^2} + 2\frac{du}{dt}\frac{dC}{dt} + u\frac{d^2C}{dt^2} \tag{7.16}$$

Substituting (7.16) in (7.15), and taking into account that $\frac{di(u)}{dt} = \frac{di}{du}\frac{du}{dt}$, we obtain the full differential equation of the system:

$$C(t)\frac{d^2u}{dt^2} + 2\frac{dC}{dt}\frac{du}{dt} + \left(\frac{1}{L} + \frac{d^2C}{dt^2}\right)u - \frac{di}{du}\frac{du}{dt} = 0 \tag{7.17}$$

If the frequency of the system is not modulated (i.e., $c(t)$ = const), this equation is reduced to the usual conservative equation of a tuned circuit with parallel nonlinearity $i(t)$:

$$C\frac{d^2u}{dt^2} + \frac{1}{L}u - \frac{di}{dt}\frac{du}{dt} = 0 \tag{7.18}$$

Let us derive (7.17) by the symbolical method. We enter the symbolical conductivity of the circuit

$$Y_{ss} = \frac{1}{j\omega L} + j\omega C = \frac{1 + \left[(j\omega)^2 LC\right]}{j\omega L} \tag{7.19}$$

Substituting (7.19) in the symbolical equation of the tuned circuit $i = Y_{SS}(j\omega)u$, we obtain

$$i(u) = \frac{1 + \left[\left(j\omega^2\right)LC\right]}{j\omega L}u \tag{7.20}$$

Replacing $j\omega$ with the differential operator d/dt, we obtain the required equation

$$L\frac{di}{du}\frac{du}{dt} = u + \frac{d^2}{dt^2}(LCu) \tag{7.21}$$

which accurately coincides with (7.17) if we take into account the necessity of differentiation of both functions of time: $u(t)$ and $C(t)$.

7.3.2 Differential Equations of a Parallel Dissipative LC Circuit with Variable Capacitance and an Active Two-Pole

This basic circuit is shown in Figure 7.4(b). Operating as in the previous case, we find the full differential equation of the dissipative circuit with nonlinearity and FM:

$$C(t)\frac{d^2u}{dt^2} + 2\frac{dC}{dt}\frac{du}{dt} + \left(\frac{1}{L} + \frac{d^2C}{dt^2}\right)u - \left(\frac{di}{du} - \frac{1}{R}\right)\frac{du}{dt} = 0 \tag{7.22}$$

If the frequency is not modulated (i.e., $C(t)$ = const), the equation is reduced to the usual dissipative equation of a circuit with parallel nonlinearity $i(u)$:

$$C\frac{d^2u}{dt^2} + \frac{1}{L}u - \left(\frac{di}{dt} - \frac{1}{R}\right)\frac{du}{dt} = 0 \tag{7.23}$$

Let us derive (7.23) by the symbolical method. We enter symbolical conductivity of the circuit

$$Y_{ss} = \frac{1}{j\omega L} + \frac{1}{R} + j\omega C = \frac{R + j\omega L + \left[(j\omega)^2 LCR\right]}{j\omega LR} \tag{7.24}$$

Substituting (7.24) in the symbolical equation $i = Y_{SS}(j\omega)u$, we obtain

$$i(u) = -\frac{R + j\omega L + \left[(j\omega^2)LCR\right]}{j\omega LR}u \tag{7.25}$$

Replacing here $j\omega$ with the differential operator d/dt yields the required equation:

$$L\frac{di}{du}\frac{du}{dt} = u + \frac{L}{R}\frac{du}{dt} + \left[\left(\frac{d^2}{dt^2}\right)LCu\right] \tag{7.26}$$

In transformations it will again be necessary to take into account the differentiation of both functions of time $u(t)$ and $C(t)$.

It is clear that the full differential equations derived in this section apply to cases of independent tuned circuits, when the external current i is zero, and to self-oscillatory systems in which the external current i is developed by an active element and compensates, in the mode of stationary oscillations, for the losses in the oscillatory circuit and the generator load.

7.4 ABBREVIATED DIFFERENTIAL EQUATIONS OF SINGLE-TUNED OSCILLATORS WITH SINUSOIDAL FM

We will consider a procedure for derivation of the abbreviated differential equations of single-tuned oscillators. The basic circuit of such a generator at high frequency is shown in Figure 7.5. The active element is assumed for concreteness to be a bipolar transistor, which for simplicity is considered to be an inertialess device with large input resistance at the operating frequency. Under the influence of control signal $u(t)$ the transistor develops a current $i(t)$ flowing into the tuned circuit and compensating for the common losses. The control voltage u is coupled to the output u_{SS} through the feedback factor $k_{fb} = -u/u_{SS}$, determined by the circuit parameters.

We will consider that ohmic losses of the circuit are concentrated in inductances L_1 and L, and that they are proportional to those inductances: $r_1/r = L_1/L$. Sinusoidal modulation of frequency described by

$$\omega(t) = 1/\sqrt{L_{total}C_{total}(t)} = \sqrt{LC(t)} = \omega_0(1+\varepsilon\cos\Omega_m t) \tag{7.27}$$

is provided with modulation of circuit capacitance

$$C(t) = C_0(1-2\varepsilon\cos\Omega_m t) \tag{7.28}$$

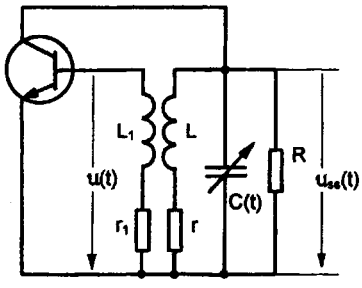

Figure 7.5 Basic circuit of the single-tuned transistor generator controlled in frequency.

Now we may write a system of full differential equations of the problem from which (7.22) follows. This equation of the second order is not especially complex and can be reduced directly to abbreviated equations. The procedure is quite tedious for more complex oscillatory systems and those with automatic bias, where execution of the direct truncation procedure without mistakes is very difficult. Therefore, we use the approach of simple derivation of the abbreviation equations developed in this chapter, and we will describe an example in detail.

We write the symbolical admittance of the system, as shown in the example of Section 7.3.2, in the following form:

$$Y_{ss}(j\omega,\mu)=\frac{R+j\omega L+(j\omega)^2 LCR}{j\omega LR}=\frac{1+\left(\frac{j\omega}{\omega_0}\right)\frac{\rho}{R}+\left(\frac{j\omega}{\omega_0}\right)^2\left(\omega_0^2\right)LC}{\left(\frac{j\omega}{\omega_0}\right)\rho}$$

$$=\frac{1+\left(\frac{j\omega}{\omega_0}\right)\delta+\left(\frac{j\omega}{\omega_0}\right)^2\left(1-2\varepsilon\cos\Omega_m t\right)}{\left(\frac{j\omega}{\omega_0}\right)\delta R}$$

Here, $\omega_0 = 1/LC_0 = \text{const}$ is the constant component of the oscillation frequency around which the frequency is modulated according to (7.27), $j\omega$ is the differential operator, and $\rho = \omega_0 L$ is the characteristic impedance of the circuit.

Now we determine the decomposition factors in Taylor series in ω for the numerator and denominator of the symbolical admittance $Y_{ss}(j\omega,\mu)$:

$$\alpha_0=1,\ \alpha_1=\frac{\delta}{\omega_0},\ \alpha_2=\frac{1-2\varepsilon\cos\Omega_m t}{\omega_0^2},\ \beta_0=0,\ \beta_1=\frac{R}{\omega_0}$$

In the case at hand only one factor α_2 depends on time.

We now express the decomposition factors of all coefficients in a Taylor series in δ:

$$\alpha_{00}=1,\ \alpha_{01}=0,\ \alpha_{10}=0,\ \alpha_{11}=\frac{1}{\omega_0},$$

$$\alpha_{20}=\frac{1-2\varepsilon\cos\Omega_m t}{\omega_0^2},\quad \beta_{00}=0,\ \beta_{10}=\frac{R}{\omega_0}$$

Now we write the abbreviated equation for complex amplitudes:

$$j\delta\dot{U}+j\frac{1-2\varepsilon\cos\Omega_m t}{\omega_0^2}\dot{U}\left(j\omega\Delta\omega\right)+2j\omega_0\left(j\omega\frac{1-2\varepsilon\cos\Omega_m t}{\omega_0^2}\dot{U}\right)=j\delta\omega_0\frac{R}{\omega_0}\dot{I} \tag{7.29}$$

Substituting $\Delta\omega = \omega(t) - \omega_0 = \varepsilon\omega_0\cos\Omega_m t$, we obtain:

$$\dot{U}+\frac{1-2\varepsilon\cos\Omega_m t}{\delta\omega_0^2}\dot{U}\left(j\omega\varepsilon\omega_0\cos\Omega_m t\right)+\frac{2}{\omega_0\delta}\left(j\omega\left[1-2\varepsilon\cos\Omega_m t\right]\dot{U}\right)=R\dot{I} \tag{7.30}$$

Now enter a circuit time constant $T = 2/\omega_0\delta$ and rewrite (7.30) as:

$$\dot{U}+T\frac{1-2\varepsilon\cos\Omega_m t}{2}\dot{U}\left(j\omega\varepsilon\cos\Omega_m t\right)+T\left(j\omega\left[1-2\varepsilon\cos\Omega_m t\right]\dot{U}\right)=R\dot{I} \tag{7.31}$$

Substituting the expressions for complex amplitudes $\dot{U}=Ue^{j\varphi}$ and $\dot{I}=Ie^{j\varphi}$ (taking into account that the active element is inertialess), we obtain

$$Ue^{j\varphi}+T\frac{1-2\varepsilon\cos\Omega_m t}{2}\varepsilon Ue^{j\varphi}\left(\frac{d}{dt}\cos\Omega_m t\right)+T\left(\left[\frac{d}{dt}\right]\left[1-2\varepsilon\cos\Omega_m t\right]Ue^{j\varphi}\right)=RIe^{j\varphi} \tag{7.32}$$

Differentiating, we obtain:

$$Ue^{j\varphi}+T\frac{1-2\varepsilon\cos\Omega_m t}{2}\varepsilon Ue^{j\varphi}\left(-\Omega_m\sin\Omega_m t\right)+T\left\{\left[-2\varepsilon\Omega_m\sin\Omega_m t\right]Ue^{j\varphi}+\left[1-2\varepsilon\cos\Omega_m t\right]\left(\frac{dU}{dt}e^{j\varphi}+jUe^{j\varphi}\frac{d\varphi}{dt}\right)\right\}=RIe^{j\varphi} \tag{7.33}$$

Dividing by the exponential factor yields

$$U+T\frac{1-2\varepsilon\cos\Omega_m t}{2}\varepsilon U\left(-\Omega_m\sin\Omega_m t\right)+T\left(\left[-2\varepsilon\Omega_m\sin\Omega_m t\right]U+\left[1-2\varepsilon\cos\Omega_m t\right]\left(\frac{dU}{dt}+jU\frac{d\varphi}{dt}\right)\right)=RI \tag{7.34}$$

Now separate the real and imaginary parts to obtain

$$T(1-2\varepsilon\cos\Omega_m t)\frac{dU}{dt}+U-\varepsilon\Omega_m TU\sin\Omega_m t\frac{1-2\varepsilon\cos\Omega_m t}{2} \\ -2\varepsilon\Omega_m TU\sin\Omega_m T=RI(U) \tag{7.35}$$

$$TU\left(1-2\varepsilon\cos\Omega_m t\right)\frac{d\varphi}{dt}=0 \tag{7.36}$$

These are the required abbreviated equations of the FM generator. In the absence of FM (i.e., for $\varepsilon = 0$) these equations are reduced to those of Chapter 6. From (7.36) it follows that $d\varphi/dt = 0$ (i.e., the steady-state and transient frequency is exactly equal to the modulated frequency of the circuit). It is clear that, within the framework of the *first approximation*, the frequency with an inertialess active element does not depend on amplitude.

In considering these equations it can be noted that ε is small, and it is possible to neglect the terms with ε in comparison with 1 and terms with ε^2 in comparison with ε. Then (7.35) will become

$$T\frac{dU}{dt}+U(1-\frac{5}{2}\varepsilon\Omega_m T\sin\Omega_m t)=RI(U) \tag{7.37}$$

This is the equation that should be solved in considering parasitic amplitude modulation of the generator.

It is possible to show that for all single-tuned FM oscillators the structure of the abbreviated equation for amplitude will resemble (7.37), but the factor in the term $\varepsilon\Omega_m T\sin\Omega_m t$ will vary. For a circuit with transformer feedback it is $-5/2$, from (7.37). For a circuit with an inductive three-port, considered in Chapter 8, the factor is $-3/2$. For other single-tuned FM oscillator circuits (for example, for a capacitor three-port), this multiplier will have other values (see Chapter 8).

7.5 PARASITIC AMPLITUDE MODULATION IN AUTODYNES FOR VARIOUS TYPES OF FREQUENCY MODULATION

Let the oscillation frequency of the autodyne now be modulated under the any law using a variable capacitance:

$$\omega = 1/\sqrt{L_{total}C_{total}(t)} = \sqrt{LC(t)} = \omega_0[(1+\varepsilon\gamma(t)] \tag{7.38}$$

The capacitance for this purpose varies as $C(t) = C_0[1 + \beta F(t)]$. Let us find the connection between these relationships:

$$\omega(t)=\frac{1}{\sqrt{LC_0}}\frac{1}{\sqrt{1+\beta F(t)}} \quad \text{or}$$
$$\frac{1}{1+\beta F(t)}=[1+\varepsilon\gamma(t)]^2 \tag{7.39}$$

Considering small modulation factors $\beta << 1$, $\varepsilon << 1$, then we find that $1 - \beta F(t) \approx 1 + 2\varepsilon\gamma(t)$, or

$$\beta F(t) = -2\varepsilon\gamma(t) \tag{7.40}$$

Thus, if oscillation frequency is modulated according to (7.38), modulation of circuit capacitance has the form

$$C(t)=C_0[1+\beta F(t)]=C_0[1-2\varepsilon\gamma(t)] \tag{7.41}$$

The symbolical admittance in this case will be obtained according to Section 7.4, but instead of the multiplier $(1 - 2\varepsilon\cos\Omega_m t)$ in the numerator there will appear as the multiplier $[1 - 2\varepsilon\gamma(t)]$. As earlier, we will express decomposition factors in a Taylor series of the numerator and denominator of the symbolical admittance:

$$\alpha_0=1,\ \alpha_1=\frac{\delta}{\omega_0},\ \alpha_2=\frac{1-2\varepsilon\gamma(t)}{\omega_0^2},\ \beta_0=0,\ \beta_1=\frac{R}{\omega_0}$$

Expressing the decomposition coefficients of all factors in Taylor series in δ:

$$\alpha_{00}=1,\ \alpha_{01}=0,\ \alpha_{10}=0,\ \alpha_{11}=\frac{1}{\omega_0}$$
$$\alpha_{20}=\frac{1-2\varepsilon\gamma(t)}{\omega_0^2},\ \beta_{00}=0,\ \beta_{10}=\frac{R}{\omega_0}$$

we obtain the abbreviated equation for complex amplitudes

$$j\delta\dot{U}+j\frac{1-2\varepsilon\gamma(t)}{\omega_0^2}\dot{U}(j\omega\Delta\omega)$$
$$+2j\omega_0\left(j\omega\frac{1-2\varepsilon\gamma(t)}{\omega_0^2}\dot{U}\right)=j\delta\omega_0\frac{R}{\omega_0}\dot{I} \tag{7.42}$$

Substituting $\Delta\omega = \omega(t) - \omega 0 = \varepsilon\omega_0\gamma(t)$, we obtain

$$\dot{U}+\frac{1-2\varepsilon\gamma(t)}{\delta\omega_0^2}\dot{U}\left[j\omega\varepsilon\omega_0\gamma(t)\right]+\frac{2}{\omega_0\delta}\left(j\omega\left[1-2\varepsilon\gamma(t)\right]\dot{U}\right)=R\dot{I} \qquad (7.43)$$

Substituting now the expressions for complex amplitudes $\dot{U}=Ue^{j\varphi}$ and $\dot{I}=Ie^{j\varphi}$ (here it is assumed that the active element is inertialess), and differentiating, we find:

$$\begin{aligned}&Ue^{j\varphi}+T\frac{1-2\varepsilon\gamma(t)}{2}\varepsilon Ue^{j\varphi}\left(\frac{d\gamma}{dt}\right)\\&+T\left(\left[-2\varepsilon\frac{d\gamma}{dt}\right]Ue^{j\varphi}+\left[1-2\varepsilon\gamma(t)\right]\left(\frac{dU}{dt}e^{j\varphi}+jUe^{j\varphi}\frac{d\varphi}{dt}\right)\right)=RIe^{j\varphi}\end{aligned} \qquad (7.44)$$

Dividing by the exponential multiplier and dividing the real and imaginary parts, we have:

$$\begin{aligned}T\left(1-2\varepsilon\gamma[t]\right)\frac{dU}{dt}+U-\varepsilon UT\frac{d\gamma}{dt}\frac{1-2\varepsilon\gamma(t)}{2}\\-2\varepsilon TU\frac{d\gamma}{dt}=RI(U)\end{aligned} \qquad (7.45)$$

$$TU\left[1-2\varepsilon\gamma(t)\right]\frac{d\varphi}{dt}=0 \qquad (7.46)$$

These are also the required abbreviated equations of the FM generator for any type of frequency modulation. If the common case of small frequency deviation (i.e., $\varepsilon << 1$), (7.45) becomes:

$$T\frac{dU}{dt}+U(1-\frac{5}{2}\varepsilon T\frac{d\gamma}{dt})=RI(U) \qquad (7.47)$$

This is the equation that should be solved in considering parasitic amplitude modulation (PAM) of the generator. As earlier, for all single-tuned FM oscillators the structure of the abbreviated equations for amplitude will be resemble (7.47), but the factor multiplying $\varepsilon T d\gamma/dt$ will vary: for a circuit with a transformer feedback it is –5/2, and for the circuit with an inductive three-port it is –3/2.

Let us determine now the PAM signal for common types of frequency modulation. Let the autodyne response with PAM be

$$U=U_0+\eta_{PAM}(t)+\eta_{ad}(t) \qquad (7.48)$$

where U_0 is the amplitude of the HF voltage of the autodyne at its operating point (without PAM), $\eta_{ad}(t)$ is the autodyne signal, and $\eta_{PAM}(t)$ is the PAM signal. We consider, as usual, that $\eta_{PAM} << U_0$, $\eta_{ad} << U_0$. If the problem is to determine the level of PAM signal in the absence of an autodyne response for different modulation types $\gamma(t)$, then at the usual PAM levels it is possible to make (7.47) a linear one, having substituted (7.48) in it instead of U for $\eta_{ad} = 0$:

$$T\frac{dU_0}{dt} + T\frac{d\eta_{PAM}}{dt} + (U_0 + \eta_{PAM})(1 - \frac{5}{2}\varepsilon T\frac{d\gamma}{dt}) = R[I(U_0) + \frac{d(GU)}{dU}\eta_{PAM}] \tag{7.49}$$

We rewrite this equation as:

$$T\frac{dU_0}{dt} + T\frac{d\eta_{PAM}}{dt} + U_0\left(1 - \frac{5}{2}\varepsilon T\frac{d\gamma}{dt}\right) + \eta_{PAM}\left(1 - \frac{5}{2}\varepsilon T\frac{d\gamma}{dt}\right) = RI(U_0) + R\left[U_0\frac{dG}{dU}\eta_{PAM} + G_0\eta_{PAM}\right]$$

and excluding from this the equation of the stationary mode, we obtain

$$T\frac{d\eta_{PAM}}{dt} - \eta_{PAM}\frac{5}{2}\varepsilon T\frac{d\gamma}{dt} = R\left[U_0\frac{dG}{dU}\eta_{PAM}\right] + \frac{5}{2}U_0\varepsilon T\frac{d\gamma}{dt}$$

Neglecting the product $\eta_{PAM}\varepsilon$ as being of the second order, we have finally:

$$T\frac{d\eta_{PAM}}{dt} - \frac{U_0}{G_{ss}}\frac{dG}{dU}\eta_{PAM} = \Phi(t) \tag{7.50}$$

where

$$\Phi(t) = \frac{5}{2}U_0\varepsilon T\frac{d\gamma}{dt} \tag{7.51}$$

Equation (7.50) describes a PAM transient signal for a single-tuned autodyne with any type of frequency modulation, determined through (7.51). The common result of (7.50) has the form

$$\eta_{PAM}(t) = \frac{1}{T}e^{-t/T}\int e^{t/T}\Phi(t)dt. \tag{7.52}$$

7.5.1 Sine Wave Frequency Modulation

In this case $\gamma(t) = \cos\Omega_m t$ and

$$\Phi(t) = -\frac{5}{2} U_0 \varepsilon \Omega_m T \sin\Omega_m t \tag{7.53}$$

Now from (7.52) we obtain

$$\eta_{PAM}(t) = -\frac{5}{2} U_0 \varepsilon \Omega_m e^{-t/T'} \int e^{t/T'} \sin\Omega_m t dt \tag{7.54}$$

and from (7.54) we obtain, integrating by parts:

$$\begin{aligned} \eta_{PAM}(t) &= -\frac{5}{2} U_0 \varepsilon \Omega_m e^{-t/T'} \int e^{t/T'} \sin\Omega_m t dt \\ &= -\frac{5}{2} U_0 \varepsilon \Omega_m e^{-t/T'} \left\{ e^{t/T'} \frac{1}{\Omega_m} (-\cos\Omega_m t) + T' \sin\Omega_m t e^{t/T'} + C \right\} \\ &= \frac{5}{2} U_0 \varepsilon \left\{ \cos\Omega_m t - \Omega_m T' \sin\Omega_m t \right\} + C e^{-t/T'} \end{aligned} \tag{7.55}$$

where C is a constant of integration. Entering $\tan\Psi_1 = \Omega_m T'$ we find

$$\begin{aligned} \eta_{PAM}(t) &= \frac{5}{2} U_0 \varepsilon \left\{ \cos\Omega_m t - \tan\Psi_1 \sin\Omega_m t \right\} + C e^{-t/T'} \\ &= C e^{-t/T'} + \frac{5 U_0 \varepsilon \cos(\Omega_m t - \Psi_1)}{2\sqrt{\left(\frac{U_0}{G_{ss}} \frac{\partial G}{\partial U} \right)^2 + (\Omega_m T)^2}} \end{aligned} \tag{7.56}$$

Thus, the PAM signal with sine wave modulation consists of an exponential multiplier, describing a PAM signal transient, and a sine wave component with the modulation frequency (actually a PAM signal). The phase shift of the PAM signal is determined by the modulation frequency and the normalized time constant of the circuit: $\Psi_1 = \arctan(\Omega_m T')$. The PAM amplitude is proportional to the amplitude of high-frequency oscillations and to the frequency modulation index, depending in a complex way on the autodyne regime through the normalized derivative $(U_0/G_{SS})(\partial G/\partial U)$.

7.5.2 Binary Frequency Modulation

The mathematical expression for binary frequency modulation is

$$\omega = \omega_{fr} + \frac{4\Delta\omega}{\pi}\sum_{k=1}^{\infty}\frac{1}{2k-1}\sin(2k-1)\Omega_m t = \omega_{fr}\left[1+\varepsilon\gamma(t)\right] \tag{7.57}$$

where: $\varepsilon = \Delta\omega/\omega_{fr}$,

$$\gamma(t) = \frac{4}{\pi}\sum_{k=1}^{\infty}\frac{\sin(2k-1)\Omega_m t}{2k-1},$$

ω_{fr} is the frequency of free oscillations,
$\Delta\omega$ is the frequency deviation,
Ω_m is the modulation frequency, and
k is a whole positive number.

Now the function $\Phi(t)$ in (7.51) becomes:

$$\Phi(t) = \frac{5}{2}U_0\varepsilon T\frac{d\gamma}{dt} = \frac{10}{\pi}U_0\varepsilon\Omega_m T\sum_{k=1}^{\infty}\cos(2k-1)\Omega_m t \tag{7.58}$$

Substituting this in (7.54), we obtain the expression for PAM signal amplitude with binary frequency modulation:

$$\eta_{PAM}(t) = Ce^{-t/T} + \frac{10}{\pi}U_0\varepsilon\Omega_m T\sum_{k=1}^{\infty}\frac{\cos\left[(2k-1)\Omega_m t - \Psi_{2k-1}\right]}{\sqrt{\left(\frac{U_0}{G_{ss}}\frac{\partial G}{\partial U}\right)^2 + \left[(2k-1)\Omega_m T\right]^2}} \tag{7.59}$$

where the phase Ψ_{2k-1} is found from $\tan\Psi_{2k-1} = (2k-1)\Omega_m T$. So again the PAM signal consists of the same exponential component and the enforced component whose amplitude can be found from (7.59).

7.5.3 Frequency Modulation by an Asymmetrical Sawtooth

The mathematical expression for asymmetrical sawtooth frequency modulation is

$$\omega = \omega_{fr} + \frac{2\Delta\omega}{\pi}\sum_{k=1}^{\infty}\frac{(-1)^{k+1}}{k}\sin k\Omega_m t = \omega_{fr}\left[1+\varepsilon\gamma(t)\right] \tag{7.60}$$

where $\gamma(t) = \frac{2}{\pi}\sum_{k=1}^{\infty}\frac{(-1)^{k+1}\sin k\Omega_m t}{k}$.

Now the function $\Phi(t)$ in (7.51) becomes:

$$\Phi(t) = \frac{5}{2} U_0 \varepsilon T \frac{d\gamma}{dt} = \frac{5}{\pi} U_0 \varepsilon \Omega_m T \sum_{k=1}^{\infty} (-1)^{k+1} \cos k\Omega_m t \tag{7.61}$$

Substituting these expressions in (7.54), we obtain the expression for the amplitude of the PAM signal with this type of frequency modulation:

$$\eta_{PAM}(t) = Ce^{-t/T} + \frac{5}{\pi} U_0 \varepsilon \Omega_m T \sum_{k=1}^{\infty} (-1)^{k+1} \frac{\cos\left[k\Omega_m t - \Psi_k\right]}{\sqrt{\left(\frac{U_0}{G_{ss}} \frac{\partial G}{\partial U}\right)^2 + \left[k\Omega_m T\right]^2}} \tag{7.62}$$

where $\tan\Psi_k = k\Omega_m T$.

7.5.4 Frequency Modulation with a Symmetrical Sawtooth

The mathematical expression for symmetrical sawtooth frequency modulation is

$$\omega = \omega_{fr} + \frac{8\Delta\omega}{\pi} \sum_{k=1}^{\infty} \frac{(-1)^{k+1}}{(2k-1)^2} \sin(2k-1)\Omega_m t = \omega_{fr}\left[1 + \varepsilon\gamma(t)\right] \tag{7.63}$$

where $\gamma(t) = \frac{8}{\pi} \sum_{k=1}^{\infty} \frac{(-1)^{k+1} \sin(2k-1)\Omega_m t}{(2k-1)^2}$.

Now function $\Phi(t)$ in (7.51) becomes:

$$\Phi(t) = \frac{5}{2} U_0 \varepsilon T \frac{d\gamma}{dt} = \frac{20}{\pi} U_0 \varepsilon \Omega T \sum_{k=1}^{\infty} (-1)^{k+1} \frac{\cos(2k-1)\Omega_m t}{2k-1} \tag{7.64}$$

Substituting these expressions in (7.54), we obtain the expression for the amplitude of the PAM signal with this type of frequency modulation:

$$\eta_{PAM}(t) = Ce^{-t/T} + \frac{20}{\pi} U_0 \varepsilon \Omega_m T \sum_{k=1}^{\infty} \frac{(-1)^{k+1}}{2k-1} \frac{\cos\left[(2k-1)\Omega_m t - \Psi_{2k-1}\right]}{\sqrt{\left(\frac{U_0}{G_{ss}} \frac{\partial G}{\partial U}\right)^2 + \left[(2k-1)\Omega_m T\right]^2}} \tag{7.65}$$

where, as before, $\tan\Psi_{2k-1} = (2k-1)\Omega_m T$.

References

[1] Bogachev, V. M., V. G. Lysenko, and S. M. Smolskiy, *Transistor Generators and Autodynes* (in Russian), Moscow: Publishing House of MPEI, 1993.

[2] Bogachev, V. M., and S. M. Smolskiy, "General Abbreviated and Characteristic Equations of the Transistor Oscillator," *Radiotechnika*, Vol. 28, No. 3, 1973, pp. 51-59.

[3] Bogachev, V. M., and S.M. Smolskiy, "General Equations of the Anisochronous Oscillator Synchronized by External Periodic Force," collection *Semiconductor Devices in Telecommunication Engineering*, (I. F. Nikolaevskiy, ed.), Release 12, 1973, Moscow, pp. 160-173.

[4] Bogachev, V. M., V. G. Lysenko, and S. M. Smolskiy, *Transistor Autodynes*, manual for the course "Sets of Generation and Control of Radio Signals," Moscow, MPEI, 1984.

[5] Smolskiy, S. M., "Short-Range Radar-Tracking Systems Based on Controlled Oscillators," thesis for a doctor's degree, Moscow, 1993.

Chapter 8

Output Voltage of a Frequency-Controlled Oscillator

As a general rule, the amplitude of oscillator output varies with any frequency control, be it tuning discretely in time (switching), continuous tuning (frequency wobbling), or frequency modulation (FM). There are several reasons for dependence of oscillator amplitude on frequency in the steady-state mode of operation. It can occur because of change during tuning of the resonant resistance of the tuned circuit, of the tuned circuit insertion coefficient in the output circuit of the active element, of the feedback factor, or of the transfer characteristic slope of the active element, together with immediate influence on amplitude of the change of a reluctance element parameter (a capacitor or an inductance, depending on which frequency control element is used). By immediate influence we mean the influence on the oscillation amplitude of the change in the reluctance element parameter other than the variation of resonant resistance of a tuned circuit caused by this change, and also by possible variations in some oscillators of the insertion coefficient of the tuned circuit in the output circuit and by the feedback factor of the oscillator.

The purpose of this chapter is to estimate the degree of output amplitude change for oscillators of different types, to define the influence of circuit parameters, and to establish the relation between frequency and amplitude, allowing us to estimate amplitude change with frequency control.

Steady-state regimes are considered separately for tuning discretely in time (the complete frequency range of the oscillator in this case can be arbitrary), and for steady-state regimes with FM (frequency deviation in this case is much less, compared with the carrier frequency, than is typical of frequency modulation). It is obvious that the results obtained during the investigation of the first case are valid as well for rather slow frequency control that is continuous in time, as is typical for swept oscillators.

To make clearer the physical reasons for the immediate influence of reluctance element parameter changes on the amplitude of output voltage, which are typical for oscillators with rapid frequency control, the parasitic amplitude modu-

lation (PAM) accompanying FM in ideal (lossless) *LC*-tuned circuits is examined separately.

8.1 CHANGE OF OUTPUT VOLTAGE FOR OSCILLATORS TUNED DISCRETELY IN TIME

The oscillator designs that will be investigated can be reduced to the block diagram shown in Figure 8.1. It contains, as usual, a tuned circuit, a nonlinear active element, and a positive feedback circuit. The oscillations appear in the tuned load, the active device gets energy from power supplies and converts it to energy of oscillations compensating for losses in the load, and the feedback circuit drives the active device. In the case of oscillators using a single-tuned circuit, the subject of this chapter, the tuned load is usually an *LC*-tuned circuit.

The oscillator output voltage is usually obtained from the tuned load or an element of it, and thus in the case of a real feedback factor k the voltage U_{ss} on the load is related to the amplitude of the driving voltage U, acting on the active device driving input, by $U_{ss} = U/k$. As the feedback factor is assumed to be constant, the change of output voltage with tuning is equal to the change of amplitude U.

For simplicity of initial discussions we will assume that the active device of the oscillator is inertialess. Then with a real feedback factor, according to (6.34), the amplitude of the driving voltage U is described by the following abbreviated equation:

$$T\frac{dU}{dt} = RI_1(U) - U \tag{8.1}$$

where T is the time constant of the tuned circuit, $p = d/dt$ is the differentiation operator, R is the so-called driving resistance, and I_1 is the amplitude of the first harmonic of the active device output current, which depends nonlinearly upon the amplitude U and the bias voltage E.

The bias voltage E is usually supplied by an external bias voltage source E_{init}

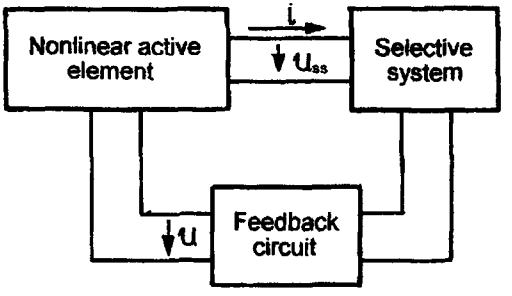

Figure 8.1 Block diagram of an oscillator.

minus the voltage drop on an autobias resistor R_{com} due to the constant current I_{com0} in the common electrode of the active device (base or emitter current of a bipolar transistor, drain current of a field-effect transistor) (Figure 8.2). The voltage E is given in this case by the following abbreviated equation:

$$T_{com}\frac{dE}{dt} = E_{init} - E - R_{com}I_{com0} \tag{8.2}$$

where $T_{com} = R_{com}C_{com}$ is the time constant of the autobias circuit, and C_{com} is the capacitance of the autobias circuit.

In this section we consider variable-frequency oscillators that are tuned discretely in time. Thus, we are interested initially in steady-state regimes of operation (i.e., modes) in which the oscillator has been tuned to one of its intended frequencies, after termination of the resulting transients.

Under steady conditions the values of U and E are, by definition, constant, and consequently in (8.1) and (8.2) the left-hand parts are equal to zero. Hence, these equations become:

$$RI_1(U) - U = 0 \tag{8.3}$$

$$E_{init} - E - R_{com}I_{com0} = 0 \tag{8.4}$$

Analysis of low-frequency oscillators (i.e., those in which the inertial properties of the active device can be neglected) often uses approximations to the static characteristics of currents by a piecewise-linear model. In this case, harmonic analysis of electrode currents (i.e., definition of harmonics of a base frequency in the current of each electrode) can be carried out quite easily and we obtain

$$I_1 = S\gamma_1(\theta)U$$

$$I_0 = S_{com}\gamma_0(\theta)U$$

where S is the slope of the approximated characteristics of the output current, S_{com}

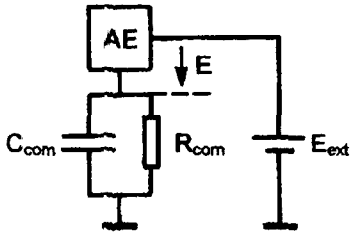

Figure 8.2 Equivalent scheme of a bias circuit.

is that of the current whose constant component flows through resistor R_{com}, $\gamma_1(\theta)$ and $\gamma_0(\theta)$ are coefficients of decomposition of cosine impulses, and θ is the cutoff angle of both currents (we consider that both approximated characteristics come from the same point of the abscissa and consequently the cutoff angles of both currents are identical). Substituting these expressions for currents I_1 and I_{com} in (8.3) and (8.4), we find:

$$SR\gamma_1(\theta) - 1 = 0 \tag{8.5}$$

$$E_{init} - E - S_{com}R_{com}U\gamma_0(\theta) = 0 \tag{8.6}$$

These equations allow us to estimate quantitatively the change of amplitude U with tuning of ω. Then from (8.6) and the expression $\cos\theta = -(E - E')/U$, where E' is the cutoff voltage of active device currents, we have

$$U = \frac{(E_{init} - E')}{S_{com}R_{com}\gamma_0(\theta) - \cos\theta} \tag{8.7}$$

Having determined at the given frequency ω the cutoff angle θ using the expression following from the equation (8.5)

$$\gamma_1(\theta) = 1/(SR) \tag{8.8}$$

it is possible from (8.7) to calculate the amplitude U for any frequency in the tuning range of the oscillator.

For interpretation of the results that will be obtained later, we normalize the amplitude U and frequency ω to values U_{180} and ω_{180}, applicable to the cutoff angle $\theta = 180°$. From (8.7), it follows that

$$U_{180} = \frac{E_{init} - E'}{S_{com}R_{com} + 1}$$

and consequently

$$\frac{U}{U_{180}} = \frac{S_{com}R_{com} + 1}{S_{com}R_{com}\gamma_0(\theta) - \cos\theta} \tag{8.9}$$

From (8.8), we have

$$\gamma_1(180) = 1 - \frac{1}{SR(1)}$$

and

$$\gamma_1(\theta) = \frac{R(1)}{R(\omega/\omega_{180})} \tag{8.10}$$

where $R(1)$ is the driving resistance of the oscillator at $\omega = \omega_{180}$ and $R(\omega/\omega_{180})$ is that for arbitrary ω.

Let us consider expression (8.10) for a specific oscillator, namely one with transformer feedback and a tuned circuit in the output circuit of the active device (Figure 8.3). Here and in subsequent discussion of other oscillator types we will assume, as is usually the case, that the loss resistance r of coils is much less than their reactance ωL in the range of the oscillator tuning (i.e., $r << \omega L$), and that for all inductance coils the ratio r/L has the same value (strictly speaking, r depends on frequency). For an oscillator with transformer feedback coupling (Figure 8.3), the coupling coefficient of the tuned circuit at the output of the active device is $p_k = L_1/L$, where $L = L_1 + L_2$ is the total inductance of the tuned circuit, the characteristic resistance of the tuned circuit is $\rho = \omega L$, and the resonant resistance of the tuned circuit is $R_{ss} = p_k^2 \rho Q(\omega) = (L_1^2/L)Q(\omega)\omega$. Here, $Q(\omega)$ is the quality factor of the tuned circuit, generally dependent on ω. As the feedback factor for this oscillator is $k = M/L_1$, then for the driving resistance of the oscillator we have $R = kR_{ss} = (ML_1/L)Q(\omega)\omega$. From this and (8.10), we can write in the general case for the oscillator with transformer feedback coupling

$$\gamma_1(\theta) = \frac{Q(1)/Q(\omega/\omega_{180})}{\omega/\omega_{180}} \tag{8.11}$$

where $Q(1)$ is the quality factor of the tuned circuit for $\omega = \omega_{180}$ and $Q(\omega/\omega_{180})$ is that for an arbitrary value of ω. When the quality factor of the tuned circuit varies so little over the tuning range that it can be considered constant, (8.11) becomes

$$\gamma_1(\theta) = 1/(\omega/\omega_{180}) \tag{8.12}$$

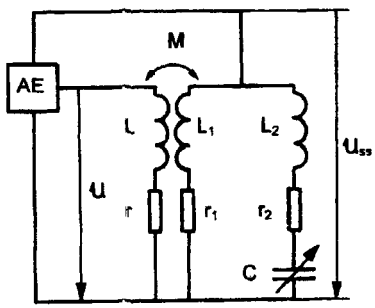

Figure 8.3 Tunable oscillator with a transformer feedback circuit.

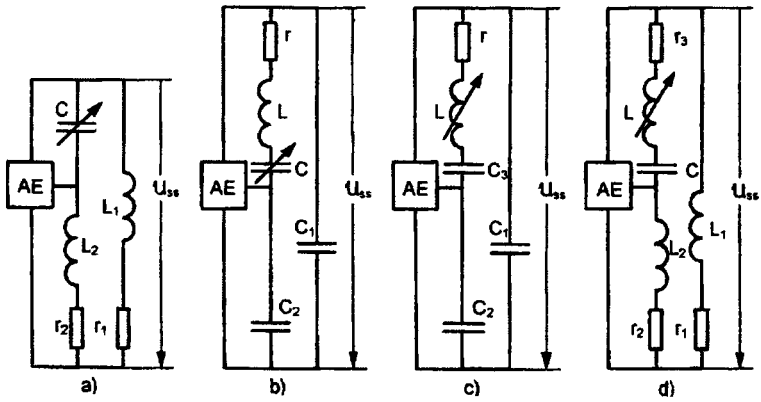

Figure 8.4 Main types of tunable oscillators using single-tuned circuits.

In Figure 8.4 the RF circuits of several variants of tunable single-tuned oscillators are shown. The frequency controller is the variable element of the tuned circuit. Note that the oscillators implemented using the circuits of Figure 8.4(c) and 8.4(d) are not now practically applied. However, if there appear in the future small-sized electrically controllable inductors capable of competing with varicaps, they will certainly be used. One feature of oscillators as shown in Figure 8.4(a) and (b) is that the normalized output voltage U_{ss} is proportional to the voltage acting only on a fixed capacitance [Figure 8.4(b)] or on a constant inductance coil of the tuned circuit [Figure 8.4(d)].

In Table 8.1 expressions are given for the coupling coefficient p_k of the tuned circuit in an active device output circuit having a characteristic resistance ρ and

Table 8.1

Calculation Formulas for Key Parameters of Controlled Generators for Circuits in Figure 8.4

Generator Circuit	*Figure 8.4(a)*	*Figure 8.4(b)*	*Figure 8.4(c)*	*Figure 8.4(d)*
p_k	$\frac{L_1}{L}$	$\frac{C}{C_1}=\frac{1}{C_1L\omega^2}$	$\frac{C}{C_1}$	$\frac{L_1}{L}=L_1C_1\omega^2$
ρ	ωL	ωL	$1/(\omega C)$	$1/(\omega C)$
R_{ss}	$\frac{L_1^2Q(\omega)\omega}{L}$	$\frac{Q(\omega)}{C_1^2L\omega^3}$	$\frac{CQ(\omega)}{C_1^2\omega}$	$L_1^2CQ(\omega)\omega^3$
k	$\frac{L_2}{L_1}$	$\frac{C_1}{C_2}$	$\frac{Q(1)\omega}{Q(\omega/\omega_{180})\omega_{180}}$	$\frac{Q(1)\omega^3}{Q(\omega/\omega_{180})\omega_{180}^3}$
R	$\frac{L_1L_2Q(\omega)\omega}{L}$	$\frac{Q(\omega)}{C_1C_2L\omega^3}$	$\frac{CQ(\omega)}{C_1C_2\omega}$	$L_1L_2CQ(\omega)\omega^3$
$\gamma_1(\theta)$	$\frac{Q(1)\omega_{180}}{Q(\omega/\omega_{180})\omega}$	$\frac{Q(1)\omega^3}{Q(\omega/\omega_{180})\omega_{180}^3}$	$\frac{Q(1)\omega}{Q(\omega/\omega_{180})\omega_{180}}$	$\frac{Q(1)\omega^3}{Q(\omega/\omega_{180})\omega_{180}^3}$

resonant resistance R_{ss}, for the feedback factor k and for the oscillator driving resistance R for all oscillator circuits shown in Figure 8.4. The relevant expressions for $\gamma_1(\theta)$, found on the basis of (8.10), are also shown.

Note that the expressions for $\gamma_1(\theta)$ for an oscillator with a transformer feedback coupling (Figure 8.3) coincide with those for an inductive three-point [Figure 8.4(a)]. This is because in both oscillators the frequency controller is the variable capacitor, and the coefficients p_k and k do not depend on frequency. In general, any oscillator tuned by a variable capacitor with constant feedback factor, having frequency dependence of its active device output tuned circuit coupling coefficient similar to one of the oscillators shown in Figure 8.4, will have the same formula for the coefficient of expansion $\gamma_1(\theta)$.

In Figure 8.5(a-d) the normalized amplitude of the driving voltage U/U_{180} is plotted as a function of the normalized frequency ω/ω_{180} for oscillators implemented by the circuits of Figure 8.4(a-d), respectively. The calculations were made using (8.9) with expressions for $\gamma_1(\theta)$ as shown in Table 8.1; thus, it was assumed that the tuned circuit quality factors remained practically constant over the tuning range [i.e., $Q(\omega/\omega_{180}) = Q(1)$]. From these curves we can see that the change of normalized amplitude U/U_{180} with oscillator tuning is reduced as the product $S_{com}R_{com}$ increases.

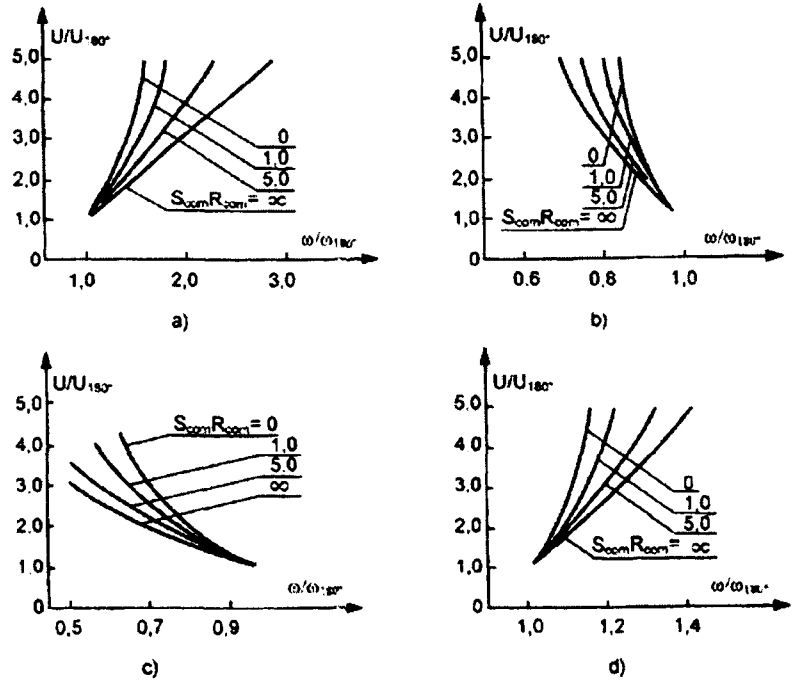

Figure 8.5 Dependence of normalized oscillation amplitude on normalized frequency for different tunable oscillator circuits with different autobias parameters.

8.2 PARASITIC AMPLITUDE MODULATION OF OSCILLATIONS IN IDEAL SINGLE-TUNED CIRCUITS WITH MODULATION OF THEIR NATURAL FREQUENCIES

In the previous section, the change of output voltage in different single-tuned oscillators was explored for discrete control of frequency in time (frequency tuning) or slow continuous control of frequency (frequency wobbling). For short-range radar the use of frequency modulated carriers is typical, and therefore the changes of output voltage in those oscillators will be further explored, but for frequency modulation (i.e., for the case in which the tuning can be rapid). In order to better understand the reason for additional amplitude change with rapid tuning, the voltages U_{ss} in ideal tuned circuits (i.e., without losses) shown in Figure 8.6 are considered, with modulation of their natural frequencies.

The tuned circuits shown in Figure 8.6 correspond to those in Figure 8.4 under the assumption that all resistance losses r are equal to zero. Thus the voltage U_{ss} here is proportional to the output voltage of the corresponding oscillator in Figure 8.4. It is obvious that the relative change of amplitude for voltage U_{ss} will be identical to that previously derived.

We assume that the natural angular frequency $\omega_{ss} = 1/\sqrt{LC}$ of the tuned circuits varies with modulation according to expression

$$\omega_{ss} = \omega_{ss0}(1 + \varepsilon \cos \Omega_m t) \tag{8.13}$$

where L and C are the total inductance and capacitance of the tuned circuit, ω_{ss0} is frequency in the absence of FM, ε is the peak frequency deviation, and Ω_m is the angular frequency of modulation. We will assume that requirements typical for FM, $\varepsilon < 1$, and $\Omega_m < \omega_{ss0}$ are observed. In ideal tuned circuits (Figure 8.6) with frequency modulation the amplitude of the output voltage will vary [i.e., there will be a parasitic amplitude modulation (PAM)]. It is possible to prove this by considering the energy in such tuned circuits. We will show this for an example of the circuit in Figure 8.6(a).

It is obvious that at frequency ω_{ss0} the energy in the tuned circuit can be expressed as $W_{ss0} = C_0 U_{ss0}^2/2$, where C_0 is the circuit capacitance and U_{ss0} is the voltage on it in the absence of FM. An increase of tuned circuit resonant frequency by

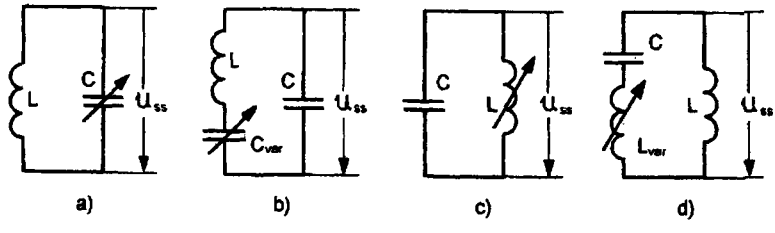

Figure 8.6 Different types of ideal variable-frequency oscillators.

$\Delta\omega_{ss} = \varepsilon\omega_{ss0}$ increases of the energy of the tuned circuit by ΔW_{ss}. The validity of this assertion is most obvious by considering that the variable capacitor C, being the modulator of frequency, represents a capacitor consisting of two plates, and that the variation of its capacitance is carried out by the change of distance d between the plates. Then, a frequency increase by $\Delta\omega_{ss} = \varepsilon\omega_{ss0}$, requiring the reduction of capacitance by $\Delta C = 2\varepsilon C_0$, is obtained by increasing the distance between plates by Δd. It is obvious that some work A must be executed, corresponding to the increase of energy ΔW_{ss}. This operation is linked with the necessity, in separating the plates, of overcoming the attractive force effective between them. The total energy of the tuned circuit $W_{ss0} + \Delta W_{ss}$ can be expressed as

$$C_0(1-2\varepsilon)U_{ss0}^2(1+m)^2/2 = W_{ss0}(1-2\varepsilon)(1+m)^2$$

where $C_0(1 - 2\varepsilon)$ is the capacitance of the tuned circuit and $U_{ss0}(1 + m)$ is the voltage on it, applicable at the greatest frequency $\omega_{ss} = \omega_{ss0}(1 + \varepsilon)$. Using

$$W_{ss0} + \Delta W_{ss} = W_{ss0}(1-2\varepsilon)(1+m)^2$$

it is easy to show that

$$m = \varepsilon + \frac{\Delta W_{ss}}{2W_{ss0}} \tag{8.14}$$

Similarly, considering the reduction of frequency by $\Delta\omega_{ss} = \varepsilon\omega_{ss0}$, assuming then a voltage on capacitance equal to $U_{ss0}(1 - m)$, we obtain again (8.14). Thus, the modulation of frequency of the tuned circuit shown in Figure 8.6(a) is fundamentally accompanied by PAM of the output voltage U_{ss}, and the coefficient of PAM is determined by (8.14).

Unfortunately, it is difficult to express completely the coefficient of PAM for all the tuned circuits shown in Figure 8.6 through the peak frequency deviation ε by means of the energy approach. It is much easier to derive it through the differential equations describing oscillatory processes occurring in tuned circuits. We will first consider tuned circuits in which a variable capacitor [Figure 8.6(a, b)] is used as the modulator. The differential equation describing behavior of a charge q, accumulated in capacitance C, appears as:

$$\frac{d^2q}{dt^2} + \omega_{ss}^2 q = 0 \tag{8.15}$$

Here again it is assumed that the angular frequency ω_{ss} is described by (8.13). Then (recalling that $\varepsilon < 1$ and $\Omega_m < \omega_{ss0}$) an adequate solution of (8.15) corresponds to an FM oscillation [1]:

$$q = Q_0\left(1-\frac{\varepsilon}{2}\cos\Omega_m t\right)\cos\left[\omega_{ss0}t+\varepsilon\frac{\omega_{ss0}}{\Omega_m}\sin\Omega_m t\right] \tag{8.16}$$

where Q_0 is the average value of charge q. It is obvious that the capacitance in the circuit with change of frequency ω_{ss} should vary according to (8.13) relative to the average value $C_0 = 1/(L\omega_{ss0}^2)$ by

$$C = C_0(1-2\varepsilon\cos\Omega_m t) \tag{8.17}$$

From (8.16) and (8.17), we obtain for a voltage U_{ss} effective on the capacitance C [Figure 8.6(a)]

$$U_{ss} = \frac{Q_0\left(1-\frac{\varepsilon}{2}\cos\Omega_m t\right)}{C_0(1-2\varepsilon\cos\Omega_m t)} \tag{8.18}$$

After simple transformation and dropping terms of a higher order of smallness from (8.18), we get:

$$U_{ss} = U_{ss0}\left(1+\frac{3}{2}\varepsilon\cos\Omega_m t\right) \tag{8.19}$$

where $U_{ss0} = Q_0/C_0$ is the average value of U_{ss}.

When the voltage U_{ss} acts only on a fixed capacitance C [Figure 8.6(b)], we similarly obtain:

$$U_{ss} = \frac{Q_0}{C}\left(1-\frac{\varepsilon}{2}\cos\Omega_m t\right) = U_{ss0}\left(1-\frac{\varepsilon}{2}\cos\Omega_m t\right) \tag{8.20}$$

We convert now to tuned circuits in which the modulator is a variable inductance [Figure 8.6(c, d)]. In this case it is more convenient to approach the problem from the differential equation of oscillations of the magnetic flux Φ of the total inductance L:

$$\frac{d^2\Phi}{dt^2}+\omega_{ss}^2\Phi = 0 \tag{8.21}$$

As (8.15) and (8.21) are similar in form, the approximate solution for magnetic flux Φ can be presented in a form similar to (8.16):

$$\Phi = \Phi_0\left(1-\frac{\varepsilon}{2}\cos\Omega_m t\right)\cos\left[\omega_{ss0}t+\varepsilon\frac{\omega_{ss0}}{\Omega_m}\sin\Omega_m t\right] \tag{8.22}$$

where Φ_0 is the average value of flux Φ.

We determine the voltage acting on the inductance L [Figure 8.6(c)] using the relationship $U_{ss} = d\Phi/dt$. Dropping terms of a higher order of smallness in the result of differentiation of (8.22), we obtain

$$U_{ss} = U_{ss0}(1 + \frac{\varepsilon}{2}\cos\Omega_m t) \tag{8.23}$$

where $U_{ss0} = \Phi_0\omega_{ss0}$.

For a voltage acting on the constant inductance L [Figure 8.6(d)], we can write $U_{ss} = L(di/dt) - L[d(\Phi/L_{ss})/dt]$, where $i = \Phi/L_{ss}$ is the current flowing in the tuned circuit. As $\varepsilon < 1$, using $L_{ss} = 1/(C\omega_{ss}^2) = 1/[C\omega_{ss0}^2(1 + \varepsilon\cos\Omega_m t)^2]$ we find, for use of a variable inductance as the modulator, that the total inductance of the tuned circuit varies about the average value $L_{ss0} = 1/(C\omega_{ss0}^2)$ following an expression similar to (8.17):

$$L_{ss} = L_{ss0}(1 - 2\varepsilon\cos\Omega_m t) \tag{8.24}$$

Substituting now (8.23) in $U_{ss} = Ld(\Phi/L_{ss})/dt$, applying one of the approximate equalities used above and again dropping from the result of differentiation terms of a higher order of smallness, we obtain

$$U_{ss} = U_{ss0}(1 + \frac{5}{2}\varepsilon\cos\Omega_m t) \tag{8.25}$$

Here, $U_{ss0} = (L/L_{ss0})\omega_{ss0}\Phi_0$.

From (8.19), (8.20), (8.23), and (8.25) it follows that in all the tuned circuits of Figure 8.6, with frequency modulation, a parasitic amplitude modulation of an output voltage is observed as well. Thus the comparison of (8.19), (8.20), (8.23) and (8.25) shows that the coefficient of PAM depends on the type of modulating element (variable capacitor or inductance), and depending on how the output voltage is obtained can reach values from 1.5ε to 2.5ε. The phase of the voltage envelope U_{ss} relative to that of the frequency deviation can equal 0 or 180°.

8.3 PARASITIC AMPLITUDE MODULATION OF OUTPUT VOLTAGE IN SINGLE-TUNED OSCILLATORS WITH FREQUENCY MODULATION

Let us consider now the change of output voltage taking place for frequency modulation of actual single-tuned oscillators, the circuits of which are shown in Figure 8.4. As in the previous section, we will consider that FM is carried out by a sinusoidal change of a resonant frequency of the tuned circuits:

$$\omega_{ss} = \frac{1}{\sqrt{LC}} = \omega_{ss0}(1 + \varepsilon \cos \Omega_m t) \tag{8.26}$$

where $\varepsilon << 1$, and $\Omega_m << \omega_{ss0}$. Thus, for application of a variable capacitor [Figure 8.4(a, b)] or a variable inductance [Figure 8.4(c, d)] as the modulator, the total capacitance or inductance of the tuned circuit should vary according to expressions $C = C_0(1 - 2\varepsilon \cos \Omega_m t)$ or $L = L_0(1 - 2\varepsilon \cos \Omega_m t)$.

To examine the dependence of amplitude on an oscillator that is tuned discretely in time over a wide range, the abbreviated equation (6.34) was used. As shown in Chapter 7, it is impossible to use this in our case. The problem is that the Evtianov method, with which (8.1) was obtained, assumes that the reactance elements of the load (a tuned circuit or coupled circuits in case of a multiple loop oscillator) are constant. Such an assumption allows us to obtain the abbreviated oscillator equations using the symbolical expression for complex impedance of the load $Z(j\omega)$, representing the resistance of the load to a sinusoidal current with frequency ω, in which $j\omega$ is considered as the differentiation operator p. In our case, where the modulator is a variable capacitance or inductance in the tuned circuit, this is impossible. Besides, as it will be shown below, the transition from instantaneous amplitudes of currents and voltages to their complex amplitudes, with variable tuned-circuit reactance elements, requires application of more complex formulas than in the usual application of the method of the symbolical abbreviated equations (Chapter 6).

Thus, we must obtain new abbreviated equations (depending on whether the modulator uses a variable capacitor or inductance and on the method of extraction of the output), distinct from (8.1), that will allow us to examine the case specified in the beginning of this section. In principle it can be done on the basis of the general approach (Chapter 7), but we will approach it in detail by a direct approach for the oscillator considered, such as that using the inductive three-point [Figure 8.4(a)]. Assuming an active device input current of zero, $r_1/r_2 = L_1/L_2$ and letting $\eta = C/C_0$, we can write for the oscillator of Figure 8.4(a) the differential equation linking oscillator output voltage U_{ss} to the output current i of the active device:

$$\left[(p + \omega_{ss0}\delta_0)p\eta + \omega_{ss0}\right]u_{ss} = \delta_0 R\left\{\left[\left(\frac{\omega_{ss0}}{p_k}\right) + \eta\frac{1 - p_k}{p_k}(p + \omega_{ss0}\delta_0)p\right]\frac{\eta}{\omega_{ss0}}(p + \omega_{ss0}\delta_0)\right\}i \tag{8.27}$$

where $p = d/dt$ is the differentiation operator, $\delta_0 = r/(\omega_{ss0}L)$ is the attenuation of the tuned circuit in the absence of FM, $R_{ss} = p_k^2 L/(rC_0\eta) = R_{ss0}/\eta$ is the resistance of the tuned circuit at its connection to the output of the active device, $p_k = L_1/L$; $r = r_1 + r_2$, and $L = L_1 + L_2$.

Attenuation in tuned circuits is a small quantity. Under the assumed restrictions ($\varepsilon << 1$, $\Omega << \omega_{ss0}$), ω_{ss0} and C are slowly varying functions of time, and therefore derivatives $p\eta$ and $p^2\eta$ are also small. As in the expression of PAM it is sufficient to maintain in (8.27) only terms of the first order of smallness; we will neglect the terms including $\delta_0 p\eta$, $p^2\eta$, δ_0^2, and δ_0^3 to obtain

$$\left(2\langle p\eta\rangle p + \eta p^2 + \omega_{s\cdot 0}\delta_0\eta p + \omega_{ss0}{}^2\right)u_{ss} = \delta_0 R\left[\frac{\omega_{ss0}\eta p}{p_k} + \frac{1-p_k}{p_k}\frac{\eta^2}{\omega_{ss0}}p^3\right]i \tag{8.28}$$

where the brackets <...> limit the activity of the functional operator p inside them.

Let us write the oscillator output voltage u_{ss} and the first harmonics i_1 of the output current of the active device in the form:

$$u_{ss} = \dot{U}_{ss}\exp(j\int\omega_{ss}dt) = U_{ss}\exp(j\varphi)\exp(j\int\omega_{ss}dt) \tag{8.29}$$

$$i_1 = \dot{I}_1\exp(j\int\omega_{ss}dt) = I_1\exp(j\varphi)\exp(j\int\omega_{ss}dt) \tag{8.30}$$

where U_{ss}, I_1, and φ are slowly varying functions of time (because of the smallness of δ_0, ε, and Ω_m/ω_{ss0}). The abbreviation of the differential equations discussed in Chapter 6 assumes transition from instantaneous functions u_{ss} and i_1 to complex amplitudes $\dot{U}_{ss}$, $\dot{I}_1$. It can be realized using (8.29), (8.30), and the following formulas, which can easily be obtained:

$$\begin{cases} pA\exp(j\int\omega_{ss}dt) = \exp(j\int\omega_{ss}dt) \\ p^2A\exp(j\int\omega_{ss}dt) = \exp(j\int\omega_{ss}dt)\left[\left(j\omega_{ss}+p\right)^2 + \langle p(j\omega_{ss})\rangle\right]A \\ \cdots\cdots\cdots\cdots\cdots\cdots\cdots\cdots\cdots\cdots\cdots\cdots\cdots\cdots\cdots\cdots\cdots\cdots \end{cases} \tag{8.31}$$

Having substituted (8.29), (8.30) in (8.28), transitioning with (8.31) from instantaneous functions u_{ss} and i to complex amplitudes $\dot{U}_{ss}$ and $\dot{I}_1$, and maintaining only terms of zero and first orders of smallness (because of slow change in I_1 and ω_{ss} derivatives with p, p^2, and p^3 terms of first, second, and third orders of smallness respectively), we find:

$$\left\{2\langle p\eta\rangle j\omega_{ss}+\left[\left(-\omega_{ss}{}^2+j2\omega_{ss}p\right)+\langle p(j\omega_{ss})\rangle\right]+\omega_{ss0}\delta_0\eta j\omega_{ss}+\omega_{ss0}{}^2\right\}\dot{U}_{ss}$$
$$=\delta_0 R\left[(\omega_{ss0}\eta j\omega_{ss})/p_k+(1/p_k-1)(\eta^2/\omega_{ss0})(-j\omega_{ss}{}^3)\right]\dot{I}_1 \tag{8.32}$$

Taking into account that $\omega_{ss}=\omega_{ss0}/\sqrt{\eta}$, $I_1 = S_1 k U_{ss}$, $R = kR_{ss}$, $2/(\omega_{ss0}\delta_0) = T_0$ (where k is the feedback factor of the oscillator), we can write (8.32) in the form

$$\left[\ T_0 p+0.25MT_0\langle p\eta\rangle+1\ \right]\dot{U}_{ss}=S_1 R\dot{U}_{ss} \tag{8.33}$$

where S_1 is the average slope of current I, R is the driving resistance, T_0 is the time constant of the tuned circuit in the absence of FM, and M is a number which for the selected oscillator circuit is equal to 3.

Just as (8.33) was found, the abbreviated equations were obtained for complex amplitude $\dot{U}_{ss}$ for oscillators shown in Figure 8.4(b-d). All have the same form as (8.33) and differ only in the value of M, equal to -1, 1, and 5, respectively. Having expressed in (8.33) complex amplitude $\dot{U}_{ss}$ through U_{ss} and phase φ, we find

$$T_0\frac{dU_{ss}}{dt}+0.25MT_0U_{ss}\frac{d\eta}{dt}=S_1RU_{ss} \tag{8.34}$$

$$\frac{d\varphi}{dt}=0 \tag{8.35}$$

Note from (8.29) that the oscillator frequency $\omega = \omega_{ss} + d\varphi/dt$, and hence from (8.35) it follows that $\omega = \omega_{ss}$. Thus, the oscillator frequency is equal to the natural frequency of the tuned circuit and is determined by (8.26).

Equations (8.34) and (8.35) were obtained under the assumption that tuned circuit loss resistances r do not depend on oscillator frequency ω and are included in tuned circuits according to Figure 8.1. However, it is possible to show that these equations are valid as long as the attenuation from loss resistance and other tuned circuit elements is small.

We will now express the resonant circuit resistance R_{ss}, included in the driving resistance $R = kR_{ss}$ and present on the right side of (8.34), as:

$$R=R_0(1+m_R\cos\Omega_m t) \tag{8.36}$$

where m_R is the modulation index of resistance R. For the oscillator using an inductive three-point [Figure 8.4(a)] $R = R_0/\eta = R_0(1 - 2\varepsilon\cos\Omega_m t)$, and hence, $m_R = -2\varepsilon$. Recall that the expression $R = R_0/\eta$ assumes resistance r independent of frequency ω (i.e., of the variable capacitance C). It is easy to show that generally,

when the modulator is a variable capacitor, $m_R = -2\varepsilon(C_0 / R_0)(dR / dC)|_{C=C_0}$, and when it is a variable inductance, $m_R = -2\varepsilon(L_0 / R_0)(dR / dL)|_{L=L_0}$.

The examination of PAM in FM oscillators with autobias requires the joint solution of (8.34) and abbreviated equations for the autobias circuit (Figure 8.2):

$$T_{com}\frac{dE}{dt} = E_{init} - E - R_{com}I_{com0} \tag{8.37}$$

where E is the bias voltage, E_{init} is the initial bias voltage, I_{com0} is the slowly varying current flowing through the autobias circuit, R_{com} and C_{com} are the auto bias resistor and the capacitor shunting it. The current I_{com0} can be expressed through the average slope S_{com0}:

$$I_{com0} = S_{com0}(U, E)kU_{ss} \tag{8.38}$$

The assumed earlier sinusoidal type of modulation (8.26) allows neglecting the higher harmonics, to present expressions for output voltage U_{ss} and voltage E in the steady-stated mode of modulation in the form:

$$U_{ss} = U_{ss0} + V_1\cos\Omega_m t + V_2\sin\Omega_m t \tag{8.39}$$

$$E = E_0 + e_1\cos\Omega_m t + e_2\sin\Omega_m t \tag{8.40}$$

As slopes S_1 and S_{com0} are functions of U_{ss} and E, on the basis of (8.39) and (8.40) it is possible to present them as:

$$S_1 = S_1(U_{ss0}, E_0) + \left[\frac{\partial S_1}{\partial U_{ss}}V_1 + \frac{\partial S_1}{\partial E}e_1\right]\cos\Omega_m t + \left[\frac{\partial S_1}{\partial U_{ss}}V_2 + \frac{\partial S_1}{\partial E}e_2\right]\sin\Omega_m t \tag{8.41}$$

$$S_{com} = S_{com}(U_{ss0}, E_0) + \left[\frac{\partial S_{com}}{\partial U_{ss}}V_1 + \frac{\partial S_{com}}{\partial E}e_1\right]\cos\Omega_m t + \left[\frac{\partial S_{com}}{\partial U_{ss}}V_2 + \frac{\partial S_{com}}{\partial E}e_2\right]\sin\Omega_m t \tag{8.42}$$

where all partial derivatives of functions S_1 and S_{com} with respect to U_{ss} and E are determined at $U_{ss} = \overset{\circ}{U}_{ss}$ and $E = \overset{\circ}{E}$ (i.e., calculated at points of steady-state operation).

Now there are all expressions for the joint solution of the equations (8.34) and (8.37). The solution is obtained by a usual method of harmonics balance. For this purpose we will substitute (8.36), (8.39), and (8.41) in (8.34) with $\eta = 1 - 2\varepsilon\cos\Omega_m t$, and (8.38) - (8.40) and (8.42) in (8.37). Expressing the sepa-

rate equations with the appropriate signs, constant components, and coefficients of $\cos\Omega_m t$ and $\sin\Omega_m t$, and neglecting the small terms, we obtain six equations whose joint solution allows us to find U_{ss0}, E_0, V_1, V_2, e_1, and e_2. Thus

$$\begin{cases} V_1 = \dfrac{\varepsilon}{2}\dfrac{M\Omega_m T_0 F - 2(m_R/\varepsilon)P}{F^2+P^2}, \\ V_2 = \varepsilon\dfrac{(m_R/\varepsilon)F + M\Omega_m T_0 P}{F^2+P^2} \end{cases} \tag{8.43}$$

where

$$F = \Omega_m T_0 - \frac{\partial S_1}{\partial E}\frac{U_{ss0}R_0 A\Omega_m T_b}{(\Omega_m T_0)^2 + B^2}$$

$$P = \frac{\partial S_1}{\partial U_{ss}}U_{ss0}R_0 - \frac{\partial S_1}{\partial U_{ss}}\frac{R_0 AB}{(\Omega_m T_0)^2 + B^2}$$

$$A = kR_b\left[S_{com0}(U_{ss0}, E_0) + \frac{\partial S_{com0}}{\partial U_{ss}}U_{ss0}\right]$$

$$B = kR_{com}\frac{\partial S_{com0}}{\partial E}U_{ss0} + 1$$

From (8.39) and (8.43) we can see that FM in the oscillators being studied is accompanied by PAM, the coefficient of which is

$$m = \frac{\sqrt{V_1^2 + V_2^2}}{U_{ss0}} = \frac{1}{2}\left[\frac{M^2(T_0^2) + 4(m_R/\varepsilon)^2}{F^2+P^2}\right]^{1/2} \tag{8.44}$$

The phase shift between the frequency deviation $\Delta\omega = \varepsilon\omega_{ss0}\cos\Omega_m t$ and envelope $V = V_1\cos\Omega_m t + V_2\sin\Omega_m t = mU_{ss0}\cos(\Omega_m t + \Psi)$ can be defined using (8.43) and

$$\Psi = \Psi_0 + \arctan(V_2/V_1) \tag{8.45}$$

where $\Psi_0 = 0$ for $V_1 > 0$ and $\Psi = 180°$ for $V_1 < 0$, with $-\pi/2 < \arctan(V_2/V_1) < \pi/2$.

Let us study the influence of autobias on parasitic AM in these oscillators, considering that they operate in the unsaturated regime. Let us calculate first the coefficient of parasitic AM at low modulation frequencies ($\Omega_m \sim 0$). Assuming in (8.44) that $\Omega_m \to 0$, we find:

$$m = \frac{|m_R|/(U_{ss0}R_0)}{\left|\frac{\partial S_1}{\partial U_{ss}} - \frac{\partial S_1}{\partial E}\left\{\frac{kR_{com}\left[S_{com}(U_{ss0},E_0)+\frac{\partial S_{com}}{\partial U_{ss}}U_{ss0}\right]}{kR_{com}\frac{\partial S_{com}}{\partial E}U_{ss0}+1}\right\}\right|} \tag{8.46}$$

The equations obtained from the fixed terms of (8.34) and (8.37) describe the cutoff and bias diagrams (Chapter 6) in the absence of FM and allow us to find expressions for the tangents to them:

$$\mathrm{X} = \frac{dU_{ss}}{dE} = -\frac{\partial S_1/\partial E}{\partial S_1/\partial U_{ss}}\Big|_{E=E_0,U_{ss}=U_{ss0}} \tag{8.47}$$

$$\mathrm{X}_b = \frac{dU_{ss}}{dE} = -\frac{kR_{com}U_{ss0}(\partial S_{com}/\partial E)+1}{kR_{com}\left[S_{com}(U_{ss0},E_0)+U_{ss0}(\partial S_{com}/\partial E)\right]}\Big|_{E=E_0,U_{ss}=U_{ss0}} \tag{8.48}$$

Substituting (8.47) and (8.48) in (8.46) we obtain

$$m = \frac{|m_R|}{\frac{\partial S_1}{\partial E}\left(\frac{1}{\mathrm{X}}-\frac{1}{\mathrm{X}_b}\right)U_{ss0}R_0} \tag{8.49}$$

Depending on the magnitude of SR_0 the coefficient X is either positive-going or negative, while X_b is always negative. In the case $X > 0$, both terms in the denominator of (8.49) have the same sign, and in accordance with (8.48) the autobias reduces the coefficient of parasitic AM, thus reducing m as R_{com} increases. (We assume that U_{ss0} is maintained constant by a corresponding change in E_{init}.) In the case where $X < 0$, the stable regime will be realized for $X_b > X$ [2] (i.e., if in the denominator (8.49) the magnitude of the second term is greater than the first). Thus, coefficient m is also reduced with increasing R_b.

Let us consider now the parasitic AM at modulation frequencies Ω_m, which are significantly greater than $\delta_0 = 1/(\omega_{ss0}T_0)$. It is easy to conclude that δ_0 is equal to half the fractional bandwidth of the tuned circuit in the absence of FM. From (8.44) with $\Omega_m/\delta_0 > 1$ we have: $m = |M|\varepsilon/2$ (i.e., for rather high modulation frequencies the autobias does not affect the coefficient of parasitic AM). Substituting in the expression $m = |M|\varepsilon/2$ the applicable values of M for each of the oscillators in Figure 8.4, we find that for $\Omega_m/\delta_0 > 1$ the parasitic stray AM coefficients appear to be the same as the those obtained above for FM in lossless tuned circuits (Figure 8.6).

Confining the analysis for concreteness to oscillators with modulators represented by a variable capacitor [Figure 8.4(a, b)], we will consider now the parasitic AM for all modulation frequencies. Using the accepted approximation to an output current i supplying automatic bias, we have:

$$S_1 = S\gamma_1(\theta), \qquad S_{com0} = S_{com}\gamma_0(\theta)$$

where S and S_{com} are the slopes of the approximated current characteristics I and i_{com}, $\gamma_1(\theta)$ and $\gamma_0(\theta)$ are the decomposition coefficients of cosine impulses, and θ is the cutoff angle. Having introduced coefficients $\gamma_1(\theta)$ and $\gamma_0(\theta)$, and using three terms of their expansion in a series for $\cos\theta$, we have:

$$S_1 = S\left(\frac{1}{2} - \frac{2}{\pi}\cos\theta + \frac{1}{3\pi}\cos^3\theta\right)$$

$$S_{com0} = S\left(\frac{1}{\pi} - \frac{1}{2}\cos\theta + \frac{1}{2\pi}\cos^2\theta\right)$$

The calculations using these formulas give sufficiently precise values of slopes S_1 and S_{com0} at angles θ lying within the limits 40° to 140°. Applying the last expressions for slopes S_1 and S_{com0} and the expression $\cos\theta = (E - E')/kU_{ss}$, the derivatives of S_1 and S_{com0} with respect to U_{ss} and E can easily be obtained:

$$\begin{cases} \dfrac{\partial S_1}{\partial U_{ss}} = S\left(\dfrac{2}{\pi}\cos\theta_0 - \dfrac{1}{\pi}\cos^3\theta_0\right)/U_{ss0} \\ \dfrac{\partial S_1}{\partial E} = S\left(\dfrac{2}{\pi} - \dfrac{1}{\pi}\cos^2\theta_0\right)\dfrac{1}{kU_{ss0}} \\ \dfrac{\partial S_{com0}}{\partial U_{ss}} = S_{com}\left(\dfrac{1}{2}\cos\theta_0 - \dfrac{1}{\pi}\cos^2\theta_0\right)/U_{ss0} \\ \dfrac{\partial S_{com0}}{dE} = S_{com}\left(\dfrac{1}{2} - \dfrac{1}{\pi}\cos\theta_0\right)/U_{ss0} \end{cases} \tag{8.50}$$

Substituting (8.50) in (8.43) yields (8.46) as obtained before (note that the feedback factor k, included in these formulas, is abbreviated), it is possible to obtain equations suitable for calculation of the coefficient m and the angle Ψ.

In Figure 8.7 the dependence of the normalized coefficient of stray AM m/ε and phase angle Ψ on dimensionless frequency $\Omega_m/\delta_0 = \Omega_m T_0$ are introduced (calculated using the above equations) for oscillators using the inductive three-point [Figure 8.4(a), continuous lines] and the Klapp scheme [Figure 8.4(b), broken lines]. The curves correspond to $SR_0 = 1.5$ (small regeneration), $SR_0 = 4.35$ (large

regeneration), $S_{com}R_{com} = 0.04$, 0.57 and 5.13 at $SR_0 = 1.5$, and $S_{com}R_{com} = 7.5$ and 23.7 at $SR_0 = 4.35$.

The values of the ratio m_R/ε used in these calculations are found assuming that the circuit $Q = \omega L/r$ is constant over the frequency range of oscillation. The curves calculated for $T_b = T_0$ differ slightly from those shown in Figure 8.7, for which $T_b = 0.1T_0$. The curves shown in Figure 8.7 allow us to revise the definitions of "low frequencies of modulation" and "high frequencies of modulation" used in the equations above. The former (i.e., the frequencies at which the parasitic AM coefficient is approximately derivable from the static modulation characteristic) should meet condition $\Omega_m \leq 0.1\delta_0$ (for large values $S_{com}R_{com}$ this condition is less rigid, and in the case of the inductive three-point and independence of circuit Q from frequency ω_{ss}, the coefficient m is independent of modulation frequency). The latter [i.e., the frequencies at which the parasitic AM coefficient is essentially independent of the autobias (and $S_{com}R_{com}$) and are close to those based on FM in separate lossless tuned circuits] should meet the condition $\Omega_m \geq \delta_0$. At modulation frequencies Ω_m smaller than δ_0, as follows from Figure 8.7, the increase in product $S_{com}R_{com}$ reduces m and Ψ and simultaneously aligns their values in the modulating frequency range.

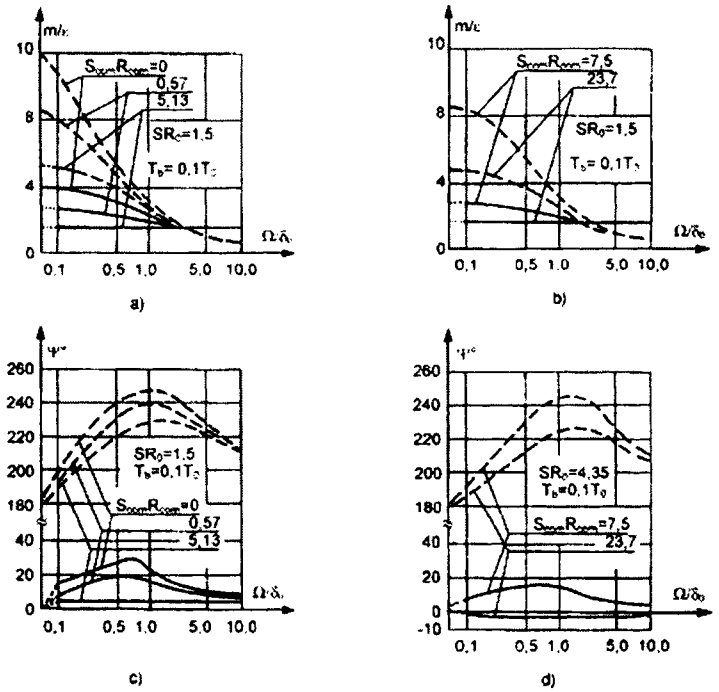

Figure 8.7 Dependence of normalized PAM factor (a, b) and phase shift Ψ (c, d) upon modulation frequency for the inductive three-point scheme and Klapp scheme for small (a, c) and large (b, d) regeneration factors.

We attempt now to give an energy-based explanation of the results. As was already noted in Section 8.1, compensation for energy losses in the output load of the oscillator (i.e., in its tuned system) is provided by input of energy from an active device in the load. Thus, in the case of a fixed frequency oscillator under steady-state conditions, the compensating energy arriving during each oscillation period and the energy lost during that period are made equal. Owing to the nonlinear properties of active devices and the dependence of load resistance (i.e., resonant circuit resonance resistance at points of connection to the active element) on the oscillation frequency, this equalizing of energy occurs at different oscillation amplitudes for different frequencies. Therefore, the voltage output of the oscillator depends on frequency.

For FM with low modulation frequencies ($\Omega_m \leq 0.1\delta_0$), there is enough time for the oscillator amplitude to be adjusted, by equalizing of the energies lost and gained, at each of the frequencies over which the oscillator sweeps. This means that the oscillation amplitude at each frequency during the modulation cycle is close to that of the oscillator under fixed frequency (without FM), steady-state conditions for that frequency. However, with increase in modulation frequency the oscillation amplitude is increasingly influenced by the following two factors: the bandwidth of the tuned circuit and the effect on tuned circuit energy of modulator reactance. Considering FM oscillations in an ideal single-tuned circuit, it has been established that these variations result in an increase in energy in the tuned circuit during one half-cycle of modulation followed by a decrease during the succeeding half-cycle. The minor effect of the second factor for low frequencies of modulation ($\Omega_m < 0.1\delta_0$), as compared to the case of FM in an ideal single-tuned circuit where it occurs irrespective of the modulation frequency, is caused by tuned circuit losses and their link to the active device. For high frequencies of modulation ($\Omega_m >> \delta_0$), the influence of both factors is so significant that oscillation amplitude is completely determined by them. Thus, because of tuned circuit inertia, the equalization of energy supplied by the active device and that lost in the tuned circuit is controlled only by the energy within the modulation period rather than that in the oscillation period. If the changes in modulator reactance did not result in variations of tuned circuit energy, oscillation amplitude would remain constant, but as these changes do occur the amplitude is also affected. For high frequencies of modulation ($\Omega_m >> \delta_0$), the changes in modulator reactance causing alternating addition and withdrawal of energy in the tuned circuit are so rapid that the tuned circuit inertia precludes influence on circuit power losses and their compensation. This allows us to consider single-tuned FM oscillators (Figure 8.4) at high modulation frequencies to be ideal single-tuned circuits (Figure 8.6). It also shows that the parasitic AM coefficients for the oscillators analyzed in this paragraph, for $\Omega_m >> \delta_0$, are the same as those derived earlier by consideration of FM tuned circuits assumed to be ideal.

As the tuned circuit inertia and effect of modulator reactance on oscillation frequency (i.e., on parasitic AM coefficient) have no effect in the case of FM with low modulation frequencies ($\Omega_m < 0.1\delta_0$), the influence on amplitude will be

minor also in cases of large, slow continuous tuning, although the relationship between variations of amplitude and generated frequency will now certainly be different because of nonlinear properties of the active device and frequency dependence of resonance resistance of the tuned circuit. With reference to continuous periodic tuning (as, for example, in swept oscillators), the last assertion can be rendered more concrete. If the oscillator is swept at frequency F and if the harmonics up to n are essential to system operation, this assertion can be considered valid for $F < 0.1\delta_0/(2\pi n)$. From this it follows that for $F < 0.1\delta_0/(2\pi n)$, the variation of oscillator amplitude as considered in this chapter can be calculated using expressions obtained in Section 8.1.

8.4 USE OF A VARICAP AS THE FREQUENCY CONTROLLER

Varicaps are often applied as frequency controllers (tuning elements, FM modulators) in modern oscillators. The dependence of oscillator amplitude on frequency for discrete tuning in time, and also for slow continuous tuning (propositions made in the closing part of the Section 8.3 are valid here) can again be obtained using (8.7) and (8.8), valid for oscillators operating at fixed frequency and in the steady-state regime.

When the modulation frequencies cannot be considered low, we must apply the differential equations describing FM oscillator processes in order to find the dependence of parasitic AM coefficient on frequency deviation, as was done in the previous section. When using varicap modulators there will be additional terms in these equations, as compared to those considered earlier, because the capacitance of the varicap depends not only on the modulating voltage but also on the RF voltage imposed on the varicap by the oscillator. For study of parasitic AM using the approximation set forth in this chapter, these terms can practically be neglected, and the results can be applied also to oscillators with frequency modulators using varicaps.

However, in a series of publications [1, 3], in which FM oscillators using varicap modulators were investigated, results differing from those above were obtained. This is explained by the fact that in many publications the differential equations were solved with some inaccuracy. We describe below the nature of this inaccuracy.

Formulating the differential equations for FM oscillators with varicap modulators, we must use the expression for the high frequency component of current flowing through the varicap. Let us write this expression, proceeding from the known formula for differential capacitance of a single varicap:

$$C_V(e) = C_{V0}\left(\frac{\varphi_c}{\varphi_c + e}\right)^n$$

where e is the external voltage applied to the varicap, C_{V0} is the capacitance of the varicap at $e = 0$, φ_c is the contact potential difference, and $n = 2$ or 3 for a sharp or smoothly varying p-n junction, respectively.

Because, by definition, the current i, as a function variation of the charge q, is equal to dq/dt, and the capacitance $C_V(e) = dq(e)/dt$, the current flowing through the varicap is:

$$i = \frac{dq}{dt} = \frac{dq(e)}{de}\frac{de}{dt} = C_V(e)\frac{de}{dt} \tag{8.51}$$

From (8.51) it follows that if constant bias E and a high frequency component u are applied to the varicap (i.e., if $e = E + u$), then

$$i = C_V(e)\frac{du}{dt} \tag{8.52}$$

where $C_V(e) = C_{V0}(e)[\varphi_c/(\varphi_c + E + u)]^n$. If, in addition to voltages E and u, the modulating component e_m is applied to the varicap (i.e., if $e = E + u + e_m$) from (8.51) follows:

$$i = C_V(e)\left(\frac{de}{dt} + \frac{du}{dt}\right) = C_V(e)\frac{de}{dt} + C_V(e)\frac{du}{dt} \tag{8.53}$$

As the high frequency voltage u appears in the expression for $C_V(e)$, the first term of the right part of (8.53) must be taken into account in determining the high frequency component of oscillator modulation current. However, in many published articles this was not done: instead the high frequency component of current flowing through the varicap was determined by (8.52) with $C_V(e) = C_V(E + e_m + u)$.

In [3], the FM oscillators were studied for a modulator based on back-to-back varicaps with sharp p-n junctions. It was assumed there that the equivalent capacitance of both varicaps is defined by:

$$C_{Veq}(e) = C_{Veq0}\left[\frac{\varphi_c}{\varphi_c + E + e_m + u/N}\right]^n \tag{8.54}$$

where $C_{Veq0} = C_{V01}C_{V02}/(C_{V01} + C_{V02})$,

$N = |(C_{V01} + C_{V02})/(C_{V01} - C_{V02})|$, and

C_{V01} and C_{V02} are the capacitances of the varicaps with no voltages on them.

But as follows from [2], (8.54) cannot be used generally when $N \neq 1$. It is valid only for one special case ($N = 1$), namely, when the modulator is a single varicap and $C_{V01} \to \infty$ or $C_{V02} \to \infty$ and $C_{Veq} = C_{V2}(C_{Ve0} = C_{V02})$ or $C_{Veq} = C_{V1}(C_{Ve0} = C_{V01})$, respectively. Thus, as in the earlier case, the capacitances C_{V1} and C_{V2} are differential capacitances defined as $C_V = dq(e)/de$, where $e = E + e_m + u$. Results obtained in [3] as well as in [1] are incorrect for this special case because the high frequency current flowing through the varicap is also determined by (8.52), if it is assumed that $C_V = C_V(E + e_m + u)$ (i.e., the component, conditioned by the first term in (8.53), is also left out).

In summary, as indicated above, we study free oscillations in an ideal single-tuned circuit with a varicap (Figure 8.8) with modulation of varicap capacitance and thereby the frequency of resonant oscillations. Thus we will consider for concreteness that the varicap has a sharp p-n junction.

It appears that for our tuned circuit the following differential equation applies:

$$L\frac{di}{dt} + u = 0 \tag{8.55}$$

where i is the high frequency current flowing in the tuned circuit, and consequently through the varicap, and u is the high frequency voltage applied to the varicap. For a solution to (8.55), we shall substitute into it the expression for the current of the varicap (8.53)

$$i = C_V(e)\frac{d(e_m + u)}{dt} \tag{8.56}$$

where $C_V(e) = C_{V0}[\varphi_c/(\varphi_c + E + e_m + u)]^{1/2}$. The fact that (8.56) also includes the low frequency component of the current imposed by the modulating voltage e_m applied to the varicap is not a hindrance to the study, as the method of solution of (8.55) selected below (the method of harmonic balance) will subsequently allow us to take into account only those components that are interesting. So, having substituted (8.56) in (8.55), performed transformations, and entered a series of identifications, the following equation can be obtained:

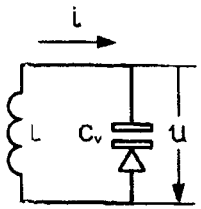

Figure 8.8 Ideal tuned circuit with varicap.

$$-0.5(1+x+y)^{-3/2}\left(\frac{d(x+y)}{dt}\right)^2+(1+x+y)^{-1/2}\frac{d^2(x+y)}{dt^2}+\omega_0{}^2x=0 \quad (8.57)$$

where: $x = u/(\varphi_c + E)$ is the dimensionless high frequency voltage on the varicap,
$y = e_m/(\varphi_c + E)$ is the dimensionless modulating voltage,
$\omega_0{}^2 = 1/[LC_V(E)]$, and
$C_V(E) = C_{V0}(\varphi_c + E)$.

It appears that ω_0 is the angular frequency of resonant oscillations in the tuned circuit for $x \to 0$ and $y = 0$.

Multiplying all terms of (8.57) by $2(1 + x + y)^{3/2}$ and transferring from the derivatives $d(x + y)/dt$ and $d^2(x + y)/dt^2$ to derivatives $d(x + y)/d\tau$ and $d^2(x + y)/d\tau^2$, where $\tau = \omega_0 t$ is dimensionless time, we change (8.57) to a more suitable form for further solution:

$$-\left[\frac{d(x+y)}{d\tau}\right]^2+2(1+x+y)\frac{d^2(x+y)}{d\tau^2}+2(1+x+y)^{3/2}x=0 \quad (8.58)$$

For solution of (8.58) we will be confined to the case $x \le 0.6$ and $y << 1$. The first of these inequalities is usually met in oscillators where frequency is controlled by a varicap, and the second corresponds to the case of small frequency deviations usually characterizing FM. These limitations allow us to decompose the expression $(1+ x + y)^{3/2}$ in an ascending power series:

$$(1+x+y)^{3/2}=\frac{1+3(x+y)}{2}+\frac{3(x+y)^2}{8}-\frac{(x+y)^3}{16}+\ldots \quad (8.59)$$

As opposed to the case in which $x \to 0$ and $y \to 0$, where (8.59) degenerates to the customary equation of a sinusoidal oscillator $d^2x/d\tau^2 + x = 0$ with the solution $x = X\sin\tau = X\sin\omega_0 t$, in our case x does not tend to zero, the resonant angular frequency of oscillations ω will not be equal to ω_0, and the solution of (8.59) will include higher harmonics as well. Having designated a first harmonic of oscillations as $x_1 = X_1\sin\theta$, where $\theta = \int \omega dt = \int (\omega/\omega_0) d\tau$, and having substituted it in place of x in (8.59), after the applicable angular transformations we see that the latter contains the terms including $\cos 2\theta$ and $\cos 3\theta$. Neglecting the third harmonic [inclusion of this and higher harmonics actually present in the solution of (8.59) results in insignificant corrections to magnitudes given below], we can search for a solution to (8.59) in the form:

$$x = X_1 \sin\theta + X_2 \cos 2\theta \quad (8.60)$$

Note that from substitution of $x_1 = X_1 \sin\theta$ in (8.59) it follows that the amplitude X_2 has an order not greater than X_1^2 (i.e., $X_2 \approx X_1^2$).

Assuming that the modulation of tuned circuit resonant frequency is by a sinusoidal voltage $e = \varepsilon \sin \Omega_m t$, where Ω_m is the angular modulation frequency, and substituting $y_m = \varepsilon/(\varphi_c + E)$, we can introduce a dimensionless modulating voltage in the form $y = y_m \sin \Omega_m t$. Transferring to dimensionless time $\tau = \omega_0 t$ and substituting $\alpha = \Omega_m/\omega_0$, we obtain

$$y = y_m \sin \alpha\tau \tag{8.61}$$

It was assumed above that $y_m << 1$, and we shall consider also that $\alpha << 1$ (the inequality $\Omega_m << \omega_0$ is characteristic of FM radar). As $y_m << 1$, we will also have rather small variations of amplitudes X_1 and X_2 and magnitude $d\theta/d\tau$, relative to their values in the absence of modulation (X_{10}, X_{20}, θ_0) (i.e., of order y_m, too). As they will vary with frequency $\Omega_m = \alpha\omega_0$, we will find $dX_1/d\tau \approx \alpha y_m X_1$, $d^2X_2/d\tau^2 \approx \alpha^2 y_m X_2$, and $d^2\theta/d\tau^2 \approx \alpha y_m d\theta/d\tau$. By virtue of the negligible value of the derivative $d^2X_2/d\tau^2 \approx \alpha^2 y_m X_2$, hereinafter we need consider only the derivatives $d^2X_1/d\tau^2$ and $d^2\theta/d\tau^2$.

Substituting now (8.60) and (8.61) in (8.59) and applying the standard trigonometric formulas, we obtain an equation composed of the permanent terms, including functions $\sin\theta$, $\cos\theta$, $\sin 2\theta$, $\cos 2\theta$, $\sin 3\theta$, and $\cos 3\theta$. Let us solve these equations, proceeding from the method of harmonic balance, pursuant to which the equation will contain all reduced trigonometric functions. Thus, for expressing the parasitic modulation of resonant oscillations in the tuned circuit, applicable to frequency modulation, it is sufficient to use only equations balancing the terms with functions $\sin\theta$, $\cos\theta$, and $\cos 2\theta$. These are

$$\begin{aligned} &7X_1X_2\left(\frac{d\theta}{d\tau}\right)^2 - 2X_1\left(\frac{d\theta}{d\tau}\right)^2 - 2y_mX_1\left(\frac{d\theta}{d\tau}\right)^2 \sin\alpha\tau + 2X_1 - 3X_1X_2 \\ &+3y_mX_1 \sin\alpha\tau + \frac{9}{16}X_1^3 - \frac{3}{2}y_mX_1X_2 \sin\alpha\tau = 0 \end{aligned} \tag{8.62}$$

$$4X_2\frac{dX_1}{d\tau}\frac{d\theta}{d\tau} - 2\alpha y_mX_1\frac{d\theta}{d\tau}\cos\alpha\tau + 4\frac{dX_1}{d\tau}\frac{d\theta}{d\tau} + 2X_1\frac{d^2\theta}{d\tau^2} - X_1X_2\frac{d^2\theta}{d\tau^2} = 0 \tag{8.63}$$

$$\begin{aligned} &\frac{1}{2}X_1^2\left(\frac{d\theta}{d\tau}\right)^2 - 8X_2\left(\frac{d\theta}{d\tau}\right)^2 - 8y_mX_2\left(\frac{d\theta}{d\tau}\right)^2 \sin\alpha\tau + 2X_2 \\ &-\frac{3}{2}X_1^2 + \frac{3}{2}y_mX_2 \sin\alpha\tau - \frac{3}{4}y_mX_1^2 \sin\alpha\tau = 0 \end{aligned} \tag{8.64}$$

Note that in writing (8.62) - (8.64) the terms of order of smallness higher than X_1^3 were dropped (it was assumed that $X_2 \approx X_1^2$), and also (assuming that $dX_1/d\tau \approx \alpha y_m X_1$ and $d^2\theta/d\tau^2 \approx \alpha y_m d\theta/d\tau$) among the terms including $\sin\alpha\tau$ and $\cos\alpha\tau$, those containing products αy_m^2 or $\alpha^2 y_m^2$ were dropped as considerably smaller than those containing y_m or product αy_m.

For $y = 0$ and $x \to 0$, the solution of (8.59) gives $d\theta/d\tau = 1$ (i.e., $\omega = \omega_0$). For $x < 0.5$ (as assumed above) but not approaching zero we should expect that the value $d\theta/d\tau$ will be approximated by $d\theta/d\tau = \alpha + \Delta d\theta/d\tau$. Thus, proceeding from the condition $x < 0.5$, we can assume that $\Delta\theta << 1$. The presence of a modulating signal ($y \neq 0$) will result in modulation of the tuned circuit resonant frequency, and having confined the calculation only to the first harmonics of frequency variation, we find that $d\theta/d\tau = 1 + \Delta d\theta/d\tau + e\sin\alpha\tau$. By virtue of the small magnitude of $\Delta d\theta/d\tau$ and higher harmonics of variation of tuned circuit resonant frequency, the magnitude ε will appear practically as a relative frequency deviation.

The presence of FM should result in the appearance of parasitic AM. In the study of AM in an ideal tuned circuit where the modulator was a linear capacitance, it was found that the variation of the voltage on this capacitance coincides in phase with variation in tuned circuit frequency. This circumstance permits us to drop as negligible the higher harmonics of amplitude variation and to search hereinafter for magnitude X_1 in the form $X_1 = X_{10} + a\sin\alpha\tau$.

Substituting the expressions $d\theta/d\tau = 1 + \Delta d\theta/d\tau + e\sin\alpha\tau$ and $X_1 = X_{10} + a\sin\alpha\tau$ in (8.64), and dropping all small terms (noting that $\Delta d^2\theta/d\tau^2 = 0$, $\alpha << 1$, $\varepsilon << 1$, $y_m << 1$), we obtain

$$X_2 = -X_{10}^2/6 \tag{8.65}$$

We now substitute the following expressions in (8.62):

$$X_1 = X_{10} + a\sin\alpha\tau$$

$$d\theta/d\tau = 1 + \Delta d\theta/d\tau + e\sin\alpha\tau$$

$$X_2 = -X_{10}^2/6$$

Dropping terms of a higher order of smallness and retaining in one case only permanent terms, and in the other the terms including a trigonometric ratio $\sin\alpha\tau$ (i.e., again applying a method of harmonic balance), we obtain two new equations. From the first we find

$$\Delta\frac{d\theta}{d\tau} = -\frac{5}{192}X_{10}^2 \tag{8.66}$$

The second equation gives the relative frequency deviation ε:

$$\varepsilon = \frac{1}{4} y_m \tag{8.67}$$

And finally, substituting following expressions in (8.63):

$$X_1 = X_{10} + a\sin\alpha\tau$$

$$d\theta/d\tau = 1 + \Delta d\theta/d\tau + e\sin\alpha\tau$$

$$X_2 = -X_{10}^2/6$$

Again dropping the small terms, we obtain:

$$a = \frac{3}{2}\varepsilon X_{10} \tag{8.68}$$

From (8.68) we obtain, for the parasitic AM coefficient $m = a/X_{10}$

$$m = \frac{3}{2}\varepsilon$$

Thus, within the limits of the accuracy with which the coefficients of parasitic AM of the voltage on the modulating capacitance were derived, we obtain for FM in an ideal tuned circuit using as the modulator a linear variable capacitor (Section 4.2) the same result as for the varicap (this section).

It is interesting to note following circumstances. We often use the known Thompson formula $\omega = 1/\sqrt{LC}$ to determine the influence of a high frequency voltage $u = U\sin\omega t$, applied to the varicap that parallels the coil, on the frequency of a tuned-circuit oscillator. Thus, instead of capacitance C the investigator often substitutes the expression for equivalent capacitance of the varicap C_{Veq}, expressed in terms of the constant capacitance

$$C_V = C_{V0}[\varphi_c/(\varphi_c + E + u)]^{1/2}$$

or as a ratio Q_1/U, where Q_1 is the first harmonic of a charge present in the varicap:

$$q = 2C_{V0}\varphi_c/[(\varphi_c + E + u)/\varphi_c]^{1/2}$$

Entering the value $x = X_{10}\sin\omega t = [U/(\varphi_c + E)]\sin\omega t$ and assuming $X_{10} << 1$, we thus obtain, keeping only the terms up to X_{10}^2:

$$C_{Veq} = C_{V0}(E)\left(1 + \frac{3}{16} X_{10}^2\right)$$

$$C_{Veq} = C_{V0}(E)\left(1+\frac{X_{10}^{\ 2}}{16}\right)$$

respectively. From these, the expressions for oscillator frequency become

$$\omega \approx \omega_0\left(1-\frac{3}{32}X_{10}^{\ 2}\right)$$

$$\omega \approx \omega_0\left(1-\frac{X_{10}^{\ 2}}{16}\right)$$

respectively, where ω is the oscillation frequency for $X_{10} \to 0$ (i.e., $U \to 0$). Comparing the frequency changes indicated by these equations to that resulting from a high frequency voltage applied to the varicap, as derived above by solution of differential equation (8.58)

$$\frac{\Delta\omega}{\omega_0} = \frac{\Delta d\theta}{d\tau} = -\frac{5}{192}X_{10}^2$$

(i.e., by the more precise method), we can see that the more precise method yields a significantly smaller change.

References

[1] Artym, A. D., *The Theory and Methods of Frequency Modulation*, (in Russian), Moscow: Gosenergoizdat, 1964.

[2] Evtianov, S. I., *Lamp Generators*, (in Russian), Moscow: Svyaz, 1967.

[3] Sokolinskiy, V. G., Frequency Distortions of Signals in Oscillators with Frequency Modulation, *Radiotechnika i Electronica*, Volume 17, No. 8, 1972, pp. 1607-1612.

Chapter 9

Nonlinearity and Linearization in Varactor Control of FM Oscillators

It is convenient to use electric methods for frequency control of oscillators such as those used in sweep generators and in FM systems, including those used in short-range radar. Thus, the relationship between frequency and control signal (a voltage or a current) should be as close as possible to linear. This requirement is essential for short-range FM radar, as has been shown in the first part of this book.

The most widely applicable electronic controller of oscillator frequency is the varactor, a special semiconductor diode whose capacitance depends on a constant reverse voltage, or several varactors connected in an inverse-parallel or inverse-series manner. This makes it necessary to study the nonlinearity of frequency dependence upon the control voltage applied to the varactor or varactors. This problem is solved in this chapter.

In the first investigation phase we will consider that the active component of the oscillator is inertialess at the operating frequency, and that the feedback factor of the oscillator is a real quantity. These assumptions allow us to consider the oscillation frequency equal to the resonant circuit frequency. It confines the analysis to consideration of oscillators using a single-tuned circuit, (i.e., analysis in isolation from active components).

In practice the resonant circuits of all single-tuned oscillators controlled by varactors can be reduced to the two types shown in Figure 9.1 (if the frequency controller uses several varactors, it can be always reduced to a single equivalent varactor). We can consider capacitive coupling of the varactor to the oscillator circuit as shown in Figure 9.1(a) or autoinductive coupling as in Figure 9.1(b). The fixed capacitors (C_0, C, and parasitic capacitance C_p) included in the circuits allow us to take into account not only the capacitance of oscillator circuit elements, but also self-capacitance of the active component of the oscillator and the package capacitance.

The study of nonlinearity in the dependence of resonant frequency of these circuits upon the varactor control voltage is performed below for large frequency changes (as in a sweep oscillator), and for rather small variations (the case of

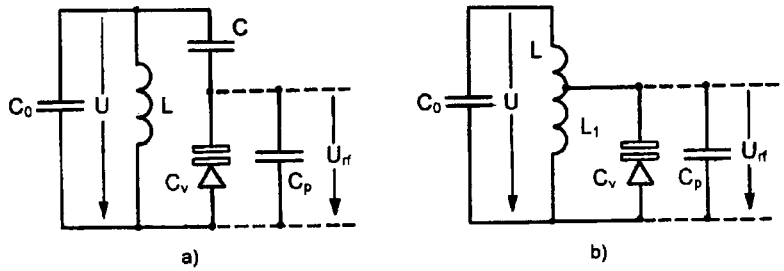

Figure 9.1 Circuits of tuned oscillators with (a) capacity and (b) autoinductive coupling to the varactor.

short-range FM radar). Thus, the consideration of large changes is restricted for brevity to the case of capacitor coupling of the varactor to the oscillator circuit of Figure 9.1(a). The fact is that with autoinductive coupling the capacitance C_0 is necessary and it must also meet the condition $C_0 > C_{v\,max} + C_p$, where $C_{v\,max}$ is the maximum value of varactor capacitance. This condition follows from the fact that with autoinductive coupling the resonant circuit of the oscillator is actually a double loop and its second resonant frequency (omitting the above-stated inequality) appears commensurable with the oscillator operating frequency. With frequency control of the oscillator, this circumstance can lead to mode jumping in frequency, precluding its use in FM radar. The availability of rather high capacity C_0 certainly does not allow large frequency changes in oscillators with autoinductive coupling.

For the first stage of study of general cases it is further assumed that the varactor capacitance depends exclusively on the control voltage applied to it (i.e., that it does not depend on the RF voltage on the varactor). The foundation for this conjecture is as follows. While the nonlinearity of the dependence of resonant frequency of these circuits upon the control voltage at predetermined limits of its variation is increased by the effect of RF voltage on the varactor, the frequency drift also simultaneously increases. In all, the influence on control nonlinearity of RF voltage on the varactor for a given frequency deviation should not lead to a significant correction. This is demonstrated further by consideration of some special cases.

It is impossible to obtain the required linearity of control voltage dependence in FM signal oscillators and resulting nonlinear distortions of the signal for large tuning ranges only by selection of circuit components. Therefore, it is often necessary to resort to special measures, some of which are also discussed in this chapter. We consider in Section 9.4 the widely used method of linearization of the control voltage dependence by predistortion of the control voltage with diode-resistor circuits. The chapter concludes with a description of several methods of reducing nonlinear distortions of the signal.

9.1 NONLINEARITY OF FREQUENCY DEPENDENCE OF SINGLE-TUNED OSCILLATORS ON CONTROL VOLTAGE OF THE VARACTOR WITH LARGE FREQUENCY CHANGES

The dependence of frequency f of oscillator circuits of Figure 9.1 upon varactor control voltage E_{vc} has a parabolic form, as shown in Figure 9.2. Let us call this dependence the oscillator control characteristic.

Let us draw a straight-line dependence $f_1(E_{vc})$ in Figure 9.2, intersecting the control characteristic at two points such that the greatest absolute frequency deviations of the oscillator within the limits of its variation f_{min} to f_{max} on the two sides of the line are equal. We will use their magnitude $(\Delta f)_{max} = |f - f_1|_{max}$ as the numerical criterion of control characteristic nonlinearity. We can see that such a criterion allows us to assert that at any point the control characteristic differs from linear by a magnitude Δf not greater than $(\Delta f)_{max}$.

Let us now move the straight line $f_1(E_{vc})$ parallel to itself downward so that it passes through the least and greatest frequencies of the tuning range (f_{min}, f_{max}) and we will designate this new dependence $f_1^*(E_{vc})$ (the dashed line in Figure 9.2).

Let us define δf as the difference between frequencies f and f_1^*. We can see that

$$(\Delta f)_{max} = 0.5(\delta f)_{max} \tag{9.1}$$

where $(\delta f)_{max}$ is the largest value of the difference $\delta f = f - f_1^*$ in the oscillator tuning range.

We will confine the discussion for brevity to the analysis of nonlinearity of the curve $f(E_{vc})$ for the circuit shown in Figure 9.1(a). The derivation of the greatest variations of f requires that the capacitances C_0 and C_p should be minimum (i.e., that they include only self-capacitance of the active component and package capacitance). In the case of autoinductive coupling of the varactor, the capacitance C_0 is important and it must be sufficiently large ($C_0 > C_{v\,max} + C_p$, where $C_{v\,max}$ is

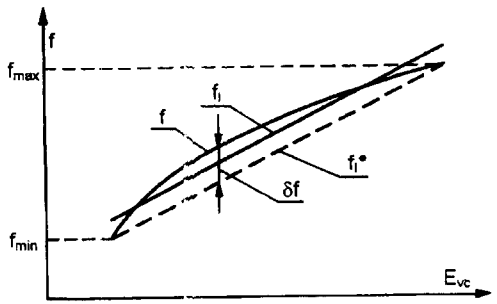

Figure 9.2 Dependence of oscillator frequency f on the voltage controlling the varactor, and its linear approximation.

the greatest value of varactor capacitance applicable to frequency f_{min}). Thus, the oscillator circuit shown in Figure 9.1(b) does not allow large tuning.

Thus, on the basis of Figure 9.1(a) we may write the following expression for generated frequency:

$$f = \frac{1}{2\pi}\sqrt{\frac{C + C_p + C_v}{L\left[CC_p + C_pC_0 + CC_0 + C_v(C + C_0)\right]}} \tag{9.2}$$

For capacitance of the varactor we have the known expression:

$$C_v = C_{v0}\sqrt[\gamma]{\frac{\varphi_c}{\varphi_c + E_{vc}}} = C_{v\max}(1+\beta)^{-1/\gamma} \tag{9.3}$$

where C_{v0} is the capacitance of the varactor at $E_{vc} = 0$, φ_c is the contact potential difference, γ is the power of the radical, equal to two for sharp *p-n* junction and to three for a smooth one, and $C_{v\max} = C_v(E_{vc\,\min})$ is the capacitance of the varactor at $E_{vc} = E_{vc\,\min}$, $\beta = (E_{vc} - E_{vc\,\min})/(\varphi_c + E_{vc\,\min})$. Having substituted (9.3) in (9.2), it is easy to obtain, for frequency f

$$f = \frac{1}{2\pi\sqrt{LC_{v\max}}}\sqrt{\frac{(a+b)(1+\beta)^{1/\gamma} + 1}{(ab + bd + ad)(1+\beta)^{1/\gamma} + (a+d)}} \tag{9.4}$$

where $a = C/C_{v\,\max}$, $b = C_n/C_{v\,\max}$, and $d = C_0/C_{v\,\max}$. Finally, assuming that

$$f_{\min} = \frac{1}{2\pi\sqrt{LC_{v\max}}}\sqrt{\frac{a+b+1}{ab + bd + ad + (a+d)}} = \frac{1}{2\pi\sqrt{LC_{\max}}}$$

where $C_{\max}$ is the value of selective system capacitance C_{ss} applicable to minimum frequency $f_{\min}$, we rewrite (9.4) in the form:

$$\frac{f}{f_{\min}} = \sqrt{z}\sqrt{\frac{(a+b)(1+\beta)^{1/\gamma} + 1}{(ab + bd + ad)(1+\beta)^{1/\gamma} + (a+d)}} \tag{9.5}$$

where $z = C_{ss\,\max}/C_{v\,\max}$.

From Figure 9.2 it follows that the frequency f_1^* is related to the control voltage E_{vc} by

$$f_1^* = f_{\min} + \frac{f_{\max} - f_{\min}}{E_{vc\,\max} - E_{vc\,\min}}(E_{vc} - E_{vc\,\min}) \tag{9.6}$$

Having divided and multiplied the second member in the right part by $\varphi_c + E_{vc\,min}$, it is easy to reduce (9.6) in the form:

$$f_1^* / f_{min} = 1 + (K_f - 1)\beta / \beta_{max} \tag{9.7}$$

where: $K_f = f_{max}/f_{min}$ is the frequency coverage coefficient, and
$\beta_{max} = (E_{vc\,max} - E_{vc\,min})/(\varphi_c - E_{vc\,min})$.

Having at our disposal (9.5) and (9.7), it would be possible to substitute them in a differential $(\delta f)/f_{min} = f/f_{min} - f_1^*/f_{min}$, and then, considering it as a function of the magnitude β, to find its maximum. However, to obtain an analytical expression for $(\delta f)_{max}/f_{min}$ (still strict only for the special case) we will hold constant the first term in the right side of this differential, and change the second member of (9.7) from the variable β/β_{max} to a variable f/f_{min}. This is not difficult to see using (9.7), assuming that the magnitude β_{max} corresponds to frequency f_{max}. Having performed this change and substituted the new expression for f_1^*/f_{min} in a differential

$$(\delta f)/f_{min} = f/f_{min} - f_1^*/f_{min},$$

we obtain:

$$\frac{\delta f}{f_{min}} = \frac{f}{f_{min}} - 1 - (K_f - 1)\frac{\left[\dfrac{z - (f/f_{min})^2(a+d)}{(f/f_{min})^2(ab+bd+ad) - z(a+b)}\right]^{\gamma} - 1}{\left[\dfrac{z - K_f^2(a+d)}{K_f^2(ab+bd+ad) - z(a+b)}\right]^{\gamma} - 1} \tag{9.8}$$

We will consider in the beginning the special case in which the capacitance of the varactor C_v is the only capacitance of the resonant circuit (i.e., the capacitors C, C_0, and C_p shown in Figure 9.1 are omitted). Then $z = 1$, $a \to \infty$, $b = 0$, $d = 0$, and (9.8) becomes:

$$\frac{\delta f}{f_{min}} = \frac{f}{f_{min}} - 1 - \frac{K_f - 1}{K_f^{2\gamma} - 1}\left[\left(\frac{f}{f_{min}}\right)^{2\gamma} - 1\right] \tag{9.9}$$

Study of the differential $\delta f/f_{min}$ shows that it reaches a maximum value at

$$\frac{f}{f_{min}} = \left[\frac{K_f^{2\gamma} - 1)}{2\gamma(K_f - 1)}\right]^{1/(2\gamma - 1)}. \tag{9.10}$$

Now substituting (9.10) into (9.9), we obtain the expression for the ratio

$$\frac{(\delta f)_{max}}{f_{min}} = \left[\frac{(K_f^{2\gamma}-1)}{2\gamma(K_f-1)}\right]^{1/(2\gamma-1)} - 1 - \frac{(K_f-1)}{(K_f^{2\gamma}-1)}\left[\left\{\frac{(K_f^{2\gamma}-1)}{2\gamma(K_f-1)}\right\}^{2\gamma/(2\gamma-1)} \gamma - 1\right] \tag{9.11}$$

In Figure 9.3 we show with solid curves the dependence of the ratio $(\delta f)_{max}/f_{min}$ upon the oscillator frequency coverage coefficient for values $\gamma = 2$ (varactor with sharp *p-n* junction) and $\gamma = 3$ (varactor with smoothly varying *p-n* junction), calculated using (9.11). The calculation of the ratio $(\delta f)_{max}/f_{min}$ for $\gamma = 3$ was restricted to values $K_f < 1.6$, as larger values are not encountered in cases of a varactor with smoothly varying *p-n* junction. We see that for equal values of the coverage coefficient K_f, the deviation from a straight line of the oscillator control characteristic is larger for the varactor with a smoothly varying *p-n* junction.

We note from (9.10) that ratios of frequencies at which the magnitude $(\delta f)/f_{min}$ appears maximal for given coefficient K_f practically coincide with those for $(K_f + 1)/2$. This circumstance (assuming that a maximum of dependence of the dimensionless differential $(\delta f)/f_{min}$ on the dimensionless quantity f/f_{min} is not sharply expressed) allows us to determine $(\delta f)_{max}/f_{min}$ by a substitution $f/f_{min} = (K_f + 1)/2$ in (9.9). Thus, we obtain one further expression for $(\delta f)_{max}/f_{min}$:

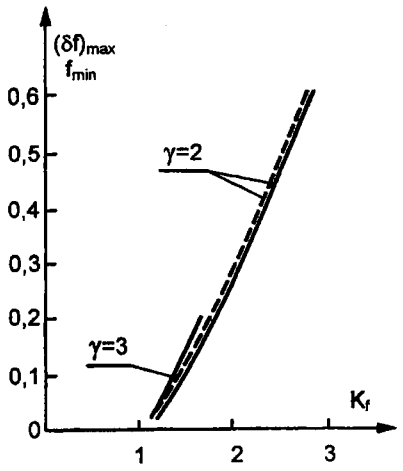

Figure 9.3 Dependence of the ratio $(\delta f)_{max}/f_{min}$ on the frequency coverage coefficient with (- - - -) and without (——) considering the radio frequency voltage on the varactor.

$$\frac{(\delta f)_{\max}}{f_{\min}} = \frac{(K_f + 1)}{2} - 1 - \frac{K_f - 1}{K_f^{2\gamma} - 1}\left[\left(\frac{K_f + 1}{2}\right)^{2\gamma} - 1\right] \tag{9.12}$$

The dependence of $(\delta f)_{\max}/f_{\min}$ on coefficient K_f calculated with (9.12) agree completely with those (solid curves) derived using (9.11), within the plotting scale of the ordinate of Figure 9.3.

Let us show now for the special case $z = 1$, $a \to \infty$, $b = 0$, $d = 0$ that the calculation of the influence of an RF voltage on varactor capacitance does not introduce significant correction in the result obtained by determination of nonlinearity of the oscillator control characteristic with (9.11) or (9.12). Naturally, we will consider that the tuning range of the oscillator (i.e., coverage coefficient K_f) is fixed. Thus we will be confined to the case in which the influence of an RF voltage on varactor capacitance is most significant, namely when the varactor with sharp *p-n* junction is used.

It is possible to show (see Chapter 8) that an RF voltage with amplitude U acting on a varactor with sharp *p-n* junction changes the resonant frequency of the circuit of Figure 9.1, with $C_0 = C_p = 0$ and $C = \infty$, by the correction

$$\frac{\Delta\omega}{\omega_0} = -\frac{5}{192} X_{10}^2 = -\frac{5}{192}\left(\frac{U}{\varphi_c + E_v}\right)^2$$

This correction allows us, instead of expressing the differential capacitance of the varactor by (9.3) for $\gamma = 2$, to use an expression depicting its equivalent capacitance, in the following form:

$$C_{veq} = C_{v0}\sqrt{\frac{\varphi_c}{\varphi_c + E_{vc}}}\left[1 + \frac{5}{96}\left(\frac{U}{\varphi_c + E_{vc}}\right)^2\right] \tag{9.13}$$

where U is the amplitude of the RF voltage at the varactor. Having taken advantage of the earlier identification

$$\beta = (E_{vc} - E_{vc\,\min})/(\varphi_c + E_{vc\,\min})$$

it is easy to reduce (9.13) to the form

$$C_{veq} = C_{v\max}(1+\beta)^{-1/2}\left[1 + \frac{5}{96}\left(\frac{U}{\varphi_c + E_{vc\,\min}}\right)\left(\frac{1}{1+\beta}\right)^2\right] \tag{9.14}$$

where, as earlier, $C_{v\max} = C_{v0}\sqrt{\varphi_c/(\varphi_c + E_{vc\min})}$.

The amplitude of the RF voltage U appearing in (9.13) and (9.14) varies, as a rule, with tuning of the oscillator (i.e., it depends on the control voltage E_{vc}). However, as its effect on capacitance C_{veq} is significant only for small values of voltage E_{vc}, we may consider the amplitude to be constant and equal to that value which it has for the minimum voltage $E_{vc\,\min}$. Thus, as the influence of amplitude on capacitance C_{veq} will be greatest for $E_{vc\,\min} + \varphi_c = U$, we consider that this applies (smaller values $E_{vc\,\min}$ are excluded, as they would cause the opening of the varactor p-n junction, which for many reasons is undesirable). Thus (9.14) now becomes:

$$C_{veq} = C_{v\max}(1+\beta)^{-1/2}\left[1+\frac{3}{16}\left(\frac{1}{1+\beta}\right)^2\right] \tag{9.15}$$

Supposing now that $E_{vc} = E_{vc\,\min}$ (i.e., $\beta = 0$), we find from (9.15) the following expressions for the maximum value of the effective capacitance of the varactor:

$$C_{veq\max} = C_{v\max}\left(1+\frac{3}{16}\right) \tag{9.16}$$

As for arbitrary and minimum generated frequencies we have $f = 1/(2\pi\sqrt{LC_{veq}})$ and $f_{\min} = 1/(2\pi\sqrt{LC_{v\max}})$, we obtain an expression for the ratio of frequencies $f/f_{\min}$ from (9.15) and (9.16):

$$\frac{f}{f_{\min}} = \frac{(1+3/16)^{1/2}(1+\beta)^{1/4}}{\left[1+(3/16)\left(\frac{1}{1+\beta}\right)^2\right]^{1/2}} \tag{9.17}$$

Unfortunately (9.17) does not allow us to obtain a formula with which we could calculate the ratio $(\delta f)_{\max}/f_{\min}$ for a given frequency coverage coefficient K_f, as was possible when the RF voltage acting on the varactor was ignored in (9.11). However, resorting to computer facilities and using (9.7) and (9.17), we can find the ratio $(\delta f)_{\max}/f_{\min}$ (recalling that $(\delta f)_{\max}/f_{\min} = (f - f^*)/f_{\min} = f/f_{\min} - f^*/f_{\min}$). The resulting dependence of $(\delta f)_{\max}/f_{\min}$ on coefficient K_f for a varactor with sharp p-n junction, taking into account presence of an RF voltage on the varactor, is shown in Figure 9.3 (dashed line) together with curves obtained by disregarding this voltage.

From the curves shown in Figure 9.3, we see that the relative error in the value of $(\delta f)_{\max}/f_{\min}$ caused by ignoring the RF voltage on the varactor does not exceed 10%, when the varactor has a sharp p-n junction ($\gamma = 2$) and is the only

capacitance of the resonant circuit. It is also apparent that in the case of the varactor with smoothly varying junction ($\gamma = 3$), this inaccuracy will be even less, because of the smaller influence on its equivalent capacitance C_{veq} of an RF voltage.

We now return to the general case, in which the capacitances C_0, C_p, and C of Figure 9.1(a) do not obey the conditions $C_0 = 0$, $C_p = 0$, and $C = \infty$. Unfortunately, (9.8) in this case does not allow us to obtain an analytical expression for the magnitude $(\delta f)_{max}/f_{min}$. However, it is not difficult to calculate it with adequate accuracy. In this chapter, the case of rather large frequency tuning is interesting to us. The derivation of such changes is possible only in the case where the capacitance of the varactor plays a significant role in the total capacity of the oscillator circuit (i.e., when the inequalities $C_v > C_0$. $C_v > C_p$, and $C_v < C$ apply). This circumstance leads to a ratio f/f_{min}, applicable to magnitude $(\delta f)_{max}/f_{min}$, that is still close to $f/f_{min} = (K_f + 1)/2$. And as the maximum of dependence of a dimensionless differential $\delta f/f_{min}$ on the dimensionless frequency f/f_{min} at $C_0 \neq 0$, $C_p \neq 0$, $C \neq \infty$ is expressed only approximately, a more precise value for it can be obtained with (9.8), in which $f/f_{min} = (K_f + 1)/2$.

These calculations demonstrate that with a given frequency coverage coefficient K_f the dimensionless differential $(\delta f)_{max}/f_{min}$ is reduced (i.e., the oscillator control characteristic is more linear), as the inequalities $C_v > C_0$, $C_v > C_p$, and $C_v < C$ apply more strongly.

Thus, we may meet the requirement for linearity of the oscillator control characteristic by appropriate choice of the oscillator circuit and capacitors included in it, if the allowable deflection from a straight line of that characteristic $(\Delta f)_{max} = 0.5(\delta f)_{max}$ is within the value given by (9.11) or (9.12). If this is not the case, and also when the permissible variation $(\Delta f)_{max}$ is less than the value from (9.11) or (9.12), it is necessary to resort to different methods of linearization of the control characteristic. In particular, it can be the method considered in Section 9.3.

9.2 NONLINEAR DISTORTIONS WITH FREQUENCY MODULATION USING VARACTORS

The derivation of formulas for calculation of nonlinear signal distortions is carried out below for FM oscillators using varactors. This derivation is based on the widely applicable method of series expansion in terms of $\omega(\beta_\Omega)$, where ω is the radian frequency of oscillations and $\beta_\Omega = U_\Omega/E_{vs}$ is the ratio of modulating voltage to an initial (bias) voltage on the varactor in the absence of modulation. The series obtained below converge if $\beta_\Omega < 1$. Under the usual condition $E_{vs} - U_\Omega \leq U_{rf}$, where U_{rf} is the amplitude of the RF voltage at the varactor, these series always converge. As can be demonstrated from the calculations, they converge quickly enough for $\beta_\Omega < 0.7$, and therefore in subsequent analysis we need consider only the first three members of the series. In general the third harmonic is of great importance in the case of S-shaped control characteristics. The control characteristics

of most FM oscillators with varactors resemble a parabola and the fourth member of the series is negligible as compared with the third member. This is demonstrated below in an example of capacity coupling of the varactor to the resonant circuit with $C_0 = 0$.

The effect of RF voltages on varactor capacitance is initially neglected in analysis of nonlinear distortions for the general case (where the oscillator circuits with parasitic capacitance are as shown in Figure 9.1), as was assumed for the case of large frequency changes. For the special case in which the circuits shown in Figure 9.1 are reduced to a circuit with only the capacitance of the varactor, it will be shown that this omission is quite acceptable.

9.2.1 Nonlinear Distortions for Capacitor Coupling of the Varactor to the Oscillator Circuit

The expression for the natural radian frequency of the oscillator circuit shown in Figure 9.1(a) is:

$$\omega = \sqrt{\frac{C + C_p + C_v}{L(CC_p + C_pC_0 + C_v(C + C_0)}} \tag{9.18}$$

The capacitance of the varactor is represented as

$$C_v = C_{v0}\sqrt[\gamma]{\frac{\varphi_c}{\varphi_c + E_{vs} + U_\Omega \cos\Omega_m t}} = C_{vs}\frac{1}{\sqrt[\gamma]{1 + \beta_\Omega \cos\Omega_m t}} \tag{9.19}$$

where $C_{vs} = C_{v0}\sqrt[\gamma]{\varphi_c/(\varphi_c + E_{vs})}$ is the capacitance of the varactor with no modulation, $\beta_\Omega = U_\Omega/(\varphi_c + E_{vs})$ is the relative amplitude of a control voltage, and Ω_m is the radian frequency of the modulating signal.

Substituting (9.19) in (9.18), decomposing the resulting expression in a power series in $\beta_\Omega \cos\Omega_m t$ and restricting the series to three members, we obtain

$$\omega = \omega_s(1 + A_1 \cos\Omega_m t - A_2 \cos^2\Omega_m t) \tag{9.20}$$

where

$$A_1 = \frac{\beta_\Omega}{2\gamma}\frac{a_s^2}{[(a_sb_s + b_sd_s + a_sd_s) + a_s + d_s](a_s + b_s + 1)}$$

and

$$A_2 = \frac{\beta_\Omega^2 a_s^2\left[2(a_sb_s + b_sd_s + a_sd_s)\{(\gamma+1)(a_s + b_s) + 2\gamma\} + 2(\gamma - 1)(a_s + d_s) + (2\gamma - 1)a_s^2)\right]}{8\gamma^2[(a_sb_s + b_sd_s + a_sd_s) + a_s + d_s]^2(a_s + b_s + 1)^2}$$

Here, ω_s is the oscillation frequency for the initial condition of no modulation (i.e., $C_s = C_{vs}$, $a_s = C/C_{vs}$, $d_s = C_0/C_{vs}$, and $b_s = C_p/C_{vs}$). Utilizing the known formula $\cos^2\Omega t = (1 + \cos 2\Omega t)/2$ and assuming that the nonlinear distortion coefficient K_2 for the second harmonic is the ratio of coefficients for $\cos 2\Omega_m t$ and $\cos\Omega_m t$, we find:

$$K_2 = 0.5A_2 / A_1 \tag{9.21}$$

As the magnitude A_2 from (9.20) is simply the relative frequency deviation (i.e., $A_2 = \Delta\omega/\omega_s$), (9.21) can be written:

$$K_2 = 0.5(A_2 / A_1^2)(\Delta\omega / \omega_s). \tag{9.22}$$

Substituting in (9.22) the magnitudes A_2 and A_1, we obtain the following dependence of the nonlinear distortion coefficient of the second harmonic upon the relative frequency deviation $\Delta\omega/\omega_s$ and upon parameters of the circuit:

$$K_2 = \frac{2(a_s b_s + b_s d_s + a_s d_s)\left[(\gamma+1)(a_s + b_s) + 2\gamma\right] + 2(\gamma-1)(a_s + d_s) + (2\gamma-1)a_s^2}{4a_s^2} \times \frac{\Delta\omega}{\omega_s} \tag{9.23}$$

In the specific case where $C \to \infty$, $C_p = 0$, $C_0 = 0$ (i.e., for $a_s \to \infty$, $b_s = 0$, and $d_s = 0$) we obtain from (9.23)

$$K_2 = \frac{2\gamma - 1}{4} \frac{\Delta\omega}{\omega_s} \tag{9.24}$$

From (9.23) and (9.24), it follows that for a given relative frequency deviation $\Delta\omega/\omega_s$ the nonlinear distortion coefficient is minimum in the case where the capacitance of the varactor is the only capacitance of the oscillator circuit:

$K_{2\min} = 0.75\Delta\omega/\omega_s$ for $\gamma = 2$ (sharp *p-n* junction), and
$K_{2\min} = 1.25\Delta\omega/\omega_s$ for $\gamma = 3$ (smooth *p-n* junction).

For the special case in which $C_0 = 0$ (i.e., for $d_s = 0$), the fourth member of (9.20) was obtained. This allows us to determine the nonlinear distortion coefficient for the third harmonic:

$$K_3 = \frac{K_2}{6}\frac{3a_s^2 - 6a_sAB + 4B^2\left\{\left[A(2\gamma-1) - b_s(\gamma+1)\right](b_s+1) + 3b_sA\right\}}{a_s(a_s+2AB)} \times \frac{\Delta\omega}{\omega_s} \tag{9.25}$$

where $A = b_s(\gamma + 1) + \gamma - 1$, and $B = a_s + b_s + 1$. For $C \to \infty$ and $C_p = 0$ (differently than for $a_s \to \infty$ and $b_s = 0$), it follows from (9.25) that

$$K_3 = \frac{4\gamma - 1}{6}\frac{\Delta\omega}{\omega_s} \tag{9.26}$$

(i.e., the ratio K_3/K_2 is of the same order as the relative frequency deviation $\Delta\omega/\omega_s$). Table 9.1 shows the ratio $(K_3/K_2)/(\Delta\omega/\omega_s)$, calculated for representative values of a_s and b_s. From this table we can see that for $C \neq \infty$, $C_n \neq 0$ the ratio $(K_3/K_2)/(\Delta\omega/\omega_s)$ is increased, as contrasted to the case where the varactor is the only capacitance of the oscillator circuit. However, for $C \to \infty$ and $C_p = 0$ it is possible to obtain a rather large relative frequency deviation $\Delta\omega/\omega_s$. The presence of the finite capacitance C and nonzero capacitance C_p usually reduces the peak value of deviation, especially in case of the varactor with smoothly varying *p-n* junction. Therefore, in many conditions the nonlinear distortion coefficient of the third harmonic is less by an order of magnitude that that of the second harmonic.

Table 9.1
Calculated Values of the Normalized Ratio of Nonlinear Distortion Coefficients

	$a_s \to \infty, b_s = 0$	$a_s = 1, b_s = 0$	$a_s \to \infty, b_s = 1$	$a_s = 1, b_s = 1$
$\gamma = 2$	1.17	2.1	2.7	7.7
$\gamma = 3$	1.83	2.9	4.1	11.8

9.2.2 Nonlinear Distortions for Autoinductive Coupling of the Varactor to the Oscillator Circuit

For analysis of nonlinear distortions in this case we find, as earlier, the expression for the radian frequency of oscillations. For Figure 9.1(b)

$$\omega = \frac{1}{\sqrt{L(C_0 + p^2C_p + p^2C_v)}} \tag{9.27}$$

where $p = L_1/L$ is the sensitivity coefficient of the varactor and capacitance C_p in the resonant circuit. Let us substitute (9.19) in (9.27) and decompose the resulting expression as a power series in $\beta_\Omega \cos\Omega_m t$. Considering three members of the series, we again obtain (9.21) for the nonlinear distortion coefficient of the second harmonic K_2, but in which the constants are now

$$A_1 = \frac{\beta_\Omega}{2\gamma} \frac{p^2}{d_s + p^2 b_s + p^2} \text{ and}$$

$$A_2 = \frac{\beta_\Omega^2}{8\gamma^2} \frac{p^2\left[p^2(2\gamma - 1) + 2(\gamma + 1)\left(d_s + p^2 b_s\right)\right]}{\left(d_s + p^2 b_s + p^2\right)^2}$$

where d_s and b_s have the same sense as earlier.

Given the expressions for A_1 and A_2, with (9.22) we now establish the following relation of the nonlinear distortion coefficient K_2 to the relative frequency deviation $\Delta\omega/\omega_s$ and parameters of the resonant circuit:

$$K_2 = \frac{p^2(2\gamma - 1) + 2(\gamma + 1)(d_s + p^2 b_s)}{4p^2} \frac{\Delta\omega}{\omega_s} \tag{9.28}$$

Assuming in (9.28) $p = 1$, $d_s = 0$, and $b_s = 0$, (i.e., assuming $C_0 = 0$ and $C_p = 0$), we obtain again (9.26): $K_2 = (2\gamma - 1)\Delta\omega/4\omega_s$ (i.e., we again find that for a given relative frequency deviation the nonlinear distortion coefficient is minimum in the case where the varactor is the only capacitance of the oscillator circuit). For set values of magnitudes d_s and b_s, the nonlinear distortion coefficient is reduced with increase of the sensitivity coefficient p of the varactor in the oscillator circuit.

9.2.3 Nonlinear Distortions in the Case of a Single-Tuned Oscillator Circuit with Allowance for RF Voltage on the Varactor

We assume now that in the oscillator circuit of Figure 9.1 $C_0 = 0$, $C_p = 0$, $C \to \infty$, and $p = 1$. In this case the two circuits degenerate into one composed only of a series-connected inductor and varactor. Let us now take into account the influence of an RF voltage on varactor capacitance. As in earlier consideration of the nonlinear oscillator control characteristic, we will confine the analysis to the case in which this effect is most significant, namely where a varactor with sharp junction ($\gamma = 2$) is used.

The expression of interest to us, for equivalent capacitance of the varactor, can be obtained from (9.13) by substitution in the last term of E_c for $E_{vs} + U_\Omega \cos\Omega_m t$, and is

$$C_{veq} = C_{v0}\sqrt{\frac{\varphi_c}{\varphi_c + E_s + U_\Omega \cos\Omega_m t}}\left[1+\frac{3}{16}\left(\frac{U_{rf}}{\varphi_c + E_{vs} + U_\Omega \cos\Omega_m t}\right)^2\right] \quad (9.29)$$

Using the known relationship $\beta_\Omega = U_\Omega/(\varphi_c + E_{vs})$, and also $a = U_v/(\varphi_c + E_{vs})$, we reduce (9.29) to the form

$$C_{veq} = C_{vs}\left[(1+\beta_\Omega \cos\Omega_m t)^{-1/2} + (3/16)a^2(1+\beta_\Omega \cos\Omega_m t)^{-5/2}\right] \quad (9.30)$$

where, as earlier, $C_{veq} = C_{v0}\sqrt{\varphi_c/(\varphi_c + E_s)}$ is the capacitance of the varactor with no modulation and disregarding any RF voltage.

We note that the amplitude of an RF voltage U_{rf} on the varactor with FM is normally included in a. However, we will subsequently approximate a as a constant, considering that it is generally difficult to take these variations into account, that it is possible to make these variations small by stabilizing the output voltage amplitude, and that the result obtained has only qualitative value.

Having now substituted (9.30) in the formula for oscillator circuit frequency $\omega = 1/\sqrt{LC_{veq}}$ and considering only three members of the series in $\beta_\Omega \cos\Omega_m t$, we obtain

$$\omega = \omega_{seq}(1 + A_{1eq}\cos\Omega_m t - A_{2eq}\cos^2\Omega_m t)$$

$$A_{1eq} = \frac{\beta_\Omega}{4}\frac{1+(15/16)a^2}{1+(3/16)a^2} \text{ and}$$

$$A_{2eq} = \frac{3\beta_\Omega^2}{32}\left[2\frac{1+(35/16)a^2}{1+(3/16)a^2} - \left(\frac{1+(15/16)a^2}{1+(3/16)a^2}\right)^2\right]$$

where $\omega_{seq} = \omega_s[1 + (3/16)a^2]^{-1/2}$ is the oscillator frequency for the case of no modulation with allowance for influence of RF voltage on the capacitance of the varactor.

Having taken advantage in this case of (9.22), in which A_{1eq} and A_{2eq} now correspond to A_1 and A_2, using the expressions for A_{1eq} and A_{2eq} we find the following dependence between the nonlinear distortion coefficient K_2 and the relative frequency deviation $\Delta\omega/\omega_s$:

$$K_2 = \frac{3}{4}\left[2\frac{\left[1+(35/16)a^2\right]\left[1+(3/16)a^2\right]}{\left[1+(15/16)a^2\right]^2} - 1\right]\frac{\Delta\omega}{\omega_s} \quad (9.31)$$

Calculations using (9.31) demonstrate an acceptable level of error in determination of the nonlinear distortion coefficient K_2, while disregarding the RF voltage at the varactor, in the case where the varactor has a sharp p-n junction ($\gamma = 2$) and is the only capacitance of the oscillator circuit. For all reasonable values of a, the error is an order less than the value $K_2 = (3/4)\Delta\omega/\omega_s$, from the formulas obtained earlier: (9.23), (9.28), and from (9.31) with $a = 0$. It also appears that in the case of the varactor with smoothly varying junction this error will be even less.

9.3 LINEARIZATION OF DEPENDENCE OF OSCILLATOR FREQUENCY ON CONTROL VOLTAGE

It was demonstrated above that the oscillator control characteristic is nonlinear when the frequency control voltage is applied directly to the varactor. The result is the appearance of nonlinear distortions on the FM signal. In short-range FM radar, nonlinearity of the control characteristic and nonlinear distortions of the FM signal are often much less than when control voltage is applied directly to the varactor. To avoid this situation, we can apply special correcting circuits (CC). In this case, the control voltage E_c is the input to the CC input, and an output voltage E_{vc} is applied to the varactor. Thus, the CC will convert a voltage E_c to E_{vc} in such a way that the oscillator control characteristic (now understood as the dependence of frequency f on a voltage E_c, instead of on E_{vc}) is nearly linear.

We will find the form of CC transforming characteristic $E_{vc} = \Phi(E_c)$ that is necessary for a strictly linear control characteristic. For this we need the dependence of frequency f upon the varactor voltage E_{vc}, which can either be calculated or obtained experimentally. Let us now take advantage of a rectangular coordinate system (Figure 9.4), where on the ordinate we plot both the frequency f and the voltage E_{vc}, and on the abscissa the voltage E_c. Not setting any plotting scale in the figure, we select two arbitrary points, one of which corresponds to the initial value E_{cs}, and the other to the final value E_{cf} of voltage E_c. Let us draw a straight line

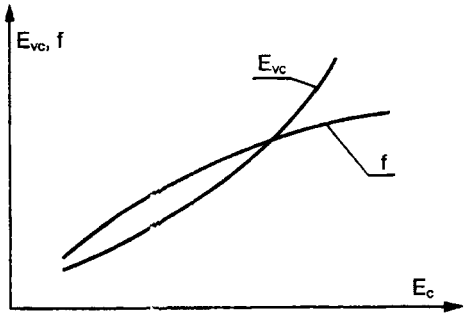

Figure 9.4 Control characteristic $f(E_c)$ and dependence $E_{vc}(E_c)$ for correction circuit.

through points with coordinates (E_{cs}, f_{min}), (E_{cs}, f_{max}), where f_{min} and f_{max} are the minimum and maximum frequencies of the control characteristic. This will define our straight-line control characteristic. Having now designated on verticals to the abscissa at the point with values E_{vc}, applicable to frequencies f of the straight-line control characteristics, intercrossed by these verticals, and having passed a curve through them, we find the form of the required CC transforming characteristic $E_{vc} = \Phi(E_c)$.

Because the dependence of oscillator frequency on the varactor voltage in single-tuned oscillators is represented in a rectangular reference system by an increasing curve with decreasing slope in accordance with increase of voltage E_{vc} (Figure 9.2), the curve $E_{vc} = \Phi(E_c)$ should always have increasing slope with increasing voltage E_c (Figure 9.4).

One of the possible simple CCs producing an optimum transforming characteristic according to Figure 9.4 is the circuit shown in Figure 9.5. Its resistors are chosen such that as E_c increases, diode D_1 is turned on first, followed by diode D_2, and so forth. After turning on diode D_1, a voltage E_{vc} will appear with increasing E_c, and turning on each subsequent diode will reduce the slope as the voltage E_c increases.

We will now obtain expressions that allow us at given points of a required curve $E_{vc} = \Phi(E_c)$ (continuous curve in Figure 9.6) to calculate the resistance of CC resistors shown in Figure 9.5, and also to determine required limits to the variation of E_c. To simplify these expressions we make the assumption that the CC diodes have indefinite resistance in the cutoff state and zero resistance in the conducting state. For same purpose, we assume that the increments of the voltage E_c between points of conduction of diodes D_1 and D_2, diodes D_2 and D_3, and so forth, and also between conduction of the diode D_m and the greatest value of a voltage E_c on the required curve $E_{vc} = \Phi(E_c)$ are all equal.

With these assumptions, instead of the required transforming characteristic $E_{vc} = \Phi(E_c)$, only the characteristic appearing as a segmented line, shown in Figure 9.6 (dashed line), need be obtained. We also note that as the actual dependence of

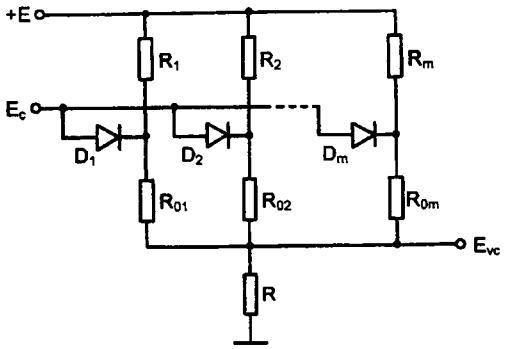

Figure 9.5 Diode-resistive correction circuit.

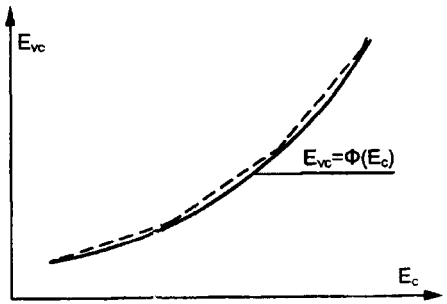

Figure 9.6 $E_{vc}(E_c)$ required for compensation and its segmented approximation with diode-resistive CC.

currents in a diode on the applied voltage is smooth rather than as assumed above, it is possible to obtain a rather smooth curve for $E_{vc} = \Phi(E_c)$. This usually allows us to closely approach the required oscillator control characteristic with few diodes in the CC.

Sometimes it is only possible to realize a CC that produces, instead of the desired characteristic $E_{vc} = \Phi(E_c)$, the form $E^*_{vc} = \Psi(E_c)$ displaced on the ordinate by some additional magnitude E_{vcadd} (i.e., $E^*_{vc} = E_{vc} + E_{vc\ add}$). The application of the required varactor voltage is then obtained by subtraction of $E_{vc\ add}$ from the voltage E^*_{vc} (Figure 9.7). We subsequently consider that adjustment of the CC can reshape the performance $E^*_{vc} = \Psi(E_c)$.

We note that in the CC shown on Figure 9.5 all resistors R_{01}, R_{02}, ... R_{0m} are equal. However, one of them, as will be shown later, should differ from others. Let us consider as those the resistance R_{0m}.

We now give to voltages E_c and E^*_{vc}, applicable to opening of diodes D_1, D_2, ... D_m, the subscripts 1, 2 ... m (apparently, $E_{cs} = E_{c1}$ and $E^*_{cs} = E^*_{c1}$) and enter identifications: $R_{01} = R_{02} = \ldots R_{0(m-1)} = R_0$, $R_{0m} = lR_0$ (l is a positive number), $R_n + R_{0n} = R^*_n$, $R_0/R_n = \chi_n$, $R_0/R = y$, and $E/E^*_{vcs} - 1 = a_n$, where $n = 1, 2, \ldots m$.

It is apparent that for output voltage E^*_{vc}, at which diode D_1 is at the boundary between conducting and open states and all remaining diodes are closed, we obtain

$$E^*_{vc1} = \frac{R}{R + 1/(1/R^*_1 + 1/R^*_2 + \ldots 1/R^*_m)} E$$

which can be easily changed to the form

$$y = A + a_1\chi_m \tag{9.32}$$

where $A = a_1(\chi_1 + \chi_2 + \ldots + \chi_{m-1})$.

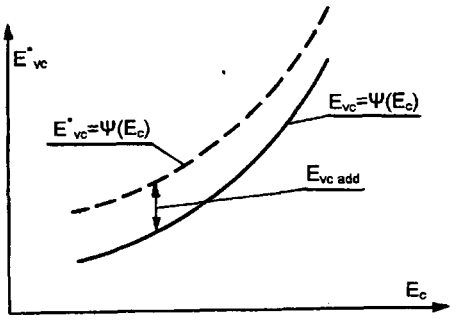

Figure 9.7 E_{vc} and E^*_{vc} versus control voltage.

For output voltage E^*_{vc} applicable to the open state of all diodes, and also to the case when the diode D_m is at the boundary between conducting and open states (i.e., $E^*_{vc} = E^*_{vcm}$), we can write

$$E^*_{vc} = \frac{R}{R + [R_0/(m-1)]R_{0m}/[R_0/(m-1) + R_{0m}]}(E_c - E'_d)$$

where E'_d is the voltage on the diode at which it begins to conduct. From here, assuming that

$$\frac{ly}{1 + l(m-1)} = B \tag{9.33}$$

we obtain the following two expressions:

$$E^*_{vcm} = \frac{1}{1+B}(E_{cm} - E'_d), \tag{9.34}$$

$$E^*_{vck} = \frac{1}{1+B}(E_{ck} - E'_d). \tag{9.35}$$

The input voltage of the CC, applicable to the boundary between open and conducting states of the arbitrary diode, apparently exceeds by E'_d the voltage at a point of connection of the diode to resistors R_n and R_{0n}. We may thus write:

$$E_{cn} = (E - E^*_{vcn})R_{0n}/R^*_n + E^*_{vcn} + E'_d$$

from which the equation system follows:

$$\begin{cases} E_{c1} = E^*_{vc1}(a_1\chi_1 + 1) + E'_d, \\ \cdots\cdots\cdots\cdots\cdots\cdots\cdots\cdots \\ E_{c(m-1)} = E^*_{vc(m-1)}(a_{m-1}\chi_{m-1} + 1) + E'_d, \\ E_{cm} = E^*_{vcm}(la_m\chi_m + 1) + E'_d \end{cases} \tag{9.36}$$

Substituting the last equation of system (9.36) into (9.34), we obtain

$$\chi_m = B/(la_m) \tag{9.37}$$

On the basis of accepting the above condition, that

$$E_{ck} - E_{cm} = E_{cm} - E_{c(m-1)} = \ldots = E_{c2} - E_{c1}$$

we can write a following system of equalities:

$$\begin{cases} E_{ck} = E_{cm} + \dfrac{1}{m-1}(E_{cm} - E_{c1}) = \dfrac{m}{m-1}E_{cm} - \dfrac{1}{m-1}E_{c1}, \\ E_{ck} = E_{cm} + \dfrac{1}{m-2}(E_{cm} - E_{c2}) = \dfrac{m-1}{m-2}E_{cm} - \dfrac{1}{m-2}E_{c2}, \\ \cdots\cdots\cdots\cdots\cdots\cdots\cdots\cdots\cdots\cdots\cdots\cdots\cdots\cdots\cdots\cdots \\ E_{ck} = E_{cm} + (E_{cm} - E_{c(m-1)}) = 2E_{cm} - E_{c(m-1)}. \end{cases} \tag{9.38}$$

Substituting now (9.38) into (9.35) and using (9.36) and (9.37), we obtain

$$\begin{cases} \chi_1 = \dfrac{1}{a_1}\left[\dfrac{mc - (m-1)}{b_1 c}(B+1) - 1\right], \\ \chi_2 = \dfrac{1}{a_2}\left[\dfrac{(m-1)c - (m-2)}{b_2 c}(B+1) - 1\right], \\ \cdots\cdots\cdots\cdots\cdots\cdots\cdots\cdots\cdots\cdots\cdots\cdots \\ \chi_{m-1} = \dfrac{1}{a_{m-1}}\left[\dfrac{2c-1}{b_{m-1}c}(B+1) - 1\right], \end{cases} \tag{9.39}$$

where $b_n = E^*_{vcn}/E^*_{vcm}$, $c = E^*_{vcm}/E^*_{vck}$.

Solving jointly (9.32), (9.33), and (9.37), we find for magnitude l

$$l = \frac{B(a_1/a_m - 1)}{B(m-1) - A} \tag{9.40}$$

Now we will obtain the formula for selection of the voltage $E_{vc\ add}$. Observing the condition $E_{c1} - E'_d \geq E^*_{vc1}$ (this is necessary, following from the first equation of system (9.36), because to $E_{c1} - E'_d = E^*_{vc1}$ there corresponds a case $\chi_1 = 0$, i.e., $R_1 \to \infty$), but, as $E_{c1} - E'_{ck} - m(E_{ck} - E_{cm})$, this condition can be represented as

$$E_{ck} = m(E_{ck} - E_{cm}) - E'_d \geq E^*_{vc1} \tag{9.41}$$

But from (9.34) and (9.35) it follows that

$$E_{ck} = \frac{E^*_{vck}}{E^*_{vcm}}(E_{cm} - E'_d) + E'_d \tag{9.42}$$

Excluding the voltages E_{ck} from (9.41) and (9.42), we obtain:

$$E_{cm} \geq \frac{E^*_{vc1}}{m - (m-1)E^*_{vck} / E^*_{vcm}} + E'_d \tag{9.43}$$

or after a substitution $E^*_{vc1} = E_{vc1} + E_{vc\ add}$, $E^*_{vcm} = E_{vcm} + E_{vc\ add}$, and $E^*_{vck} = E_{vck} + E_{vcadd}$,

$$E_{cm} \geq \frac{(E_{vc1} + E_{vcadd})(E_{vcm} + E_{vcadd})}{m(E_{vcm} + E_{vcadd}) - (m-1)(E_{vck} + E_{vcadd})} + E'_d \tag{9.44}$$

The inequality (9.44) applies when there is a positive common denominator in its right part. Otherwise the sign $\geq$ changes to $\leq$. But as the voltage E_{cm} can only be positive, the second case is not of interest. A condition for a positive denominator is the inequality:

$$E_{vadd} \geq (m-1)E_{vck} - mE_{vcm} \tag{9.45}$$

from which it follows that with $(m - 1)E_{vck} - mE_{vcm} > 0$ there can be realized only the transforming characteristic $E^*_{vc} = \Psi(E_c)$, obtained by offset of the required transforming characteristic $E_{vc} = \Psi(E_c)$ on the ordinate by $E_{v\ add}$, nonzero and defined by the inequality (9.45).

It is desirable that the voltage E_{cm} not be too large. Analysis of (9.44) demonstrates that the least possible value of a voltage E_m is reached at magnitude $E_{v\ add}$, defined by

$$E_{vcadd} = M + \sqrt{M^2 + (E_{vc1} + E_{vcm})M + E_{vc1}E_{vcm}} \tag{9.46}$$

where $M = (m - 1)E_{vck} - mE_{vcm}$.

9.4 CALCULATION OF DIODE-RESISTIVE CORRECTION CIRCUITS

The expressions obtained in Section 9.3 suggest the following procedure for calculation of the correction circuit shown in Figure 9.5:

1. For a calculated or experimentally determined oscillator control characteristic $F(E_{vc})$, we find the shape of the transforming characteristic $E_c = \Phi(E_{vc})$ (i.e., we create an arbitrary plotting scale on the abscissa) providing a linear dependence $f(E_c)$.

2. Based on tolerance requirements for linearization of the control characteristic $f(E_c)$, we choose a number of diodes m used in the CC.

3. From the transforming characteristic $E_c = \Phi(E_{vc})$ of step 1, we determine voltages $E_{vc1}, E_{vc2}, \ldots E_{vcm}, E_{vck}$.

4. Knowing the number of diodes m and voltages $E_{vc1}, E_{vc2}, \ldots E_{vcm}, E_{vck}$, we find from (9.46) the value $E_{vc\ add}$.

5. We find the voltages $E^*_{vc1} = E_{vc1} + E_{vc\ add}$, $E^*_{vc2} = E_{vc2} + E_{vc\ add}$, $E^*_{vcm} = E_{vcm} + E_{vc\ add}$, and $E^*_{vck} = E_{vck} + E_{vc\ add}$.

6. Substituting in the right side of (9.43) values m, $E_{vc1}, E_{vc2}, \ldots E_{vcm}$, and E_{vck}, we find the least possible voltage $E_{cm\ min}$ and select a voltage E_{cm} slightly greater than this. Thus, the inequality $E_{c1} > E_{vc1}$ will apply and the resistance R_1 will have a final value that will permit its implementation as a variable (as well as resistance $R_1, R_2, \ldots R_m$). This makes possible alignment of the CC at some stage of setup, the need for which can arise after its realization.

7. Using

$$E_{ck} = \frac{E_{vck}}{E_{vcm}}(E_{cm} - E'_d) + E'_d$$

which follows from (9.34) and (9.35), we calculate a voltage E_{ck}.

8. Using the expression $E_{c1} = E_{ck} - m(E_{ck} - E_{cm})$, we define the voltage E_{c1}.

9. We select a voltage E, proceeding from the condition $E > E_{ck}$ and from available possibilities.

10. We calculate magnitudes $a_1, a_2, \ldots a_m$, $(a_n = E/E_{vcn} - 1)$, $b_1, b_2, \ldots b_{m-1}$ $(b_n = E_{vcn}/E_{vcm})$, and c $(c = E_{vcm}/E_{vck})$.

11. Using $B = (E_{ck} - E'_d)/E_{vck} - 1$, from (9.35), we find the value of B.

12. Using (9.39), we find the values $\chi_1, \chi_2, \ldots \chi_{m-1}$.

13. We calculate $A = a_1(\chi_1, \chi_2, \ldots \chi_{m-1})$.

14. Using (9.40), we calculate l.

15. Using (9.37) and (9.32), we find values χ_m.

16. Having set the value of resistance R, we calculate resistances $R_0 = R$ and $R_{0m} = lR_0$.

17. We calculate magnitudes $R_1 = R_0/\chi_1$, $R_2 = R_0/\chi_2$ ... $R_m = R_0/\chi_m$ and find resistance $R_1 = R_1^* - R_0$, $R_{m-1} = R_m^* - R_0$, $R_m = R_m^* - R_{0m}$.

Having set the value R (step 16), we note that for greater R the values of resistance of all other resistors of the CC will be larger. Therefore, for greater R there will be larger input resistance to the CC as well as a higher voltage source E_c, and accordingly the power consumed by it will be less. There will be also less power consumed in this case from the source E. It is seen that for larger values of resistance in the CC, its band of operational frequencies is reduced because of the presence at its output of the varactor capacitance (for direct connection to the CC) or the input capacitance of the following stage. Thus, it is necessary to take into consideration possible requirements for quick variations of E_c.

In case of a large E_{vck}, the desired values of the voltage E and the input voltages E_{ck} obtained from CC calculation can become so large that deriving them for standard oscillators becomes inconvenient. For example, to obtain a desired value of E_{ck} may require an amplifier with a large linear dynamic range and accordingly a very large supply voltage not commonly used in modern electronic components (such as transistors, integrated circuits). In such a situation, it is convenient to repeat the CC calculation starting from new values of output voltage obtained by reducing E_{vc1}, ... E_{vck} by a factor K. The new calculated values $E_{vc\,add}$, and accordingly, E_{vc1}, E_{vc2}^*, ... E_{vcm}^* will appear reduced by K and the resulting value of the voltage E_{ck} for a suitable choice of K will be more easily realized. The deriving of required voltages on the oscillator varactor should in this case be realized by connecting an amplifier with gain K to the CC output and as before, reducing the voltage $E_{vc\,add}$ [e.g., application of a voltage $E_{vc\,add}$ to the second side of the varactor (Figure 9.7)]. The requirements on the voltage E, the transforming characteristic of the amplifier hooked up to CC output, and its supply voltage thus can be maintained within practical limits.

We will illustrate this with a specific example. In an actual oscillator, tuning from 730 MHz to 860 MHz was carried out by variation of the varactor control voltage between 3.0V and 36.0V. Calculated for a CC with four diodes, the values of voltages were found as: $E_{vc1} = 3.0$V, $E_{vc2} = 7.0$V, $E_{vc3} = 13.5$V, $E_{vc4} = 22.5$V, and $E_{vck} = 36.0$V.

We find from step 4 of the proposed method of calculation the following magnitudes: $M = (m-1)E_{vck} - mE_{vcm} = (4-1)36 - 4 \times 22.5 = 18$V.

From step 5 we find $E_{vc1}^* = 50.2$V, $E_{vc2}^* = 54.2$V, $E_{vc3}^* = 69.7$V, $E_{vc4}^* = 69.7$V, and $E_{vck}^* = 83.2$V.

We find the smallest value $E_{c4\,min} = 119.2\text{V} + E_d'$ and set it at $E_{c4} = 122$V.

Finally, from steps 7 and 8 we calculate extreme values of the voltage E_c, which is to be sent to the CC input: $E_{ck} = 145.6\text{V} + E_d'$ and $E_{c1} = 51.2\text{V} + E_d'$.

Thus, for supplying a voltage E^*_{vc} directly to the CC input, the voltage E must exceed 145.6V + E'_d and thus the amplifier output with a linear transforming characteristic should be not smaller than 145.6V + E'_d (on a reinforced voltage). An even larger supply voltage is necessary for generating that input voltage.

A reduction of the voltages E_{vcm} and E_{vck} by a factor of five ($K = 5$) will give the following results: $E^\circ_{vc1} = E_{vc1}/K = 0.6\text{V}$, $E^\circ_{vc2} = E_{vc2}/K = 1.4\text{V}$, $E^\circ_{vc3} = E_{vc3}/K = 2.7\text{V}$, $E^\circ_{vc4} = E_{vc4}/K = 4.5\text{V}$, $E^\circ_{vck} = E_{vck}/K = 7.2\text{V}$. Having repeated the calculation and now substituting in the formulas new values E°_{vcm} instead of E_{vcm} we find $E_{c4\,\min} = 23.6\text{V} + E'_d$. We accept $E_{c4} = 25\text{V} + E'_d$. Thus, we obtain: $E_{ck} = 29.9\text{V} + E'_d$, $E_{c1} = 10.8\text{V} + E'_d$.

So, in the second case the voltage E should exceed only 29.9V + E'_d and requirements on the amplifiers (or amplifier, as the deriving of CC input voltage in this case should not require the additional amplifier) appear much more reasonable. Apparently, the requirement for a linear transforming characteristic can be met with an output voltage 36V, and the supply voltage for the amplifier can be selected near 50V (convenient and equal to the supply voltage of amplifiers).

9.5 DECREASING THE NONLINEAR DISTORTION OF THE FM SIGNAL WITH A CORRECTING SIGNAL

The approach outlined in the previous paragraph for linearization of oscillation frequency with control voltage can be used as well for reduction of nonlinear distortions of the FM modulating signal. However, for small frequency deviations and high frequencies (typical for short-range radar), other methods may be better for this purpose. The first of these methods is use of a circuit with a diode compensator for nonlinear distortions, shown in Figure 9.8. In this circuit the compensation diode D_c is in its open state for any value of modulating voltage. Thus, for sinusoidal modulation, an alternating voltage with unequal amplitudes of half-waves will appear at resistance R_2 at the expense of nonlinearity of the volt-ampere characteristic of the diode. The same voltage will be applied to the varactor (a circuit

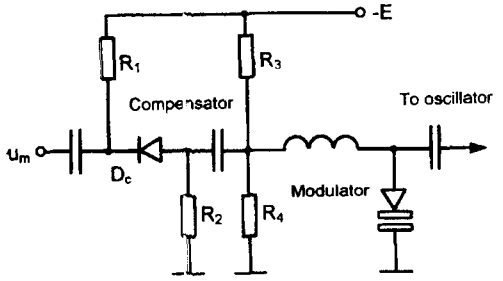

Figure 9.8 Circuit of modulator with diode compensator for nonlinear distortions.

composed of the capacitor and an inductor, between which is coupled resistor R_2 and the varactor, which should have rather low impedance at modulation frequencies). It is clear that given the polarity of the compensating diode and varactor shown in Figure 9.8, a positive half-wave of alternating varactor voltage corresponds to a reduction in varactor capacitance, and therefore an increase in oscillator frequency. Taking into consideration the form of dependence of the oscillator frequency on the varactor voltage (Figure 9.2), it becomes clear that feeding the modulating signal to the varactor according to the circuit of Figure 9.8 will allow reduction of nonlinear distortions in the FM signal. The best compensation of nonlinear distortions in the actual circuit is ensured with an appropriate selection of the compensating diode and resistors R_1 and R_2.

The nonlinearity of the transforming characteristic of transistors can also be used for reduction of nonlinear distortions of the modulating signal. Apparently, it is possible to offer different alternatives of transistor networks for compensation of modulating signal nonlinear distortions. But a necessary condition of operation of all such circuits is the forming of a sinusoidal modulating signal of alternating voltage with unequal amplitudes of half-waves and its application to the varactor so that the larger half-wave leads to a reduction of varactor capacitance.

Two circuits for compensation of nonlinear distortions are shown in Figure 9.9. In the circuit of Figure 9.9(a) the compensating transistor is included in the preamplifier for the modulating voltage. In the second circuit, Figure 9.9(b), it acts as an active component of an emitter follower, through which the modulating

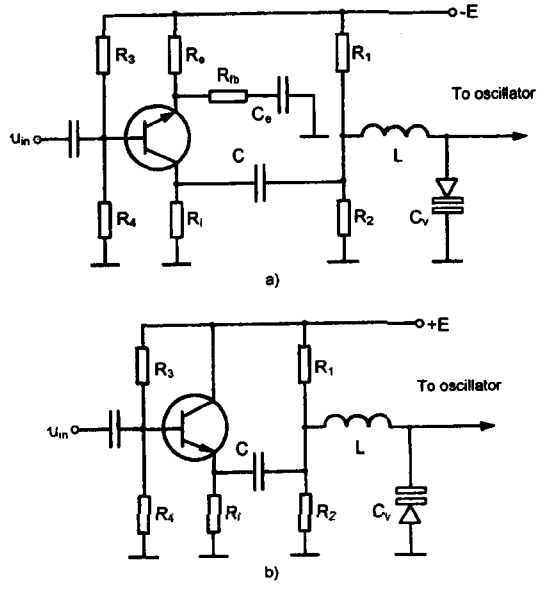

Figure 9.9 Circuit for diode-transistor modulator (a) with amplification and (b) without amplification of the modulating signal.

voltages are applied to the varactor of the FM oscillator. The alignments of both circuits to achieve minimum nonlinear distortions of the signal are conveniently realized by variation of the emitter current of the transistors, varying the resistors in emitter circuit.

Figure 9.10 shows two possibilities for compensation of nonlinear signal distortions by applying varactors as modulators in FM oscillators. The first uses the varactor (or varactors) in an intermediate oscillator circuit, the resonance frequency f_1 of which is lower than oscillator frequency f_0. The linearity of the control characteristic is thus regulated by variation of tuning of an intermediate oscillator circuit at frequency f_0. The other method of linearization is to derive the required FM oscillations by offsetting the FM oscillator frequency and use of a supplementary oscillator (local oscillator). Thus, at the output of the mixer the oscillation with the difference frequency is selected. The principle of compensation of nonlinear signal distortions in this case is quite obvious. The frequency f_0 of the FM oscillator is made much greater than the required frequency; for example, n times greater. Therefore, the maximum relative frequency deviation $\Delta f/f_1$ of these oscillations should be n times less than the required relative frequency deviation. This, as follows from (9.23) and (9.28), will lead to an n-fold decrease in nonlinear distortions as compared with conventional oscillators. This decrease will be maintained after conversion of generated FM oscillations by the mixer to the required band of frequencies (i.e., after decreasing the frequency f_0 by the factor n).

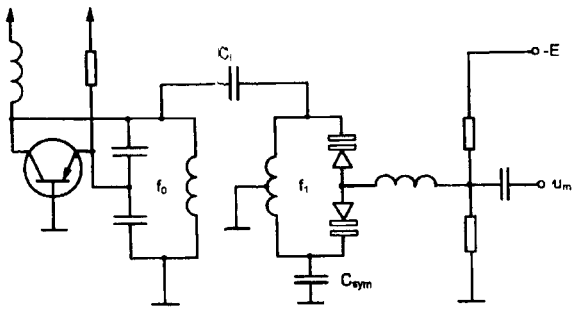

Figure 9.10 Modulator circuit with detuned intermediate oscillator circuit.

Chapter 10

Theory of the Single-Tuned Transistor Autodyne and Optimization of Its Modes

Transistor autodynes, as discussed above, are the combined microwave units which, along with generation of a radiating signal (including FM signals), perform the initial processing of a reflected signal accepted by the common antenna and carrying the information on target speed and distance. The basic circuit of the single-tuned autodyne, executed, for example, using Klapp's circuit with *external phasing capacity* C_4 and varicap C_3, is shown in Figure 10.1. High-frequency elements (C_1, C_2, C_3, L) form Klapp's circuit, and all active losses in the elements of selective system and in the antenna (losses on radiation) are expressed by an equivalent active conductivity G_{Σ}. By virtue of the fact that in the microwave

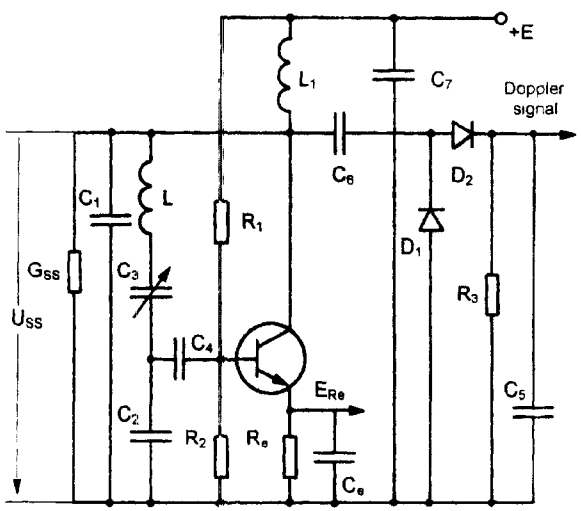

Figure 10.1 Basic circuit of Klapp's single-tuned transistor FM autodyne.

range a generator feedback circuit shifts the signal phase (i.e., the feedback factor $\dot{k}_{fb}$ is a complex value), the phasing capacitance C_4 is usually added to the circuit of the microwave oscillator, combining with transistor input conductivity the additional phase shift and improving the phasing conditions at the moment of self-excited oscillation and the stability of output frequency in the steady-state mode.

In the circuit there is an emitter automatic bias chain R_e, C_e that is used for mode stabilization of the direct current and from which the autodyne signal E_{Re} is output. Apart from this, the output of the autodyne signal as modulation of oscillation amplitude is formed by the peak detector D_1, D_2, R_3, and C_5.

10.1 ABBREVIATED DIFFERENTIAL EQUATIONS FOR THE SINGLE-TUNED TRANSISTOR AUTODYNE

We will express the abbreviated differential equations on the basis of the general abbreviated equation (7.3). For the case in which auxiliary control circuits are absent and a single emitter autobias chain is present, the equations become:

$$\begin{cases} \dot{Y}\left(U,U_{ss},\varphi,\phi,E\right)U_{ss}e^{j\varphi} = Y_{ss}(p+j\lambda)U_{ss}e^{j\varphi} + \dot{I}_{refl} \\ U_{ss}e^{j\varphi} = \dot{N}\left(U,E\right)U_{ss}e^{j\varphi} \\ E + \dfrac{J_e(U,E)}{Y_e(p)} = E_{init} \end{cases} \tag{10.1}$$

This system represents five valid equations, as the first two equations are complex. The equations define the behavior of five unknown functions of the problem: U, U_{ss}, φ, ϕ, and E. The equations are differential, and their order is determined, as in Chapter 6, by the order of the symbolic admittances Y_{ss} and Y_e.

Nonlinear complex functions $\dot{Y}$ and $\dot{N}$ are determined, according to [1, 2], by the parameters k and y_σ of the high-frequency circuit and by complex y-parameters of the transistor, averaged on the first harmonic of signals, which depend on the mode:

$$\dot{N}\left(E,U\right) = \dot{U}_{ss}/\dot{U} = -1/\dot{k}_{fb} = -\frac{y_{11}+y_\sigma}{y_{12}-ky_\sigma} \tag{10.2}$$

$$\dot{Y}(U,E) = \frac{\left(y_{21}-ky_\sigma\right)\left(y_{12}-ky_\sigma\right)}{y_{11}+y_\sigma} - y_{22} - k^2 y_\sigma \tag{10.3}$$

We can see that if it is necessary to take into account the nonlinearity (dependence on operating point) of all four averaged parameters of the transistor, y_{ij}, where $i,j = 1, 2$, then both functions N and Y appear dependent on the operating point, and the analysis becomes complicated. If the input conductivity y_{11} and the conductivity of the return reaction y_{12} may be neglected, then $N = -1/k = \text{const}$ and the analysis becomes simpler.

By virtue of sharp selectivity of the autodyne oscillatory system, the voltages u_{ss} and u are approximately sinusoidal:

$$u_{ss}(t) = \mathrm{Re}\left\{U_{ss}(t)\exp\left(j\left[\omega_{fr}t + \varphi(t)\right]\right)\right\} \tag{10.4}$$

$$u(t) = \mathrm{Re}\left\{U(t)\exp\left(j\left[\omega_{fr}t + \phi(t)\right]\right)\right\} \tag{10.5}$$

where ω_{fr} is the frequency of free oscillations of the autodyne.

The received reflected signal is delayed relative to that radiated by a time $\tau = 2r/c$, where r is the distance between the target and the autodyne and c is the speed of light:

$$i_{refl}(t) = \mathrm{Re}\left\{\kappa U_{ss}(t-\tau)\exp\left(j\left[\omega_{fr}(t-\tau) + \varphi(t-\tau)\right]\right)\right\} \tag{10.6}$$

Here, κ is the factor accounting for reduction of the microwave signal voltage between transmission and reception. For the definition of κ consider the ratio connecting the power P_{rec} of the received signal, the active component of the antenna input conductivity G_{ss}, and the amplitude I_{refl} of the received current: $I_{refl} = \sqrt{8P_{rec}G_{ss}}$. Taking into account that the power P_{rec} is proportional to radiated power P_{rad}:

$$P_{rec} = \chi P_{rad} = \chi U_{ss}^2 G_{ss}/2$$

we obtain: $I_{refl} = 2U_{ss}G_{ss}\sqrt{\chi}$; that is,

$$\kappa = 2G_{ss}\sqrt{\chi} \tag{10.7}$$

Factor χ in the case of a point target varies inversely as the fourth power of range r [3]:

$$\chi = \frac{\lambda_{fr}^2 G_{ant}^2 F_{ant}^4 \sigma}{64\pi^3 r^4} \tag{10.8}$$

and in the case of a distributed object inversely as the square of r:

$$\chi = \frac{\lambda_{fr}^2 G_{ant}^2 F_{ant}^4 N_0^2}{64\pi^2 r^2} \tag{10.9}$$

where λ_{fr} is the wavelength in free space, G_{ant} is antenna power gain, F_{ant} is a function of antenna orientation, σ the radar cross section, and $N_0 = 0.3$ to 1 is the factor accounting for losses in reflection from a distributed object.

We will now enter the frequency difference $\lambda = \omega_{fr} - \omega_0$ between the frequency of free fluctuations ω_{fr} and the carrier frequency ω_0, and we will copy expressions for complex amplitudes of signals (10.4) - (10.6) as follows:

$$\dot{U}_{ss} = U_{ss}(t)\exp\left(j\left[\lambda t + \varphi(t)\right]\right), \quad \dot{U} = U(t)\exp\left(j\left[\lambda t + \phi(t)\right]\right) \tag{10.10}$$

$$\dot{I}_{refl} = \kappa U_{ss}(t-\tau)\exp\left(j\left[\lambda t - \omega_{fr}\tau + \varphi(t-\tau)\right]\right) \tag{10.11}$$

Let us now substitute (10.10) and (10.11) in (10.1), and having applied the theorem of displacement for operational fractional-rational functions [4], we obtain:

$$U_{ss}e^{j\varphi} = N(E,U)Ue^{j\phi} \tag{10.12}$$

$$\begin{aligned} Y_{ss}(p+j\lambda)U_{ss}\exp(j\varphi) = {} & Y(E,U)U_{ss}\exp(j\varphi) \\ & + \kappa U_{ss}(t-\tau)\exp\left(j\left[-\omega_{fr}\tau + \varphi(t-\tau)\right]\right) \end{aligned} \tag{10.13}$$

If automatic bias is used in the autodyne then the system (10.12) - (10.13) for the high-frequency part of the circuit must be augmented by the equation for the bias chain, which is usually that for a single RC chain (as in Figure 10.1):

$$T_e \frac{dE}{dt} + E - J_e(E,U)R_e = E_{init} \tag{10.14}$$

where $T_e = R_e C_e$ is the time constant of the bias circuit, and J_e is a constant component of emitter current, depending on the operating point.

The system of the equations (10.12) - (10.14) forms the system of general abbreviated equations of an autodyne, describing with a consistent approach all the processes involved. Equation (10.13) includes the signal delay that predetermines the basic complexity of the autodyne systems analysis.

At the same time, estimation using (10.7) - (10.9) shows that in all practically important cases the parameter κ is small (i.e., $I_{refl} = \kappa U_{ss} \approx \delta U_{ss}$) and as a conse-

quence an inequality $\tau << T_{syn}$ applies, where T_{syn} is the time constant describing duration of the synchronization process influencing the generator of a signal with amplitude I_{refl}. This means that for a delay τ varying slowly as a function of time, $U_{ss}(t-\tau)$ and $\varphi(t-\tau)$ can be neglected (i.e., we may consider $U_{ss}(t-\tau) \approx U_{ss}(t)$ and $\varphi(t-\tau) \approx \varphi(t)$). In this case the subsequent analysis becomes simpler.

10.2 LINEARIZED DIFFERENTIAL EQUATIONS OF AUTODYNES FOR SMALL REFLECTED SIGNALS

In actual short-range radar systems the level of the reflected signal appears quite weak, in spite of the fact that the target range is rather small. If the received signal is entirely absent an autodyne mode is characterized uniquely by values U_{ss}^0, U^0, E^0, φ^0, ϕ^0 which are defined by the equations of the steady-state mode (i.e., by the abbreviated equations in which the operator p is zero). In the case of weak reflected signals (i.e., for $I_{refl} \approx \delta U_{ss} G_{ss}$) we can assume that the variations of the steady-state mode resulting from the reflected signal (i.e., the autodyne signal) are rather small:

$$U_{ss} = U_{ss}^0 + \xi,\ U = U^0 + \eta,\ E = E^0 + \varepsilon,\ \varphi = \varphi^0 + \alpha,\ \phi = \phi^0 + \varsigma$$

We will expand nonlinear functions $U_{ss}e^{j\varphi}$, $NUe^{j\phi}$, and $YU_{ss}e^{j\varphi}$ in Taylor's series for powers of the small deviations and reject terms above the first order of smallness (i.e., we will linearize the equations):

$$U_{ss}e^{j\varphi} = U_{ss}^0 e^{j\varphi^0} + e^{j\varphi^0}\left(\xi + jU_{ss}^0\alpha\right),\ \alpha = \varsigma$$

$$NU = N^0U^0 + \left(N^0 + U^0\frac{\partial N^0}{\partial U}\right)\eta + U^0\frac{\partial N^0}{\partial E}\varepsilon$$

$$YU_{ss}e^{j\varphi} = Y^0U_{ss}^0e^{j\varphi^0} + e^{j\varphi^0}\left\{Y^0\xi + U_{ss}^0\frac{\partial Y^0}{\partial U}\eta + U_{ss}^0\frac{\partial Y^0}{\partial E}\varepsilon + jY^0U_{ss}^0\alpha\right\}$$

Having substituted these decompositions in system (10.12) - (10.13) in view of the equations of the steady-state mode, we obtain a system of linearized high-frequency equations:

$$\begin{aligned}\left[Y_{ss}(p+j\lambda) - Y^0\right]\xi - U_{ss}^0\frac{\partial Y^0}{\partial U}\eta - U_{ss}^0\frac{\partial Y^0}{\partial E}\varepsilon \\ + jU_{ss}^0\left[Y_{ss}(p+j\lambda) - Y^0\right]\alpha = I_{refl}\exp\left(-j\omega_{fr}\tau\right)\end{aligned} \tag{10.15}$$

$$\xi - N^0(1+n^0)\eta - U^0\frac{\partial N^0}{\partial E}\varepsilon = 0 \tag{10.16}$$

where $n = (U/N)(\partial N/\partial U)$ is a function not equal to zero if the feedback factor of the generator $\dot{k}_{fb}$ depends on the mode. If autobias is used in the autodyne, one more linearized equation is added to (10.15) - (10.16):

$$\frac{\partial J_e^0}{\partial U}\eta + \left\{\frac{\partial J_e^0}{\partial E} + Y_e(p)\right\}\varepsilon = 0 \tag{10.17}$$

We will consider as a simplification the case in which the feedback factor does not depend on the operating point, and write for this case the linearized equations in matrix form:

$$\begin{Vmatrix} -U\dfrac{\partial G}{\partial U} & -U\dfrac{\partial G}{\partial E} & -\left[Y_{im}(p,\lambda)-B\right]U \\ -U\dfrac{\partial B}{\partial U} & -U\dfrac{\partial B}{\partial E} & \left[Y_{re}(p,\lambda)-G\right]U \\ \dfrac{\partial J_e}{\partial U} & \dfrac{\partial J_e}{\partial E}+Y_e(p) & 0 \end{Vmatrix} X \begin{Vmatrix} \eta \\ \varepsilon \\ \alpha \end{Vmatrix} = \begin{Vmatrix} I_{refl}k\cos\omega_{fr}\tau \\ -I_{refl}k\sin\omega_{fr}\tau \\ 0 \end{Vmatrix} \tag{10.18}$$

where $G = \mathrm{Re}Y$, $B = \mathrm{Im}Y$, $Y_{re}(p,\lambda) = \mathrm{Re}Y_{ss}(p + j\lambda)$, $Y_{im}(p,\lambda) = \mathrm{Im}(p + j\lambda)$, and all functions of the regime are calculated at a point of the autonomous mode (the index "0" of functions is omitted for simplicity).

Using (10.18) it is possible to analyze the influence of the received signal on the autodyne and to establish a relationship between the output signal, the input amplitude I_{refl}, and the autodyne parameters. For this purpose we must find under Kramer's formulas the operational expressions for increments of oscillation amplitude, bias voltage, and phase:

$$\eta = \Delta_\eta/\Delta,\ \varepsilon = \Delta_\varepsilon/\Delta,\ \alpha = \Delta_\alpha/\Delta \tag{10.19}$$

and then proceed to the originals (required functions of time). Here, Δ is a characteristic determinant of system (10.18), and Δ_i ($i = \eta, \alpha, \varepsilon$) is a determinant formed from Δ by replacement of the column made of factors at a required variation i, by the column consisting of functions images in the right part of (10.18). Acting in the specified way, it is easy to determine *transfer factors* of an autodyne for any variation η,α,ε resulting from I_{refl}.

10.3 EQUIVALENT CIRCUITS OF AUTODYNES FOR SMALL REFLECTED SIGNALS

We may use, as the useful signal in an autodyne, the deviation of any parameter (amplitude, frequency, etc.) from the stationary value, caused by external influence. In short-range radar autodyne systems this may be an increment of a high-frequency voltage appearing at the peak detector or an increment of current in any of the active element electrodes.

For designing a method of low-frequency signal processing and a choice of detection parameters we must know the form (or spectral structure) of the autodyne output voltage. For this purpose it is necessary to calculate increments η and α of the amplitude and the phase of the voltage $u(t)$. We will write the equations determining these increments, having excluded from (10.18) an increment ε:

$$\begin{aligned} Y_{11}(p)\eta + Y_{12}(p)U^0\alpha &= I_{refl}k\cos\omega_{fr}\tau \\ Y_{21}(p)\eta + Y_{22}(p)U^0\alpha &= -I_{refl}k\sin\omega_{fr}\tau \end{aligned} \tag{10.20}$$

where

$$\begin{aligned} Y_{11}(p) &= Y_{re}(p,\lambda) - G^0 - U^0\frac{\partial G^0}{\partial U}\left[1 - W(p)\right] \\ Y_{21}(p) &= Y_{im}(p,\lambda) - B^0 - U^0\frac{\partial B^0}{\partial U}\left[1 - W(p)\right] \\ Y_{12}(p) &= B^0 - Y_{im}(p,\lambda), \quad Y_{22}(p) = Y_{re}(p,\lambda) - G^0 \\ W(p) &= \frac{\dfrac{\partial J_e}{\partial U}}{\dfrac{\partial J_e}{\partial E} + Y_e(p)}\frac{1}{\cos\theta}, \quad \cos\theta = \frac{E' - E}{U} \end{aligned} \tag{10.21}$$

and where E' is the bias voltage at which the collector current of the transistor begins to flow (the cutoff voltage).

The system of equations (10.20) characterizes the linear two-port network shown in Figure 10.2, with parameters Y_{ij}, on which the external currents $I_{refl}k\cos\omega_{fr}\tau$ and $-I_{refl}k\sin\omega_{fr}\tau$ operate, causing the voltages η and $U^0\alpha$ at the input and output of the two-port network.

We will note that equality to zero of a determinant

$$Y_{11}(p)Y_{22}(p) - Y_{21}(p)Y_{12}(p) = 0 \tag{10.22}$$

determines the characteristic equation of the system describing local stability of single-frequency oscillations in the transistor generator (Chapter 6).

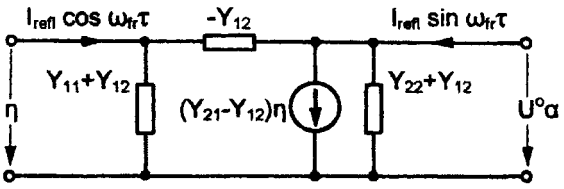

Figure 10.2 The equivalent small-signal circuit of single-tuned autodyne for calculation of increments.

We will consider some special cases of expressions (10.21). If the active element of the generator is inertialess at the carrier frequency (for example, an electronic lamp or a field-effect transistor at moderately high frequencies), then $B = 0$, $\partial B/\partial U = 0$, and factors Y_{ij} become:

$$Y_{11}(p) = Y_{re}(p,\lambda) - G^0 - U^0 \frac{\partial G^0}{\partial U}[1 - W(p)] \qquad (10.23)$$

$$Y_{12} = Y_{21} = -Y_{im}(p,\lambda), \quad Y_{22} = Y_{re}(p,\lambda) - G^0$$

For an autodyne using an inertialess two-pole active element with fixed autobias ($Y_e \to \infty$ and $W(p) = 0$), the expressions for Y_{ij} become even more simpler:

$$Y_{11} = Y_{re}(p,\lambda) - G^0 - U^0 \frac{\partial G^0}{\partial U} \qquad (10.24)$$

$$Y_{21} = -Y_{12} = Y_{im}(p,\lambda), \quad Y_{22} = Y_{re}(p,\lambda) - G^0$$

The application of linearized equivalent circuits significantly simplifies the analysis of specific autodynes with small reflected signals and allows us to establish some of their common properties.

10.4 THE FORM AND SPECTRUM OF THE OUTPUT SIGNAL OF A SINGLE-TUNED TRANSISTOR AUTODYNE

In this section we will obtain in an obvious form the expressions in time for amplitude and frequency of oscillations of the single-tuned transistor autodyne and analyze the spectrum of the output signal. We will assume a chain of autobias for the most common case as inertial, and neglect the internal autodyne noise.

For the single-tuned case $Y_{ss}(p) = G_{ss}(1 + pT)$, where G_{ss} is the active conductivity of the selective system at resonance, $T = 2/\omega_0\delta$ is the time constant of the loop, and δ is its attenuation. In the case considered, the abbreviated differential

equations of the autodyne are obtained from the general equations (10.12) - (10.14):

$$G_{ss}\left[1+(p+j\lambda)T\right]U_{ss}\exp(j\varphi)=\dot{Y}(U,E)U_{ss}\exp(j\varphi)+I_{refl}\exp\left(-j\omega_{fr}\tau+j\varphi\right) \tag{10.25}$$

$$U_{ss}\exp(j\phi)=\dot{N}(U,E)U\exp(j\phi) \tag{10.26}$$

$$T_e\frac{dE}{dt}=E_{init}-E-J_e(U,E)R_e \tag{10.27}$$

We will express these five equations in an obvious form:

$$\begin{aligned} &T\frac{dU_{ss}}{dt}+U_{ss}\left[1-\frac{G(U,E)}{G_{ss}}\right]=\frac{I_{refl}}{G_{ss}}\cos\omega_{fr}\tau, \quad U_{ss}=NU \\ &TU_{ss}\frac{d\varphi}{dt}+U_{ss}\left[\lambda T-\frac{B(,E)}{G_{ss}}\right]=-\frac{I_{refl}}{G_{ss}}\sin\omega_{fr}\tau \\ &T_e\frac{dE}{dt}=E_{init}-E-J_e(U,E)R_e, \quad \varphi=\varphi_N(U,E)+\phi \end{aligned} \tag{10.28}$$

where φ_N and N are the argument and magnitude of the complex function $\dot{N}$.

This system of equations (10.28) describes the autodyne mode of the single-tuned circuit with any amplitude of reflected signal. For small reflected signals, the linearized equations may be obtained from (10.18) or on the basis of the linearized equivalent circuits of Figure 10.2, in which for our case

$$\begin{aligned} &Y_{11}(p)=G_{ss}pT-U^0\frac{\partial G^0}{\partial U}\frac{1-\gamma+pT_e'}{1+pT_e'}; \quad Y_{12}=0 \\ &Y_{21}(p)=-U^0\frac{\partial B^0}{\partial U}\frac{1-\gamma+pT_e'}{1+pT_e'}; \quad Y_{22}(p)=pTG_{ss} \end{aligned} \tag{10.29}$$

where $T_e'=\dfrac{T_e}{1+R_e\left(\partial J_e/\partial E\right)}$ is the normalized autobias time constant, and

$\gamma=\dfrac{\partial G/\partial E}{\partial G/\partial U}\dfrac{\partial J_e/\partial U}{\partial J_e/\partial E+1/R_e}=\dfrac{1}{\cos\theta}\dfrac{\partial J_e/\partial U}{\partial J_e/\partial E+1/R_e}$ is the factor determined by the slope of the cutoff and bias diagrams at a stationary point (Section 6.3).

Let us assume further that the target moves towards the autodyne antenna at a constant speed v (i.e., $r = vt$ and $\tau = 2r/c = 2\,vt/c$). Then

$$\omega_{fr}\tau = \omega_{fr}(2vt/c) = \Omega_D t$$

where Ω_D is the Doppler frequency. Now from (10.29) we finally obtain the linearized equations:

$$T'T'_e\frac{d^2\eta}{dt^2} + \left(T' + T'_e\right)\frac{d\eta}{dt} + (1-\gamma)\eta = -\frac{I_{refl}k/G_{ss}}{\dfrac{U}{G_{ss}}\dfrac{\partial G}{\partial U}}\left(\cos\Omega_D t - \Omega_D T'_e \sin\Omega_D t\right) \quad (10.30)$$

$$T'T'_e U\frac{d^2\alpha}{dt^2} + T'U\frac{d\alpha}{dt} + \frac{\partial B/\partial U}{\partial G/\partial U}(1-\gamma)\eta + \frac{\partial B/\partial U}{\partial G/\partial U}T'_e\frac{d\eta}{dt} = -\frac{I_{refl}k/G_{ss}}{\dfrac{U}{G_{ss}}\dfrac{\partial G}{\partial U}}\left(\sin\Omega_D t + \Omega_D T'_e\cos\Omega_D t\right) \quad (10.31)$$

where $T' = T\Big/\left(\dfrac{U}{G_{ss}}\dfrac{\partial G}{\partial U}\right)$ is the normalized selective system time constant.

Now the final expression for the signal will be determined following the solution of (10.30) - (10.31) and will become:

$$u(t) = \left[U^0 + \eta(t)\right]\cos\left[\omega_{fr}t + \varphi^0 + \alpha(t)\right] \quad (10.32)$$

We shall consider (10.30) whose right-hand side has the form:

$$\frac{I_{refl}k/G_{ss}}{\dfrac{U}{G_{ss}}\dfrac{\partial G}{\partial U}}\sqrt{1+\left(\Omega_D T'_e\right)^2}\cos(\Omega_D t - \Psi_1)$$

where $\Psi_1 = \arctan(\Omega_D T'_e)$. Then the solution (10.30) will be written as the sum of a free and a forced component:

$$\eta(t) = C_1 e^{j\alpha_1 t} + C_2 e^{j\alpha_2 t} + \frac{(I_{refl}k/G_{22})\sqrt{1+(\Omega_D T'_e)^2}\cos(\Omega_D t + \pi - \Psi_1 - \Psi_2)}{(U/G_{ss})(\partial G/\partial U)\sqrt{\left[1-\gamma-\Omega_D^2 T'T'_e\right]^2 + \Omega_D^2(T'+T'_e)^2}}$$

where α_1 and α_2 are the roots of the characteristic equation describing local stability,

C_1 and C_2 are constants of integration, and

$$\Psi_2 = \arctan\frac{\Omega_D(T_e' + T')}{1-\gamma-\Omega_D^2 T' T_e'}.$$

If the independent mode is steady (only in this case it is meaningful to speak about an autodyne mode) free components of the solution decay, and the forced component represents the autodyne signal with a voltage:

$$\eta(t) = \bar{\eta}\cos(\Omega_D t + \Psi_\eta) \tag{10.33}$$

where the phase $\Psi_\eta = \pi - \Psi_1 - \Psi_2$, and the amplitude is determined from

$$\bar{\eta} = \frac{(I_{exi}k/G_{22})\sqrt{1+(\Omega_D T_e')^2}}{\frac{U}{G_{ss}}\frac{\partial G}{\partial U}\sqrt{\left(1-\gamma-\Omega_D{}^2 T' T_e'\right)^2 + \Omega_D^2\left(T'+T_e'\right)^2}} \tag{10.34}$$

We will now address the definition of the autodyne signal with phase $\alpha(t)$, for which we shall consider (10.31), the right-hand side of which, after finding of a signal $\eta(t)$, will become:

$$A\cos(\Omega_D t + \Psi_\eta) + B_1\sin(\Omega_D t + \Psi_\eta) + C\sin\Omega_D t + D\cos\Omega_D t \tag{10.35}$$

where

$$A = -\frac{\partial B/\partial U}{\partial G/\partial U}(1-\gamma)\bar{\eta},\quad B_1 = \frac{\partial B/\partial U}{\partial G/\partial U}\Omega_D T_e'\bar{\eta},\quad C = -\frac{I_{refl}k/G_{ss}}{\frac{U}{G_{ss}}\frac{\partial G}{\partial U}},\quad D = C\Omega_D T_e'$$

Now we will transform the right-hand side of (10.31) to the form

$$\frac{A_1}{\cos\beta}\cos(\Omega_D t - \beta),$$

where $A_1 = A\cos\Psi_\eta + B_1\sin\Psi_\eta + D$, $\tan\beta = A_2/A_1$, $A_2 = -A\sin\Psi_\eta + B_1\cos\Psi_\eta + C$.

Free components of the solution $\alpha(t)$ decay, and the forced component (the autodyne signal) becomes:

$$\alpha(t) = \bar{\alpha}\cos(\Omega_D t + \Psi_\alpha) \tag{10.36}$$

where $\Psi_\alpha = \pi - \beta - \Psi_1$, $\bar{\alpha} = \dfrac{A_1/U}{\Omega_D T' \sqrt{1+(\Omega_D T_e')^2}\cos\beta}$.

Now it is possible to find the expression for frequency of the autodyne oscillations:

$$\omega(t) = \omega_{fr} + \frac{(A_1/U)\cos(\Omega_D t + \Psi_\alpha)}{T'\sqrt{1+(\Omega_D T_e')^2}\cos\beta} \tag{10.37}$$

Thus, for an object moving with constant speed, the increments of amplitude and oscillation frequency (autodyne signals) are sinusoidal functions of time at the Doppler frequency. We will now determine the spectrum of the generated signal of the autodyne, having taken advantage of (10.33) and (10.36):

$$u(t) = U^0\left[1 + m_U\cos(\Omega_D t + \Psi_\eta)\right]\cos\left[\omega_{fr}t + \varphi^0 + \bar{\alpha}\cos(\Omega_D t + \Psi_\alpha)\right] \tag{10.38}$$

where $m_U = \bar{\eta}/U^0$ is the amplitude modulation index.

As we can see, the high-frequency signal of the autodyne represents an oscillation, simultaneously modulated in amplitude and phase, and the frequencies of modulation are equal to the Doppler frequency. For an exact definition of spectral components we expand $u(t)$ in a Fourier series and obtain, assuming for simplicity $\Psi_\eta = \varphi_0 = 0$, $\Psi_\alpha = \pi/2$:

$$u(t) = U^0\sum_{n=-\infty}^{\infty}\left\{J_n(\bar{\alpha})\left[1+(m_U/\bar{\alpha})n\right]\cos(\omega_{fr} + n\Omega_D)t\right\} \tag{10.39}$$

where $J_n(\bar{\alpha})$ is the Bessel function of the first kind.

From this expression we can see that the spectrum of the output signal of the autodyne is asymmetrical about the carrier frequency (i.e., amplitudes of the components with frequencies $\omega_{fr} + n\Omega_D$ and $\omega_{fr} - n\Omega_D$ are unequal).

If the maximal phase deviation $\bar{\alpha}$ is small, the decomposition into sine wave components (10.39) becomes simpler, as the Bessel functions of an order greater than unity are negligible. In this case the spectrum of the autodyne signal contains five components:

$$\begin{aligned} u(t)/U^0 = {} & J_0(\bar{\alpha})\cos\omega_{fr}t + \left[J_1(\bar{\alpha}) + m_U J_0(\bar{\alpha})/2\right]\cos(\omega_{fr} + \Omega_D)t \\ & + \left[m_U J_0(\bar{\alpha})/2 - J_1(\bar{\alpha})\right]\cos(\omega_{fr} - \Omega_D)t \\ & + \frac{m_U J_1(\bar{\alpha})}{2}\cos(\omega_{fr} + 2\Omega_D)t - \frac{m_U J_1(\bar{\alpha})}{2}\cos(\omega_{fr} - 2\Omega_D)t \end{aligned} \tag{10.40}$$

If both modulation indices are small (i.e., $(\bar{\alpha}) << 1$, $m_U << 1$), then it is possible to neglect the harmonics with frequencies $\omega_{fr} \pm 2\Omega_D$, and the three remaining components of the spectrum will become:

$$u(t)/U^0 = \cos\omega_{fr}t + \frac{m_U + \bar{\alpha}}{2}\cos(\omega_{fr} + \Omega_D)t + \frac{m_U - \bar{\alpha}}{2}\cos(\omega_{fr} - \Omega_D)t \qquad (10.41)$$

From (10.41) it follows that in this case the amplitudes of spectral sidebands differ from each other in amplitude by $\bar{\alpha}$.

So, we have established that the spectrum of the signal at the autodyne generator output contains sinusoidal components shifted by $n\Omega_D$, and is asymmetrical about the frequency of free oscillations. Asymmetry of the spectrum indicates the presence of amplitude and phase modulation simultaneously. Therefore, autodyne signal processing can be performed either by peak methods (as is usually done), or by phase.

We will now discuss what occurs in an autodyne with complex selective system and autobias circuits. In this case the order of the equations determining $\eta(t)$ and $\alpha(t)$ will be high, but for small reflected signals they will remain linear. Therefore, their solutions will again include decaying free components (in the steady-state mode) and forced components having the form (10.33) and (10.36), as in a single-tuned case. Differences will consist only in more difficult definitions of amplitudes and phases of increments. From here it follows that all conclusions concerning the structure of the output signal spectrum may be completely transferred to the case of the more complex oscillatory system.

10.5 FORM AND SPECTRUM OF THE HIGH-FREQUENCY SIGNAL FROM AN FM TRANSISTOR AUTODYNE

With frequency modulation of the carrier, the analysis of the output signal spectrum becomes significantly more complicated. In this case, an increment of amplitude $\eta(t)$ will contain not only the autodyne signal (10.33) with amplitude (10.34), but also a PAM signal determined for any law of modulation by (7.52). Thus, in the FM autodyne we have:

$$\eta(t) = \bar{\eta}\cos(\Omega_D t + \Psi_\eta) + \frac{1}{T}e^{-t/T'}\int e^{t/T'}\Phi(t)dt \qquad (10.42)$$

where $\bar{\eta} = \dfrac{(I_{refl}k/G_{22})\sqrt{1+(\Omega_D T_e')^2}}{\dfrac{U}{G_{ss}}\dfrac{\partial G}{\partial U}\sqrt{\left(1-\gamma-\Omega_D{}^2 T'T_e'\right)^2+\Omega_D{}^2\left(T'+T_e'\right)^2}}$ is the autodyne signal,

and the function $\Phi(t)$, reflecting the effect of the PAM signal, is defined differently for different laws of modulation (see Chapter 7).

We will address the analysis of the oscillation phase increment, which is calculated from (10.31). In this formula, in addition to an increment of phase α there also enters an increment of amplitude η that consists of an autodyne signal and a PAM signal. From (10.31) we can see that the PAM signal enters into the equation if high frequencies are considered (i.e., $\partial B/\partial U \neq 0$). From (10.31), we obtain for an inertialess autobias case (i.e., $T_e \approx 0$):

$$\begin{aligned}\alpha(t) &= -\frac{1}{T'U}\frac{\partial B/\partial U}{\partial G/\partial U}(1-\gamma)\int \eta(t)dt - \frac{1}{\Omega_D TU}\frac{I_{refl}k}{G_{ss}}\cos\Omega_D t \\ &= \frac{1}{T'U}\frac{\partial B/\partial U}{\partial G/\partial U}(1-\gamma)\int \bar{\eta}(t)\cos(\Omega_D t - \Psi_1)dt - \frac{1}{\Omega_D TU}\frac{I_{refl}k}{G_{ss}}\cos\Omega_D t \\ &\quad -\frac{1}{T'U}\frac{\partial B/\partial U}{\partial G/\partial U}(1-\gamma)\int\left[\frac{1}{T}e^{-t/T'}\int e^{t/T'}\Phi(t)dt\right]dt\end{aligned} \tag{10.43}$$

where $\Psi_2 = \arctan[\Omega_D T'/(1-\gamma)]$. Having integrated in (10.43) the autodyne increments:

$$\begin{aligned}\int \bar{\eta}(t)\cos(\Omega_D t + \pi - \Psi_1) &= \frac{T'}{T}\frac{I_{refl}k}{G_{ss}}\frac{1}{\sqrt{(1-\gamma)^2 + (\Omega_D T')^2}}\int \cos(\Omega_D t - \Psi_1)dt \\ &= \frac{T'}{\Omega_D T}\frac{I_{refl}k}{G_{ss}}\frac{1}{\sqrt{(1-\gamma)^2 + (\Omega_D T')^2}}\sin(\Omega_D t - \Psi_1)\end{aligned}$$

we obtain:

$$\begin{aligned}\alpha(t) &= \frac{1}{U}\frac{\partial B/\partial U}{\partial G/\partial U}(1-\gamma)\frac{1}{\Omega_D T}\frac{I_{refl}k}{G_{ss}}\frac{1}{\sqrt{(1-\gamma)^2 + (\Omega_D T')^2}}\sin(\Omega_D t - \Psi_1) \\ &\quad -\frac{1}{\Omega_D TU}\frac{I_{refl}k}{G_{ss}}\cos\Omega_D t - \frac{1}{T'U}\frac{\partial B/\partial U}{\partial G/\partial U}(1-\gamma)\int\left[\frac{1}{T}e^{-t/T'}\int e^{t/T'}\Phi(t)dt\right]dt\end{aligned} \tag{10.44}$$

It is obvious that the two first terms of the right-hand side of (10.44) are connected to the reflected signal and may be transformed to:

$$A_1 I_{refl}\cos(\Omega_D t - \Psi_1) + A_2 I_{refl}\cos\Omega_D t$$

where amplitudes A_1 and A_2 of the signal are connected to the autodyne circuit parameters and its mode. In the absence of a reflected signal ($I_{refl} = 0$) these terms vanish.

Let us now consider the last term in the right part, determining the conversion of the modulation signal to a phase increment. We note at once that for an inertialess transistor ($\partial B/\partial U = 0$), the last term vanishes. In the case of a sine wave modulation function, $\Phi(t)$ is defined by (7.51):

$$\Phi(t) = \frac{5}{2} U_0 \varepsilon T \frac{df}{dt} = \frac{5}{2} U_0 \varepsilon T \cos \Omega_m t$$

Now

$$\int e^{t/T'} \Phi(t) dt = \frac{5}{2} U_0 \varepsilon T \int e^{t/T'} \cos(\Omega_m t)\, dt = \frac{5}{2} U_0 \varepsilon \frac{T}{\Omega_m T'} e^{t/T'} \frac{\sin(\Omega_m t - \Psi_{\alpha 1})}{\sqrt{1 + (\Omega_m T')^2}}$$

Finally we have:

$$\begin{aligned} &\frac{1}{T'U} \frac{\partial B/\partial U}{\partial G/\partial U} (1-\gamma) \int \frac{1}{T} e^{-t/T'} \frac{5}{2} U_0 \varepsilon \frac{T}{\Omega_m T'} e^{t/T'} \frac{\sin(\Omega_m t - \Psi_{\alpha 1})}{\sqrt{1 + (\Omega_m T')^2}} dt \\ &= -\frac{\partial B/\partial U}{\partial G/\partial U} (1-\gamma) \frac{5}{2} \frac{1}{(\Omega_m T')^2} \frac{\varepsilon}{\sqrt{1 + (\Omega_m T')^2}} \cos(\Omega_m t - \Psi_{\alpha 1}) \end{aligned} \tag{10.45}$$

So the last term defines the modulation signal in a phase increment. Now we represent the autodyne output signal as:

$$\begin{aligned} u(t) = &\left\{ U_0 + \bar{\eta}_{ad} \cos(\Omega_D t + \Psi_{ad}) + \bar{\eta}_{PAM} \cos(\Omega_m t + \Psi_{PAM}) \right\} \\ &\times \cos \left\{ \begin{array}{l} \omega_{fr} \left(1 + \varepsilon \cos \Omega_m t\right) t + \varphi_0 + \bar{\alpha}_{ad} \cos(\Omega_D t + \Phi_{ad}) \\ \qquad + \alpha_{PAM} \cos\left(\bar{\Omega}_m t + \Phi_{PAM}\right) \end{array} \right\} \end{aligned} \tag{10.46}$$

where subscripts *ad* and *PAM* designate the amplitudes and phases of the autodyne signal and the signal of parasitic amplitude modulation.

We have established that even for a rather simple law of modulation of frequency (a pure sine wave), the spectrum of high-frequency output oscillations in the autodyne is very complex. We will not write here strict expressions for amplitudes of each spectral component (it is too unwieldy), but we will estimate a spectral structure directly from (7.54).

The spectrum contains the following components:

- Those with frequency ω_{fr} of free oscillations;
- Components of the FM signal with frequencies $\omega_{fr} \pm n\Omega_m$;
- Components of the autodyne signal with frequencies $\omega_{fr} \pm k\Omega_D$ near the carrier frequency;
- Components of autodyne signal with frequencies $\omega_{fr} \pm n\Omega_m \pm k\Omega_D$ near each component of the modulation frequency.

There are also components in the spectrum whose amplitudes are much less than these components that do not strongly influence the autodyne modes. The structure of the spectrum shows that processing of the autodyne signal can be carried out on any harmonic of the modulation frequency (most conveniently on the largest harmonic of the FM spectrum), around which it is possible to locate a signal at the Doppler frequency (autodyne signal) on which to carry out the final processing.

In the case where frequency modulation is carried out using a more complex law than the sine wave, the analysis becomes significantly complicated, but the results of the analysis of spectral structure are rather easy to predict. In the spectrum the components responsible for modulation vary, but around each of these components there are components shifted by the Doppler frequency.

10.6 TRANSFER FACTORS OF AN AUTODYNE ON A VOLTAGE AND A CURRENT AND MODE OPTIMIZATION

Theoretically, it is possible to use the change of any parameter describing the mode (amplitude, phase, bias voltage, direct currents of transistor electrodes, etc.) as the useful signal from the autodyne. In practice we more often select an autodyne amplitude signal from the peak detector, and also an increment of a constant component of the collector (emitter) current. In this section we establish the *autodyne sensitivity* for both these methods, and consider, first, in detail, the case of low frequencies for a particular transistor, and then briefly describe the results for the case of high frequencies.

First, however, it is necessary to note that it is not always possible to recommend as modes of operation those modes in which the sensitivity is high: it is necessary to carry out additional analysis of stability for these modes with various sorts of interfering influences, to reveal their potential powers, and also to determine whether it is possible to realize these modes practically.

10.6.1 Analysis for Low Frequencies for a Particular Transistor

Parameters of an autobias chain are usually selected so that with the required filter its time constant is small in comparison with the time constant of the loop ($T'_e << T'$). This is necessary for prevention of faltering generation (Chapter 6). Assuming $T'_e = 0$, we obtain from (10.34):

$$K_U = \frac{1}{\sqrt{(1-\gamma)^2\left(\frac{U}{G_{ss}}\frac{\partial G}{\partial U}\right)^2 + (\Omega_D T)^2}} \tag{10.47}$$

where $K_U = \dfrac{\bar{\eta}}{I_{refl}k/G_{ss}}$ is the *voltage transfer factor* of the autodyne.

For calculation of K_U let us assume, as earlier, a piecewise linear approximation of the transistor static characteristics. Then

$$G(U,E) = G(\cos\theta) = Sk\gamma_1(\theta),\ J_e(U,E) = S_e U\gamma_0(\theta) \tag{10.48}$$

where S and S_e are the slopes of the linearized characteristics of collector and emitter currents, and $\gamma_{0,1}(\theta)$ are decomposition factors of a cosine impulse of current that depend on the cutoff angle in the usual manner:

$$\gamma_0(\theta) = (\sin\theta - \theta\cos\theta)/\pi,\ \ \gamma_1(\theta) = (\theta - \sin\theta\cos\theta)/\pi \tag{10.49}$$

We will now determine the formulas for the derivatives that are included in the expression for function γ:

$$\begin{aligned}
\frac{\partial G}{\partial U} &= \frac{dG}{d\cos\theta}\frac{\partial\cos\theta}{\partial U} = -Sk\frac{d\gamma_1}{d\cos\theta}\frac{\cos\theta}{U} = \frac{Sk}{\pi U}\sin 2\theta \\
\frac{\partial G}{\partial E} &= \frac{dG}{d\cos\theta}\frac{\partial\cos\theta}{\partial E} = -Sk\frac{d\gamma_1}{d\cos\theta}\frac{1}{U} = \frac{2Sk}{\pi U}\sin\theta \\
\frac{\partial J_e}{\partial U} &= S_e\gamma_0(\theta) + S_e U\frac{d\gamma_0}{d\cos\theta}\frac{\partial\cos\theta}{\partial U} = \frac{S_e}{\pi}\sin\theta \\
\frac{\partial J_e}{\partial E} &= S_e U\frac{d\gamma_0}{d\cos\theta}\frac{\partial\cos\theta}{\partial E} = S_e\frac{\theta}{\pi}
\end{aligned} \tag{10.50}$$

Now we will find a connection between the function γ, included in (10.47), and the cutoff angle in an obvious form:

$$\gamma = \frac{1}{\cos\theta}\frac{b\left[\gamma_0 + (\theta\cos\theta)/\pi\right]}{1+b\theta/\pi} = \frac{(b\tan\theta)/\pi}{1+b\theta/\pi} \tag{10.51}$$

where $b = S_e R_e$ is the *autobias parameter*. Note that if we analyzed a case of combined emitter and base autobias, the formula for γ would be similar, but the magnitude of b would change to $b = S_e R_e + S_b R_b$. We calculate the normalized derivative, which is included in (10.47):

$$\frac{U}{G_{ss}}\frac{\partial G}{\partial U} = \frac{U}{G}\frac{\partial G}{\partial U} = \frac{\sin 2\theta}{\pi\gamma_1(\theta)} \tag{10.52}$$

Substituting now (10.51) and (10.52) in (10.47), we obtain the final expression for the voltage transfer factor of the autodyne:

$$K_U = \frac{1}{\sqrt{\left(\frac{b\gamma_0 - \cos\theta}{1 + b\theta/\pi}\right)^2 \left(\frac{2\sin\theta}{\pi\gamma_1}\right)^2 + (\Omega_D T)^2}} \tag{10.53}$$

As we can see, this formula is quite complex. However, analyzing it qualitatively, it is possible to draw a number of important conclusions.

We first consider the term $(2\sin\theta)/\pi\gamma_1$. For $\theta = \pi$ (at the point of self-excitation of the autodyne), $\gamma_1 = 1$ according to (10.49), and $\sin\theta = \sin\pi = 0$. Therefore, at point $\theta = \pi$ this term is zero (i.e., K_U has a maximum).

Let us consider the term $(b\gamma_0 - \cos\theta)/(1 + b\theta/\pi)$. If the autobias parameter is selected so that

$$b\gamma_0(\theta) - \cos\theta = 0 \tag{10.54}$$

then K_U again reaches the maximal value. We will call the value of the autobias parameter, appropriate to this maximum, "*optimum*" B_{opt}.

We note that the presence of a maximum of the voltage transfer factor of the autodyne at the point of initial oscillation excitation was found by I. L. Bershtein in 1946. The physical treatment of this fact is clear, as at the point of excitation any external influence results in a strong mode change.

We now consider the autodyne properties of the single-tuned generator in the case when the increment of the constant component of collector current of the transistor is observed. As this increment does not enter directly in the linearized equation (10.18), we will connect it with a variation of amplitude:

$$\Delta J(t) = \frac{dJ}{dU}\eta(t) = \bar{\Delta J}\cos(\Omega_D t + \Psi_J) \tag{10.55}$$

where $\Delta J(t)$ is the increment of collector direct current, and $\overline{\Delta J}$ and Ψ_J are its amplitude and phase. For piecewise linear approximation $J(U,E) = SU\gamma_0(\theta)$, from which we obtain:

$$\frac{dJ}{dU} = S\gamma_0 + SU\frac{d\gamma_0}{d\cos\theta}\frac{d\cos\theta}{dU} = S\gamma_0 - SU\frac{d\gamma_0}{d\cos\theta}\left(\frac{\cos\theta}{U} + \frac{1}{U}\frac{dE}{dU}\right)$$

Calculating the derivative dE/dU from (10.27), we find after transformations

$$K_J = \left(1 - \frac{\theta}{\pi\gamma_0}\frac{b\gamma_0 - \cos\theta}{1 + b\theta/\pi}\right)K_U \qquad (10.56)$$

where $K_J = \dfrac{\overline{\Delta J}/I_{refl}k}{\gamma_0/\gamma_1}$ is the *current transfer factor* of the autodyne.

Therefore, we have established that the voltage and current transfer factors of an autodyne are connected in a complex manner. Nevertheless, from (10.56) it is possible to draw a number of the important conclusions. At the point $\theta = \pi$, as follows from (10.54), the function K_U has a maximum equal to $1/(\Omega_D T)$. From (10.56) it follows that at this point $K_J = 0$. The second maximum of K_U is at the point $b = b_{opt} = (\cos\theta)/\gamma_0$. We can see that at this point K_J is also maximal, and therefore $K_J(\theta_{opt}) = K_U(\theta_{opt}) = 1/(\Omega_D T)$. Since it is possible to show that the term in parentheses in (10.56) is a monotonic function of $\cos\theta$, then K_J has no other extrema.

We note that the theoretically derived equality of voltage and current transfer factors of the autodyne at an optimum point does not provide a basis to judge equivalence of both methods of extraction of the useful signal. So the question of absolute size of the useful signal (in millivolts) that corresponds to the chosen method of forming the response is frequently important.

In Figure 10.3, the calculated family of diagrams of voltage transfer factor of an autodyne as a function cutoff angle is shown for different b, and in Figure 10.4 similar diagrams are shown for the current transfer factor. We can see that K_u has two zones of maximal values: at the point of oscillation excitation ($\cos\theta = -1$) and in the point appropriate to small cutoff angles ($\theta \le 90°$). The shape of the curves varies slightly with change of the Q-factor of the loop, natural frequency, or Doppler frequency. Dependence of K_J on the cutoff angle has a monotonic character, but the zone of the large values also is very narrow.

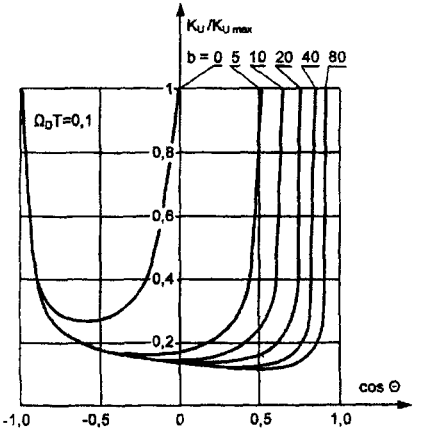

Figure 10.3 Dependence of autodyne voltage transfer factor on cutoff angle, for different values of the bias parameter.

10.6.2 The High-Frequency Case

Analysis of the autodyne mode for high frequencies for the transistor (i.e., for frequencies exceeding the boundary frequency of the transistor for slope f_S) becomes significantly more complicated. For calculations, it is possible here to take advantage of the *high-frequency piecewise-linear model* of the transistor and of analysis using an *equivalent high-frequency cutoff angle.*

The basic results of calculation of voltage and current transfer factors of the autodyne are shown for the case of high frequencies in Figures 10.5 and 10.6. As we see, the basic character of diagrams does not vary, a maximum K_U at $\theta = \pi$

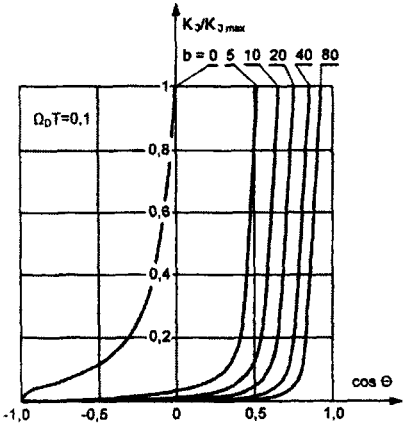

Figure 10.4 Dependence of autodyne current transfer factor on cutoff angle for different values of the bias parameter.

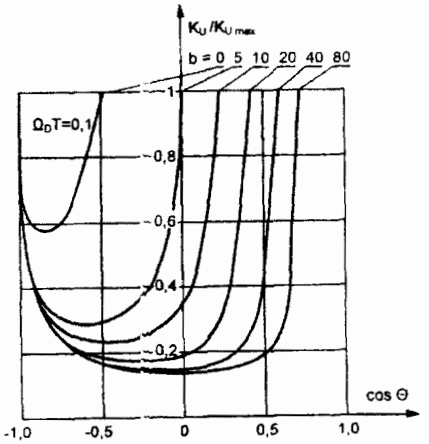

Figure 10.5 Dependence of autodyne voltage transfer factor on cutoff angle for different frequencies.

remains in place, and the second maximum is displaced by increased cutoff angles. The same situation is characteristic for current transfer factors.

10.6.3 Choice of Mode with High Autodyne Sensitivity

Consideration of mode choice for an autodyne for reception with high autodyne sensitivity is connected to the analysis of some specific phenomena, characteristic of transistor self-oscillatory systems at high frequencies and beyond the frame-

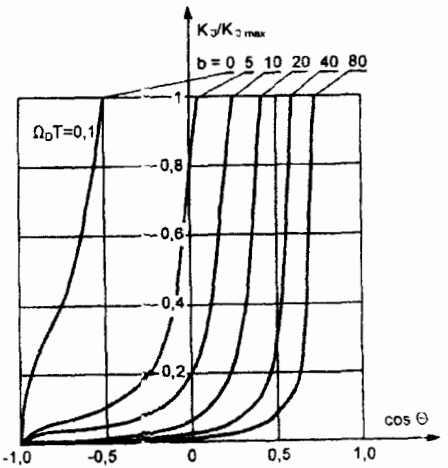

Figure 10.6 Dependence of autodyne current transfer factor on cutoff angle for different frequencies.

works of this book. We will therefore discuss only the results that are of practical importance.

It was shown above that the first zone of the maximum of voltage transfer factor corresponds to the point of self-excitation. However, it is impossible to recommend the mode $\theta = \pi$ for practical use under the following circumstances.

1. The amplitude of the reflected signal I_{refl} at the input to the autodyne is proportional to the amplitude of the radiated signal U_{ss}. The point of excitation corresponds to small amplitudes of oscillation, and therefore I_{refl} and the absolute value of the autodyne signal are also small, despite the large values of K_U.

2. Power efficiency of the mode $\theta = \pi$ is low, as there is a low operating ratio of collector voltage that results in a sharp decrease in the efficiency factor. This circumstance may be very significant, especially for onboard systems.

3. The mode close to the cutoff of oscillations is also unprofitable because it is unstable globally: oscillation in the autodyne may fail for insignificant variations of parameters (e.g., voltages of power supplies), and hence the radar may fail to function. The same circumstance may be important if it is necessary to deploy a large batch of devices without individual testing.

The mode of large oscillations at $b = b_{opt}$, which we have theoretically called the "optimum," corresponds to intersection of the cutoff curve of the generator with the asymptote of the bias curves, and is thus the point of crossing curves (the point of autodyne steady state) that exists only at infinity and cannot be achieved in practice. This asymptotical mode is certainly not realized in practice because of the proximity to the so-called *overstrained mode*. Detailed consideration shows that it is necessary to choose $b \approx 0.7b_{opt}$ and to operate in a *critical mode* (at the boundary between *understressed* and *overstrained* modes). This mode (as opposed to the mode at the point of oscillation excitation) is favorable in every respect: it is stable globally, easily realized, and the output power and efficiency factor are large.

References

[1] Bogachev, V. M., V. G. Lysenko, and S. M. Smolskiy, *Transistor Generators and Autodynes* (in Russian), Moscow: MPEI, 1993.

[2] Bogachev, V. M., V. G. Lysenko, and S. M. Smolskiy, *Transistor Autodynes*, Manual for the course "Sets of Generation and Control of Radio Signals," Moscow: MPEI, 1984.

[3] Kogan, I. M., *Theoretical Base of Short-Range Radar Tracking* (in Russian), Moscow: Sovetskoje Radio, 1978.

[4] Angot, A., *Mathematics for Electrical and Radio Engineers*, Moscow: Nauka, 1968.

Chapter 11

Autodyne Modes of Transistor Oscillators with Strong Interference

In Chapter 10 it was shown that the delayed reflected signal in an autodyne causes a complex periodic mode in which the increments of oscillation amplitude and phase, and other resulting increments (e.g., the direct emitter current), are quasi-sinusoidal functions of time, varying with the Doppler frequency. The choice of an autodyne mode for operation in a short-range radar is chosen to achieve high autodyne sensitivity (i.e., a strong response to a target moving in the radar antenna beam). The necessary sensitivity is often not too high to preclude use of simple circuits. However, in some cases autodynes must have properties that can be extremely difficult to achieve without certain complications or improvement of the circuit structure.

So, for example, in systems where autodynes are used over long periods (in steady-state moving target detectors, security devices, instruments for measuring of substance parameters, etc.) there arise major issues of maintaining high frequency stability of the signal. We note that in modern security systems the requirements of electromagnetic compatibility in certain regions of the frequency range often preclude use of autodyne variants having low frequency stability. In onboard short-range radar the opposite situation applies: often, because of the short duration of the autodyne operation a high frequency stability is not required, but the basic problem is reliability and speed of range measurement. In such systems, the most important issue is autodyne noise immunity from various interference types, principally synchronous and repeater jammers.

Stabilization of microwave autodyne frequency in the usual ways is not always possible because of specifics of the application. The problem may be resolved to an extent by reliance on the phenomenon of external synchronization of oscillations, introducing a need for theoretical analysis of autodyne properties of synchronized microwave generators. The same problem also arises in a number of practical cases, for example, when a powerful jamming signal whose amplitude and frequency corresponds to the band of synchronization is incident on the autodyne system, causing frequency locking to the jammer or the transfer of the auto-

dyne to a mode of quasi-sinusoidal beating. Here the synchronized jamming is sufficiently harmful that it is necessary to reduce its effects.

We must add that an erroneous opinion is held by some radar experts that the radar will fail when its autodyne is locked in frequency or transferred by jamming to a beating mode. This is actually far from being so. In this chapter the theoretical consideration of autodyne modes in the presence of an active synchronizing jammer will be carried out. The analysis is based on results of published works on the synchronization theory of self-oscillatory systems, where a certain class of circuits for synchronized transistor oscillators is investigated in detail. Such analyses are aimed at development and substantiation of concrete recommendations for design of autodynes maintaining their required properties in the mode of frequency synchronization by a powerful jammer.

The material in this chapter is developed in the following sequence: we derive again the abbreviated differential equations of the system and then briefly describe the steady-state synchronous modes, their stability, definition of the synchronization band, and the beating mode in the circuit without autodyne influences. After that, the autodyne properties in the presence of a jammer are investigated, the bifurcation of the steady-state variations in the system are considered (i.e., the transitions from behavior or variations of one type to behavior of other type), and concrete recommendations for practical use of the synchronized autodynes are developed.

11.1 THE COMMON PROPERTIES OF AUTODYNE MODES OF THE SINGLE-TUNED SYNCHRONIZED OSCILLATOR

11.1.1 Abbreviated Equations for the Synchronized Oscillator

Now let us consider again the generalized circuit of the transistor oscillator with an ideal transformer (Figure 11.1), similar to that considered in Chapters 6 and 7. We will consider that two signals – the synchronizing jammer frequency and the reflected target echoes (the useful signal) – influence the oscillator, and these are

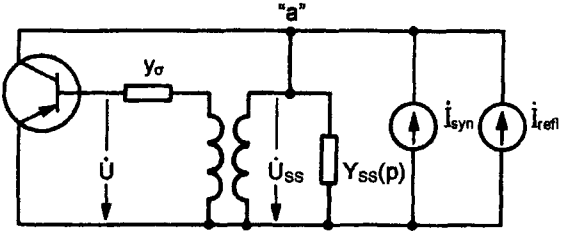

Figure 11.1 The circuit of the transistor oscillator with the ideal transformer, under the influence of a reflected signal I_{refl} and a synchronizing jammer signal I_{syn}.

represented by current sources with complex amplitudes $\dot{I}_{syn}$ (with frequency ω_{syn}) and $\dot{I}_{refl} = I_{refl}\exp\left[j(\varphi - \Omega_D t)\right]$, respectively, where, as before, φ is the phase of the high-frequency voltage on the oscillatory system $u_{ss}(t)$, and Ω_D is the Doppler frequency.

For simplicity we will characterize the transistor by a high-frequency parameter $\dot{Y}_{21}$, proportional to the complex nonlinear conductivity $\dot{Y}(U)$, which for a bipolar active element appears as:

$$\dot{Y}(U) = \dot{k}_{fb}\,\dot{S}_1(U) \tag{11.1}$$

where $\dot{k}_{fb} = \dot{U}/\dot{U}_{ss} = k$ is the complex feedback factor of the generator, which in the case of an active element represented by a two-pole is equal to the transformation factor k,

$\dot{S}_1(U) = \dot{Y}_{21}$ is the complex slope averaged over the first harmonic, and

U is the amplitude of the transistor base voltage whose complex amplitude is $\dot{U} = Ue^{j\vartheta}$.

On the basis of the approach developed in Chapter 7, based on equating the currents flowing into element "a" of the circuit in Figure 11.1, we obtain the symbolic abbreviated equation of the system as:

$$Y_{ss}(p + j\lambda)\dot{U}_{ss} = \dot{Y}(U)\dot{U}_{ss} + \dot{I}_{syn} + \dot{I}_{refl} \tag{11.2}$$

Here, Y_{ss} is the symbolic conductivity of a circuit abbreviated with respect to the carrier frequency ω_0, p is the differential operator for slowly varying functions of time $U(t)$ and $\varphi(t)$, and $\lambda = \omega_{syn} - \omega_0$ is the frequency difference between synchronized and reference signals. Dividing (11.2) as usual into its real and imaginary parts, we obtain the system of equations for the problem in an obvious form:

$$T\frac{dU}{dt} + U\left[1 - \frac{G(U)}{G_{ss}}\right] = \frac{k}{G_{ss}}\left(I_{syn}\cos\varphi + I_{refl}\cos\Omega_D t\right) \tag{11.3}$$

$$TU\frac{d\varphi}{dt} + U\left[\lambda T - \frac{B(U)}{G_{ss}}\right] = -\frac{k}{G_{ss}}\left(I_{syn}\sin\varphi + I_{refl}\sin\Omega_D t\right) \tag{11.4}$$

where T and G_{ss} are, as previously, the time constant and resonant circuit conductivity, $G(u) = \mathrm{Re}\,Y(U)$ and $B(U) = \mathrm{Im}\,Y(U)$. From system (11.3) - (11.4) there

follows, for $I_{syn} = 0$, the equations of the usual autodyne (discussed in Chapter 10), and for $I_{refl} = 0$ the equations for the synchronized oscillator investigated in our previously published works [1, 2].

A distinctive feature of (11.3) - (11.4) in comparison with the equations for the usual autodyne is that their right-hand terms are functions of a synchronizing signal, which in powerful jamming is not small. Therefore these equations cannot be analyzed using the previous approach: it is impossible to linearize them around a steady-state *independent* mode as is commonly used in autodyne analysis, as it is now impossible, even for a small target signal, to limit consideration to a small right-hand term, especially with a large synchronizing signal. In a real situation this jamming synchrosignal amplitude I_{syn} may be quite significant, especially if synchronization is carried out by a powerful active jammer. Therefore, we will no longer impose any restrictions on the synchrosignal amplitude.

The reflected signal I_{refl} is usually assumed to be small, as is typical for short-range systems. We will assume that the synchronizing signal may result in large deviations of the steady-state mode from independent, but, nevertheless, because I_{refl} is small it is possible to linearize the equations (11.3) - (11.4), but now around a steady-state *synchronous* mode. It is then possible to determine in the usual manner the transfer factors of the linearized system and to study more in detail the features of synchronized oscillator behavior for small influences of a Doppler frequency signal.

11.1.2 Abbreviated Equations in Normalized Parameters

Now we will describe, following our previous works [1, 3], the basic properties of transistor oscillator synchronous modes. For this purpose we should accept a model of nonlinearity. We will use further, following [3], a linear approximation of functions $G(U)$ and $B(U)$ around a steady-state independent point U_0:

$$G(U) = G(U_0) + \frac{dG^0}{dU}(U - U_0),\ B(U) = B(U_0) + \frac{dB^0}{dU}(U - U_0) \qquad (11.5)$$

Let us note that such a linear approximation does not correspond at all to the initial linear model of nonlinearity: for such an approach it is not the *static* characteristic but rather a *complex electronic conductivity* $Y(U) = G(U) = jB(U)$ that is approximated by the linear model (11.5), and this model of conductivity corresponds to a parabolic approximation of an *oscillatory* (instead of *static*) characteristic $\dot{I}_1(U) = \dot{Y}(U)\dot{U}$. This is illustrated in Figure 11.2 where real and approximated dependence of electronic conductivity on amplitude are shown, as well as the appropriate oscillatory characteristic.

It is possible to give one more example for acceptance of the model represented by (11.5). Frequently the model of an inertial active element is based on introduction of a so-called pure delay τ_{del}. In other words, it is considered that in

the generator feedback circuit (or inside the active element) there is a dispersion-free delay line with transfer factor $\exp(-p\tau_{del})$, and therefore the output current $i(t)$ lags behind the input voltage $u(t)$ by the phase $\varphi_{del} = \omega_{fr}\tau_{del}$. In this case an identical approximation of the real and imaginary parts of electronic conductivity of an active element is justified:

$$\dot{I}(U) = I(U)\exp\left(j\omega\tau_{del}\right) = I(U)\left(\cos\omega\tau_{del} + j\sin\omega\tau_{del}\right) \text{ and}$$

$$G(U) = \left|\dot{Y}(U)\right|\cos\omega\tau_{del},\ B(U) = \left|\dot{Y}(U)\right|\sin\omega\tau_{del}$$

Now the system of equations (11.3) - (11.4) can be rewritten in the normalized parameters as:

$$\frac{da}{d\tau} + a(a-1) = F\cos\varphi + \Phi\cos\bar{\Omega}_D t \tag{11.6}$$

$$a\frac{d\varphi}{d\tau} + a\left[\xi + (a-1)\tan\alpha\right] = -F\sin\varphi - \Phi\sin\bar{\Omega}_D t \tag{11.7}$$

Here the following parameters are used:

$a = U/U_0$ is the normalized amplitude of the synchronous fluctuations,

$\xi = \lambda T/g$ is the normalized frequency difference of the synchrosignal,

$\bar{\Omega}_D = \Omega_D T/g$ is the normalized Doppler frequency,

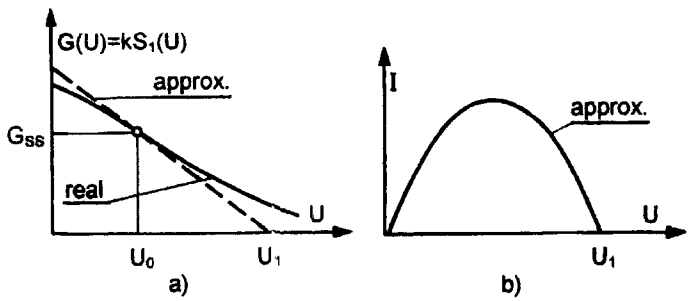

Figure 11.2 (a) Real and (b) approximated functions of electronic conductivity on amplitude and the oscillatory characteristic appropriate to approximation.

$g = -\frac{U_0}{G_{ss}}\frac{\partial G_0}{\partial U}$ is the normalized derivative,

$F = \frac{kI_{syn}}{G_{ss}U_0 g}$ is the normalized synchrosignal amplitude,

$\Phi = \frac{kI_{refl}}{G_{ss}U_0 g}$ is the normalized amplitude of the reflected signal,

$\tau = gt/T$ is dimensionless time, and

$\tan\alpha = \frac{\partial B_0/\partial U}{\partial G_0/\partial U}$ is the nonisochronism parameter in the independent mode of the oscillator.

The sense of the parameters used here is discussed in detail in [3], so we will note only that all regime functions included in these parameters are calculated at the steady-state independent point (i.e., for $I_{syn} = I_{refl} = 0$). We will consider in more detail a sense of the entered parameter α.

For a case of a pure delay we have:

$$\tan\alpha = \frac{\partial B/\partial U}{\partial G/\partial U} = -\frac{(\partial|Y|/\partial U)\sin(\omega\tau_{del})}{(\partial|Y|/\partial U)\cos(\omega\tau_{del})} = -\tan(\omega\tau_{del})$$

For the independent generator with an inertial two-pole $G(U_0) = G_{ss}$, and $B(U_0) = (\omega_{fr} - \omega_0)TG_{ss}$. From this it follows that:

$$\omega_{fr} = \omega_0 + 0.5\delta\omega_0\frac{B(U_0)}{G(U_0)} = 0.5\delta\omega_0\tan\alpha$$

Thus, in case of a pure delay a parameter $\tan\alpha$ defines the frequency deviation of free oscillations from the natural frequency of the selective system ω_0 (i.e., the *isochronism* of the generator).

In modern inertial active elements the character of dependence $G(U)$ and $B(U)$ may be the diversified, and for them the model with a pure delay is not often used. However, near the steady-state point the functions $G(U)$ and $B(U)$ are usually smooth, and it is possible to use the linear approximation (11.5) for them. Thus, the parameters $B(U_0)/G(U_0)$ and $\tan\alpha = (\partial B/\partial U)/(\partial G/\partial U)$ may not coincide, generally speaking. If the complex slope Y contains a conductivity B = const, independent of amplitude, then the capacity or inductance appropriate to it can be attributed to a circuit so as to reduce the problem to an inertialess active element. If B depends on U (e.g., due to a pure delay or an inertial process in the active

element), $\alpha \neq 0$ and the generator is anisochronous. Therefore, α in a common case is also named as the generator anisochronism parameter.

In the absence of a reflected signal, $\Phi = 0$ and the system of the equations (11.6) - (11.7) corresponds to the abbreviated equations of the synchronized generator using the normalized amplitude a and phase φ of the oscillations:

$$\frac{da}{d\tau} - a(a-1) = F\cos\varphi \tag{11.8}$$

$$a\frac{d\varphi}{d\tau} + a\left[\xi + (a-1)\tan\alpha\right] = -F\sin\varphi \tag{11.9}$$

This system of equations is investigated in detail in [1] by the phase plane method.

11.1.3 Steady-State Synchronous Modes

Now we will describe, following our previous works [1], the equations for the steady-state synchronous mode obtained from (11.8) - (11.9) with time derivatives equal to zero:

$$a(a-1) = F\cos\varphi \tag{11.10}$$

$$a\left[\xi + (a-1)\tan\alpha\right] = -F\sin\varphi \tag{11.11}$$

These equations define a family of so-called amplitude-frequency characteristics (AFCs) $a(\xi)$:

$$a^2(a-1)^2 + a^2\left[\xi + (a-1)\tan\alpha\right]^2 = F^2 \tag{11.12}$$

and phase-frequency characteristics (PFCs) $\varphi(\xi)$:

$$\xi^2 - \xi(\tan\alpha - \tan\varphi) - F\frac{\tan\alpha + \tan\varphi}{\sqrt{1+\tan^2\varphi}} = 0. \tag{11.13}$$

Local stability of steady-state synchronous modes is determined by the characteristic equation:

$$T^2p^2 + Tb_1p + b_2 = 0 \tag{11.14}$$

Stability is defined by two borders: $b_1 = 0$ (Border M) and $b_2 = 0$ (Border Q), which are set on AFC plane by the equations:

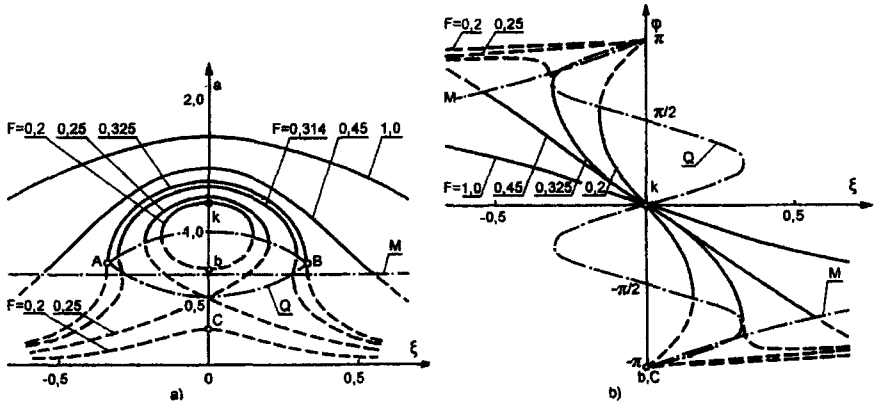

Figure 11.3 Amplitude-frequency and phase-frequency characteristics of the locked isochronous oscillator.

$$\text{Border } M - \quad 3a - 2 = 0$$

$$\text{Border } Q - \quad \xi^2 + \xi(3a-2)\tan\alpha + (a-1)(2a-1)(1+\tan^2\alpha) = 0$$

The structures of the AFCs and the PFCs are shown in Figure 11.3 for $\alpha = 0$ (the isochronous generator) and they correspond closely to known characteristics. In the same figure are shown two borders of stability for the synchronous mode (M and Q), a horizontal straight line and the stability ellipse constructed from the characteristic equation of the problem.

We can see that in the isochronous case for low amplitude synchronous jammers ($F < 0.25$), the AFCs represent closed ellipses, having vertical tangents at points of crossing with the border of stability Q (i.e., at points where stability of the synchronous mode is lost at border Q). In general, any crossings of AFCs and PFCs with border Q are accompanied by vertical tangents. For $F > 0.353$ the AFC becomes open-loop, and stability is defined by border M.

The PFC for small inputs is similar to the arcsine function and stability is lost at border Q, where the PFC has vertical tangents. For $F > 0.325$ the stability in the PFC is determined by border M.

In the anisochronous case ($\alpha \neq 0$) the AFCs and PFCs are curved (Figure 11.4), but, as before, for small F stability is determined by border Q, and at large stability by border M.

Figure 11.5 shows the dependence of the generator synchronization band on the amplitude of the synchronous jamming signal. These diagrams are constructed using the joint numerical solution of AFC and PFC equations and borders of stability. On these curves it is possible to find a band of frequencies in which the jamming results in autodyne synchronization at the given amplitude F of the

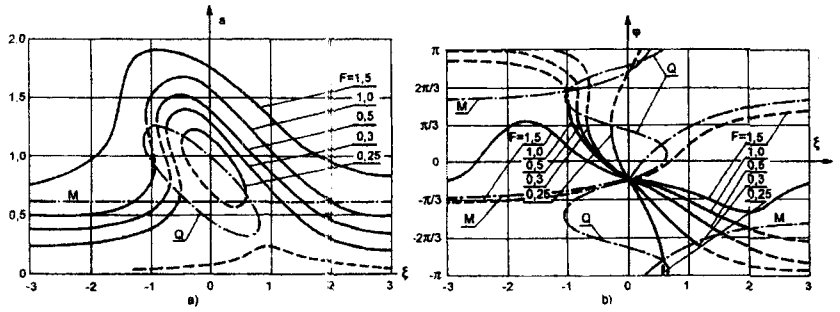

Figure 11.4 Amplitude-frequency and phase-frequency characteristics of the locked anisochronous oscillator.

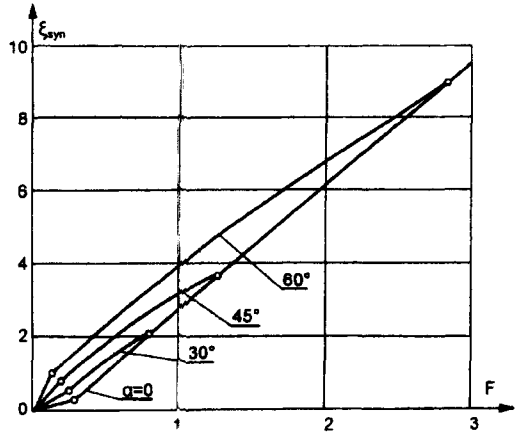

Figure 11.5 Dependence of synchronization band on amplitude of synchronous jammer signal.

jamming. Earlier this zone of synchronism was considered a failure zone of radar operation, but below it is shown that this is not so.

11.1.4 Transients at Synchronism

To understand the processes in the synchronism mode, as distinguished from the independent case (Chapter 6), we will address the analysis of phase portraits of the system (10.10) - (10.11). The equation of phase trajectories is derived from (11.10) - (11.11) by exclusion of time:

$$\frac{da}{d\varphi} = \frac{a\left[F\cos\varphi - a(a-1)\right]}{-F\sin\varphi - a\xi - a(a-1)\tan\alpha} \tag{11.15}$$

The space of conditions (phase space) represents a cylindrical surface (φ,a), which is called a phase plane.

For construction of a phase portrait - families of trajectories $a(\varphi)$ from (11.15) for given parameters F, ξ, of the system - it is necessary to obtain data on character and arrangement of so-called special trajectories: special points (conditions of balance or steady-state modes), limiting cycles, movement on which corresponds to a periodic mode (beating mode), and separatrices that divide areas corresponding to specific trajectories. Further, it is necessary to discover how the qualitative structure of the phase portrait varies for changes of system parameters, (i.e., to construct the so-called bifurcation diagrams) and to determine the features of all bifurcations: transitions from one structure of phase portraits to another. We will not do this here in detail, but discuss only the important results for later use.

For zero frequency difference (in a mode of full synchronism $\xi = 0$) there are three special points k, b, c on the phase portrait (Figure 11.6) which are, respectively, a knot, a saddle, and an unstable focus. The isoclinal lines of vertical (ILVT) and horizontal (ILHT) tangents are shown in Figure 11.6. We see that the attraction area for a steady synchronous mode at a point k is the entire phase plane. For increasing frequency difference ξ the steady knot k and the saddle b approach and finally merge on the border of stability Q, forming a special point of the *second order*: a *saddle-knot*. From the merged saddle separatrices the steady limiting cycle is formed, on which movement around the phase cylinder corresponds to a quasi-periodic beating mode. The appropriate phase portrait is shown in Figure 11.7, from which we see that the limiting cycle is globally steady (i.e., its area of attraction is the entire phase plane). If a transition from the phase portrait of Figure 11.6 is carried out by increasing jamming amplitude then the special points b and c approach each other and soon merge and disappear, leaving only the point of a synchronous generator mode locked in frequency to the jammer. If the strong jammer frequency difference is increased, the lock is broken at border M (Figure 11.4) where a steady limiting cycle of another type is formed on the phase portrait (Figure 11.8), enclosing an unstable special point, and the character of the beating

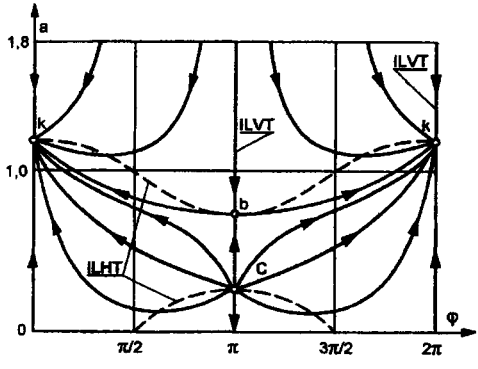

Figure 11.6 The phase portrait of the generator in a full synchronism mode.

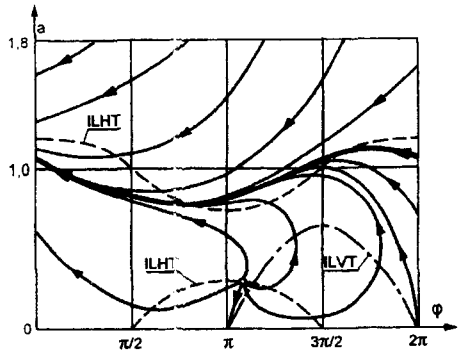

Figure 11.7 The phase portrait of the generator in a beating mode at a small synchronous jammer signal amplitude.

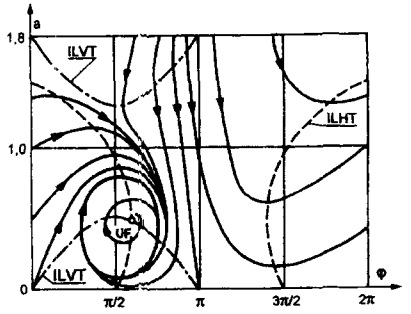

Figure 11. 8 The phase portrait of the generator in a beating mode with strong interference.

mode will thus be changed. Similarly, it is possible to inspect changes of phase portraits for all possible combinations of parameters.

The important question for us is whether the autodyne will have time during the target encounter to transition to the mode of locking to a synchronous jammer. For the answer to this question we must calculate the transition time of synchronous oscillation termination, and this can be done by numerical analysis of (11.8) - (11.9) for various combinations of parameters. Calculations have shown that the *amplitude locking time* (T_{tr}^{a}) and *phase locking time* (T_{tr}^{φ}) depend on the regeneration factor Sk/G_{ss} of the generator, as shown in Figure 11.9 for different values of circuit Q-factor and for F = 0 4, ξ = 0.2. For small jamming (but within the locking bandwidth) the amplitude of the synchronous oscillations is locked much faster than the phase. For example, with an initial phase of 45° the amplitude is locked in 110 periods of oscillation and the phase in 420 periods.

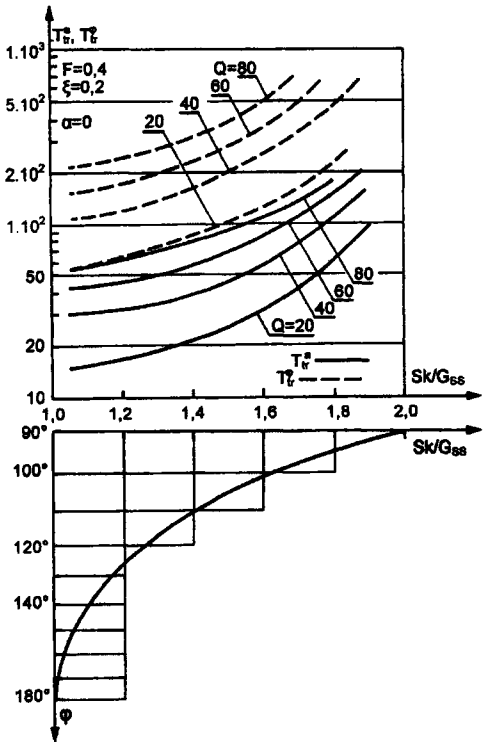

Figure 11.9 Time of autodyne locking by a jammer for different regeneration factors and Q-factors.

11.1.5 Bifurcational Diagrams of a Transistor Autodyne

To understand how locking to an active jammer occurs in the autodyne mode, we study bifurcational diagrams. The analysis shows that in the plane of parameters of input voltage F and frequency difference ξ, for each value of anisochronism parameter $\tan\alpha$, the bifurcational diagrams appear as shown in Figures 11.10 and 11.12. These establish on the plane (ξ,F) the areas corresponding qualitatively to different topological structures of variations on the integrated curve of system phase portraits. On bifurcational diagrams these areas, as distinct from the structure of phase portraits, are specified by Roman numerals, and for each of these area types the special points are identified.

For example, in area I in Figures 11.11 and 11.2 there are three special points on the phase portrait: a steady knot, a saddle, and an unstable knot (see Figure 11.6). In area V (see Figure 11.11) there are an unstable focus and a steady limiting cycle in the system (see the phase portrait in Figure 11.8). Schematically, without taking into account some transitional areas of the bifurcational diagrams

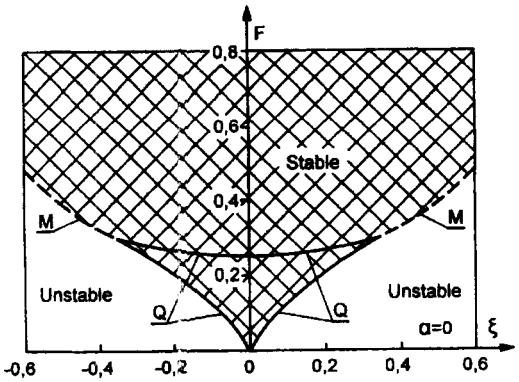

Figure 11.10 Rough splitting of generator bifurcational diagram in an isochronous case on stable and unstable areas.

(areas with Roman numbers greater than V in Figures 11.11 and 11.12), the half-plane of input voltage amplitude and its frequency difference is broken into two parts (see the areas G^* and H^* in Figure 11.11). In area G^* (above the bottom branches of borders M and Q) one globally steady steady-state synchronous mode is observed in the system to which there corresponds a steady balance condition (a special point of the knot or focus type). In area H^* (below the bottom branches of the borders) there is a beating mode corresponding to the steady limiting cycle on the phase plane a, φ.

The border between areas G^* and H^* is defined by lines Q and M. Actually, for any given F it defines the generator synchronism band. Borders M and Q are given as before by $b_1 = 0$ and $b_2 = 0$, where $b_1 = d + e$, and $b_2 = ed - bc$ are the factors of the characteristic equation (11.14) linearized around the steady-state condition a_0,φ_0 of the equations:

$$\begin{aligned} \frac{d\eta}{d\tau} + e\eta + b\gamma &= \Phi\cos\bar{\Omega}_D t, \\ \frac{d\gamma}{d\tau} + c\eta + d\gamma &= -(\Phi/a_0)\sin\bar{\Omega}_D t \end{aligned} \qquad (11.16)$$

Here, η and γ are increments of the amplitude a and the phase φ respectively, $e = 2a_0 - 1$, $b = -a_0[\xi + (a_0 - 1)\tan\alpha]$, $c = [\xi + (a_0 - 1)\tan\alpha]/a_0$, and $d = a_0 - 1$. In addition to the stability borders M and Q on Figures 11.11 and 11.12 the border $D = 0$ is shown, where D is the discriminant of the characteristic equation (11.14). The border $D = b_1^2 - 4b_2 = 0$ defines the change of the knot points to focuses.

In the presence of a small target signal Φ ($\Phi << 1$), the analysis problem of equations (11.6) - (11.7) is equivalent to that of the effect of small periodic interference with amplitude Φ and frequency $\bar{\Omega}_D$ on the system of the "autonomous"

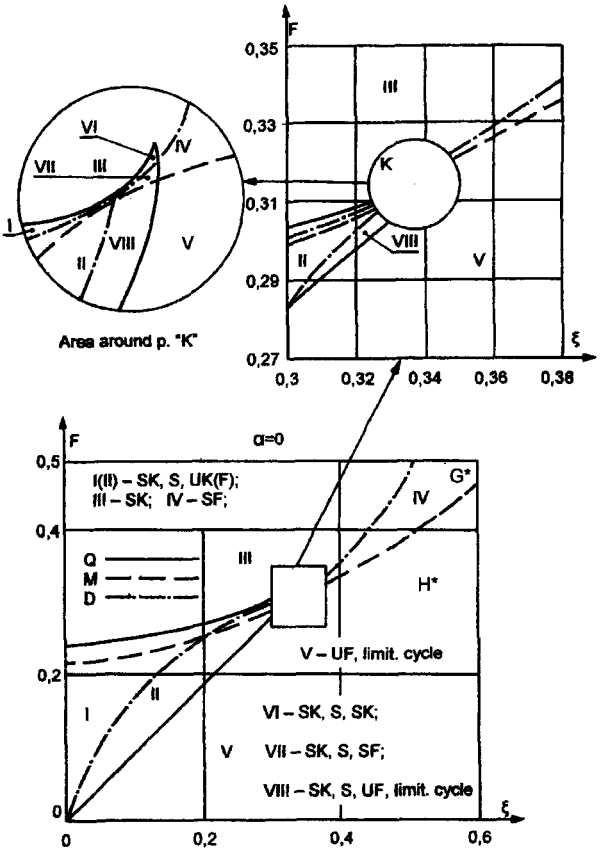

Figure 11.11 The fine picture of the bifurcational diagram for the isochronous case.

(i.e., not containing time in an obvious way) differential equations (11.6) - (11.7) of the synchronized oscillator. Therefore, for the answer to the question of behavior of (11.6) - (11.7) it is convenient to take advantage of some general results of the theory periodic interference to "autonomous" systems.

As with (11.8) - (11.9) we can see that when plotted on the phase cylinder a,φ, (11.6) - (11.7) are dissipative (the right-hand terms of (11.6) - (11.9) are limited, and for large amplitudes a the derivative $da/d\tau < 0$ for any φ). In other words, all integrated curves for large a eventually enter into the band $0 < a_0 < 1$ and none leave it. In this case it is possible to show that for (11.8) - (11.9) in the field of synchronism G^* (Figure 11.10), with small enough Φ, there is a unique steady periodic solution with a frequency equal to that of the autodyne input $\bar{\Omega}_D$. This solution also represents a useful autodyne signal. The problem of this signal size definition for different system mode parameters is therefore of interest.

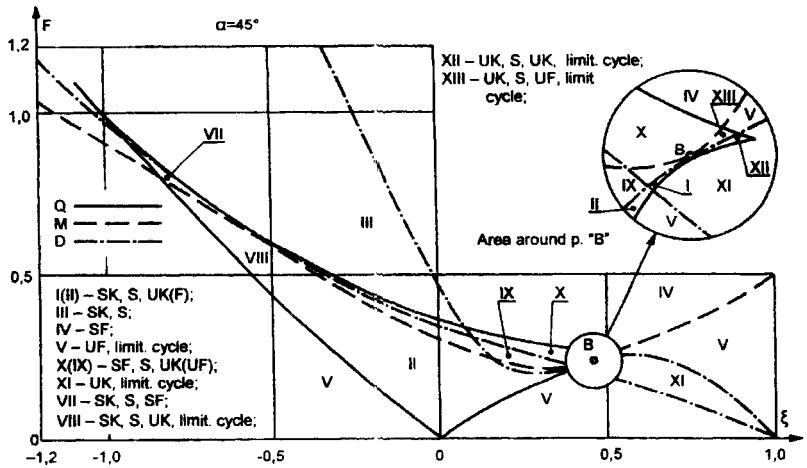

Figure 11.12 The bifurcational diagram of an autodyne for the anisochronous case.

The appropriate unstable periodic variations of (11.8) - (11.9) correspond the unstable special points of (11.6) - (11.7).

In the beating mode (area H^* of Figure 11.11), the introduction of a small periodic interfering voltage results in small changes in the course of the limiting cycle (the formation of an invariant integrated surface in the form of a bidimensional torus [4, 5]). System variations in the beating mode for this case are almost periodic (when the ratio κ of the period of interference $2\pi/\bar{\Omega}_D$ to the period of variation of the limiting cycle at $\Phi = 0$ is irrational), or are periodic (when κ is rational). In spectral language this last case implies a *multiplicity* in the spectrum of beat frequencies approaching the frequency $\bar{\Omega}_D$.

11.2 TRANSFER FACTOR OF AN AUTODYNE SUBJECT TO SYNCHRONOUS JAMMING

Steady-state (steady and unstable) periodic variations of (11.8) - (11.9) can be found as a first approximation, considering the periodic solutions of the linearized system (11.16). For simplification of the analysis we will enter, as is usual, a linear replacement of coordinates: $x = \gamma + \beta\eta$, where $\beta = -c/(p+e) = -(p+d)/b$, and p is a root of the characteristic equation (11.14). Now (11.16) can be replaced by a pair of equations:

$$\frac{dx}{d\tau} - px = \beta\Phi\cos\bar{\Omega}_D\tau - \frac{\Phi}{a_0}\sin\bar{\Omega}_D\tau \qquad (11.17)$$

where for $x = x_{1,2}$ it is necessary to use correspondingly $p = p_{1,2}$ and $\beta = \beta_{1,2}$. By direct integration from (11.17), we obtain:

$$x_{1,2} = \frac{\Phi}{p_{1,2}^2 + \bar{\Omega}_D^2}\left[\left(-p_{1,2}\beta_{1,2} + \frac{\bar{\Omega}_D}{a_0}\right)\cos\bar{\Omega}_D\,\tau + \left(\beta_{1,2}\,\bar{\Omega}_D + \frac{p_{1,2}}{a_0}\right)\sin\bar{\Omega}_D\,\tau\right] \qquad (11.18)$$

Taking into account that $\eta = (x_2 - x_1)/(\beta_2 - \beta_1)$ and $\gamma = (\beta_2 x_1 - \beta_1 x_2)/(\beta_2 - \beta_1)$, it is easy to find the appropriate transfer factors for increments of amplitude and phase in relation to the amplitude Φ of the reflected signal. For studying autodyne signal amplitudes $\bar{\eta}$ of interest, let us enter, as earlier, the voltage transfer factor of the autodyne:

$$K_U = \frac{\bar{\eta}}{\Phi} = \frac{\bar{\eta}}{\left(\frac{kI_{refl}}{U_0 G_{ss} g}\right)} = K_U(F, \xi, U_0, \alpha, \bar{\Omega}_D) \qquad (11.19)$$

Here it can be noted that the autodyne voltage transfer factor is a complex function of amplitude F and frequency ξ of the synchrosignal, the oscillation amplitude of an independent mode U_0 (i.e., a mode), the degree of anisochronism in an independent mode α, and the Doppler frequency $\bar{\Omega}_D$.

After some difficult transformations, we finally obtain:

$$K_U = \frac{A^2 + B^2}{a_0(\beta_2 - \beta_1)\left[(b_2 - \bar{\Omega}_D^2)^2 + b_1^2\bar{\Omega}_D^2\right]} \qquad (11.20)$$

where

$$A = (p_1^2 + \bar{\Omega}_D^2)(\bar{\Omega}_D - p_2\beta_2 a_0) - (p_2^2 + \bar{\Omega}_D^2)(\bar{\Omega}_D - p_1\beta_1 a_0) \text{ and}$$

$$B = (p_1^2 + \bar{\Omega}_D^2)(\beta_2\,\bar{\Omega}_D\,a_0 + p_2) - (p_2^2 + \bar{\Omega}_D^2)(\beta_1\,\bar{\Omega}_D\,a_0 + p_1)$$

Let us discuss in a general way the dependence of transfer factor K_U on parameters $F, \xi, \alpha, \bar{\Omega}_D$.

We notice again that the system of the equations (11.6) - (11.7) does not change if we put $\xi = -\xi$, $\tan\alpha = -\tan\alpha$, $\bar{\Omega}_D = -\bar{\Omega}_D$, and $\varphi = -\varphi$ (i.e., the transfer factor of an autodyne does not depend on the sign of these parameters). Thus, transfer factor K_U as function of parameters $\xi, \tan\alpha, \bar{\Omega}_D$ is symmetric about the axis $\xi = \tan\alpha = \bar{\Omega}_D = 0$. In other words, in analysis of the dependence of K_u on ξ, $\tan\alpha$, $\bar{\Omega}_D$ we need examine only those areas where one of these parameters is positive, say, $\tan\alpha > 0$.

The analysis of (11.20) shows that for $\bar{\Omega}_D \neq 0$ in the case $b_2 = \bar{\Omega}_D^2$ and $b_1 \to 0$, the size of the autodyne signal transfer factor as a first approximation approaches infinity (i.e., in a vicinity of values $b_2 = \bar{\Omega}_D^2$ and $b_1 = 0$ resonant phenomena similar to those described for similar systems are observed). In other words, a synchronized autodyne acts here as a resonant amplifier of the reflected target signal. It is not difficult to understand how valuable this property is for design of systems with increased autodyne sensitivity.

However, these resonant properties appear only in a vicinity of one point of parameter space, and the condition $b_1 = 0$ corresponds to the border M of the oscillations synchronism zones (for large input voltages F).

The beating mode corresponds to values $b_1 < 0$ when the interference appears at frequencies close to the synchrosignal, along with useful autodyne signal components.

The physical sense of the point of full resonance is that, for $b_1 = 0$ at the point $b_2 = \bar{\Omega}_D^2$ at the border of stability M, the period of variation in the limiting cycle $T = 2\pi/\sqrt{b_2}$ (on border M the limiting cycle originates from a complex focus) is closely equal to the period of the jamming $T_\Phi = 2\pi/\bar{\Omega}_D$.

For $b_1 = 0$ we have:

$$b_2 = \xi^2 - \frac{1+\tan^2\alpha}{9}$$

From this it follows that at the point of full resonance the following ratio for asymptotic value of the frequency difference applies:

$$\xi_{asym}^2 = \bar{\Omega}_D^2 + \frac{1+\tan^2\alpha}{9}$$

Dependence of the transfer factor on the synchronized autodyne voltage with frequency difference ξ at various F and $\tan\alpha$ were calculated on a computer and are given in Figures 11.13-11.15. Continuous lines in the figures show dependence of $K_U(\xi)$ for steady periodic variations of system (11.8) - (11.9) (i.e., for useful autodyne signals). Dashed lines correspond to unstable periodic variations (i.e., those variations that appear with a reflected signal near unstable balance conditions of the synchronized oscillator).

We will discuss, first of all, the results appropriate to the isochronous generator (i.e., the case $\tan\alpha = 0$). The same results apply, naturally, to the generator with an inertialess amplifying device.

The family of steady branches of resonant characteristics $a(\xi)$ of the synchronized oscillator is shown in Figure 11.13(a). As these characteristics at $a = 0$ are symmetric with respect to ξ, in the figure is shown only the right half-plane. The

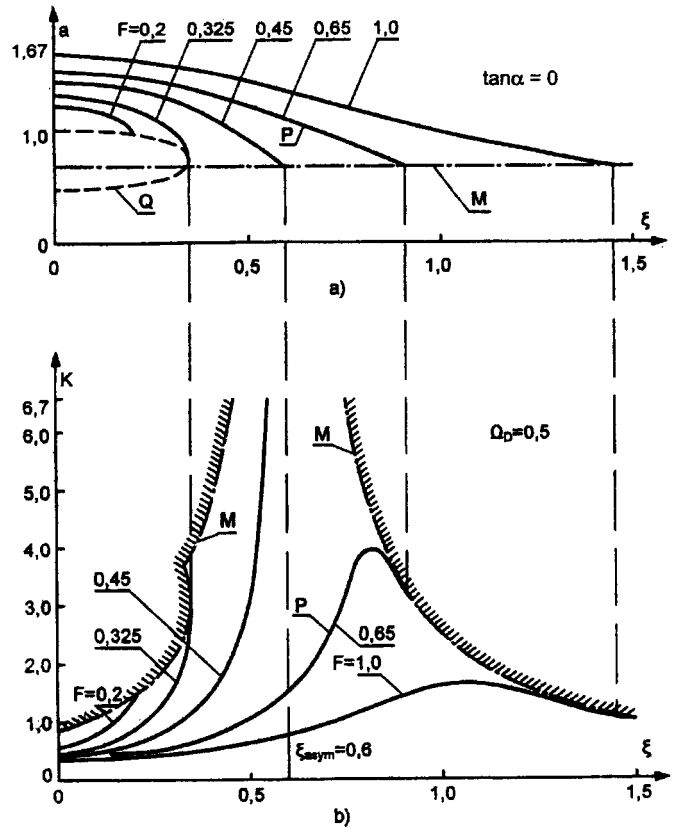

Figure 11.13 Amplitude-frequency characteristics (a), and dependence of autodyne voltage transfer factors (b) in the case of frequency locking by a jammer (for $\tan\alpha = 0$).

point of the independent mode corresponds to a case $F = 0$, $\xi = 0$, $a = 1$. For this independent point from (11.20), we obtain:

$$K_{aut} = \frac{1}{\sqrt{g^2 + (\Omega_D T)^2}} \tag{11.21}$$

which in view of designations for g coincides with (10.47) of Chapter 10, with $\gamma = 0$ for a case of fixed bias. With change of the mode U_0, the function g varies and K_U becomes maximal and equal $1/(\Omega_D T)$ at $g = 0$.

Upon introduction of the synchrosignal ($F \neq 0$) with zero frequency difference ($\xi = 0$), we have:

$$K_U = \frac{1}{\sqrt{g^2(2a-1)^2 + (\Omega_D T)^2}} \tag{11.22}$$

and, since $\xi = 0$ in the synchronous mode, $a > 1$, then K_U falls in comparison with K_{aut} [see Figure 11.13(b)]. With increase of the frequency difference for variation on the resonant curve before crossing border Q [on Figure 11.13(a)], the autodyne transfer factor increases [Figure 11.13(b)] up to the value K_Q of the boundary mode appropriate to failure of stability and transition to a beating mode:

$$K_Q = \frac{1}{\Omega_D T}\sqrt{\frac{(a-1)^2 g^2 + (\Omega_D + \lambda)^2 T^2}{(3a-2)^2 g^2 + (\Omega_D T)^2}} \tag{11.23}$$

As we can see, $K_Q > K_{aut}$ (i.e., the autodyne voltage transfer factor may exceed K at the independent point). Dependence of $K_U(\xi)$ for small F ($F < 0.325$) appear as growing parabolas [Figure 11.13(b)].

For $F > 0.325$ the stability of the steady-state synchronous mode is defined by border M [see Figure 11.13(a)], and the autodyne transfer factor K_M at this border is:

$$K_M = \frac{3g\sqrt{g^2 + 9(\Omega_D + \lambda)^2 T^2}}{\left|9\lambda^2 T^2 - 9\Omega_D{}^2 T^2 - g\right|} \tag{11.24}$$

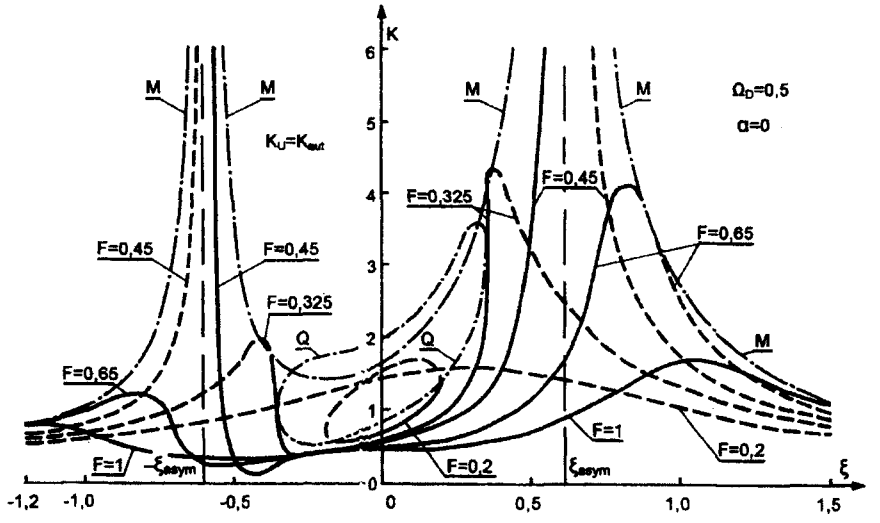

Figure 11.14 Dependence of autodyne voltage transfer factor on frequency difference in the areas of positive and negative frequency difference of a locking jamming signal.

For the marked value

$$\lambda_{asym}^2 = \frac{9\Omega_D{}^2T^2 + g^2}{9T^2}$$

or

$$\xi_{asym}^2 = \Omega_D{}^2 + \frac{1}{9}$$

(i.e., the autodyne voltage transfer factor K_U asymptotically approaches infinity) [Figure 11.13(b)].

The family showing dependence of $K_U(\xi)$ is not symmetric with respect to the axis $\xi = 0$, as we can see from Figure 11.14. Thus, for small positive ξ, the value of K_U increases with increase in the frequency difference, while for negative ξ it falls (Ω_D = const). In view of the axial symmetry in space of the parameters (ξ,Ω_D, $\tan\alpha = 0$), a similar phenomenon is observed for the family $K_U(\Omega_D)$ for ξ = const. By virtue of this, it appears possible in the synchronized autodyne to distinguish positive from negative Doppler frequencies Ω_D (i.e., the direction of target motion in space) based on the amplitude of the autodyne signal and also to receive a useful signal proportional to the frequency difference ξ or to the Doppler frequency Ω_D.

For a case of the anisochronous generator the dependence of $K_U(\xi)$ becomes complicated and even more asymmetric (Figure 11.15). Thus the marked resonant character of curves for large synchrosignal amplitudes F is maintained.

From consideration of the specified dependence $K_U(\xi,\Omega_D,F,a)$ it is possible to draw the following general conclusions. For small frequency differences ξ with respect to a line of maximum resonant characteristics the increase of synchrosignal amplitude always results in reduction of the autodyne voltage transfer factor K_U in comparison with its value for the independent mode K_{aut}. Increasing the frequency difference ξ results either in growth or reduction of K_U, depending upon values of ξ, Ω_D, and $\tan\alpha$. For small F in this case, within the limits of the synchronism band where only the useful autodyne signal exists, the change of K_U may be insignificant. For large amplitudes F increasing $|\xi|$ leads to resonant growth of K_U that was discussed in detail above. Thus it can be seen that, unless set by very large K_U, it is possible to choose values of ξ and Ω_D so that the operating point will be located far enough from the border M of the transition to the beating mode, such that the amplitude of synchronous oscillations will be close to the amplitude for the independent mode ($a \approx 1$), and thus the objective in autodyne sensitivity will be provided in comparison with an independent autodyne [see, for example, the point P in Figure 11.13(b)]. This circumstance may have major practical value.

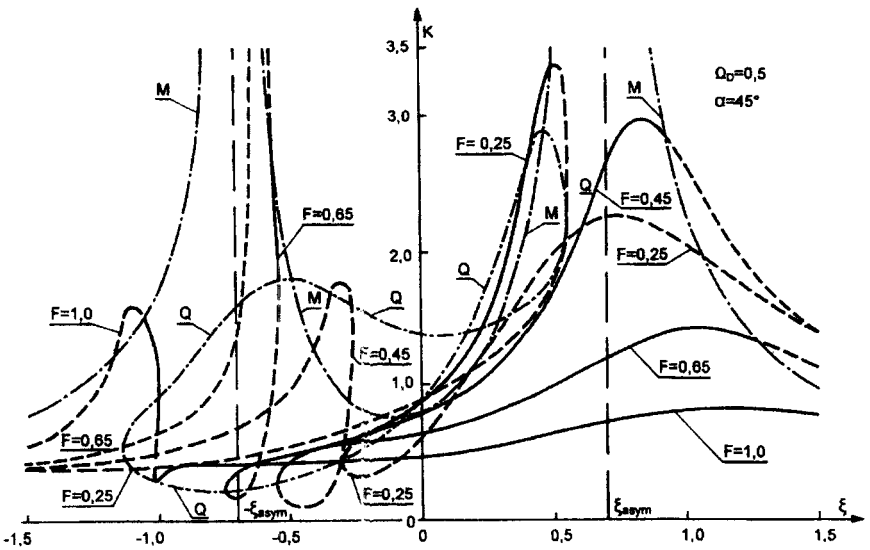

Figure 11.15 Dependence of autodyne voltage transfer factor on frequency difference in the case of an isochronous autodyne synchronized by a jammer.

11.3 BIFURCATIONS OF PERIODIC VARIATIONS IN THE SYNCHRONIZED AUTODYNE

As noted earlier, the area of resonant rise of the autodyne voltage transfer factor lies near the border of stability M of synchronous oscillations of the generator. This circumstance causes interest in further analysis of frontier areas of the bifurcation diagrams of the transistor autodyne. The results derived earlier concern the existence of an autodyne signal (steady-state periodic variation in the vicinity of the point of the synchronous mode) for any combination of parameters within the limits of the synchronism zone (Figure 11.10), in the case where the amplitude of the reflected signal Φ is small enough. However, at the given value of Φ in the vicinity of borders M and Q (and on the borders) of the bifurcation diagrams, the question of steady-state variations existing in the system and their stability remains open.

As is known, for studying bifurcation phenomena it is not enough to examine only a linearized system [i.e., behavior of system (11.6) - (11.7) is determined by nonlinear terms]. For studying the possible bifurcations we will expand the nonlinear terms of (11.6) - (11.7) in Taylor series in the vicinity of the condition of balance of system (11.8) - (11.9). The equations for increments of amplitude and phase (increments η and γ) take the form:

$$\begin{aligned}\frac{d\eta}{d\tau}+e\eta+b\gamma+\sum_{k=2}^{\infty}P(\eta^k,\gamma^k)&=\Phi\cos\Omega_D\tau\\ \frac{d\gamma}{d\tau}+c\eta+d\gamma+\sum_{k=2}^{\infty}Q(\eta^k,\gamma^k)&=-\frac{\Phi}{a_0}\sin\Omega_D\tau\end{aligned}\tag{11.25}$$

where P and Q are nonlinear forms of variables η and γ with constant factors of the order $k \geq 2$, and other designations correspond to (11.16).

We will enter, as was done earlier in Section 11.2, a linear substitution of coordinates $x_{1,2} = \gamma + \beta_{1,2}\eta$, such that (11.25) can be replaced by the following:

$$\begin{aligned}\frac{dx_1}{d\tau}-p_1x_1+\sum_{k=2}^{\infty}P'(x_1^k,x_2^k)&=\beta_1\Phi\cos\Omega_D\tau-\frac{\Phi}{a_0}\sin\Omega_D\tau,\\ \frac{dx_2}{d\tau}-p_2x_2+\sum_{k=2}^{\infty}Q'(x_1^k,x_2^k)&=\beta_2\Phi\cos\Omega_D\tau-\frac{\Phi}{a_0}\sin\Omega_D\tau,\end{aligned}\tag{11.26}$$

where factors of forms P' and Q' with order $k \geq 2$ are easily defined through the appropriate factors of forms P and Q.

As established earlier, (11.26) generally has in the vicinity of zero the periodic solution $x_{1,2} = X_{1,2}(\tau)$ with amplitude of the order Φ. Following the technique of the classical theory of bifurcation of periodic variations [6], we proceed from (11.26) to Poincaré coordinates (those normal coordinates ε,β in the vicinity of periodic system variation). We will enter the parameter $\theta = \Omega_D\tau$ on a curve of steady-state periodic variation of the system and define a vector

$$\bar{r} = \{X_1(\theta), X_2(\theta), \theta\}$$

We have a tangential vector

$$\bar{t} = \frac{\partial\bar{r}}{\partial\theta} = \{X_1'(\theta), X_2'(\theta), 1\} = \{t_x, t_y, t_z\}$$

and two normal vectors

$$\bar{n} = \bar{t}\bullet\left(\frac{\partial^2\bar{r}}{\partial\theta^2}\right) = \{n_x, n_y, n_z\} \quad \text{and} \quad \bar{b} = \bar{t}\bullet\bar{n} = \{b_x, b_y, b_z\}$$

Now it is possible to substitute coordinates in the following form:

$$x_1 = X_1(\theta) + (n_x - t_x n_z)\varepsilon + (b_x - t_x b_z)\beta$$
$$x_2 = X_2(\theta) + (n_y - t_y n_z)\varepsilon + (b_y - t_y b_z)\beta \qquad (11.27)$$

where the factors before the normal variables ε,β are periodic functions θ and have the order Φ. Substituting (11.27) in (11.26), we obtain linear equations for the case $P' = Q' = 0$ describing the variables ε and β with periodic factors.

Due to reducibility of the given system, its multipliers (and consequently the solution of the question of variation stability) will not change with a linear substitution of coordinates, which we will now write as:

$$fy_1 = (n_x - t_x n_z)\varepsilon + (b_x - t_x b_z)\beta$$
$$fy_2 = (n_y - t_y n_z)\varepsilon + (b_y - t_y b_z)\beta$$

For variables y_1, y_2 from (11.26), we obtain the following system of three equations:

$$f\frac{dy_1}{d\tau} - p_1 y_1 + \sum_{k=2}^{\infty} P^k\left\{[X_1(\theta), fy_1]^k, [X_2(\theta), fy_2]^k\right\} = 0$$
$$f\frac{dy_2}{d\tau} - p_2 y_2 + \sum_{k=2}^{\infty} Q^k\left\{[X_1(\theta), fy_1]^k, [X_2(\theta), fy_2]^k\right\} = 0 \qquad (11.28)$$
$$\frac{d\theta}{d\tau} = \Omega_D$$

from which we can see that in linear approximation ($P' = Q' = 0$) the bifurcational diagrams for (11.6) - (11.7) coincide with those for (11.8) - (11.9), since p_1 and p_2 are the roots of the characteristic equation (11.14).

For further constructions it is necessary to know the periodic solutions $X_1(\theta)$ and $X_2(\theta)$. We will consider a procedure for obtaining the asymptotic decomposition of (11.6) - (11.7), a periodic solution with the degree of parameter f.

We shall search for the solution X_1 in the form

$$X_i(\theta) = fx_i^0 + f^2 x_i^1 + f^3 x_i^2 + f^4 x_i^3 + \ldots,$$

where $i = 1,2$. Substituting the form of this solution in (11.26) and equating members of identical order in f, we obtain the following infinite system of linear nonuniform systems of differential equations with periodic right-hand parts, which may be solved consistently with use of the periodic solution of the previous equation:

$$\frac{dX_i^0}{d\tau} - p_i X_i^0 = \beta_i \cos\Omega_D \tau - \frac{1}{a_0}\sin\Omega_D \tau$$

$$\frac{dX_i^1}{d\tau} - p_i X_i^1 = -p_i^1\left[\left(X_1^0\right),\left(X_2^0\right)^2\right]$$

$$\frac{dX_i^2}{d\tau} - p_i X_i^2 = -p_i^1\left[\left(X_1^0 X_2^1\right),\left(X_1^0\right)^3,\left(X_2^0 X_1^1\right),\left(X_2^0\right)^3\right]$$

.....

here $i = 1,2$, $P'_1 = P'$, and $P'_2 = Q'$.

We will assume that an approximation of the solution $X_i(\theta)$ of the order n is thus found:

$$\sum_{k=1}^{n} f_k X_i^{k-1}$$

Having substituted this solution in (11.28), we find that in forms P', Q' all non-uniform components up to the order n inclusively will be reduced. Thus, in these forms all components except for the largest degrees of increments y will have variable factors. Then the linear system in view of members of the second order takes the form:

$$\frac{dy_i}{d\tau} - p_i y_i = -2fX_1^0(\alpha_i y_1 + \alpha_i y_2), \tag{11.29}$$

from which it is possible to find the change of the order f with respect to the size of the characteristic parameters p_i. For this purpose it is sufficient to present the fundamental system of solutions of (11.29) as:

$$Y_{ij} = Y_{ij}^0 + fY_{ij}^1$$

to substitute it in (11.29), and to find solutions of the resulting pair systems of differential equations. Further, having substituted in these solutions $\tau = T = 2\pi/\Omega_D$, we shall calculate a matrix of the system (11.29) and we define its multipliers μ_i. Then the characteristic parameters $p_i = L_n\mu_i/T$.

For consideration of bifurcations, it is possible in a similar way to construct maps of the following in view of nonlinear members. Concrete realization of these procedures is extremely unwieldy and is unjustified in our problem as the basic necessary data can be obtained, being guided by general provisions of the bifurcations theory of periodic variations in space with the help of qualitative reasons.

From this development it is clear that the multipliers of the linearized system (11.28) for small f differ little from those of system (11.16) at $f = 0$. In other words, with introduction of a small reflected signal the borders of stability M and Q of the bifurcation diagrams examined for system (11.8) - (11.9) undergo small shifts. By virtue of this, the qualitative character of borders is not generally changed. On border Q for an output from a synchronism zone there is a merging of two invariant periodic curves of system (11.6) - (11.7), one steady and one saddle-shaped, along with formation of complex periodic variation in the double beating mode (for small F), covering the phase cylinder.

Border M corresponds to a change of stability of the steady-state periodic variation curve with Doppler frequency Ω_D. Thus, as this border is a safe one, a steady two-dimensional invariant torus is established on it, consisting entirely of steady spiral phase curves for irrational values of the number of rotations κ. With change of parameters the number of rotations on this torus varies, generally speaking, so it adopts irrational or rational values when the separate steady phase curves are plotted on the torus. Corresponding generally to border M there is a passage of multiplier pairs through an individual circle. The case in which both multipliers $\mu_{1,2}$ are equal to 1 corresponds in our problem to a resonant point of a curve M, where $\sqrt{b_2} = \bar{\Omega}_D$ (i.e.,) $\mu_{1,2} = \exp\left(\pm j 2\pi \sqrt{b_2} / \bar{\Omega}_D\right) = 1$.

In the vicinity of the resonant point there may be rather complex reorganizations of system variation structures resulting from resonant excitation of amplitude oscillations with frequencies that are multiples of Ω_D. The concrete character of the bifurcations depends here significantly on the type of local nonlinearity. Solution of these bifurcations involves significant difficulties and is not necessary for us, as for small Φ the zone of resonant reorganizations is so small.

Similarly, it is possible to inspect the bifurcations in transition areas of the bifurcational diagrams (in areas VI-VIII, XII-XIII of Figures 11.11 and 11.12).

So, in summary it is possible to ascertain that as a first approximation, the zone of existence of a useful autodyne signal in a synchronized autodyne (in the absence of adjacent interference components in the spectrum) coincides with the area of existence of steady synchronous oscillations of the synchronized oscillator. Outside the specified area in the system, the mode of complex beating is observed when in a spectrum of an autodyne signal there are the parasitic components dependent on frequency and amplitude of an active synchronous jammer. The character of the transition from "synchronism" to the beating mode and back is defined, first of all, by the changes occurring in the synchronized system.

References

[1] Artemenkov, S. L., and S. M. Smolskiy, *Dynamic Properties of Synchronized Oscillators*, manual for the course "Sets for Generation and Control of Radio Signals," Moscow: MPEI, 1985.

[2] Artemenkov, S. L., and S. M. Smolskiy, "Transients in Synchronized Oscillators using Inertial Active Elements," *News of High Schools of the USSR, Series – Radiophysics*, Vol. 21, No. 11, 1977, pp. 1680-1688.

[3] Bogachev, V. M., and S. M. Smolskiy, "General Equations of an Anisochronous Oscillator Synchronized by External Periodic Force," in collection *Semi-Conductor Devices in Telecommunication Engineering*, I. F. Nikolaevskiy, ed., Release 12, 1973, Moscow, pp. 160-173.

[4] Pliss, V. A., *Integrated Sets of Periodic Systems of Differential Equations*, Moscow: Science, 1977.

[5] Pliss, V. A., *Non-Local Problems of Oscillation Theory*, Moscow: Science, 1964.

[6] Andronov, A. A., et al., *Dynamic System Bifurcation Theory on a Plane*, Moscow: Nauka, 1972.

List of Symbols

a	normalized amplitude of synchronous oscillations
b	autobias parameter
$B(U,E)$	imaginary part of the oscillator equivalent output admittance
c	velocity of electromagnetic wave propagation
$C_V(e)$	varicap capacitance
C_{V0}	varicap capacitance at $e = 0$
C_p	parasitic capacitance
E	bias voltage of autodyne (the oscillator) active element
E_{init}	initial bias voltage of active element
E_{vc}	control voltage on varicap
E'	cutoff voltage of active device currents
e	external voltage on varicap
e_1, e_2	cosine and sine components of parasitic bias signal
F	normalized amplitude of synchronizing signal
$F(t)$	law of capacity modulation
F_{ant}	function of antenna orientation
$F_p(t)$	phase modulation function of transmission
$F_r(t,\tau)$	phase modulation function of reflected signal
$F_t(t,\tau)$	phase modulation function of converted signal
Δf	frequency deviation (cycle frequency)
G_{ant}	antenna power gain
G_{SS}	resonant conductivity of selective system
$G(U,E)$	real part of the oscillator equivalent output admittance
$i(t)$	current value of the current
$i(u)$	voltage-current characteristic of active element
i_C	current flowing through condenser
i_L	current flowing through inductance coil
I_0	constant component of current
I_1	current first harmonic
$I_1(U)$	oscillatory characteristic of active element
$\dot{I}$	complex amplitude (complex envelope) of current

I_{ext} or I_{syn}	amplitude of external synchronizing signal
I_{in}	amplitude of first harmonic of active element output current
I_{in0} or J_{in}	constant component of active element input current
I_{com0} or J_{com}	constant component of current of active element common electrode
I_{out}	amplitude of first harmonic of active element output current
I_{out0} or J_{out}	constant component of active element output current
I_{refl}	amplitude of reflected signal
J_n	Bessel function of the first kind
$j\omega = d/dt$	symbolic operator of differentiation
$k_{fb} = u/u_{SS}$	feedback factor
$\boldsymbol{k}_{fb}$	complex feedback factor $-\left(\dot{U}/\dot{U}_{ss}\right)$
k_t	transformation factor of ideal transformer
K_{fb}	module of complex feedback factor
K_f	frequency coverage coefficient
K_J	current transfer factor of autodyne
K_U	voltage transfer factor of autodyne
K_2	nonlinear distortion coefficient for second harmonic
K_3	nonlinear distortion coefficient for third harmonic
L	single-tuned circuit inductance
L_{SS}	variable inductance at FM
m	coefficient of PAM
m_{com}	order of the common electrode autobias circuit
m_R	modulation index of resistance
m_{SS}	order of selective system
m_U	amplitude modulation index
M	mutual inductance
n	normalized derivative of N function
N	function opposite to feedback factor
$p = d/d\tau$	operator of differentiation in dimensionless time
$p_1 = -j\omega_{0k}$	displaced operator
p_k	coupling coefficient for single-tuned circuit
P_{rad}	radiated power
P_{rec}	power at receiver input
q	electric charge
Q_0	average value of electric charge
$Q \cdot P$	numerator and denominator of symbolic admittance
$Q(\omega_1)$	FM single-circuit quality factor for $\omega = \omega_1$
R	control resistance at resonance
R_{em}, C_{em}	resistance and capacitance of simple RC autobias chain
$R\_\_$	resistance defining slope of load straight line
R_{com}	resistance of common electrode autobias circuit

ΔR_{min}	maximum possible range resolution
r	equivalent loss resistance of sequential single-tuned circuit, distance between target and autodyne
S	slope of voltage-current characteristic of active element; slope of discriminator characteristic
S_1	slope averaged on first harmonic (a slope of oscillatory characteristic)
S_{com0}	slope of voltage-common electrode current at dc
t	time
t'	$t - \tau/2$
T	time constant of selective system
T'	normalized time constant of selective system
T_{em}	time constant of emitter autobias circuit
T'_{em}	normalized time constant of emitter autobias circuit
T_{com}	time constant of common electrode autobias circuit
T_{syn}	time constant describing the duration of synchronization process
T^a_{tr}	amplitude transient time
T^φ_{tr}	phase transient time
T_m	frequency modulating period
u	RF voltage on varicap
$u(t)$	current value of voltage
$u_{SS}(t)$	current value of selective system voltage
U	amplitude of voltage signal
U_d	the amplitude of direct signal
U_k	amplitude of k harmonic of voltage
U_p	amplitude of transmission signal
U_r	amplitude of reflected signal
U_{RF}	radio frequency voltage
U_{SS}	voltage amplitude at selective system
U_{SS0}	average amplitude of U_{SS}
U_t	amplitude of converted signal
$\overset{\circ}{U}$	value of amplitude at steady-state point
$\dot{U}$	complex amplitude (complex envelope) of voltage
$\dot{U}_{ss}$	complex amplitude of the voltage on selective system
U_{180}	voltage amplitude for $\theta = 180°$
U_Ω	modulating voltage
V_r	relative radial speed between radar and target
V_1, V_2	cosine and sine components of PAM
W_{SS0}	energy of selective system electric circuit in the absence of FM
x	dimensionless RF voltage on varicap
X	tangents to cutoff diagram
X_b	tangents to bias diagram
y_α	admittance of dispersion of ideal transformer

Y	control admittance abbreviated around reference frequency
$Y(j\Delta\omega)$	abbreviated admittance
$Y(U,E)$	equivalent output admittance of oscillator (complex electronic conductivity)
Y_0, (Y_{bi})	admittance of autobias circuit
$Y_{in}(p)$, $Y_{com}(p)$	symbolic admittance of input and common electrode autobias circuits
$Y_{SS}(p)$	symbolic admittance of selective system
$Y_{SS}(p,u)$	symbolic admittance of selective system with modulation
Y_{ij} $(i,j = 1,2)$	complex active element Y-parameters averaged for first harmonic
$Y_{ij}(p)$	parameters of autodyne small-signal equivalent scheme
$Y_{1,2,3}$	oscillator three-port circuit elements
$Z(j\omega)$	complex impedance of load
α_m	polynomial coefficients of Y_{SS} numerator
α_{mi}	polynomial coefficients of α_m decomposition in MacLaurin series
β_m	polynomial coefficients of Y_{SS} denominator
β_{mi}	polynomial coefficients of β_m decomposition in MacLaurin series
β_Ω	normalized modulating voltage
γ	factor determined by slope of cutoff and bias diagram
$\gamma(t)$	law of signal frequency modulation
$\gamma_0(\theta)$	decomposition coefficient for constant component
$\gamma_1(\theta)$	decomposition coefficient for first harmonic
δ	attenuation of selectivity system (small parameter)
$\delta\omega$	central frequency shift of direct signal
$\Delta\omega = \omega - \omega_0$	frequency difference
$\Delta\omega = \omega_{max} - \omega_{min}$	frequency deviation (radian frequency)
ε	peak frequency deviation
η	normalized capacitance controlling frequency
$\overline{\eta}$	autodyne signal amplitude
η_{PAM}	parasitic amplitude signal
η_{ad}	autodyne signal
θ	cutoff angle of cosine impulse of current
λ	frequency difference
λ_{fr}	wavelength in free space
μ	modulation parameter
ρ	characteristic impedance
$\tau = \omega_0 t$	dimensionless time; reflected signal time delay relative to transmission
τ_0	initial value of delay
τ_{hf}	delay time in high-frequency circuit

τ_{lf}	delay time in low-frequency circuit
τ_{fb}	delay time in feedback circuit
φ	current value of phase of voltage signal initial phase of control voltage u
φ_c	contact potential difference of varicap material
$\varphi_d(t)$	phase of direct signal
$\varphi_p(t)$	phase of transmission
$\varphi_r(t,\tau)$	phase of reflected signal
$\varphi_t(t,\tau)$	phase of converted signal
φ_τ	initial phase shift
φ_0	phase shift caused by reflecting properties of target
ϕ	initial phase of voltage u_{SS}
Φ	magnetic flux; normalized amplitude of reflected signal
ξ	normalized frequency difference of synchrosignal; normalized detuning
ξ_{syn}	synchronization band
ω	radian frequency
ω_k	roots of system natural equation
ω_0	natural resonant frequency of selectivity system (for single-tuned circuit $\omega_0 = 1/\sqrt{LC}$)
ω_{osc}	oscillator fluctuations frequency
ω_c	central frequency of transmission
ω_{180}	frequency for $\theta = 180°$
ω_{SS0}	initial value of frequency around which FM is taking place
ω_{syn}	frequency at synchronization mode
$j\Delta\omega/\omega_0$	frequency disturbance
Ω_D	Doppler frequency
$\bar{\Omega}_D$	normalized Doppler frequency
Ω_m	modulation frequency
$\Omega_t(t,\tau)$	instantaneous frequency of converted signal
$\Delta\Omega(t,\tau)$	frequency deviation of converted signal

About the Authors

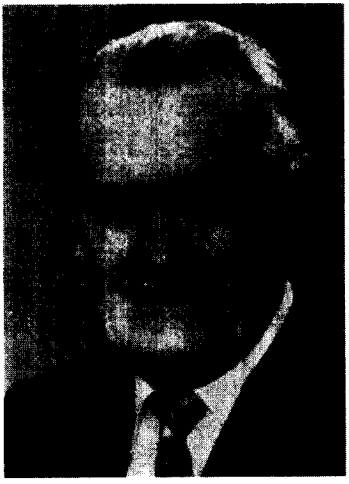

Igor V. Komarov was born in 1930 in Moscow. In 1954 he graduated from the Radio Engineering Faculty of the Moscow Power Engineering Institute (MPEI). In the same year he also began working at the Department of Radio Receivers of MPEI, where he remained until 2000. In this department, he was engaged in pedagogical and research work. He was the basic lecturer for the following lecture courses offered by the department: "Radio Receiving Devices," "The Theory of Signal Processing," "Algorithms and Devices for Signal Processing," and "Systems of Short-Range Radar."

Simultaneously with the pedagogical work, he closely cooperated with the industry in developing radar tracking devices. He was nominated as the scientific supervisor and leader of many research works of the department, part of which were carried out under decrees from the USSR government. The list of his scientific publications and inventions contains approximately 100 names and includes 2 monographs, about 30 scientific articles, 10 copyright certificates of the former USSR on inventions, and patents of the Russian Federation. Dr. Komarov has a Ph.D., and holds the honorary title Honorary Radio Specialist of the USSR.

His scientific work for the last decade in the department is connected with conversion directions of short-range radar systems development. During this period the following developments were carried out by Dr. Komarov: navigational short-range radar, medium accuracy level-measuring radar, ultrasonic level-

measuring radar, a draft of a portable navigational radar for small size sea ships, precision level-measuring radar, precision radar for measurement of very small motions, and radar for vibration measurement.

Dr. Komarov's hobbies include painting, art photography, amateur cinema, hiking, and boating. He is very fond of classical music, and also very much likes to equip his house and repair everything in it.

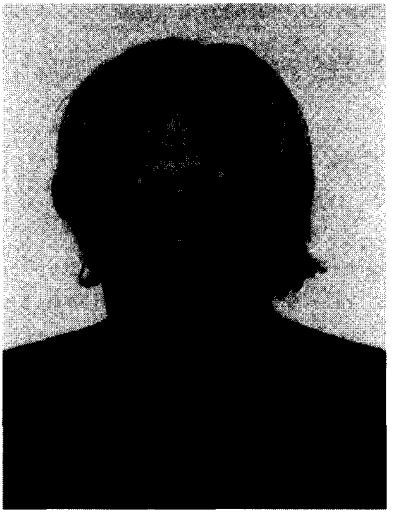

Sergey M. Smolskiy was born in 1946 in Moscow. In 1970, he graduated from the Radio Engineering Faculty of the Moscow Power Engineering Institute (MPEI). In the same year he began working in the Department of Radio Transmitting Devices of MPEI. After concluding his postgraduate study and defending his Ph.D. thesis in 1974, he continued research work in the Department of Radio Transmitting Devices, where he was engaged in theoretical and practical debates regarding transmitting stages of short-range radar development, and in various studies of transistor oscillators theory and microwave oscillations stability. He was nominated as the scientific supervisor of many scientific projects carried out under the decrees of the former USSR government. In 1993, he defended his thesis for the Doctor of Sciences degree and became a full professor. In 1995, he was appointed chairman of the Radio Receivers Department of MPEI.

Dr. Smolskiy's pedagogical experience extends over 20 years. He is the lecturer for the following courses: "Radio Transmitting Devices," "Systems of Generation and Control of Oscillations," "Nonlinear Oscillations Theory in Radio Engineering," "Analysis Methods for Nonlinear Radio-Electronic systems," and "Autodyne Short-Range Radar." The list of his scientific publications and inventions contains more than 110 scientific articles, 4 monographs, 3 copyright certificates of former USSR inventions, and more than 90 scientific and technical reports at various conferences, including international locations. He is a full member of the International Academy of Informatization, the International Academy of Electrical Engineering Sciences, and the International Academy of Sciences of Higher Educational Institutions, a member of the IEEE, and an honorary doctor of several foreign universities. He was awarded the State Order of Poland for merits in preparation of the scientific staff.

Dr. Smolskiy's scientific work during the last 10 years has been connected with conversion directions of short-range radar system engineering, radiomeasuring systems for the fuel and energy industry, systems of information acqui-

sition and transfer for industrial purposes with the use of wireless channels, and systems of medical electronics.

Dr. Smolskiy's hobbies include reading fiction in English, studying the problems of international cooperation of universities, classical music, and philately. He likes to repair electronic equipment and has issued several lecture courses on diagnostic and repair principles for students. He also loves travel and food preparation.

Index

Recent Titles in the Artech House Radar Library

David K. Barton, Series Editor

Advanced Techniques for Digital Receivers, Phillip E. Pace

Airborne Pulsed Doppler Radar, Second Edition, Guy V. Morris and Linda Harkness, editors

Bayesian Multiple Target Tracking, Lawrence D. Stone, Carl A. Barlow, and Thomas L. Corwin

Computer Simulation of Aerial Target Radar Scattering, Recognition, Detection, and Tracking, Yakov D. Shirman, editor

Design and Analysis of Modern Tracking Systems, Samuel Blackman and Robert Popoli

Digital Techniques for Wideband Receivers, Second Edition, James Tsui

Electronic Intelligence: The Analysis of Radar Signals, Second Edition, Richard G. Wiley

Electronic Warfare in the Information Age, D. Curtis Schleher

EW 101: A First Course in Electronic Warfare, David Adamy

Fourier Transforms in Radar and Signal Processing, David Brandwood

Fundamentals of Electronic Warfare, Sergei A. Vakin, Lev N. Shustov, and Robert H. Dunwell

Fundamentals of Short-Range FM Radar, Igor V. Komarov and Sergey M. Smolskiy

Handbook of Computer Simulation in Radio Engineering, Communications, and Radar, Sergey A. Leonov and Alexander I. Leonov

High-Resolution Radar, Second Edition, Donald R. Wehner

Introduction to Electronic Defense Systems, Second Edition, Filippo Neri

Introduction to Electronic Warfare, D. Curtis Schleher

Introduction to Electronic Warfare Modeling and Simulation, David L. Adamy

Microwave Radar: Imaging and Advanced Concepts, Roger J. Sullivan

Modern Radar System Analysis, David K. Barton

Multitarget-Multisensor Tracking: Applications and Advances Volume III, Yaakov Bar-Shalom and William Dale Blair, editors

Principles of High-Resolution Radar, August W. Rihaczek

Principles of Radar and Sonar Signal Processing, François Le Chevalier

Radar Cross Section, Second Edition, Eugene F. Knott et al.

Radar Evaluation Handbook, David K. Barton et al.

Radar Meteorology, Henri Sauvageot

Radar Reflectivity of Land and Sea, Third Edition, Maurice W. Long

Radar Resolution and Complex-Image Analysis, August W. Rihaczek and Stephen J. Hershkowitz

Radar Signal Processing and Adaptive Systems, Ramon Nitzberg

Radar System Performance Modeling, G. Richard Curry

Radar Technology Encyclopedia, David K. Barton and Sergey A. Leonov, editors

Range-Doppler Radar Imaging and Motion Compensation, Jae Sok Son et al.

Space-Time Adaptive Processing for Radar, J. R. Guerci

Theory and Practice of Radar Target Identification, August W. Rihaczek and Stephen J. Hershkowitz

Time-Frequency Transforms for Radar Imaging and Signal Analysis, Victor C. Chen and Hao Ling

For further information on these and other Artech House titles, including previously considered out-of-print books now available through our In-Print-Forever® (IPF®) program, contact:

Artech House
685 Canton Street
Norwood, MA 02062
Phone: 781-769-9750
Fax: 781-769-6334
e-mail: artech@artechhouse.com

Artech House
46 Gillingham Street
London SW1V 1AH UK
Phone: +44 (0)20 7596-8750
Fax: +44 (0)20 7630-0166
e-mail: artech-uk@artechhouse.com

Find us on the World Wide Web at:
www.artechhouse.com